THE UNIVERSITY OF ADELAIDE
AUSTRALIA

CRCLEME
Cooperative Research Centre for Landscape Environments and Mineral Exploration

Phyto-exploration in arid subtropical, arid mediterranean and tropical savanna environments: Biogeochemical mechanisms and implications for mineral exploration

Nathan Reid

June 2008

A thesis submitted for the degree of Doctor of Philosophy of

School of Chemical Engineering

School of Earth & Environmental Sciences

(Geology and Geophysics)

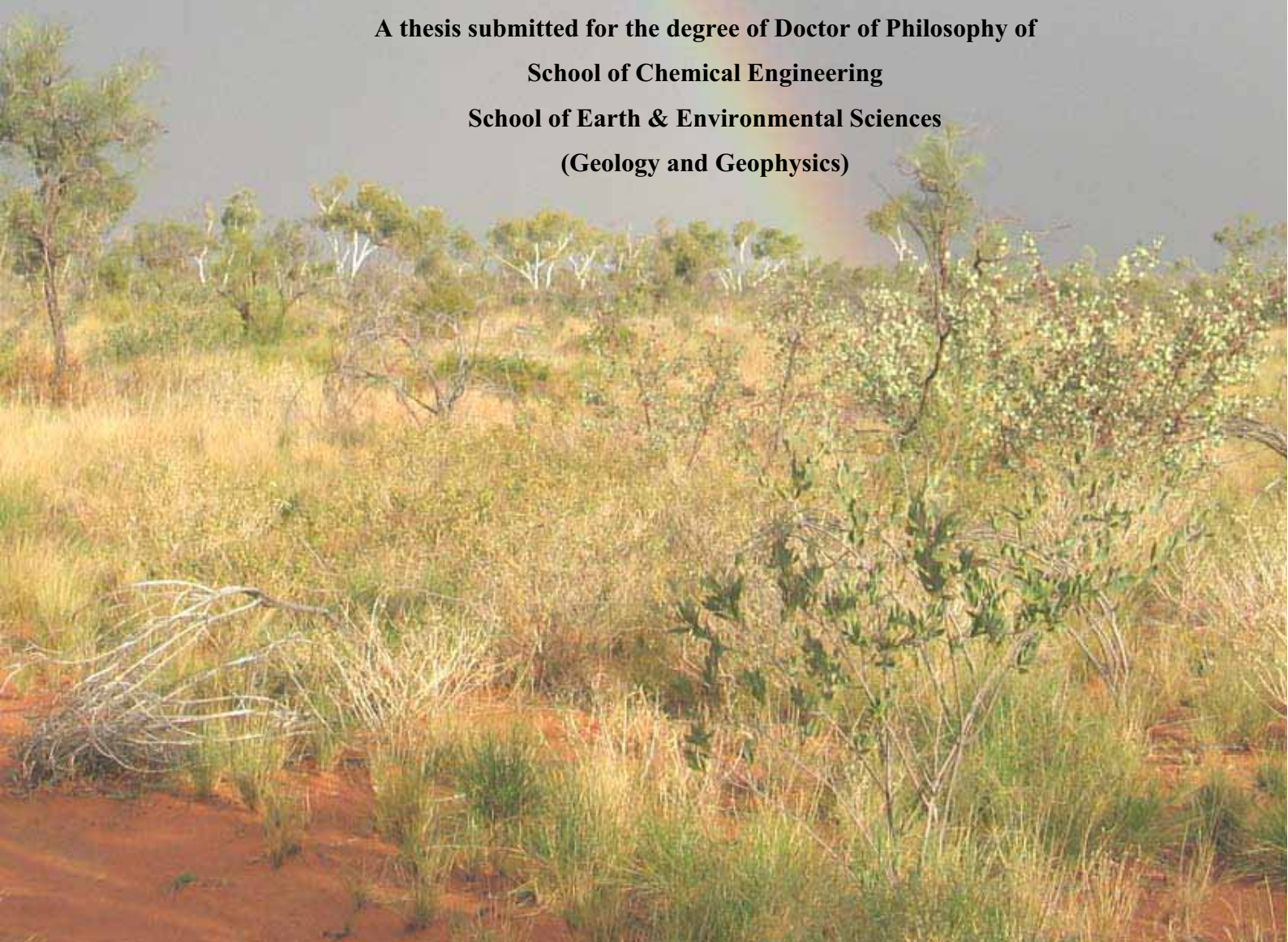

5 Tanami Region – Species Results and Discussions

5.1 Geobotany and Biogeochemistry of the Coyote Deposit

5.1.1 Site specific methods

Vegetation assemblages, tree and large shrub species and tree height were recorded along a 3 km N-S transect over the Coyote mineralisation in February 2005. This was further extended in January 2006 to include two 1.5 km transects 250 and 500 m to the east of the original transect. Biogeochemical samples were collected at 50 m spacings along all three transects and a cross line (Figure 5.1). The 3 km transect comprising 180 samples have been analysed using ICP-MS, ICP-OES and INAA techniques. This transect passed over one of the soil sampling lines that was used in the discovery of mineralisation in this prospect. The transect was along the same Easting (482325 mE, AGD84) although the soil sampling line was only 800 m with samples taken at 25 m spacings.

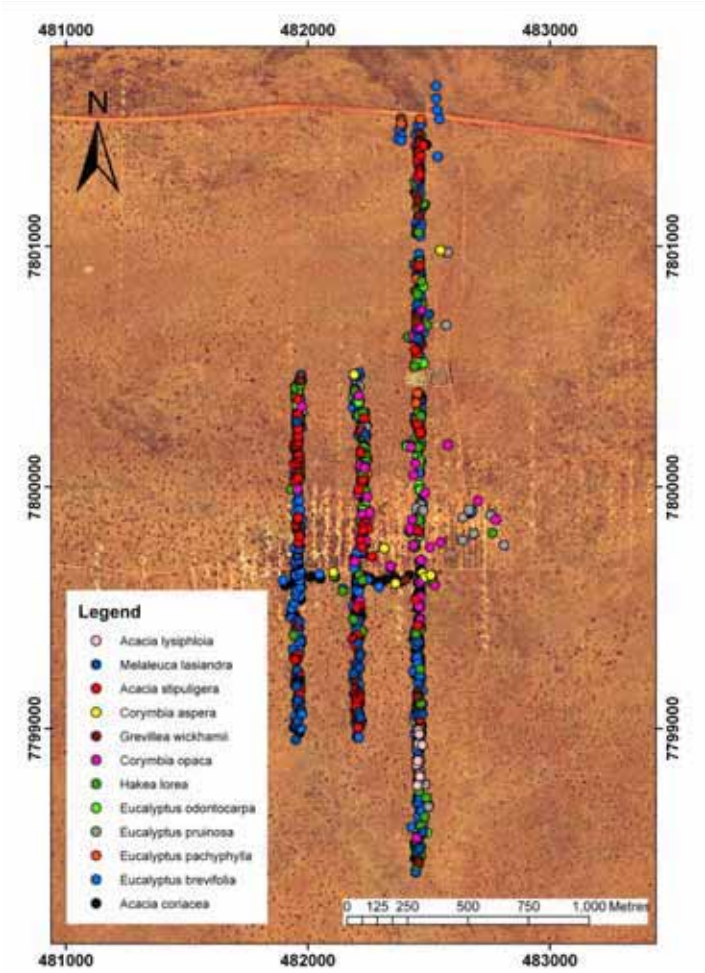

Figure 5.1: Vegetation distribution across the Coyote prospect.

The dot point vegetation map can be contoured as shown in Figure 5.2. This contour map is complicated by the large number of species growing over this site. However, some information can be determined about this landscape from this contour plot. The *Melaleuca lasiandra, Acacia stipuligera* and G*revillea wickhamii* distribution delineates the main drainage over this site. Minor drainage is shown by *Acacia stipuligera* without the *melaleuca* and *Grevillea* species. There is a wide band through the centre of the field site trending north-west to south-east. This band has no *Eucalyptus brevifolia* and more of the other Eucalypt species: *Eucalyptus pachyphylla, Eucalyptus odontocarpa, Corymbia aspera* and *Corymbia opaca*. The distribution of *Eucalyptus pruinosa* corresponds to areas where cover appears to be thinner, noted by the presence of vein quartz within the surface lag.

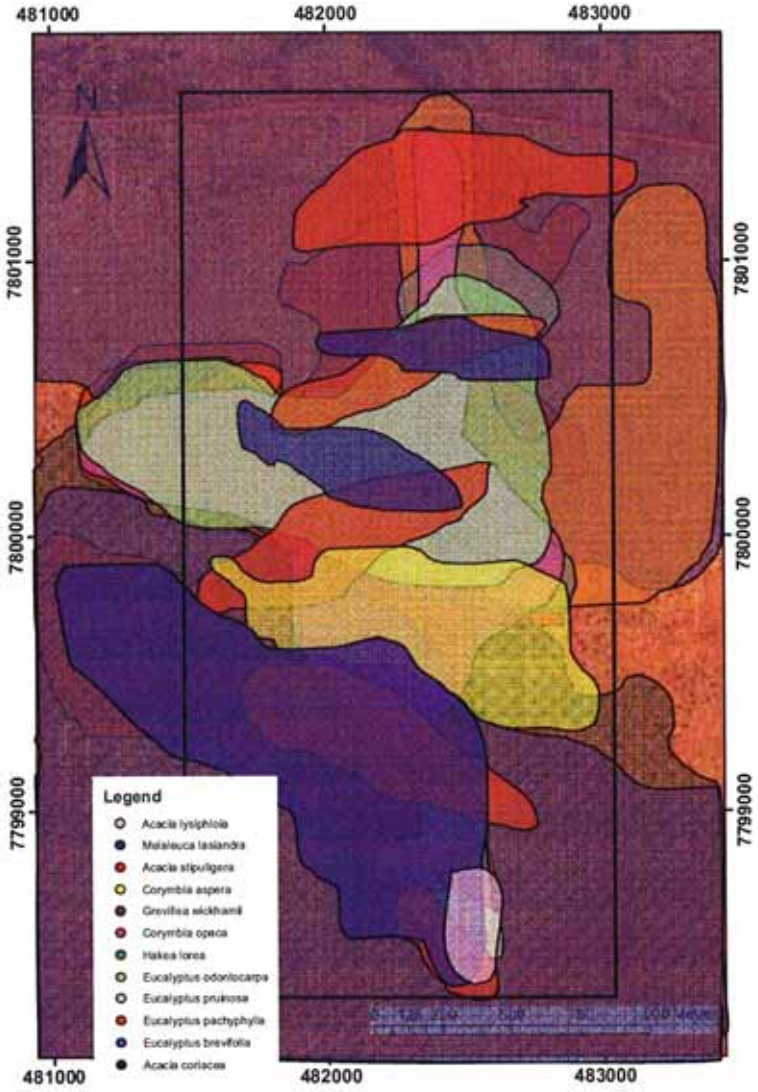

Figure 5.2: Species distribution map over the Coyote field site, with the study area within the black box. Ranges are interpreted from data points collected and remotely sensed data extrapolation.

5.1.2 *Triodia pungens* (soft spinifex)

Section 5.1.2 is an excerpt from: Reid, N., Hill, S.M., Lewis, D.M. (2008), Spinifex biogeochemical expressions of buried gold mineralisation: the great mineral exploration penetrator of transported regolith, Applied Geochemistry, 23, p76-84. See Appendix F for the full article.

The soft spinifex results show 3 distinct elemental patterns from the data:

1. Elements that are anomalous over the centre of the transect (Al, As, Au, Ba, Br, Ce, La, Mg, Mn, Na, P, S, Sc, Sm and Zn);
2. Elements anomalous to the south of the transect (K and Rb);
3. Elements anomalous to the north of the transect (Co, Mo, Nb, Nd, Ni and Sn).

There are also elements that are irregularly distributed (Cr, Cu, Fe and Sr) where Cr is also anomalously high values compared to other plants. Elements that were below analytical detection limit were Ag, Be, Bi, Ca, Cd, Cs, Eu, Ga, Hf, In, Ir, Pb, Sb, Se, Ta, Te, Th, Ti, U, V, W, Yb and Zr.

The results from the Coyote Prospect indicate that spinifex leaf chemistry show a zone of high S contents (1.2 km wide) with a dispersion tail away from the mineralisation (Figure 5.3). The highest concentrations occur over the mineralised zone (1186 ppm) with the concentrations decreasing both to the north and south of mineralisation (down to 797 ppm). This is complemented by a less extensive zone of high Zn content (600 m wide, Figure 5.3), with the highest concentrations also directly over mineralisation (34 ppm) but where the dispersion tail spreads across a shorter distance than that of S (down to 10 ppm). This difference in anomaly 'dispersion tail' or 'footprint' size is due to Zn being hydrogeochemically less mobile than S.

A high intensity zone of elevated As contents is more closely restricted to the area overlying mineralisation (Figure 5.4), with the highest values (1.2 ppm) directly above the mineralisation with the concentrations decreasing to below detection limit (0.1 ppm) within 100 m to the north and south. The rare earth elements (REE) Ce, Sm and La, all had the same chemical dispersion pattern as As with the highest values directly over the mineralisation and decreasing to below detection limit within 100 m to the north and south. Finally, detectable Au assays conform to a high intensity zone centred directly over mineralisation and has the smallest diameter anomaly 'footprint' (Figure 5.4). There are some small outlier Au anomalies to the north and south of mineralisation; however the highest magnitude assay (2.3 ppb) is still directly above mineralisation.

The Au results particularly highlight that a single element does not singularly aid in the detection of this mineralisation since only single point anomalies have been generated which are not statistically rigorous. However, when the multi-element suite is considered, several elements associated with mineralisation (in this case S, Zn, REE, As and Au) can more effectively provide a more reliable and potentially enlarged target for mineralisation.

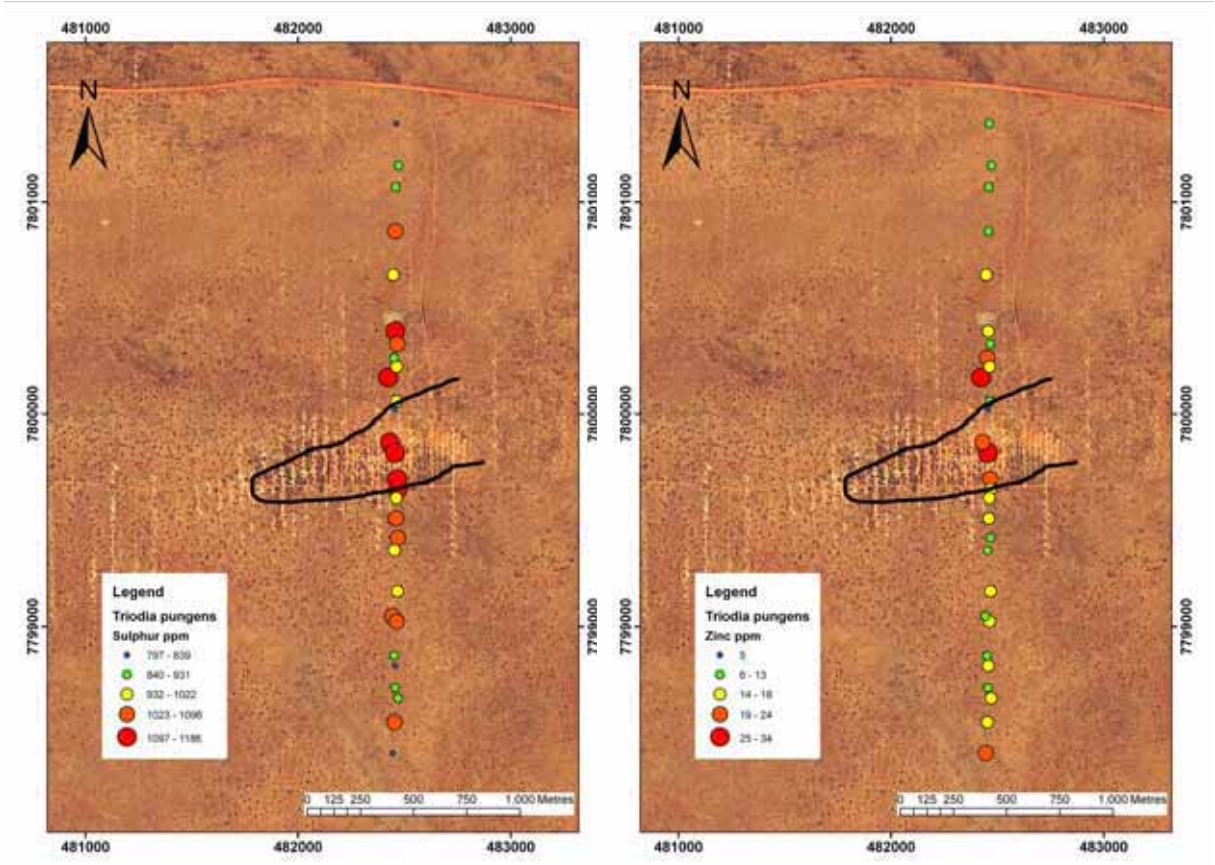

Figure 5.3: Plots of S and Zn concentration in *Triodia pungens* overlying the orthophoto of the Coyote Prospect. The Au ore body, projected from 200 m depth, is within the area delineated by the black line.

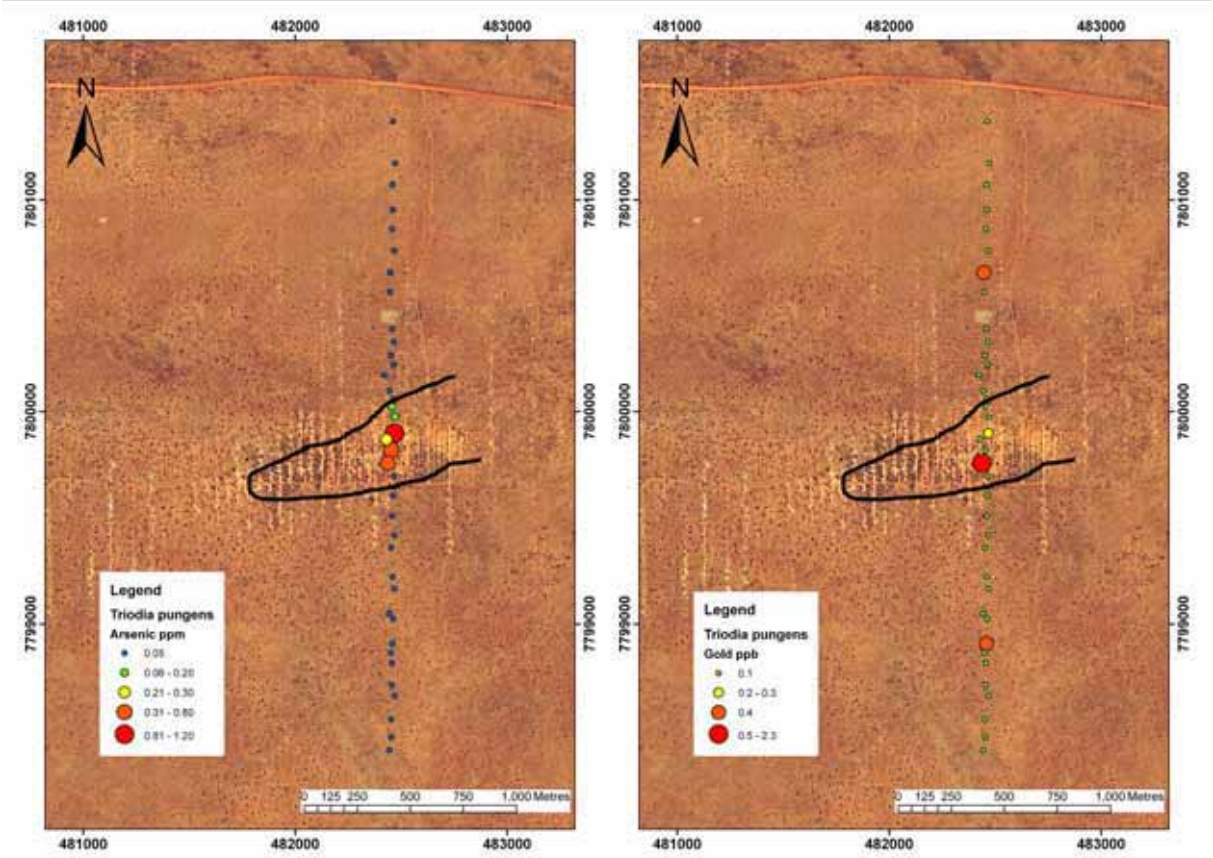

Figure 5.4: Plots of As and Au concentration in *Triodia pungens* overlying the orthophoto of the Coyote Prospect. The Au ore body, projected from 200 m depth, is within the area delineated by the black line.

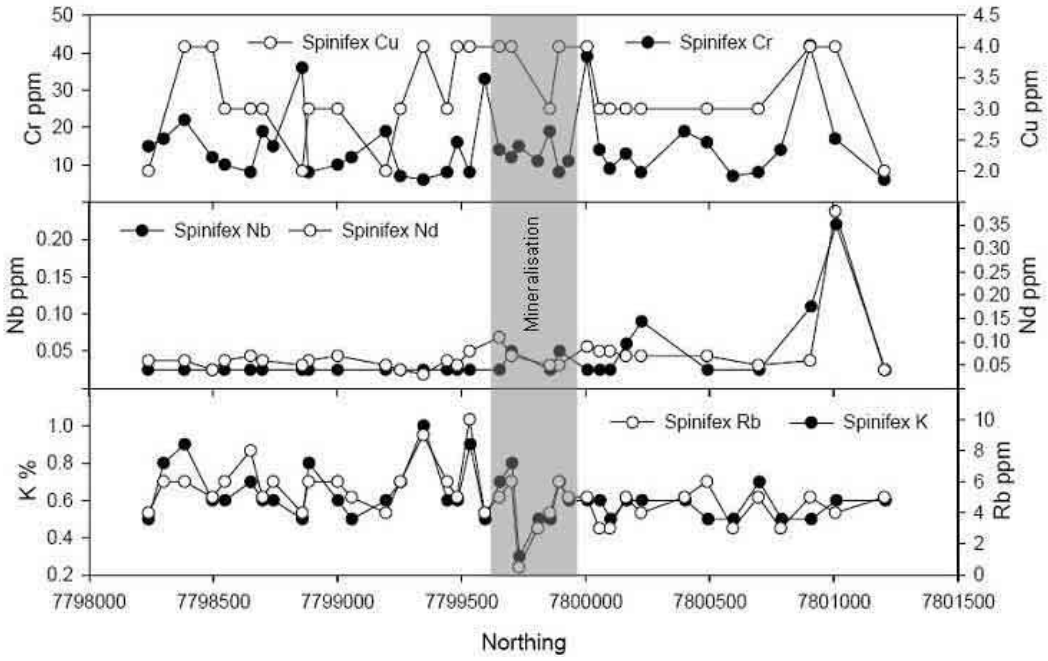

Figure 5.5: *Triodia pungens* elemental cross section across the Coyote transect

Elements higher in the South of the transect are generally elements related to plant growth, macro-nutrients and essential elements (Rb and K, Figure 5.5) the dispersion of these elements varies based upon their mobility within the substrate.

Elements higher in the North of the transect tend to focus on two areas, one directly south of the 'bag farm' (site where bags of previous drill core are dumped) which may be related to detrital contributions, and an area very close to the northern end of the transect (Nb and Nd

which are not directly related to mineralisation, Figure 5.5). This area is anomalous in several elements which may warrant further investigation.

Some of the elements had no particular associated pattern (Cr and Cu, Figure 5.5). Chromium is of particular interest because the values are particularly anomalous compared to other species; however there is no direct link for this anomalism. Copper is uniformly distributed across the site although it is present in the mineralisation, this is due to scavenging by Fe-oxides which transport Cu in groundwaters but do not allow concentration over the ore body.

The Coyote deposit was originally discovered through an As soil anomaly (-180 mesh sieve) and subsequent drilling. A plot of the As concentrations from the soil line closest to the vegetation transect (Figure 5.6) indicates that while both media detect the mineralisation zone, the soil data contains a large variation in results (possibly 'noise') compared to the spinifex which provided a direct vector to mineralisation without dispersion. Furthermore, whereas the soil samples only provided a reliable As mineralisation signature (there was no multi-element anomaly), the spinifex assays provided a multi-element expression of buried mineralisation (As, Au, Zn, S, Ce, and La). Although Au was the primary mineralisation target, As, Zn, S and REE can be used as effective biogeochemical pathfinder elements for this Au mineralisation. These elements were not all of use within the soil geochemistry results as S was not analysed and Zn was inconclusive.

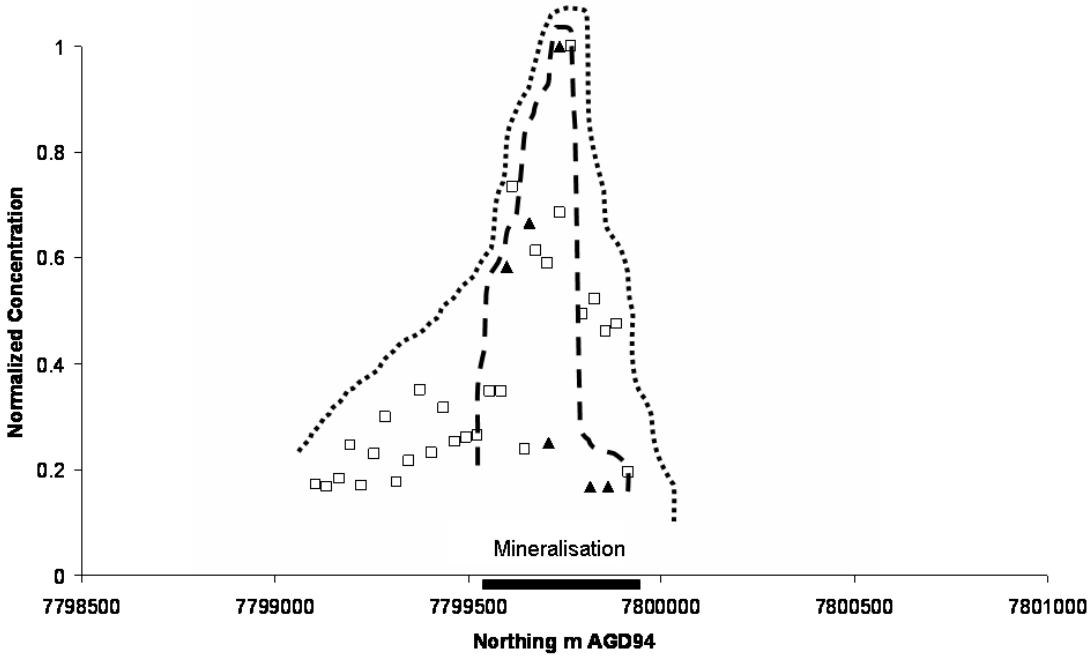

Figure 5.6: Arsenic comparison between soil and spinifex. □ represents soil data with dotted line envelope. ▲ represents spinifex data with dashed line envelope. Mineralisation marked with a rectangle.

Au concentrations were below detection in soils overlying the mineralised zone. This is not surprising given the area is regularly subjected to sheetwash erosion, which has led to the dispersion and dilution of most elements in the soil overlying mineralisation. However, since spinifex plants are deep-rooted they are able to penetrate through the surface soil and sediment and into the underlying mineralised, *in-situ* regolith.

Discussion

The chemical maps shown in Figures 5.3 and 5.4 indicate that the spinifex assays provide a multi-element expression of buried mineralisation, with different size elemental 'footprints' that are closely associated with the different solubilities of each element. In this system, S is the most soluble element and thus disperses more widely; Zn is less soluble and hence disperses over less distance. Due to its insolubility Au is only detected directly above

mineralisation; while As, being a relatively mobile element, has been bound up in the system, presumably associated with ferruginous secondary minerals and is not dispersed far from the mineralised zone. This is also reflected in the soil data for As that shows a comparable zone of elevated assays. However the soil data only detected an As anomaly directly over mineralisation and was an inconsistent data set compared to the spinifex assays that provided a very distinct and consistent chemical footprint expressing buried mineralisation.

The possibility of dust contamination has been considered during the data analysis process, and some elements have been targeted as being most likely to have been from detrital contamination. These elements are typically Ti, Zr, Al and Fe which occur in soil materials but with the exception of Fe are not essential. The levels of these elements incorporated into the plant are of such low concentrations that they would be overprinted by any particulate contamination (Kabata-Pendias & Pendias 1984). In these data Ti and Zr were below the detection limit in all plant samples, and although Fe and Al were detected their concentrations were relatively low and were consistent over the site, so there is a component of cdust contamination in the samples but it was deemed insignificant. Elemental ratios of the important ore elements versus possible detrital contaminant elements showed that the ore element signals (Zn, S, As, Au and REE) in the spinifex assays were independent of the possible contaminant elements. This indicates that soil and dust contamination had little impact upon the spinifex sample chemistry.

The lack of lateral roots or root hairs near the surface seen in soft spinifex plants examined on site indicates that any biogeochemical signal must come from deep within the regolith profile. Here, the transported cover (wind-blown or sheet-wash sands) is between 5-15 m thick, therefore the soft spinifex is ideal for use as a 'regolith penetrator' for mineral exploration sampling programs.

Since *Triodia pungens* is a deep-rooted species it is able to give localised chemical signatures for the *in-situ* regolith materials that may underlie 15 m of surface sediment. In the Tanami region, and possibly many other parts of arid Australia, the spinifex is an excellent biogeochemical exploration sampling medium, especially compared to soils, which are typically influenced by sheetflow and aeolian dispersion and dilution. The vegetation results have very sharp cut offs to the generated anomalies in this system. There are high values next to values that are below the detection limit of the analysis technique. This makes it less useful in a regional sampling program but spinifex would be an ideal sampling medium for closely spaced, detailed ore body delineation in the Tanami region and most likely in other hummock grass-dominated parts of the continent and grasslands world-wide.

5.1.3 *Eucalyptus brevifolia* (snappy gum)

Snappy gum (*Eucalyptus brevifolia*) is one of the main species growing at the Coyote Prospect. Snappy gum distribution over the Coyote Prospect can be seen in Figure 5.7. This plot shows that the snappy gum is abundant throughout the area except for a northwest to southeast band. This band is around 300 m wide and corresponds with a region of faulting that trends in this direction. The fault zone is buried and is difficult to distinguish in most geophysical imagery. Other *Eucalyptus* - *Corymbia* species (bloodwood, twin-leaf, mallee species) are more abundant in the fault zone since there is more water available in this zone and the other species are able to 'out-compete' the snappy gum.

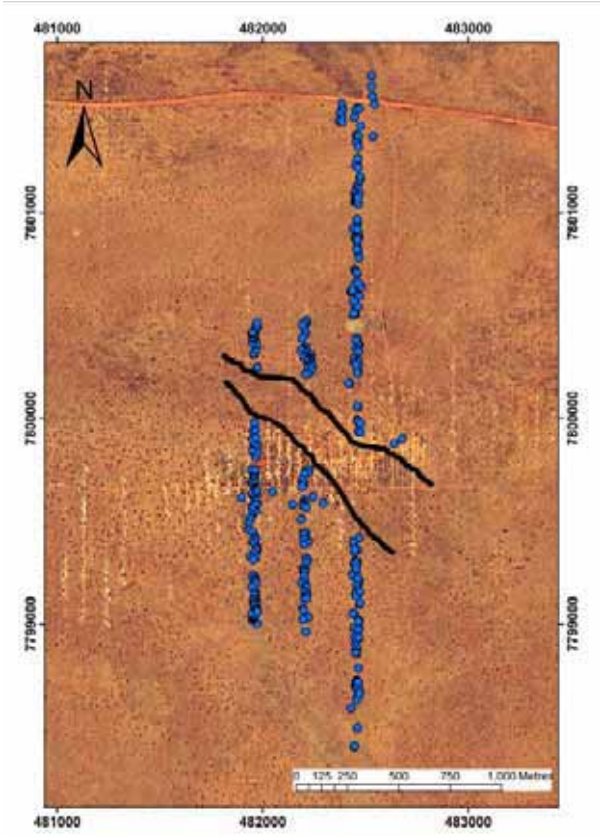

Figure 5.7: Snappy gum locations along transect surrounding Coyote mineralisation. Fault zone is enclosed within the two white lines.

The snappy gum assays show 3 distinct elemental patterns from the data:

1. Elements that are elevated over the centre of the transect (Al, As, and Ba);
2. Elements elevated to the south of the transect (Ca, Mg, P, S, Sr, and Zn); and,
3. Elements elevated to the north of the transect (Br, Ce, Co, Fe, K, Mn, Mo, Nb, Ni, Pb, Rb and Sn.).

There are also elements without distinctive associations (Cu, La, Nd and Sm). Elements that were below analytical detection level were Ag, Au, Be, Bi, Cd, Cr, Cs, Eu, Ga, Hf, In, Ir, Lu, Na, Sb, Sc, Se, Ta, Te, Th, Ti, U, V, W, Yb and Zr.

There is a chemical signature from mineralisation dispersed to the south (down slope and hydrological gradients) within the snappy gum biogeochemistry results. This can be seen in the S and Zn results (Figures 5.8 and 5.9); the more mobile elements (e.g. Ca, Mg, P, Sr) also have the same dispersion pattern. This is not a lithogeochemical signature as there is the same rock type over the whole site, with only minor textural and compositional changes within this unit. The distance of elevated assays away from the mineralisation is related to the element's relative chemical mobility. Gold, however was not detected, probably due to the lack of samples over mineralisation along this transect, therefore making Zn and S the most useful detectable ore indicator elements.

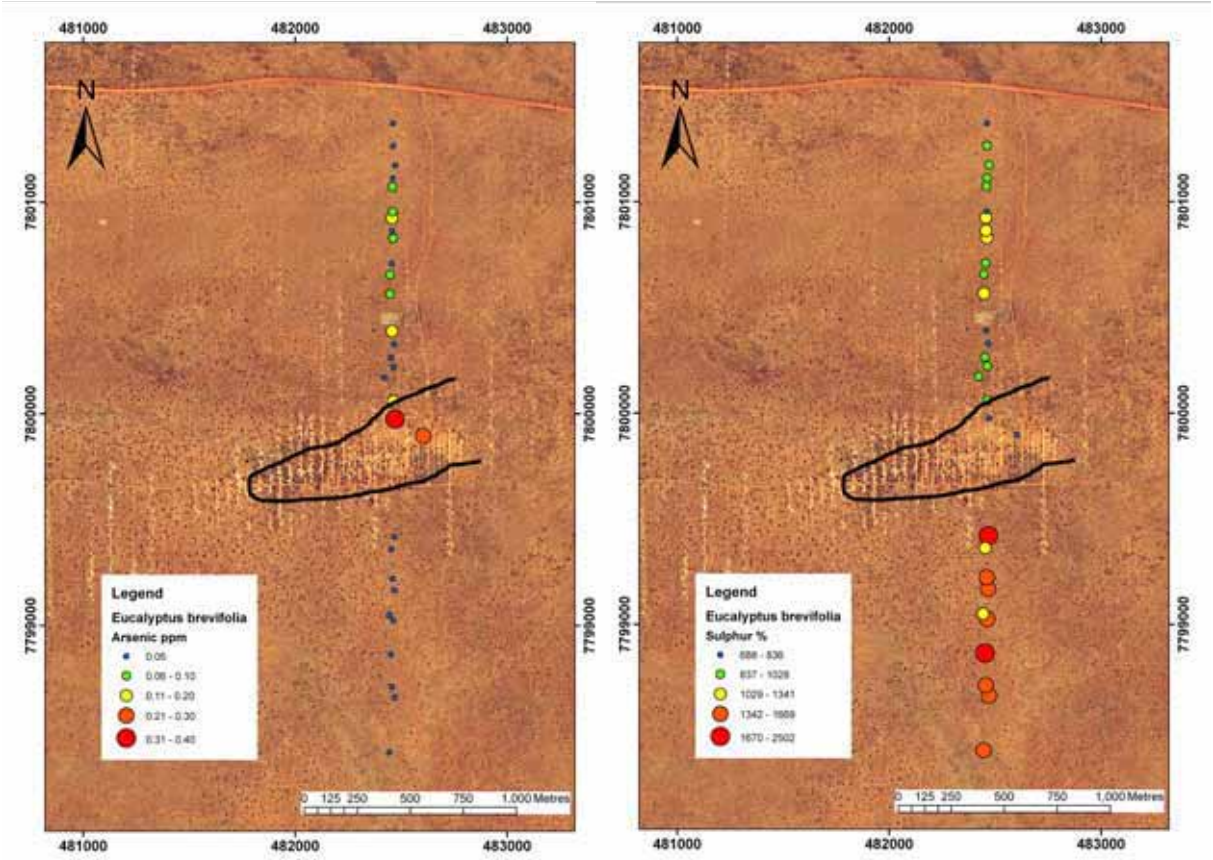

Figure 5.8: Plots of As and S concentration for *Eucalyptus brevifolia* overlying the orthophoto of the Coyote Prospect. The Au ore body, projected from 200 m depth, is within the area delineated by the black line.

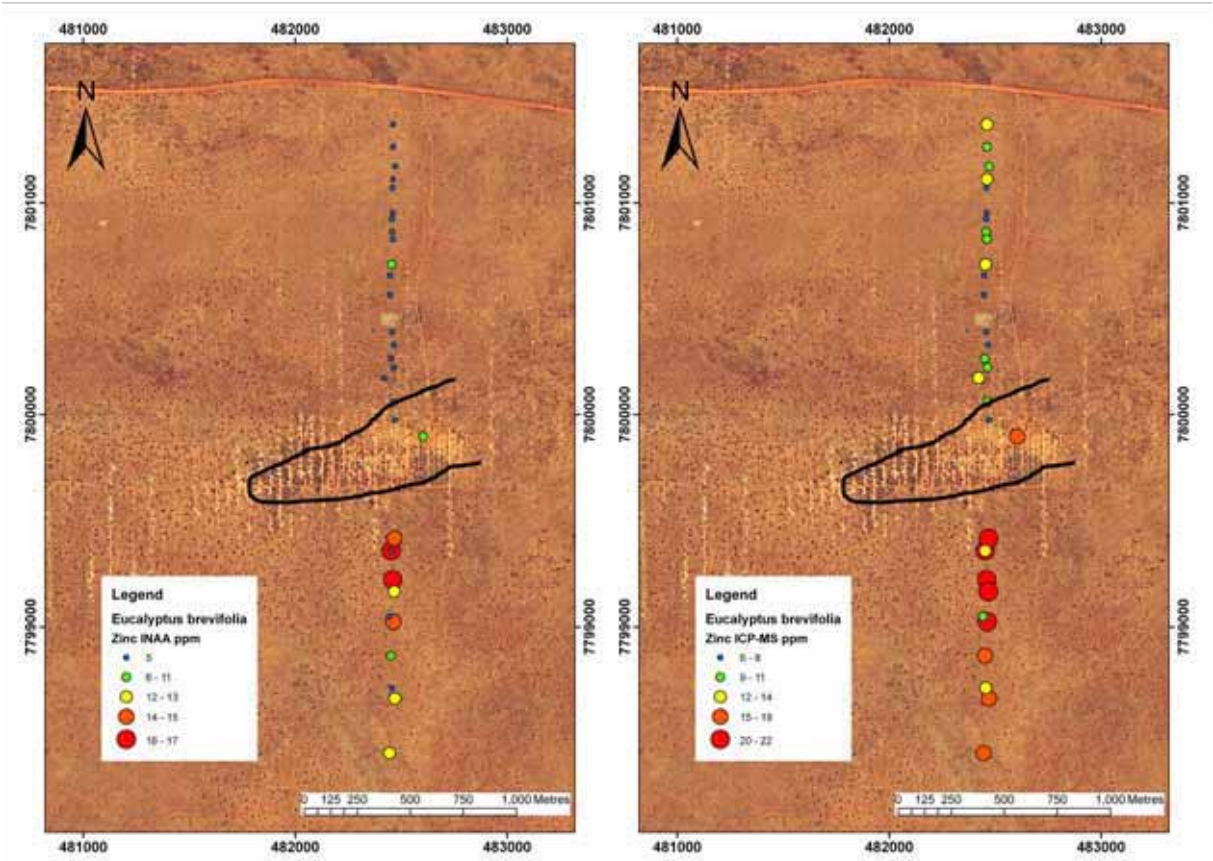

Figure 5.9: Plots of Zn (INAA) and Zn (ICP-MS) concentration for *Eucalyptus brevifolia* overlying the orthophoto of the Coyote Prospect. The Au ore body, projected from 200 m depth, is within the area delineated by the black line.

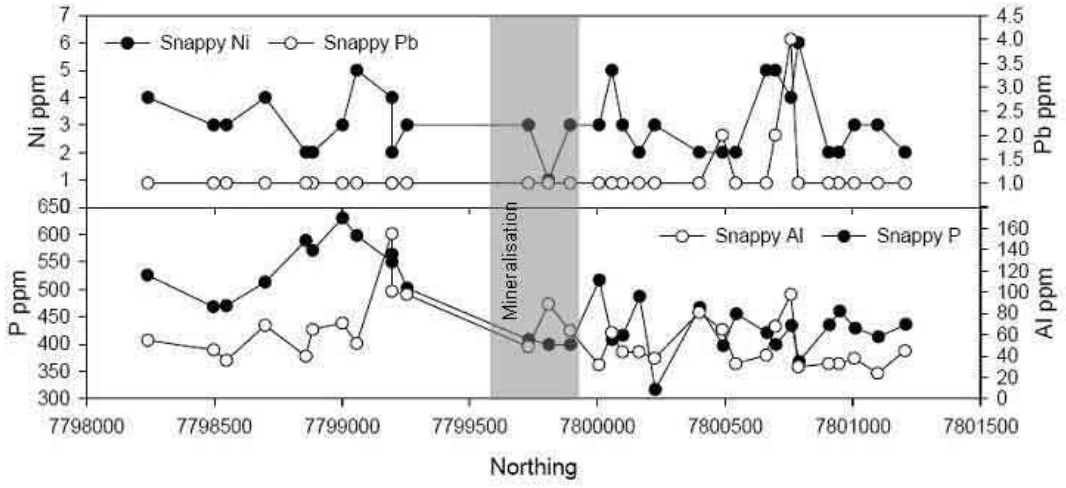

Figure 5.10: *Eucalyptus brevifolia* elemental cross sections across the Coyote transect

Arsenic concentrations were elevated in the few samples within the mineralisation zone; however this corresponds to only 2 points, which is not significant (Figure 5.8). Elements that are more abundant in the North of the transect include Ni and Pb that may relate to a buried mafic dyke (Figure 5.10).

Discussion

At the Coyote Prospect the absence of *Eucalyptus brevifolia* closely reflects the Coyote Fault zone through several metres of transported cover. There is a substrate/hydrogeochemical change associated with this fault, thought to be influencing the growth of snappy gum. This change is most likely due to increased water flow potential in the region of the faults which would then favour other *Eucalyptus/Corymbia* species. This association suggests that it might be possible to use detailed vegetation mapping in the Tanami to gain information about structural features represented by broad vegetation community changes. Hyperspectral data could be used to map the distribution of snappy gum on a regional basis and to identify gaps that could correspond with the location of bedrock structures.

The chemical maps shown in Figures 5.8-5.10 indicate that the snappy gum assays provide a multi-element expression of dispersion patterns away from buried mineralisation, with different size elemental 'footprints' reflecting element solubility. Sulphur is the most soluble element so it disperses widely; Zn is less soluble and hence travels less distance. The model developed for the mechanism for elemental uptake by snappy gum can be seen in Figure 5.11, where elements from primary mineralisation can interact with groundwater and hence enter the snappy gum roots and be transported to the aerial tissues.

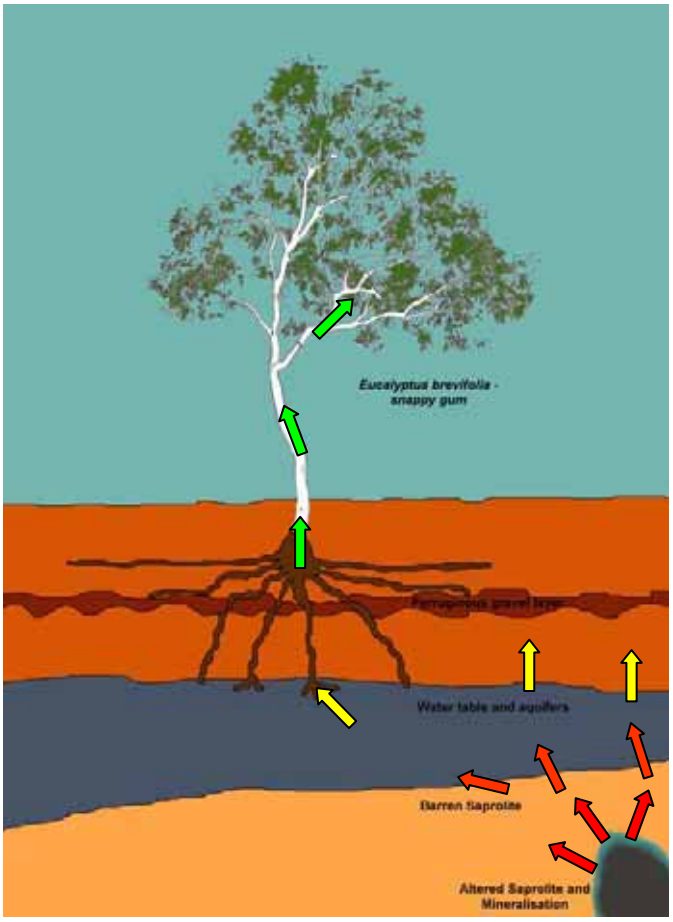

Figure 5.11: Uptake mechanism model, showing the root system of the snappy gum and its interaction with groundwater.

The mechanisms involved in this process are often complex, involving oxidation and dissolution processes to release As and S from arsenopyrite into solution. The As is oxidised to arsenate and arsenite (AsO_4^{3-} and AsO_3^{-}) or can be complexed via microbial interactions to monomethylarsonic acid (MMAA) or dimethylarsinic acid (DMAA), these compounds are transported from the ore body through the groundwater until they come into contact with the plant root zone (Abedin *et al.* 2002; Meharg & Hartley-Whitaker 2002). Metal ions can enter the plant root actively through specialised plasma membrane metal ion transporters (Salt *et al.* 1998; Meharg & Hartley-Whitaker 2002). Arsenate is the most common form of As in groundwaters and can substitute for phosphate in the plant structure (Abedin *et al.* 2002; Meharg & Hartley-Whitaker 2002; Wang *et al.* 2002) which can be critical in Australian environments where phosphate is limiting and each plant would actively uptake arsenate to fill this position. The S from sulphides are oxidised generally to sulphate (SO_4^{2-}) which is readily mobile and moves through the profile in the groundwater. There is a specific sulphate transporter in the root membrane which allows the transport of sulphate from the soil solution to the root structure (Smith *et al.* 2000). Once in the root structure the ions are either transported, transformed or stored. The transport is generally driven by transpiration causing high osmotic pressures which enable water and ion transport between the root zone and the leaf zone where the water is lost to the atmosphere (Salt *et al.* 1998).

5.1.4 *Corymbia opaca* (desert bloodwood)

Corymbia opaca distribution over the Coyote Prospect was limited to directly over the mineralisation where it was able to out-compete the snappy gum, and a few scattered plants to the north and south of the mineralised zone. Due to the restricted distribution, the

interpretation of the results is inhibited. The desert bloodwood results show 6 distinct elemental patterns from the data;

1. Elements that are elevated over the centre of the transect (Al, As, Fe, Mg, P and Ti),
2. Elements in low abundance over the centre of the transect (Br),
3. Elements elevated to the south of the transect (La, Sr and Zn),
4. Elements elevated to the north of the transect (Au, Mo and Sn),
5. Elements elevated to the centre and south (Ba, Ca, Ce, Co, Mn, Nd, Ni and Sm); and,
6. Elements anomalous to the centre and north (Cu, K, Rb and S).

Elements that were below analytical detection were Ag, Be, Bi, Cd, Cr, Cs, Eu, Ga, Hf, In, Ir, Lu, Na, Sb, Sc, Se, Ta, Te, Th, U, V, W, Yb and Zr.

The results show a 250 m wide zone of elevated As directly over mineralisation, which closely corresponds with the 200 m depth projection of mineralisation (Figure 5.12). However, the other elements that correspond this way are those assumed to be associated with detrital contamination (Al, Fe, and Ti), which could either be due to the area above mineralisation being mostly cleared and hence there was a greater amount of wind-borne dust, or because there was a greater proportion of drill spoil in this area that may have been absorbed by the lateral roots of this species.

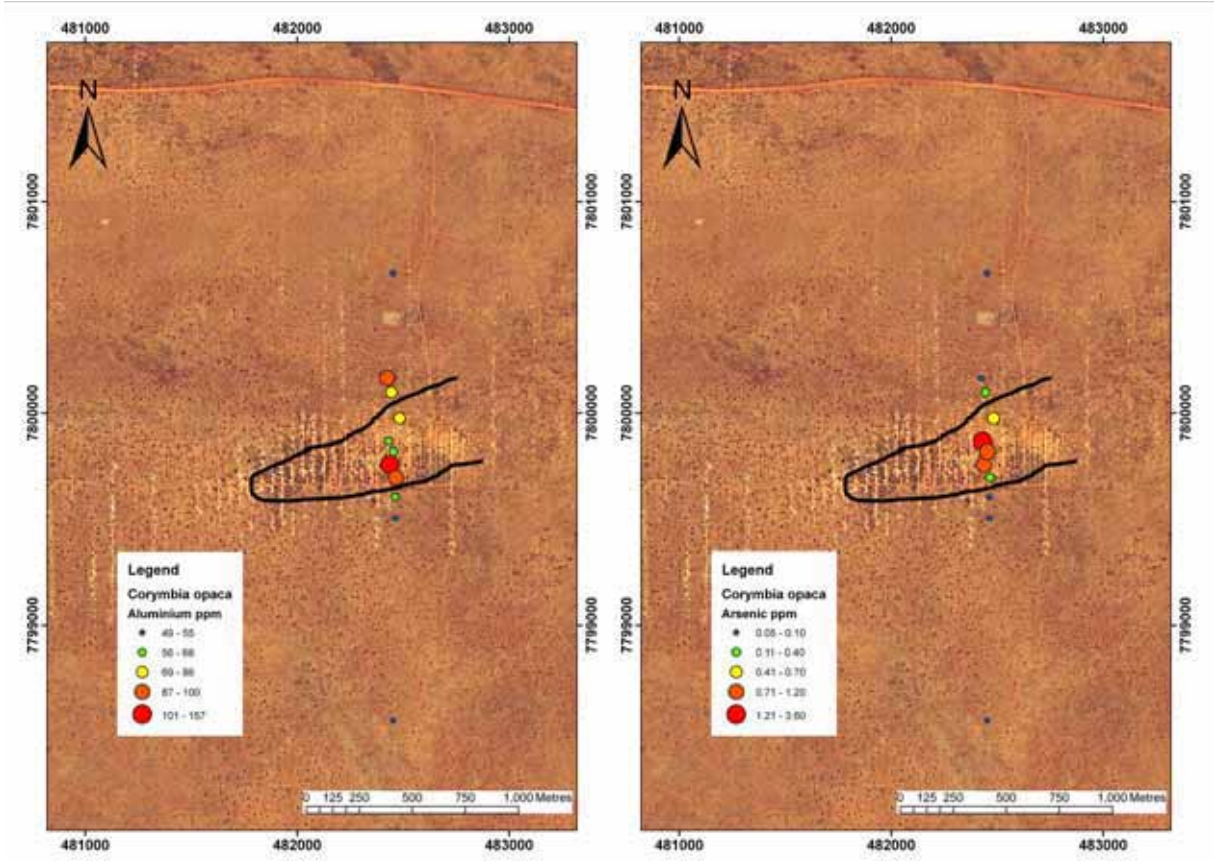

Figure 5.12: Plots of Al and As concentration for *Corymbia opaca* overlying the orthophoto of the Coyote Prospect. The Au ore body, projected from 200 m depth, is within the area delineated by the black line.

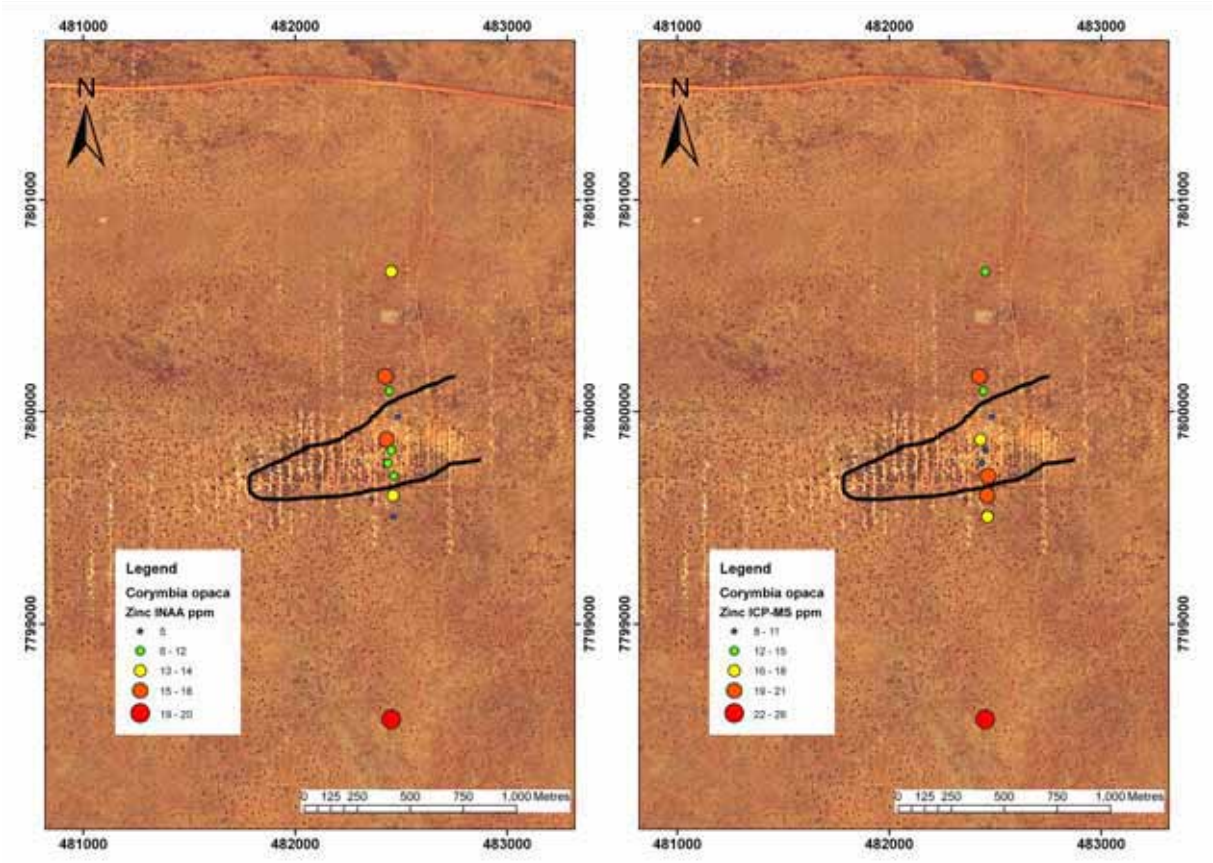

Figure 5.13: Plots of Zn (INAA) and Zn (ICP-MS) concentration for *Corymbia opaca* overlying the orthophoto of the Coyote Prospect. The Au ore body, projected from 200 m depth, is within the area delineated by the black line.

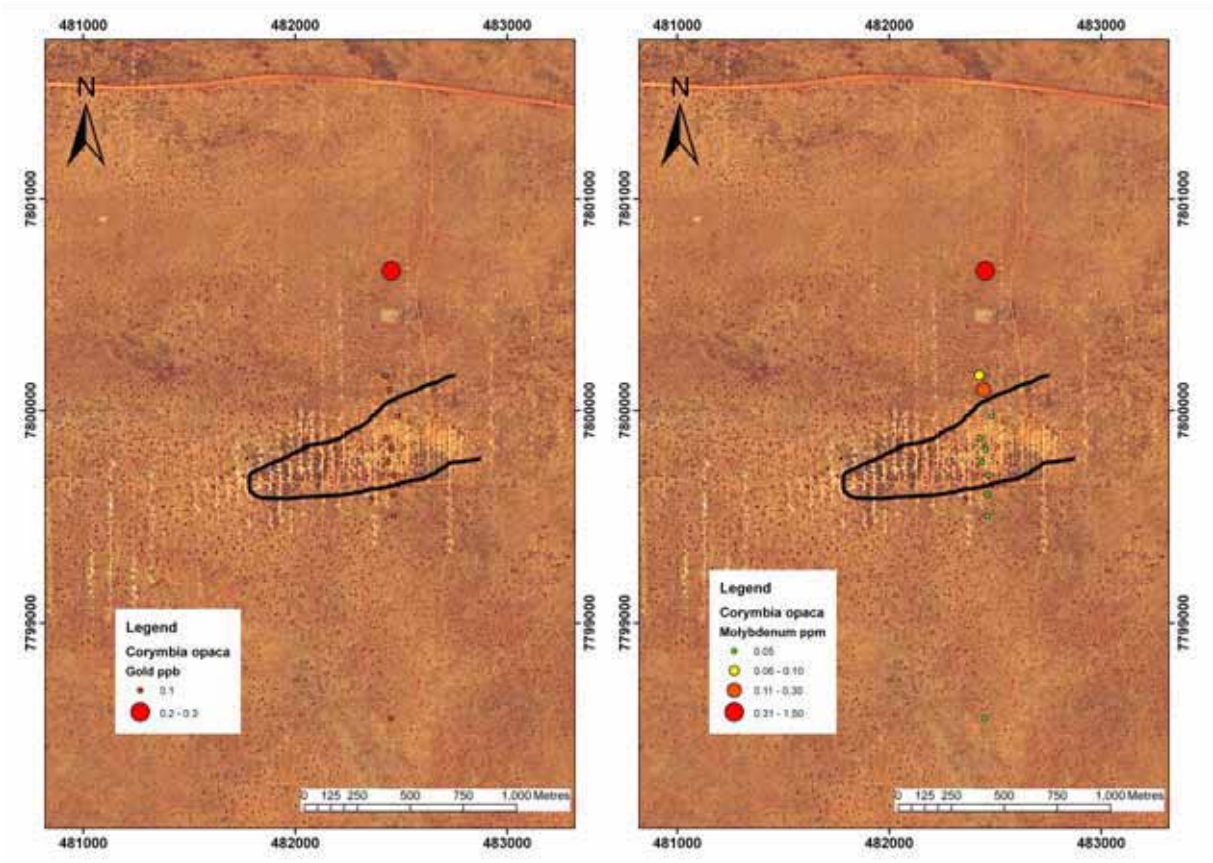

Figure 5.14: Plots of Au and Mo concentration for *Corymbia opaca* overlying the orthophoto of the Coyote Prospect. The Au ore body, projected from 200 m depth, is within the area delineated by the black line.

Some of the results showed a single point anomaly to the south of the transect (Figure 5.13). This point matches up with the results from the snappy gum, however, it is only one point which limits its significance. In this case the INAA and ICP-MS results for Zn are shown, highlighting the comparability between the two methods. The values of ICP-MS are generally slightly higher but they follow the same spatial trends.

Results showing high assay values to the north are shown by a single point anomaly, especially in Au and Mo (Figure 5.14), which corresponds with one of the single point anomalies within the spinifex results.

Discussion

The limited distribution of the desert bloodwood restricts its application as a tenement/prospect scale sampling medium. However, it detected the mineralisation within As assay (which had higher values than the spinifex results) and its behaviour and root structure appears to be very much like that of the snappy gum. It is therefore possible that this species could be used in areas where snappy gum is limited and at a regional scale with it's locally limited but regionally widespread.

5.1.5 *Acacia coriacea ssp. sericophylla* (dogwood)

The distribution of *Acacia coriacea* across the Coyote prospect was restricted to the southern half of the transect. The northern half of the transect is closer to the Tanami Highway and is subjected to repeated fire activity which is not conducive to *A. coriacea* colonisation. *A. coriacea* is a slow growing and long-lived species that does not recover well from fire. The *Acacia coriacea* results show 2 distinct elemental patterns from the data:

1. Elements that are elevated over the centre of the transect (Al, Au and P) (Figure 5.15); and,
2. Elements anomalous to the south of the transect (Ag, Cu, K, Mg, Mn, Sr and Zn) (Figure 5.16).

There are also elements that are irregularly associated (Ba, Br, Ca, Ce, Fe, La, Nd, Ni, Rb, S, Sm and Sn) (Figure 5.17). Elements that were below analytical detection were As Be, Bi, Cd, Co, Cr, Cs, Eu, Ga, Hf, In, Ir, Lu, Mo, Na, Nb, Pb, Sb, Sc, Se, Sr, Ta, Te, Th, Ti, U, V, W, Yb and Zr.

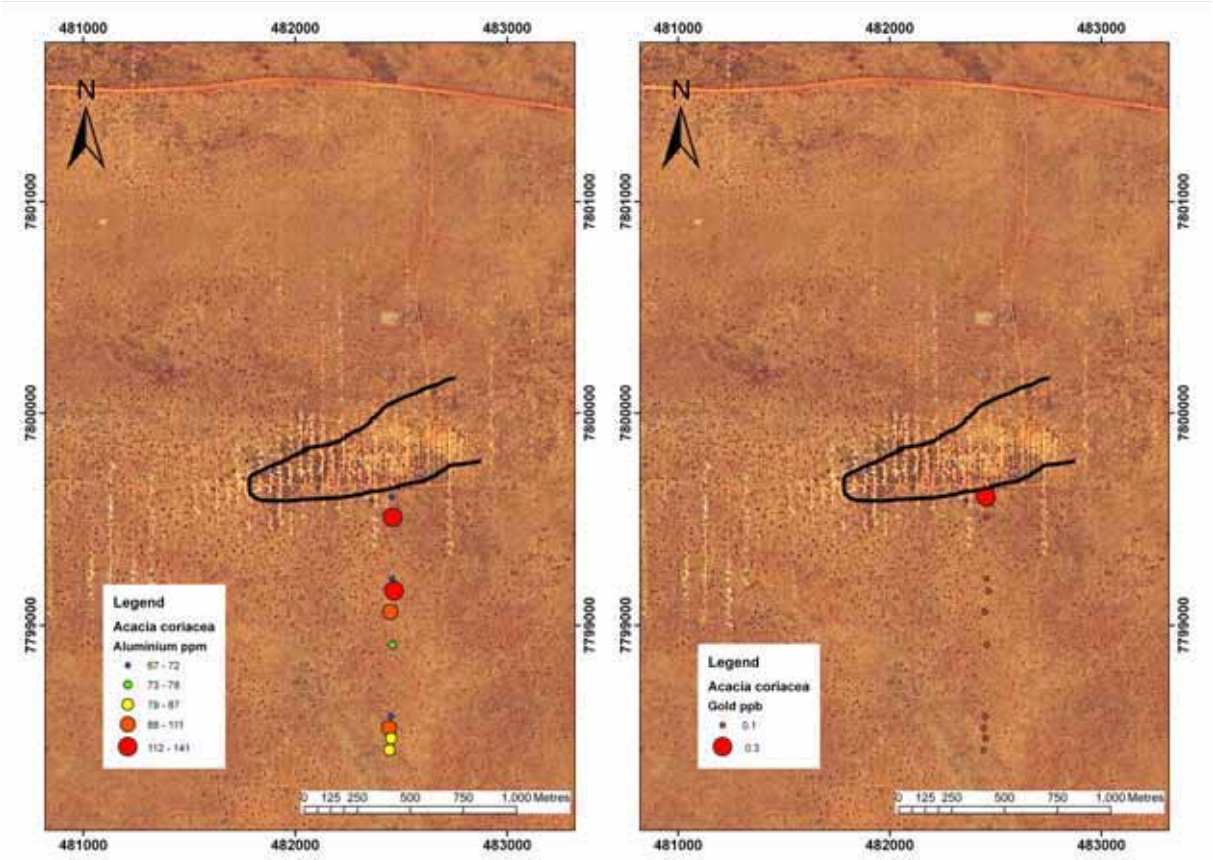

Figure 5.15: Plots of Al and Au concentration for *Acacia coriacea* overlying the orthophoto of the Coyote Prospect. The Au ore body, projected from 200 m depth, is within the area delineated by the black line.

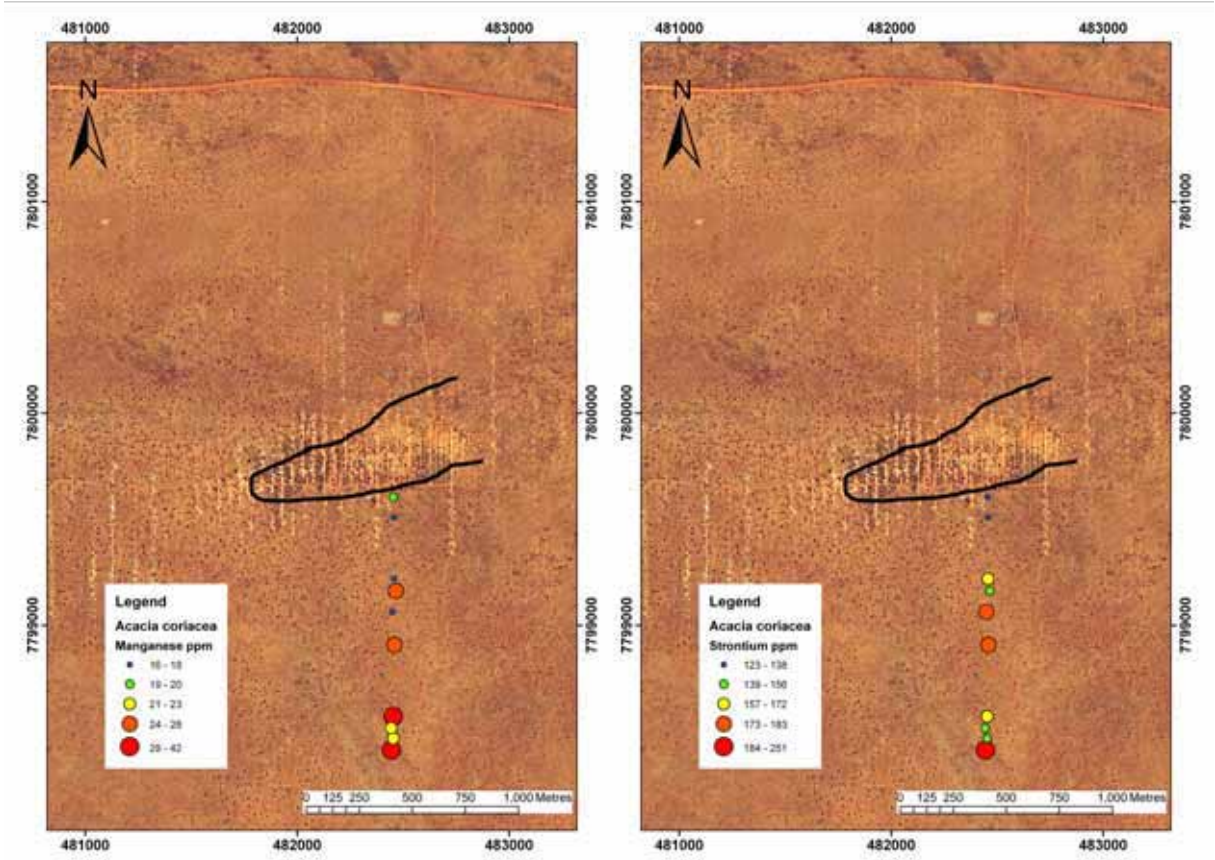

Figure 5.16: Plots of Mn and Sr concentration for *Acacia coriacea* overlying the orthophoto of the Coyote Prospect. The Au ore body, projected from 200 m depth, is within the area delineated by the black line.

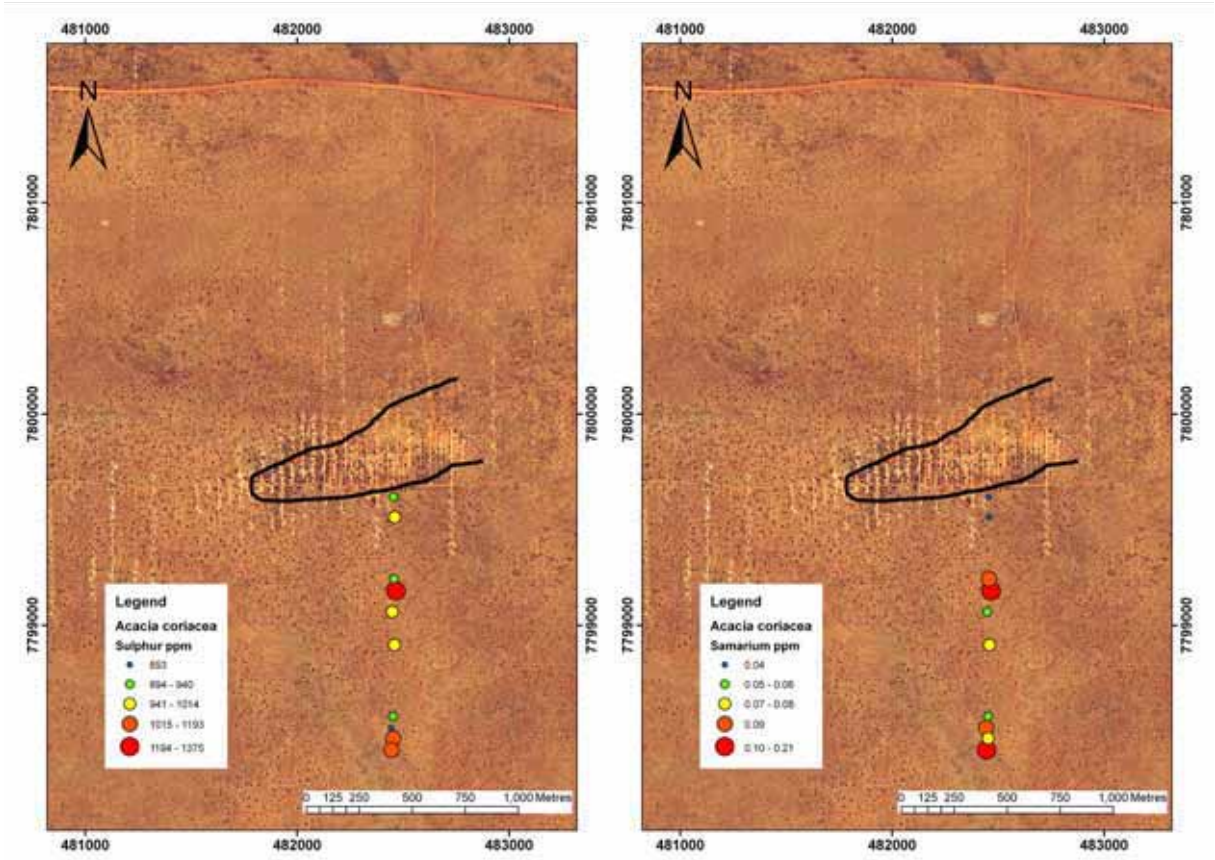

Figure 5.17: Plots of S and Sm concentration for *Acacia coriacea* overlying the orthophoto of the Coyote Prospect. The Au ore body, projected from 200 m depth, is within the area delineated by the black line.

The only sample with detectable Au was directly south of the mineralised zone (Figure 5.15). It is possible that if the distribution had extended further north over the mineralisation then the deposit may have been detected with this species, however, single point anomalies do not generate much confidence.

Discussion

The results from the *Acacia coriacea* biogeochemical assays are inconclusive due to the limited distribution across the transect. The species poor response to regular fires means that this plant would not be a useful sampling medium widely over the Tanami region as it is subjected to periodic fires.

5.1.6 *Eucalyptus pruinosa* (silver box)

Eucalyptus pruinosa has a restricted range over the Coyote Prospect. It is mostly restricted to areas with shallow transported cover, typically associated with white, angular, vein quartz lag (seen at both Coyote and Hyperion). It could therefore be possible to use this species as a geobotanical indicator for areas of quartz veins. These areas could then be narrowed down biogeochemically or lithogeochemically by testing for Au/As contents of the veins and the plants above the veins.

The *Eucalyptus pruinosa* results show 2 distinct elemental patterns from the data:

1. Elements that are anomalous over the centre of the transect (Ag, Al, As, Ce, Cu, Fe, La, Mn, P and Sm); and,
2. Elements anomalous to the south of the transect (Ni, S and Sr).

There are also elements that are irregularly associated (Ba, Br, Ca, K, Mg, Nd, Rb, Sn and Zn). Elements that were below analytical detection were Au, Be, Bi, Cd, Cr, Cs, Eu, Ga, Hf, In, Ir, Lu, Mo, Na, Pb, Sb, Sc, Se, Ta, Te, Th, Ti, U, V, W, Yb and Zr.

This species was able to detect the mineralisation with assays for As and REE (Figure 5.18) where the elevated assays were consistent and defined a zone 200 m wide. Due to the restricted distribution there were no plants sampled to the north of the prospect, and those that had high values to the south (Figure 5.19) were similar to those obtained from the snappy gum results. This included elements known from the other results to be linked to mineralisation such as S and Zn. This suggests that these plants have a similar root system. Those elements designated as having no distinct pattern (Figure 5.20) may relate to the lack of samples away from mineralisation.

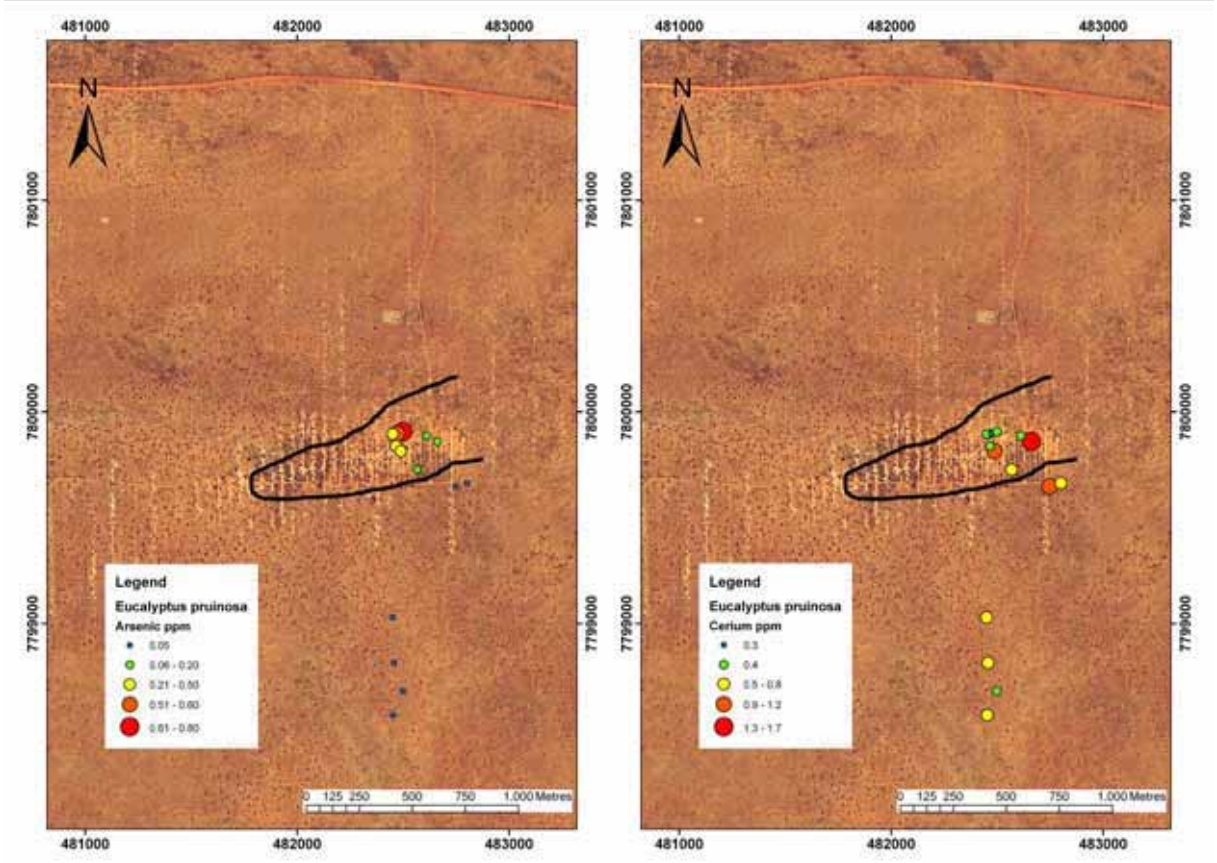

Figure 5.18: Plots of As and Ce concentration for *Eucalyptus pruinosa* overlying the orthophoto of the Coyote Prospect. The Au ore body, projected from 200 m depth, is within the area delineated by the black line.

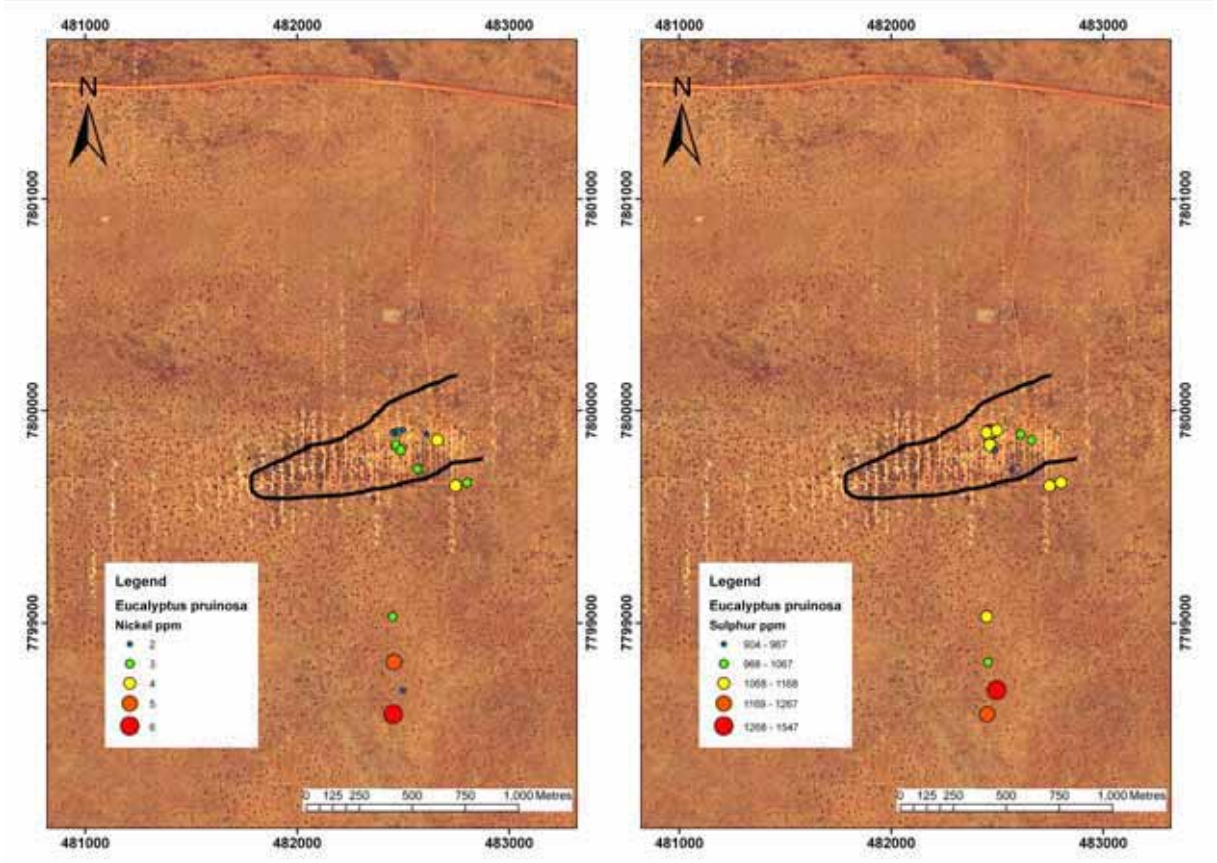

Figure 5.19: Plots of Ni and S concentration for *Eucalyptus pruinosa* overlying the orthophoto of the Coyote Prospect. The Au ore body, projected from 200 m depth, is within the area delineated by the black line.

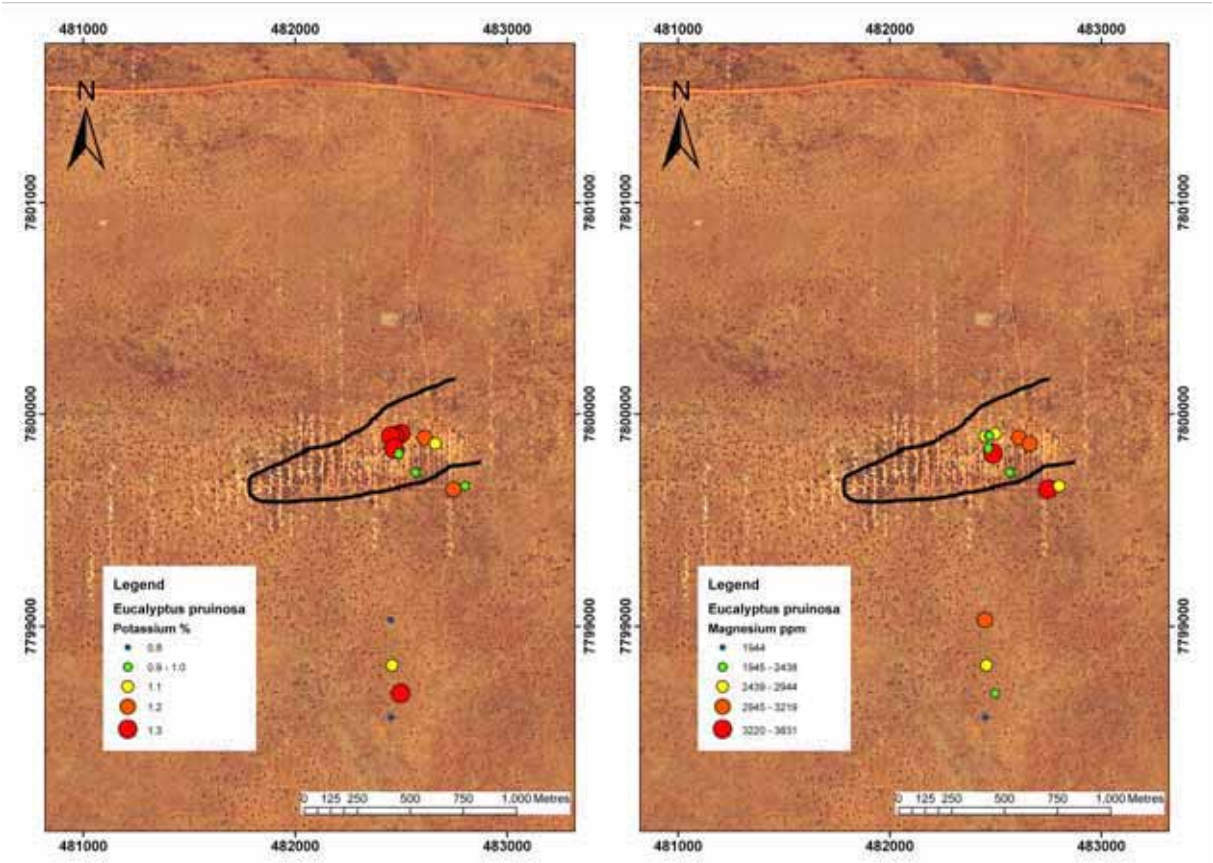

Figure 5.20: Plots of K and Mg concentration for *Eucalyptus pruinosa* overlying the orthophoto of the Coyote Prospect. The Au ore body, projected from 200 m depth, is within the area delineated by the black line.

Discussion

The silver box accurately delineated the mineralisation with a multi-element suite. Its restricted distribution however, limited its usefulness across the entire prospect.

5.1.7 Species Differences

Probability plots were created within the program IoGas for each element, using different colours for each different species from the Coyote survey. Several of the key results are shown in Figures 5.21-5.24. The X axis is 'N score' which is the 'Z' score (the divergence of the result from the most probable one as a number of standard deviations) applied to a normal distribution, and the Y axis is the concentration of the element in question (in ppm for all except Au which is ppb) Soft spinifex leaves are shown to have the highest levels of contamination of all the plants, but all species showed similar levels of contamination, which was deemed insignificant (as indicated by Al concentrations, which were determined to be from detrital contamination by clay particles).

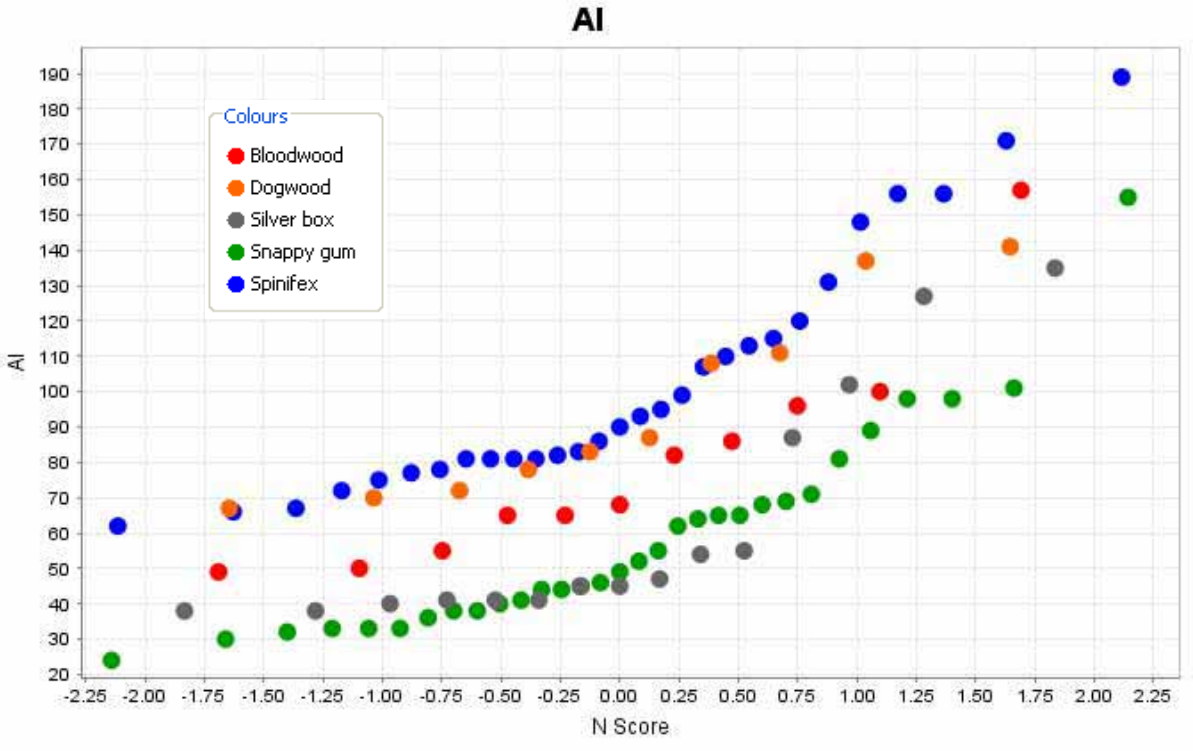

Figure 5.21: Al results split by species at the Coyote Prospect.

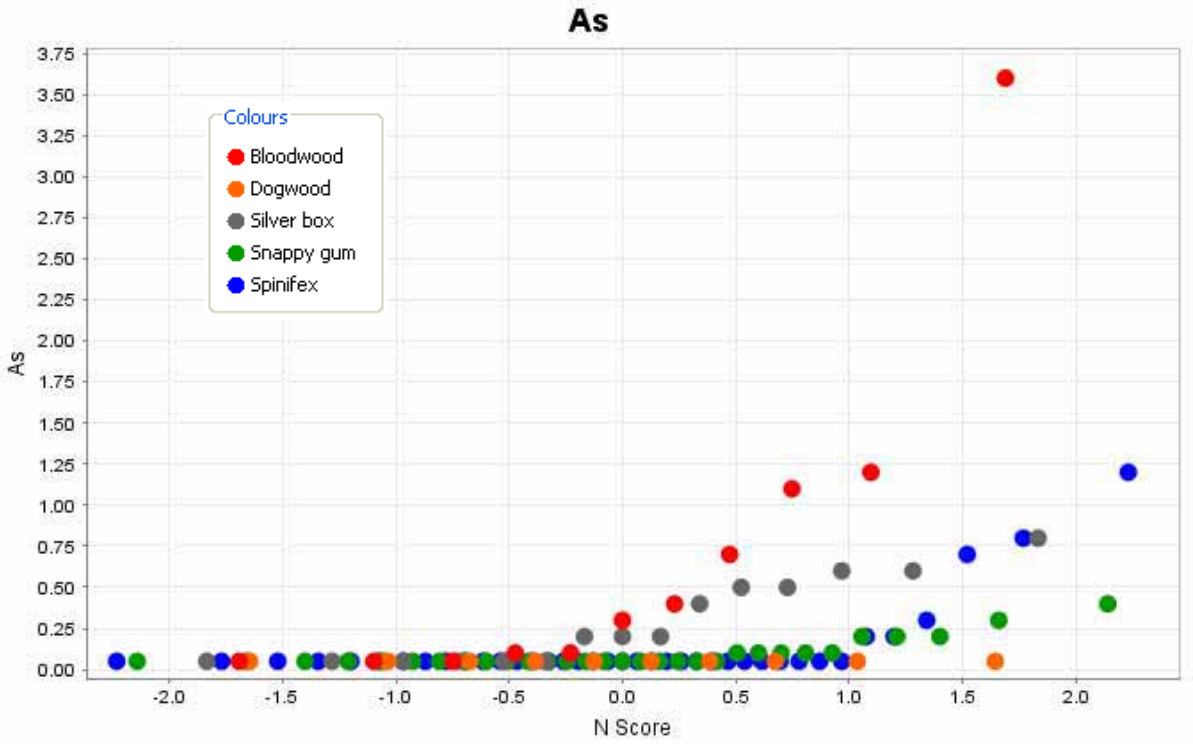

Figure 5.22: As results split by species at the Coyote Prospect.

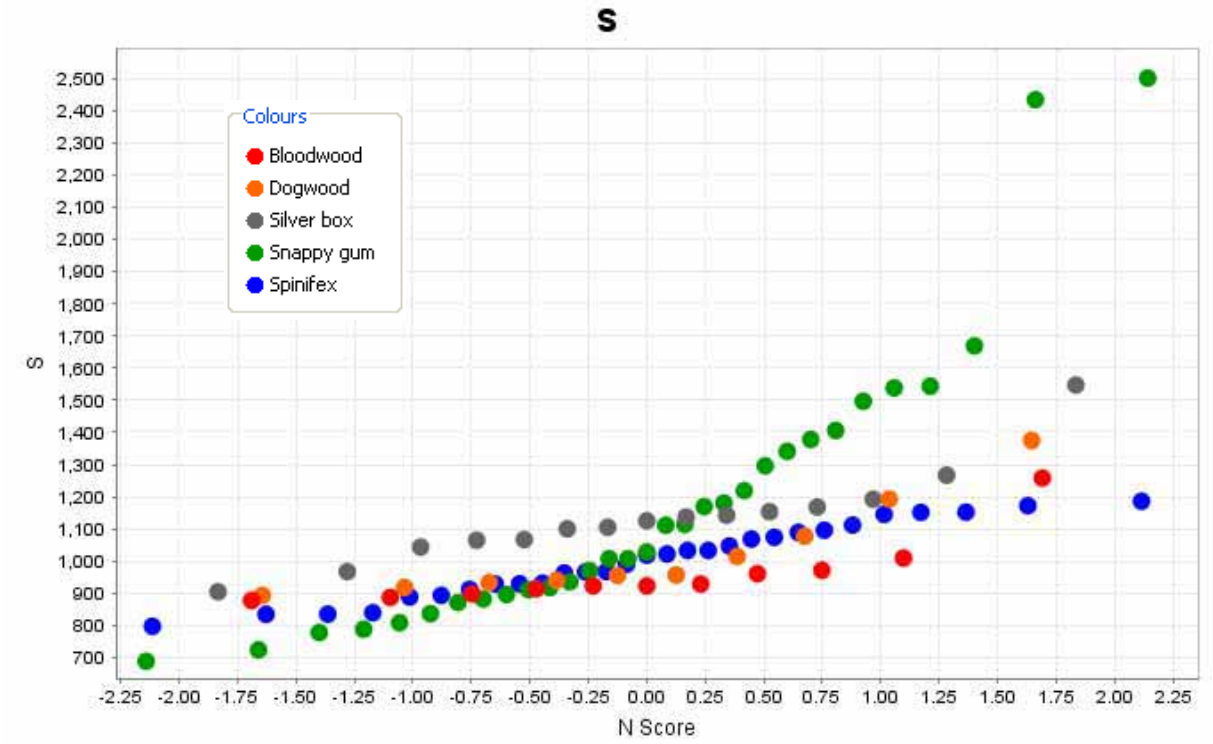

Figure 5.23: S results split by species at the Coyote Prospect.

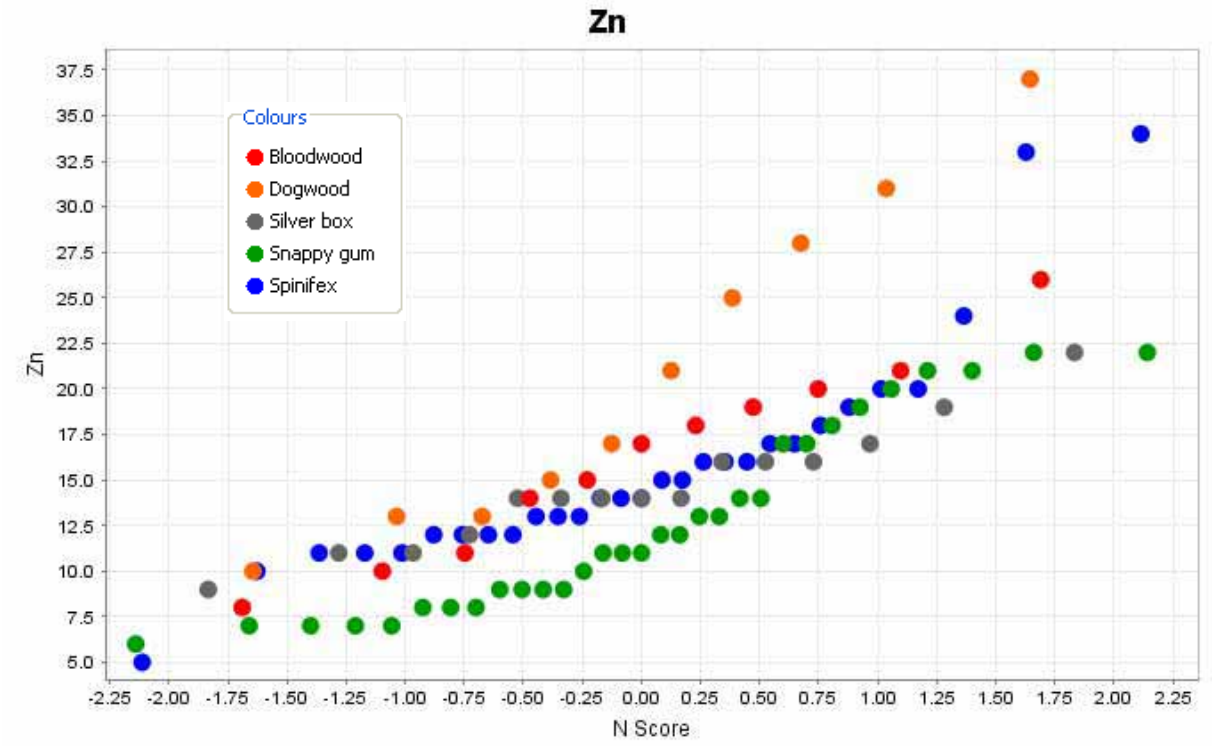

Figure 5.24: Zn results split by species at the Coyote Prospect.

Elements that are considered to be taken up by passive mechanisms (As and Au, Figure 5.22) appear to be relatively consistent between species where there is a large anomaly to background contrast. More essential elements such as S and Zn (Figures 5.23 and 5.24) have a more distinct spread (an order of magnitude difference between lowest and highest values) than the non-essentials but there is still a strong background to anomaly contrast. It is only the magnitude of this contrast which changes. The implications of this are that each of the species growing over the mineralisation are able to represent a strong background to anomaly

contrast, however, if several species were within a single data set then spurious anomalies would be generated due to the different base level for each element within each species.

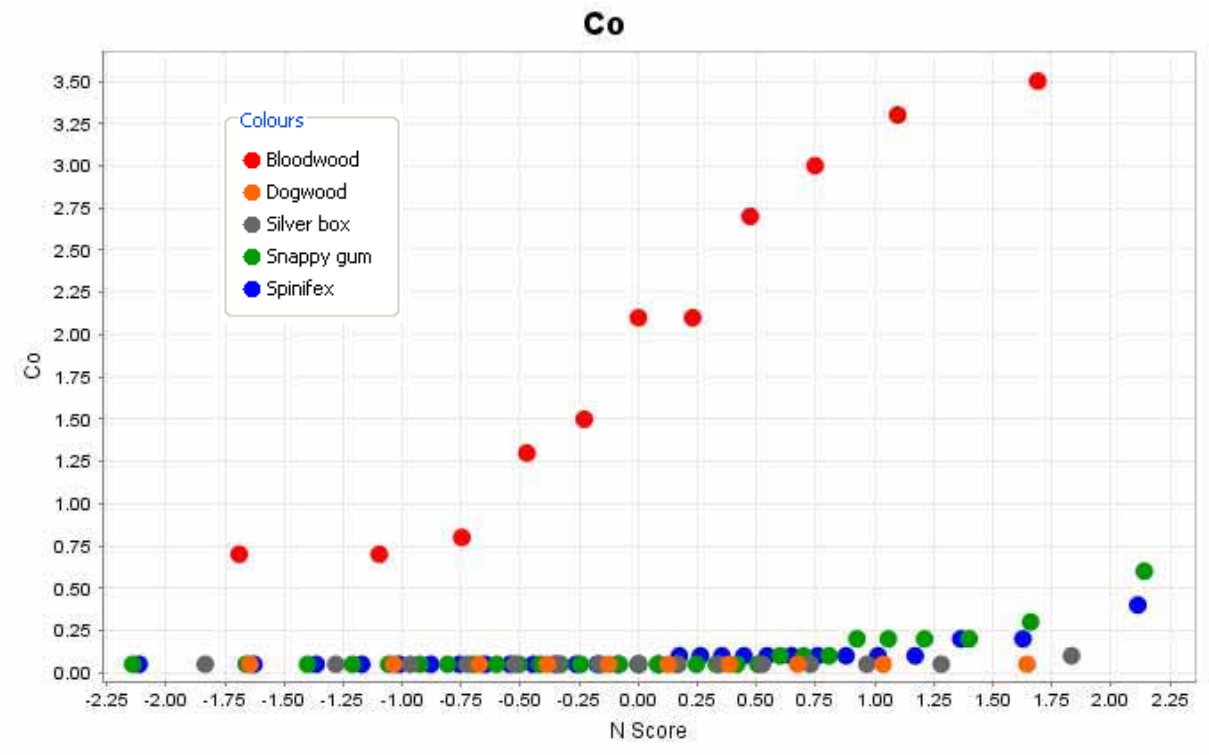

Figure 5.25: Co results split by species at the Coyote Prospect.

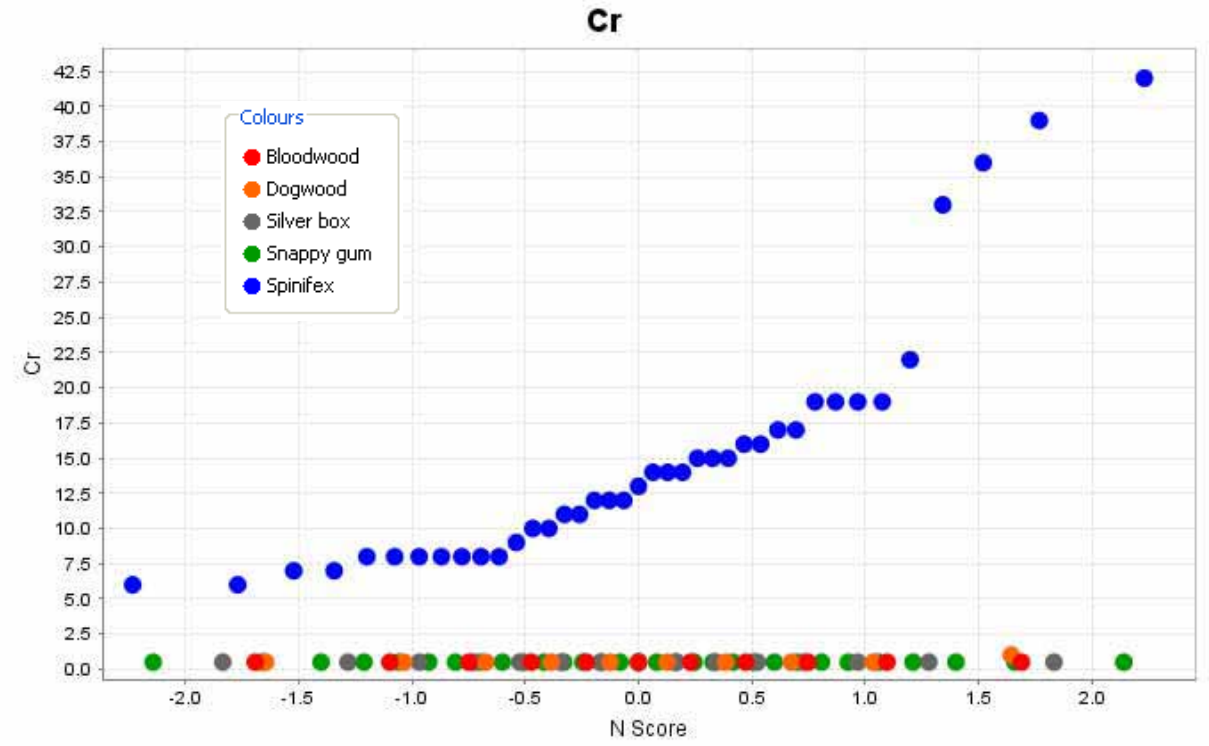

Figure 5.26: Cr results split by species at the Coyote Prospect.

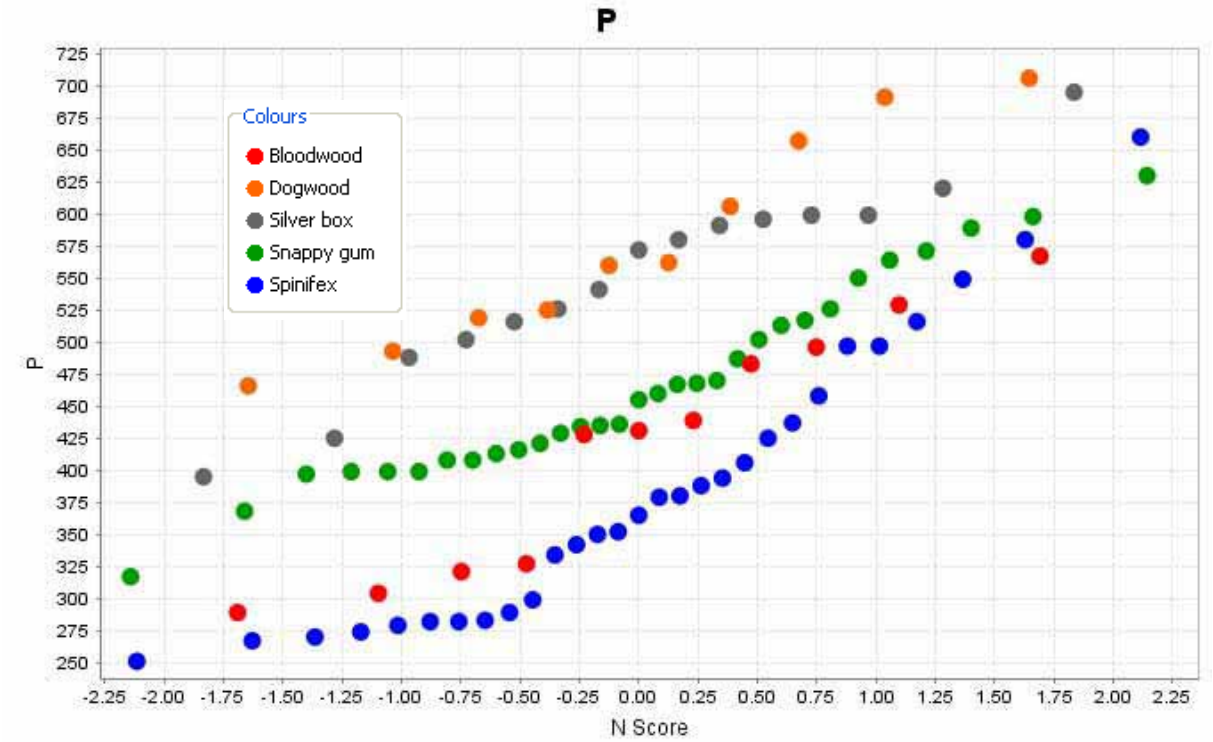

Figure 5.27: P results split by species at the Coyote Prospect.

Several of the elements were particularly different with respect to species (Figures 5.25-5.27). This shows that *Corymbia opaca* is able to uptake significantly higher Co than the other species, the reason for this is unknown (Figure 5.25). *Triodia pungens* can accumulate Cr up to 42 ppm which is over an order of magnitude greater than any other species (Figure 5.26).

Phosphorous is of particular interest in Australian environments because it is known for being a limiting factor in Australian soils. This is the reason why in agricultural areas large amounts of super-phosphates must be used to grow crops. Due to this each plant species has a very similar range of P values with some minor differences the reason for this is that since there is a limited amount of phosphorous Australian plants are adapted to using small amounts in their structure and over time this would have led to similar levels for each plant as they don't out-compete each other in this environment (Figure 5.27).

5.1.8 Elemental correlations

Correlation coefficients were calculated using Excel 2003 (Data analysis tools, correlation) for all the vegetation samples and for each individual species shown visually (X-Y plots corresponding to high calculated correlation values) in Figures 5.28-5.31. The cut-off value for strong positive correlation was values above 0.75 (75% correlation), and for a strong negative correlation was values below -0.75 (-75% correlation). The general trends for each species were very similar. All the REE correlated very well with each other (Figure 5.30), which is to be expected as the main source of REE is monazite which has all the elements in fixed concentrations. Ca and Sr correlate strongly (0.80, Figure 5.29), often with negative K (-0.88 for desert bloodwood), which matches with most geochemical signatures. P does not correlate with anything because it is limiting in this environment, so the maximum is always reached but not for the other elements.

Other elemental correlations can be used to provide information about the site. Soft spinifex showed correlations between As and the REE (Ce – 0.84, La – 0.97 and Sm – 0.80), but not

with the contaminant elements (Al, Fe, Hf, Zr), which indicates the monazites (source of REE) are from bedrock monazites (or other primary minerals) rather than transported (detrital), since the As is linked to the bedrock mineralisation.

The desert bloodwood shows correlation between As and S (0.80), which is most likely sourced from primary sulphides, or secondary sulphates directly related to the primary mineralisation.

The other important correlations shown in the tables below are the high correlation between the same element with the two different methods (INAA and ICP) (Figure 5.28, Ba - 0.95). This indicates that both techniques were showing the same concentrations from different parts of the same sample. This means that the samples were correctly homogenised before splitting, and that both methods were equivalent in releasing all Ba into solution. There was a strong correlation between Fe and Cr only within the spinifex results (Figure 5.31), which shows that spinifex does not have a barrier to Cr uptake as do the other species, and that the detection limit for Cr in this case was too high for accurate detection of the other species.

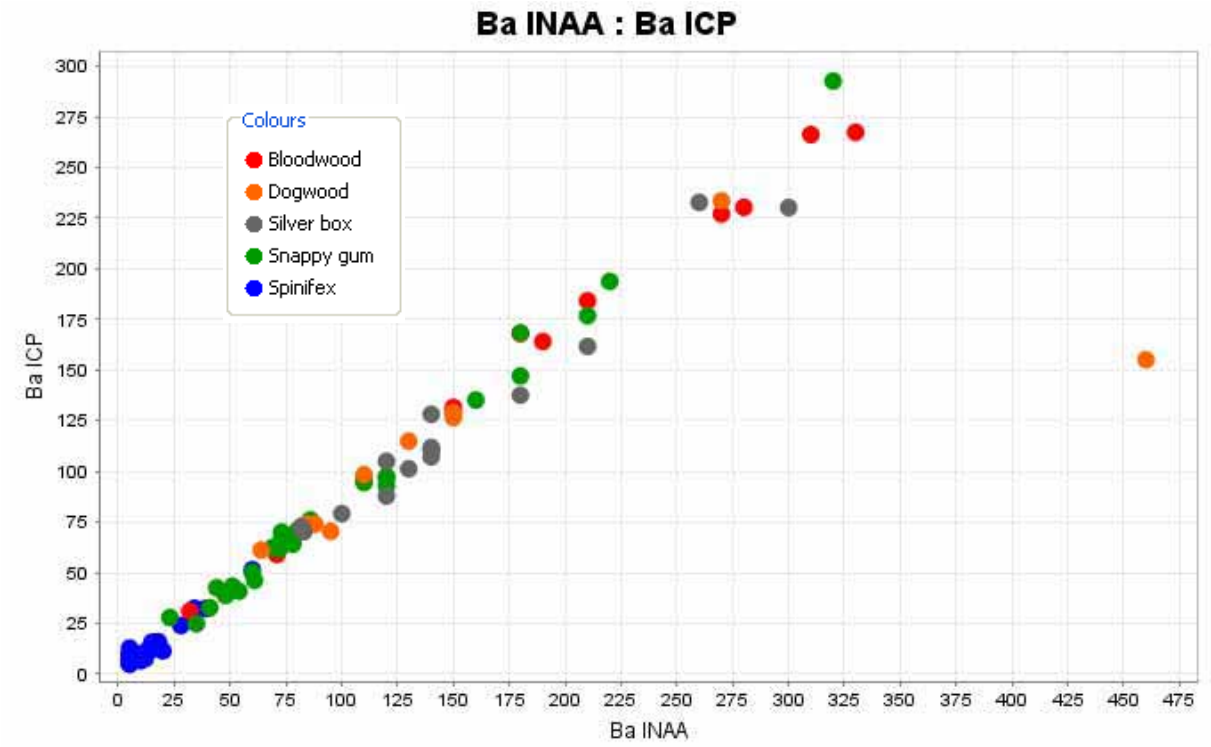

Figure 5.28: Ba INAA and Ba ICP visual correlation split by species at the Coyote Prospect.

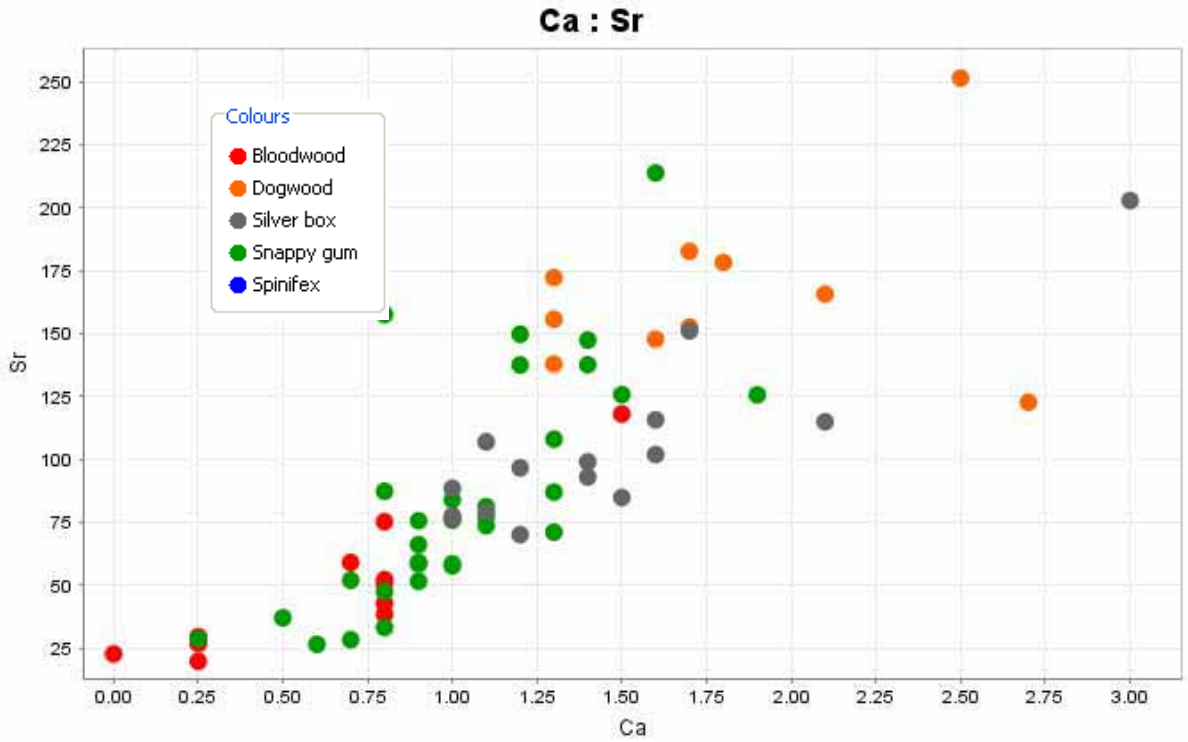

Figure 5.29: Ca and Sr visual correlation split by species at the Coyote Prospect.

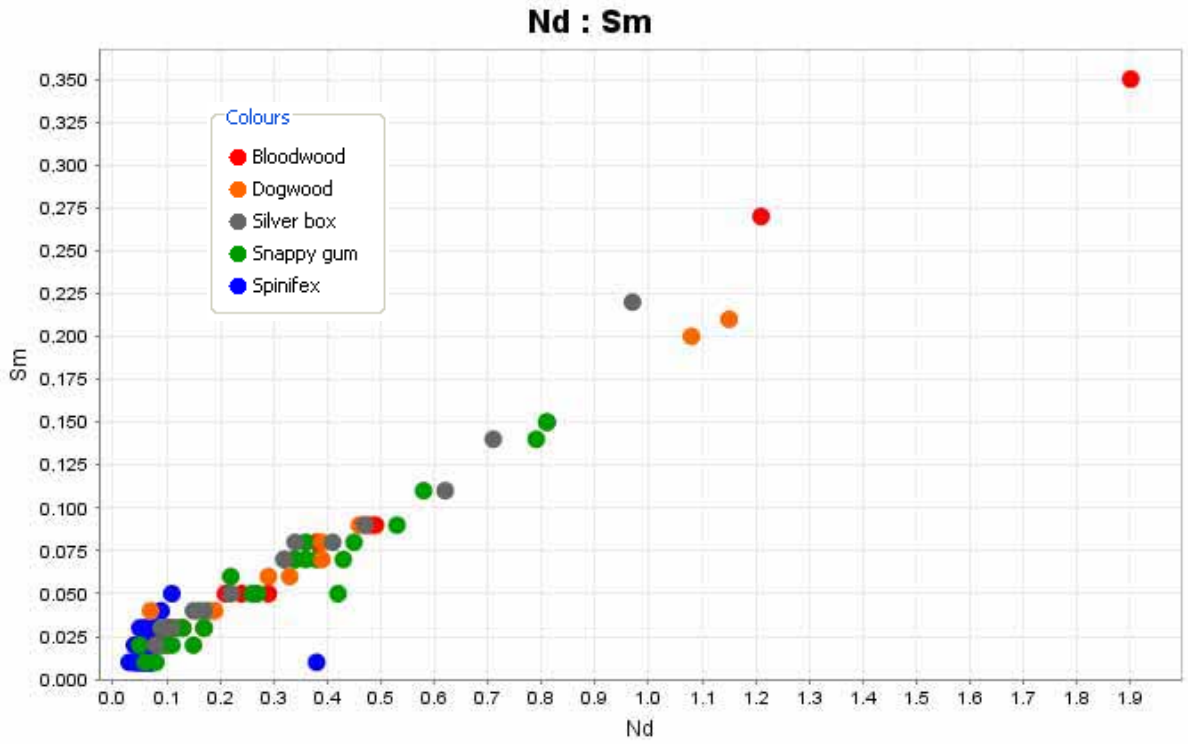

Figure 5.30: Nd and Sm visual correlation split by species at the Coyote Prospect.

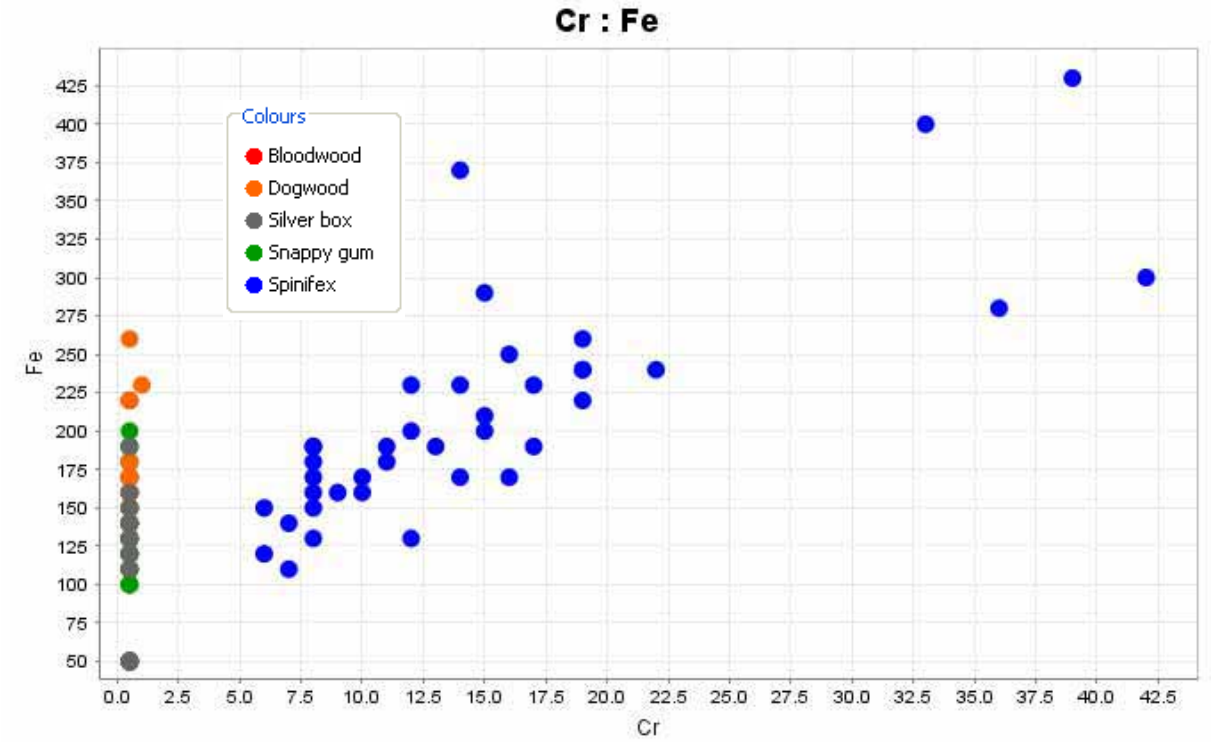

Figure 5.31: Cr and Fe visual correlation split by species at the Coyote Prospect.

5.2 Biogeochemistry of the Larranganni Prospects

5.2.1 Site specific methods

Due to time constraints only snappy gum leaves were collected from this site. This was due to ease of sampling and uniform species coverage. Thirty snappy gum samples were collected along a transect across the Sandpiper and Kookaburra mineralisation sites and extending into background sites. Three snappy gum samples were also taken from each of the other prospects visited in the Larranganni area (e.g. Osprey, Hawk, Pelican, Sandpiper, Kookaburra, and Cuckoo). These were each close to, or over mineralisation. The topography changes across the transect were less than 5 m from one end to the other. The Kookaburra mineralisation was cropping out whereas the other sites were under <1 m of transported cover.

5.2.2 *Eucalyptus brevifolia* (snappy gum)

The snappy gum results show 3 distinct elemental patterns from the data:

1. Elements that are elevated over the Sandpiper-Kookaburra mineralisation (Al, As, Au, Br, Cu, Mn, Mo, S and Zn) (Figures 5.32),
2. Elements elevated to the east of the transect (Ba and Ca); and,
3. Elements elevated over one of the outlier sites (Co, Fe, La, Ni, Pb and U) (Figures 5.33and 5.34).

There are also elements that have irregular chemical properties (Ce, K, Mg, Nd, P, Rb, Sm, Sn and Sr). Elements that were below analytical detection limit were Ag, Be, Bi, Cd, Cr, Cs, Eu, Ga, Hf, In, Ir, Lu, Na, Nb, Sb, Sc, Se, Ta, Te, Th, Ti, V, W, Yb and Zr.

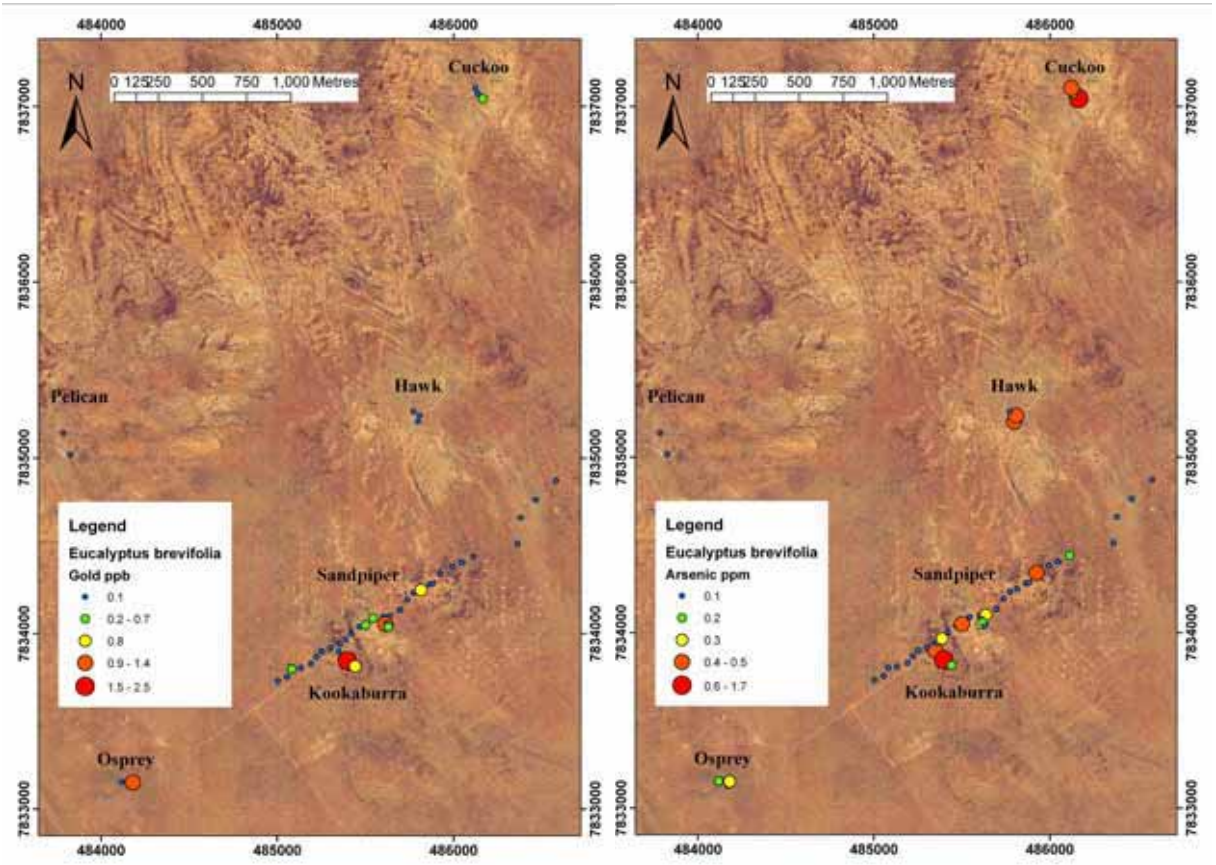

Figure 5.32: Plots of Au and As concentration for *Eucalyptus brevifolia* leaves overlying the orthophoto of the Larranganni Prospects

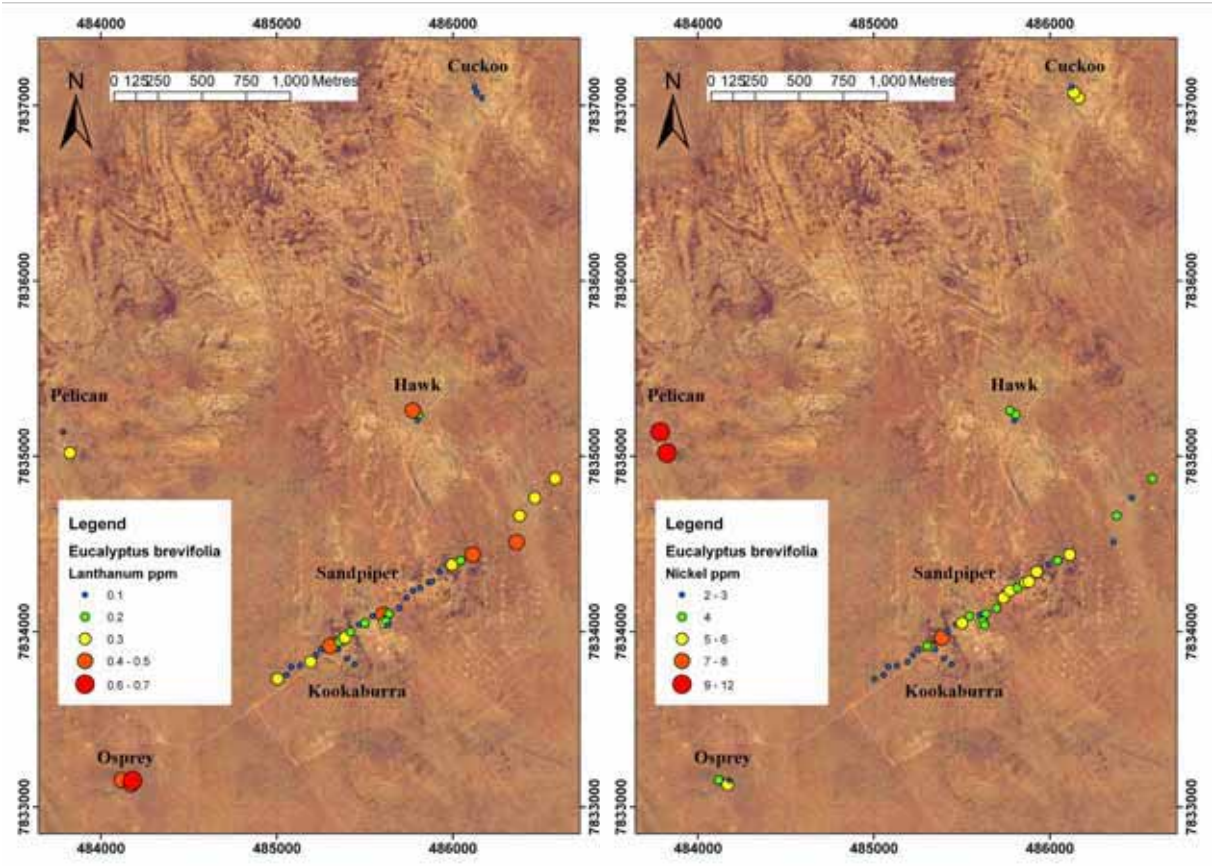

Figure 5.33: Plots of La and Ni concentration for *Eucalyptus brevifolia* leaves overlying the orthophoto of the Larranganni Prospects

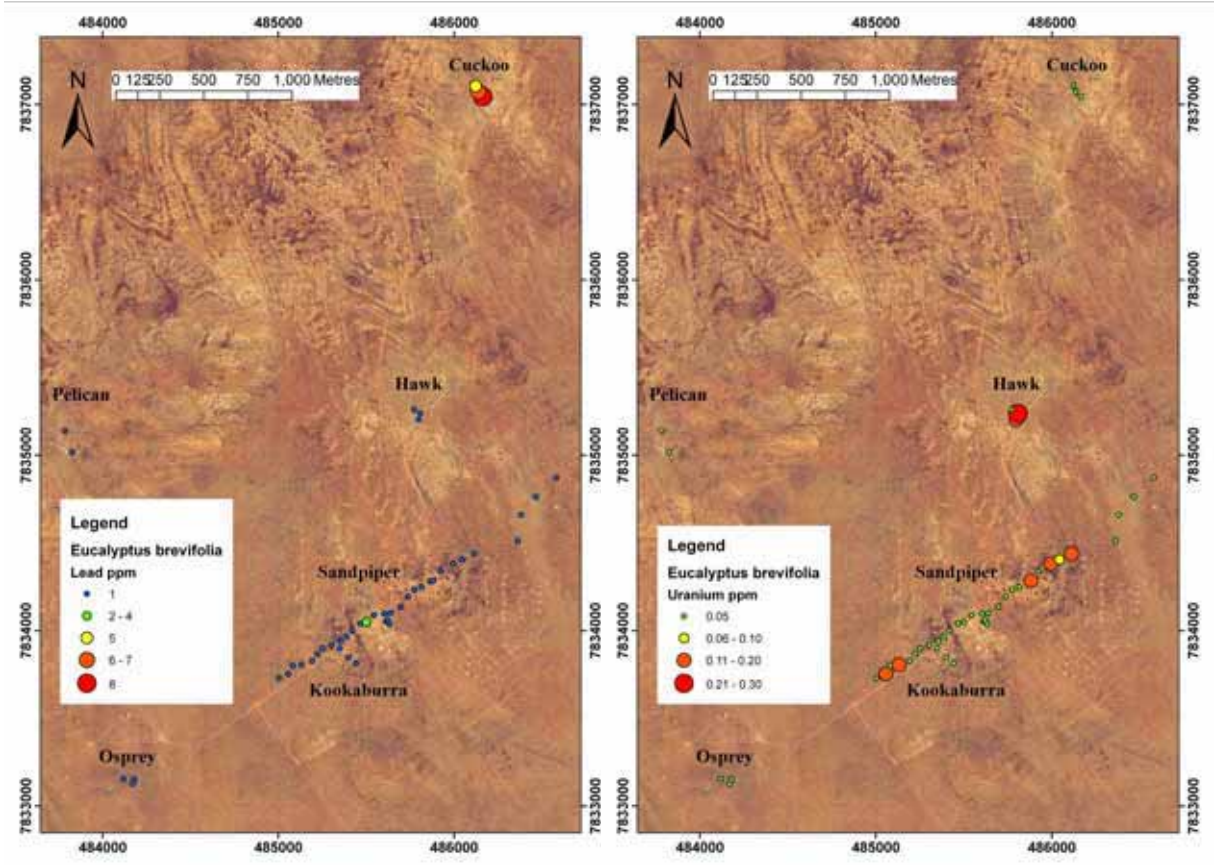

Figure 5.34: Plots of Pb and U concentration for *Eucalyptus brevifolia* leaves overlying the orthophoto of the Larranganni Prospects

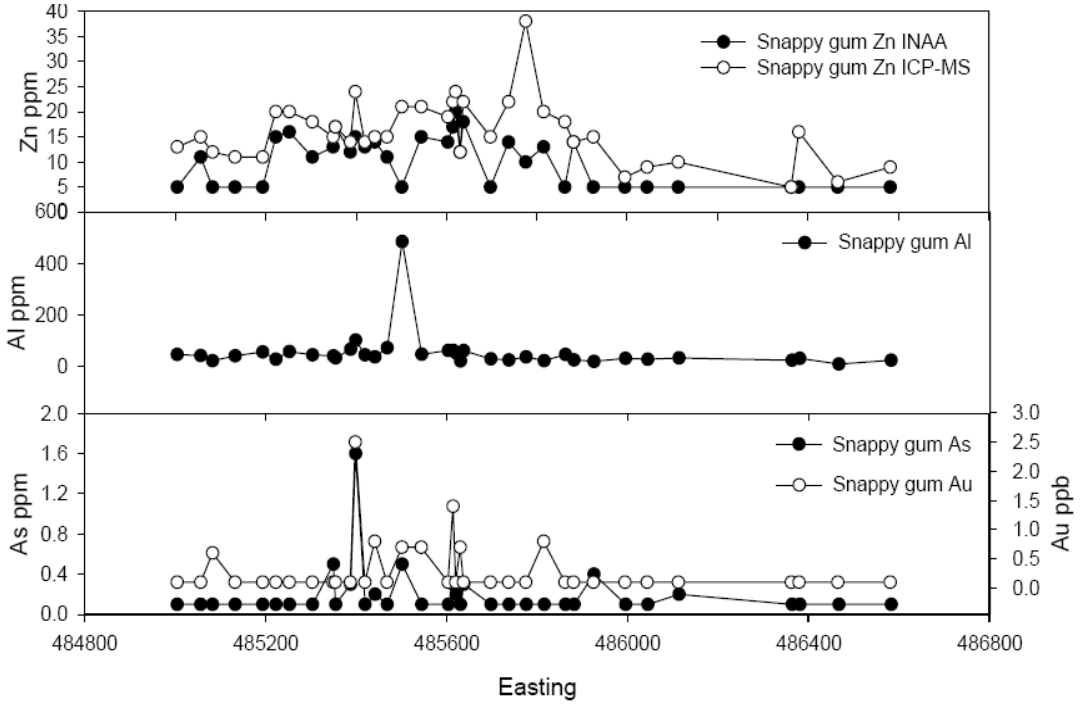

Figure 5.35: Elemental plots of *Eucalyptus brevifolia* across the Kookaburra-Sandpiper transect

The interpretations of the snappy gum results at this site are generally predictable. Since the plants were growing directly over mineralised bedrock with minimal cover, elements associated with the ore bodies were transferred to the trees directly above (Au, As, Zn and S, Figure 5.35). There are several reasons that the other sites were not as clearly detected within the Au results: the nuggetty nature of Au means that the Au could have been missed, the samples could have not been directly over the mineralisation as was the case with the Pelican

prospect, also the other sites were much smaller than the Kookaburra-Sandpiper prospects which could have presented a less viable target. There was minimal dispersion and contamination at the site due to the lack of transported materials at the site. The Al results highlight that there is very little dust contamination on these samples, as the natural Al concentrations would be below detection limit. According to the geological maps available, the Larranganni area is all within the Bald Hill formation, however, M. Green (pers. comm. 2005) showed that around the Pelican area was made up of mafic dykes within the Bald Hill formation. This corresponds with the high concentration of Ni over this site compared to the others.

5.2.3 Elemental correlations

There were very few correlations found between the elements at the Larranganni Prospects (shown visually in Figures 5.36 and 5.37). The usual correlations of the REE to each other were there (Figure 5.37) and the Ba correlation between the two techniques (0.99, Figure 5.36), and a correlation between Co and Mo (0.78) that was really a reflection of not many detectable points. There was, however, no correlation with either Fe or Al with any of the pathfinder elements which indicates low contamination within the snappy gum samples and the anomalies generated would be from the source and not drill spoil.

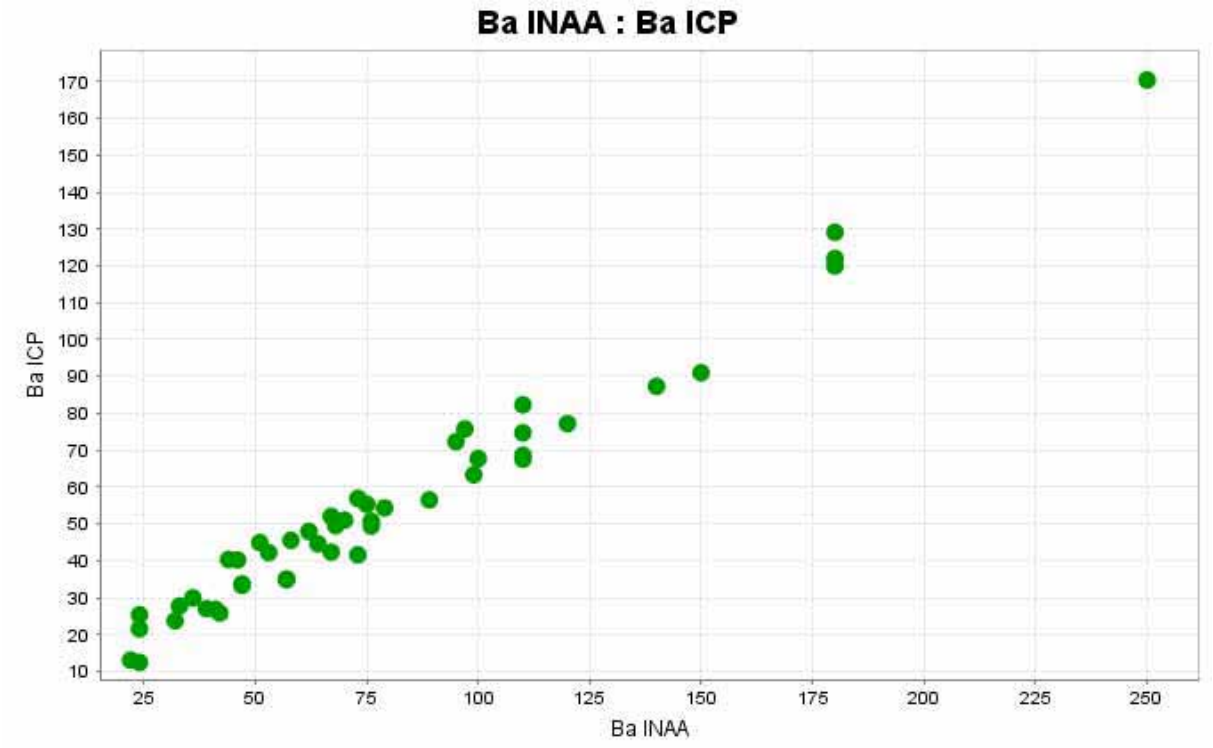

Figure 5.36: Ba INAA and Ba ICP visual correlation at the Larranganni Prospects.

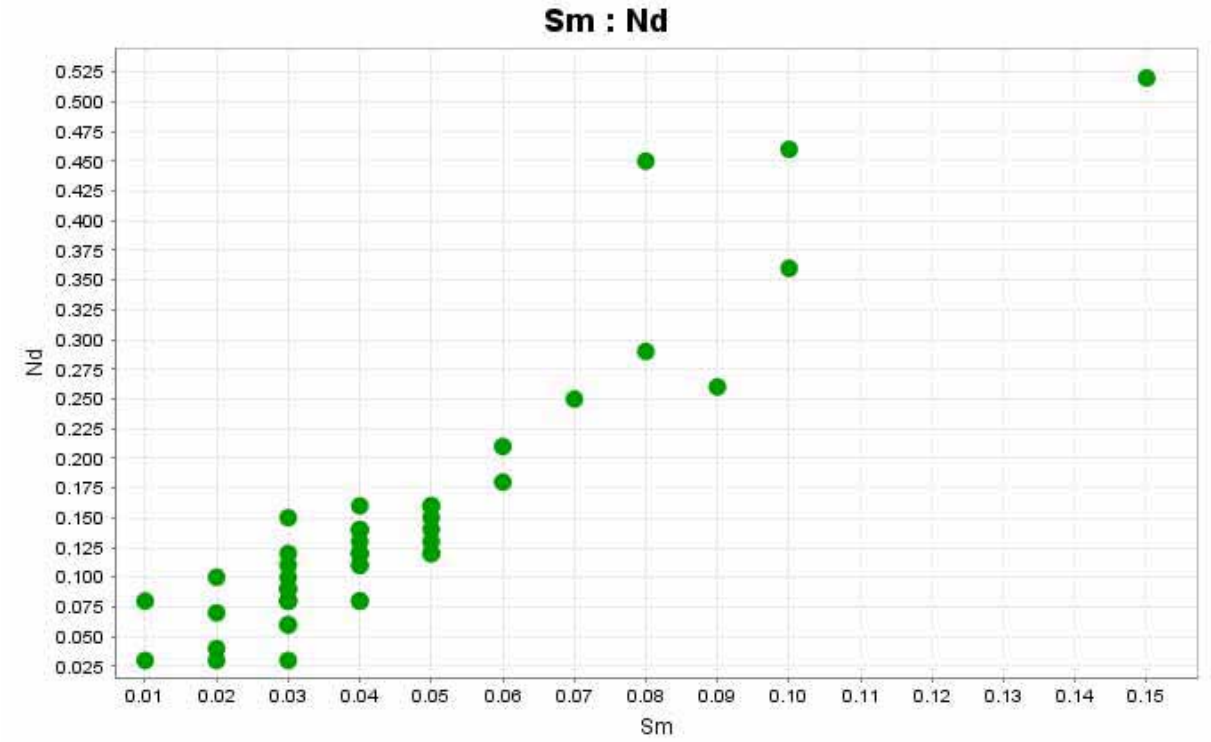

Figure 5.37: Sm and Nd visual correlation at the Larranganni Prospects.

5.3 Biogeochemistry of the Hyperion Prospect

5.3.1 Site specific methods

The study at the Hyperion Au Prospect was designed to test a 'blind' target where there has been less exploration activity than at other sites. This ended up being complicated by the previous exploration information (drill logs, geochemistry, geological information, remotely sensed imagery) being lost when members of the exploration team of Newmont Asia Pacific left the company.

Samples of snappy gum and spinifex were taken from exposed bedrock (unnamed monzogranite) in the Stony Ridge area of the Jasper Hills (to determine background concentrations) and dominant plant species were taken along a 1 km transect over the Hyperion Prospect. The sample spacing was approximately 100 m along the east-west transect at Hyperion. The sample sites and species sampled can be seen in Figures 5.38 and 5.39. At this site an extended elemental suite of 66 elements was provided by Genalysis, Perth. The transported cover thickness over the Hyperion transect was approximately 7 m determined from drillspoil piles in the area (Worrall, 2007, pers. comm.). Each elemental plot is overlying the Satellite Pour l'Observation de la Terre (SPOT) imagery, as there was no orthophoto to use.

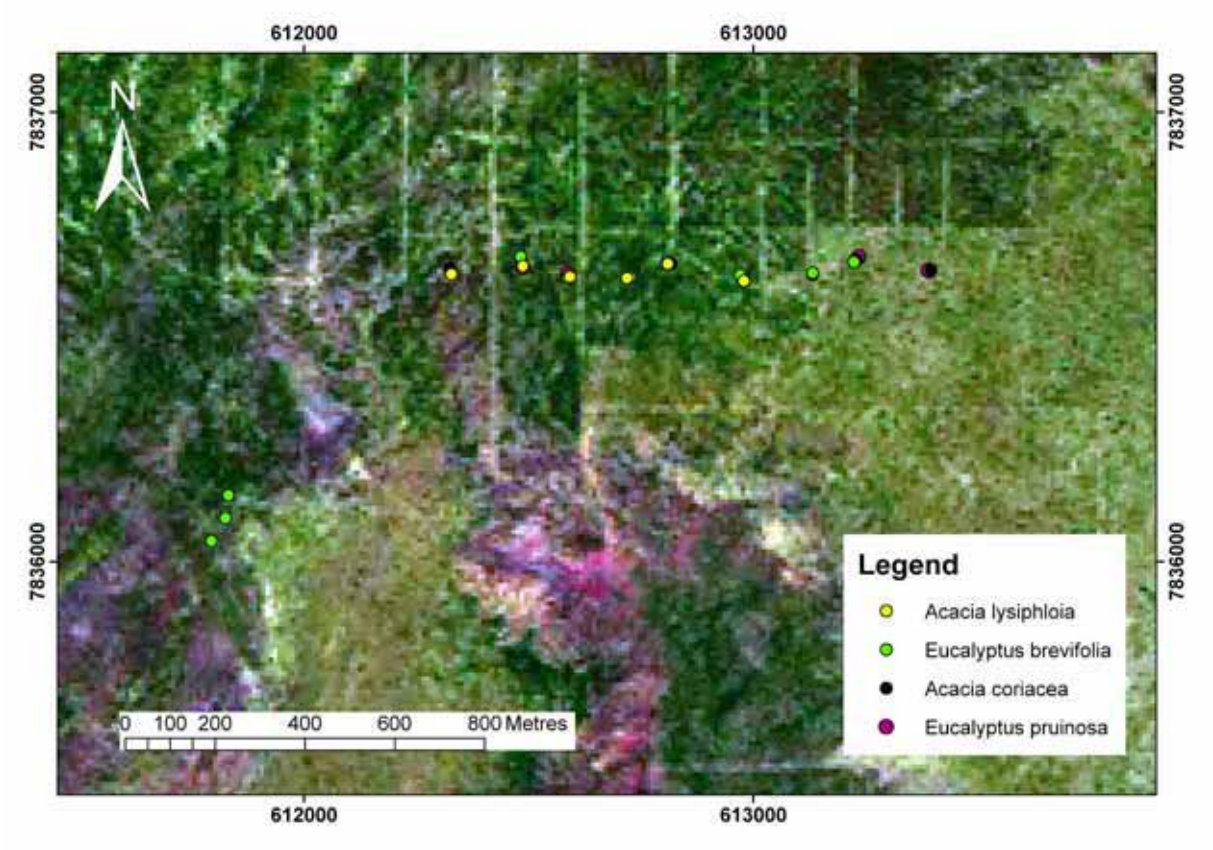

Figure 5.38: Vegetation distribution across the Hyperion Prospect overlying the SPOT imagery.

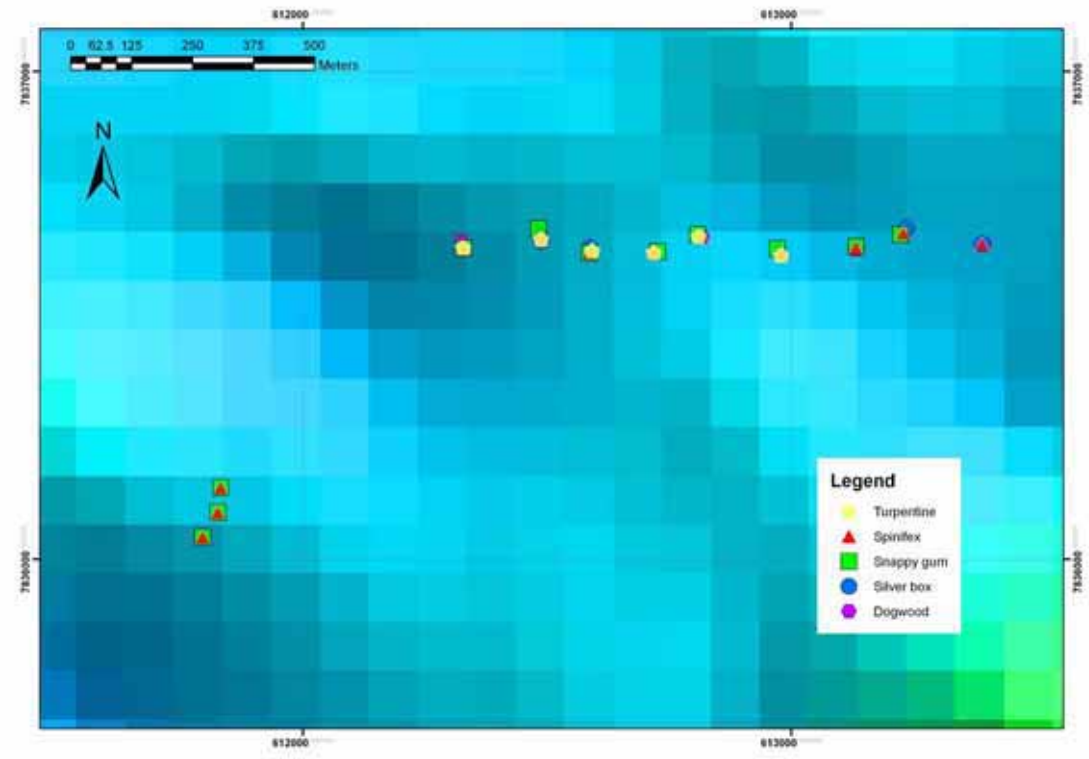

Figure 5.39: Vegetation distribution across the Hyperion Prospect overlying regional magnetics imagery

5.3.2 *Eucalyptus brevifolia* (snappy gum)

Snappy gum was abundant and widespread in this area and grew directly into the monzogranite as well as in the covered area of the Hyperion Prospect. The snappy gum results show 4 distinct elemental patterns from the data:

1. Elements that are elevated over bedrock (Ce, Co, Cs, Mo, Rb and U) (Figure 5.41);
2. Elements elevated to the east of the transect (As (and bedrock high), Ba, Br, Ca, Dy, Er, Eu, Gd, La, Lu, Nd, Pr, Sm, Sr, Th, Y and Yb) (Figure 5.42);
3. Elements elevated to the west of the transect (Mn); and,
4. Elements elevated to the centre of the transect (Au, B, Na and Ni).

There are also elements that are irregularly distributed (Al, Cu, Fe, K, Li, Mg, Ni, P, S and Zn). Elements that were below analytical detection limit were Ag, Be, Bi, Cd, Cr, Ga, Hf, Ho, In, Ir, Na, Nb, Pb, Re, Sb, Sc, Se, Sn, Ta, Tb, Te, Ti, Tl, Tm, V W and Zr.

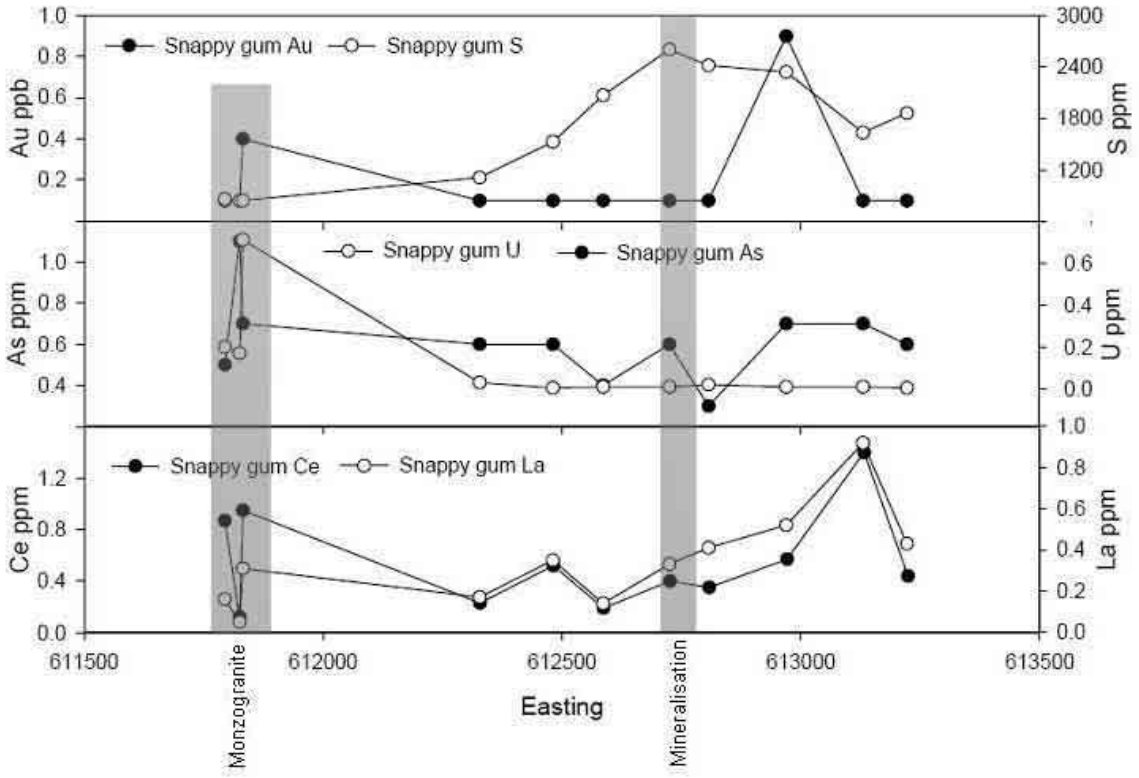

Figure 5.40: ***Eucalyptus brevifolia*** **elemental cross section across the Hyperion prospect**

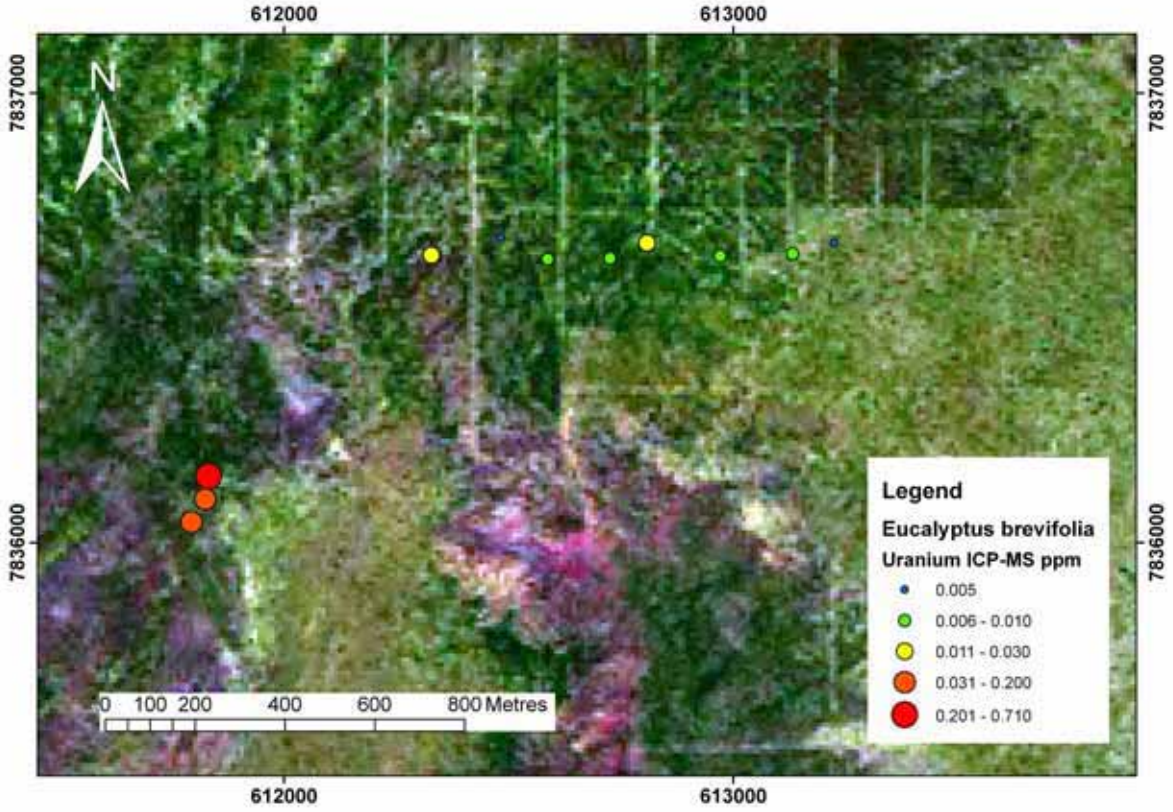

Figure 5.41: Plots of U (ICP-MS) concentration for *Eucalyptus brevifolia* overlying the SPOT of the Hyperion Prospect

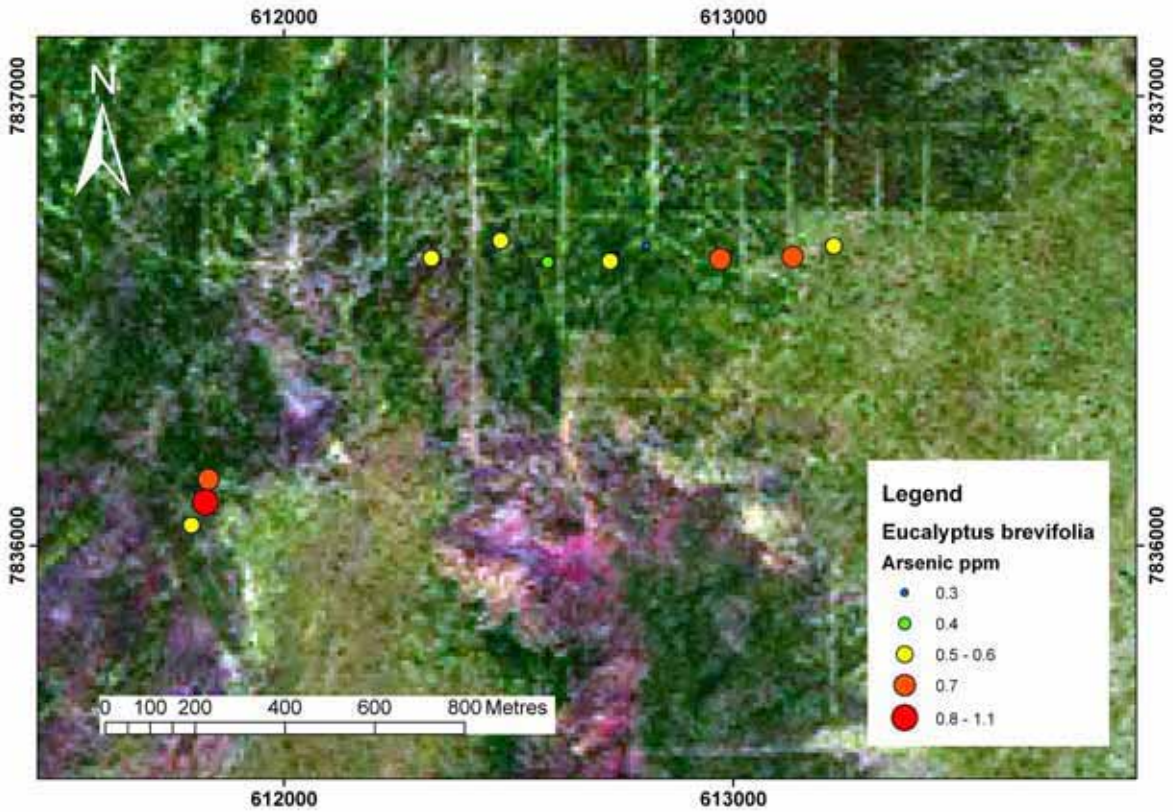

Figure 5.42: Plots of As concentration for *Eucalyptus brevifolia* overlying the SPOT of the Hyperion Prospect

Discussion
The elements that are elevated over the bedrock correspond to elements that are expected to be elevated in the bedrock (granite), and are not concentrated in the dispersed materials. Snappy gum trees in this case absorb these elements related to the amounts within the substrate geology rather than having any barrier or accumulation mechanisms in place. This is particularly important when using a species to explore for these metals.

Unfortunately there is very little background information for this area so the regional magnetics data was originally used as the spatial overlay for the geochemistry (Figure 5.39). This was chosen because it showed the most detail of the remotely sensed data provided, and also there is a distinct change in the magnetic intensity from the east to west of the transect. The midpoint of this change is where the mineralisation is thought to be hosted within a fault system. The implications of this are noted when there is a distinct change in the chemistry between the east and west halves of the transect, and in particular some elements, like Au, have a single point anomaly around that area. Recently the SPOT imagery was provided for this area providing greater detail about the materials in this area, and providing a context for the chemical results.

Gold is the best direct indicator for the mineralisation with As and the other elements dispersed to the east (REE) showing the influence of the transported cover and interactions with groundwater (Figure 5.40). However, the Au results are only a single point anomaly which cannot be considered without the multi-element suite to back it up. The results from Larranganni showed that directly over exposed mineralisation there is minor lateral dispersion, and at Coyote where there is more cover there is greater dispersion due to hydrogeochemical gradients. At Hyperion the cover thickness is intermediate, so there is some dispersion but it is of a smaller magnitude than at Coyote.

5.3.3 *Triodia pungens* (soft spinifex)

The spinifex results show 5 distinct elemental patterns:

1. Elements that are elevated over bedrock (Au, Co, Cr, Ni, Sc, Sm and Zn);
2. Elements elevated to the east of the transect (Gd, P and Sm);
3. Elements elevated to the west of the transect (B, Ce and Fe);
4. Elements elevated to the centre of the transect (Pr and U); and,
5. A double peak over the transect (Br, Ce, Dy, K, La, Mn, Na, Nd, Rb, S, Sr and Y).

There are also elements that are irregularly distributed (Al, As, Ba, Ca, Li, Mg and Zr). Elements that were below analytical detection limit were Ag, Be, Bi, Cd, Cs, Cu, Er, Eu, Ga, Hf, Ho, In, Ir, Lu, Mo, Nb, Pb, Re, Sb, Sn, Ta, Tb, Te, Th, Ti, Tl, Tm, V W and Yb.

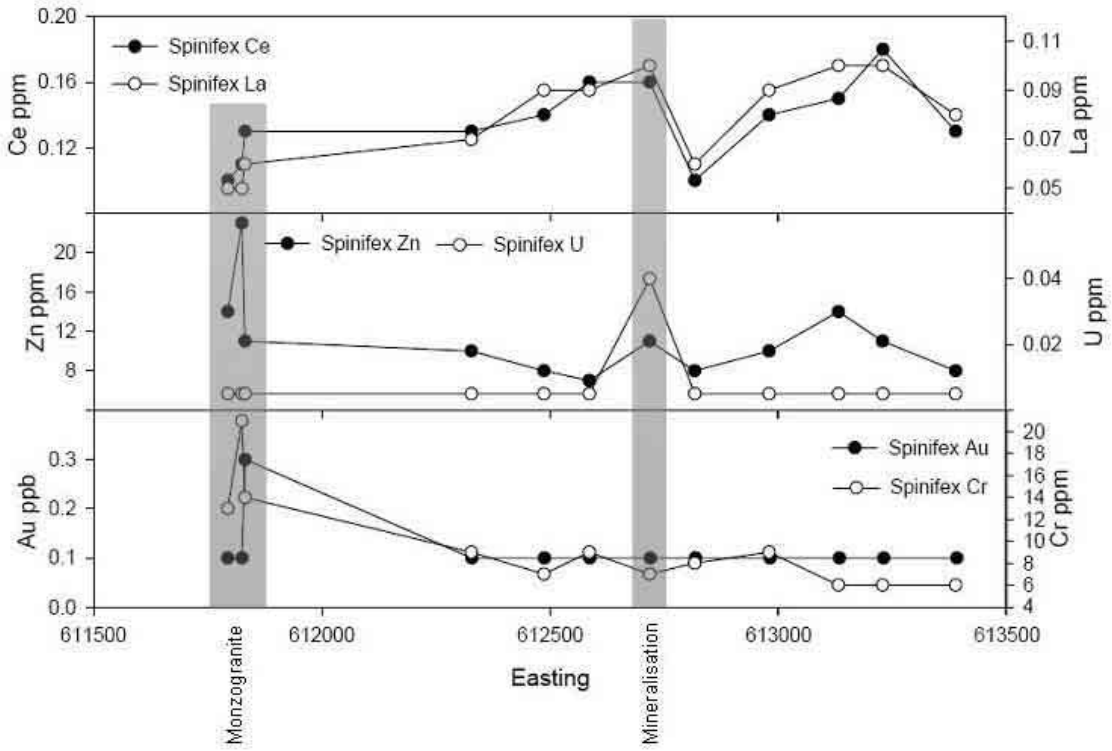

Figure 5.43: ***Triodia pungens*** **elemental cross section across the Hyperion prospect**

Discussion

In this location the soft spinifex has proven to be very variable in its chemistry. The only detectable Au value was over the bed rock and nothing along the transect (Figure 5.43). There were moderately elevated Zn assays to the east, corresponding with that in the snappy gum, but not as strong.

The only detectable point within the U results is close to the single point Au anomaly of the snappy gum rather than in the bedrock. Since the bedrock is granite, which contains a significant amount of U, spinifex must be unable to accumulate this element directly from the rock, so it either has a barrier mechanism for U, or the U must be in a more bio-available form than in the granite.

5.3.4 *Acacia coriacea ssp. sericophylla* (dogwood)

Unfortunately dogwood did not colonise the Stony Ridge area and so was only sampled along the Hyperion transect. The dogwood results show 3 distinct elemental patterns:

1. elements elevated to the east of the transect (Ce, Cs, Cu, Dy, Er, Eu, Fe, Gd, Ho, La, Li, Lu, Mn, Nd, P, Pr, S, Sm, Tl, Y, Yb and Zn);
2. Elements elevated to the west of the transect (K); and,
3. Elements elevated in the centre of the transect (Al, As, B, Ca, Mg, Mo and Ni).

There are also elements that are irregularly distributed (Ba, Br, Na, Rb, Sr and Tb). Elements that were below analytical detection limit were Ag, Au, Be, Bi, Cd, Co, Cr, Ga, Hf, In, Ir, Nb, Pb, Re, Sb, Sc, Se, Sn, Ta, Te, Th, Ti, Tm, U, V W and Zr.

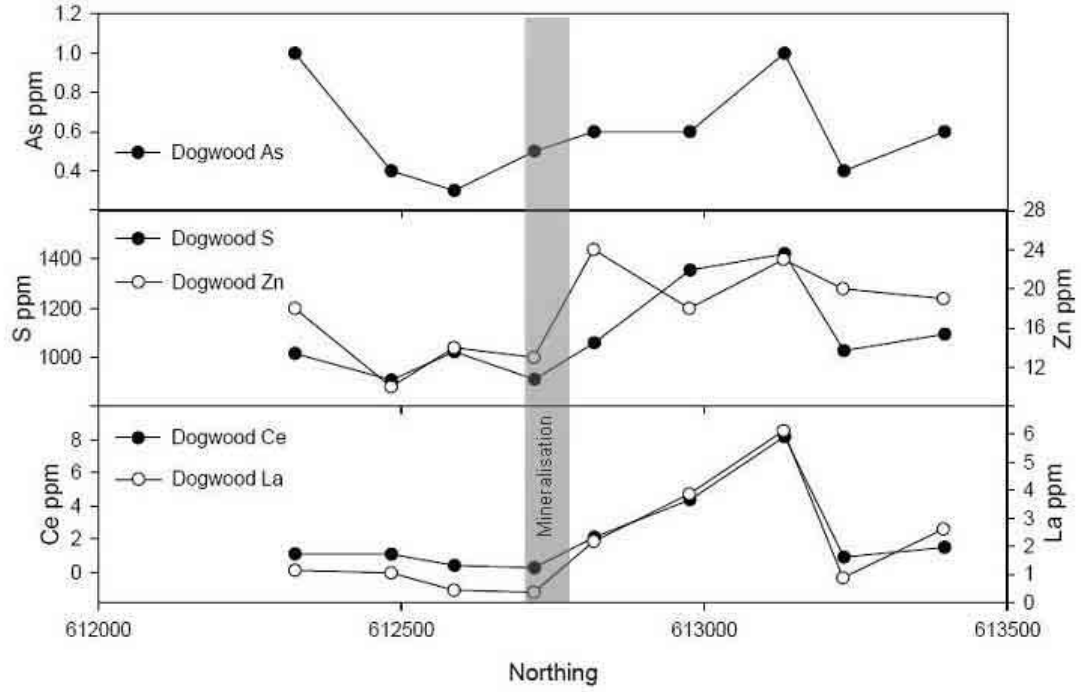

Figure 5.44: ***Acacia coriacea*** **elemental cross section across the Hyperion prospect**

Discussion

The assay results for dogwood were significant because of the large number of elements showing the same spatial patterns (Figure 5.44). All the rare earth elements assayed showed extremely high values compared to all the other plants sampled. The REE, Zn, S, As showed elevated assay values to the east of centre of the transect decreasing in value to the east. This correlates well with the snappy gum biogeochemistry. Hence, *Acacia coriacea* is able to provide a dispersed geochemical halo within a multi-element suite, however, whether this halo relates to an ore body, ground water dispersion, surficial processes or lithogeochemical differences, is difficult to determine without further knowledge about the underlying geology and chemistry of the ore body..

The higher than expected values of REE within the dogwood chemistry and the extended suite of elements meant that plots of the REE concentrations normalised to chondrite chemical compositions could be generated (Figure 5.45). This plot showed a pronounced negative Ce anomaly and a negative Eu anomaly. The Ce anomaly is normally associated with Ce being absorbed onto Fe-oxides and hydroxides hence being unavailable for uptake. This indicates that the Ce must be in the 4+ form (which is more readily adsorbed) rather than 3+ which is consistent with an oxidising environment. A negative Eu anomaly is created by Eu^{2+} being unavailable for uptake, since the other form of Eu is 3+ then this indicates reducing conditions

in the environment. This contradicts the Ce result, therefore one of them must be incorrect. Negative Eu anomalies however, are normal for most upper crustal rocks younger than the Proterozoic, with the main sources being felsic granites and sediments derived from them (Gao & Wedepohl 1995). Therefore, the Ce anomaly should reflect the current groundwater/environmental redox conditions and the Eu anomaly should reflect either the surrounding granite being younger than Proterozoic, the transported materials containing REE sourced from depleted mantle sources, or that the sediments over Hyperion were formed under reducing conditions. Unfortunately without any of the background geology or geochemistry for the site it is difficult to further constrain these possibilities.

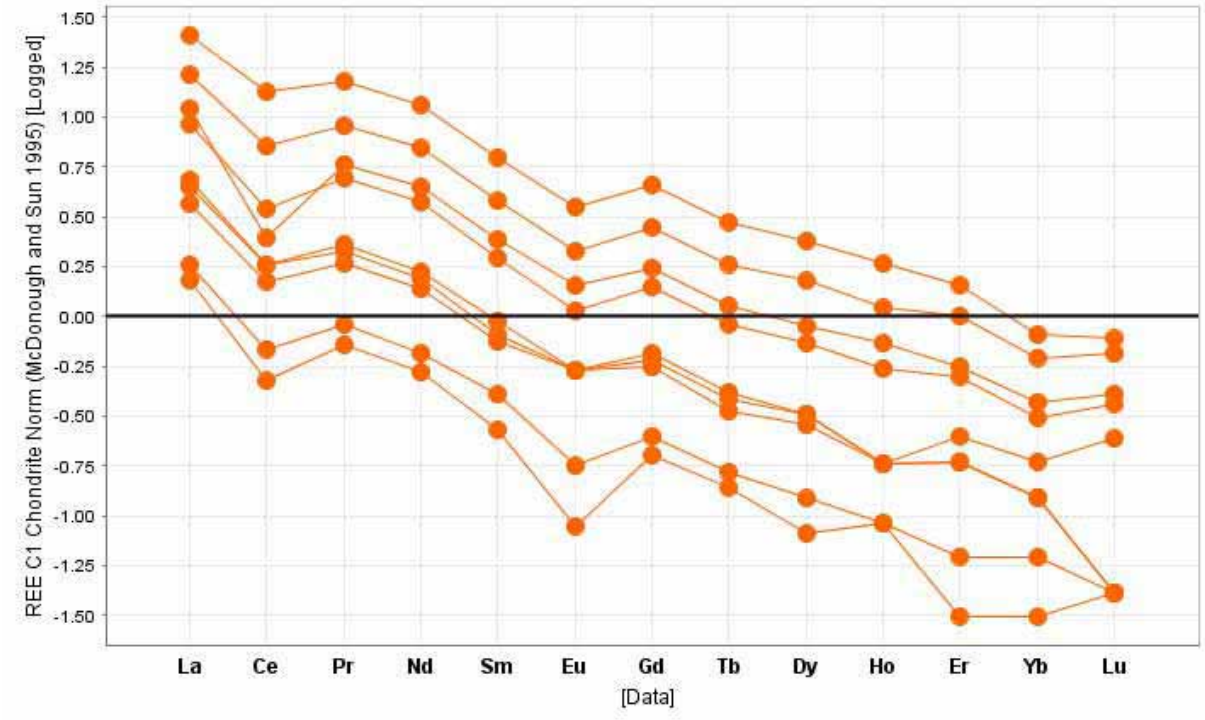

Figure 5.45: REE plot of dogwood results normalised to chondrite at the Hyperion Prospect.

5.3.5 *Eucalyptus pruinosa* (silver box)

Unfortunately there were only 4 silver box plants to sample along the transect. The results show 2 distinct elemental patterns:

1. Elements anomalous to the east of the transect (As, Au, Ba, Br, Cu, Ni, P and Zn) (Figures 5.46 and 5.47); and,
2. elements anomalous to the west of the transect (Al, B, Ca, Ce, Co, Dy, Er, Eu, Gd, Ho, La, Lu, Mn, Nd, Pr, Sm, Tb, Y and Yb) (Figure 5.48).

There are also elements that are irregularly distributed (Cs, Fe, K, Li, Mg, Rb, S, Sr and U) (Figure 5.49). Elements that were below analytical detection limit were Ag, Be, Bi, Cd, Cr, Ga, Hf, In, Ir, Mo, Na, Nb, Pb, Re, Sb, Sc, Se, Sn, Ta, Te, Th, Ti, Tl, Tm, V W and Zr.

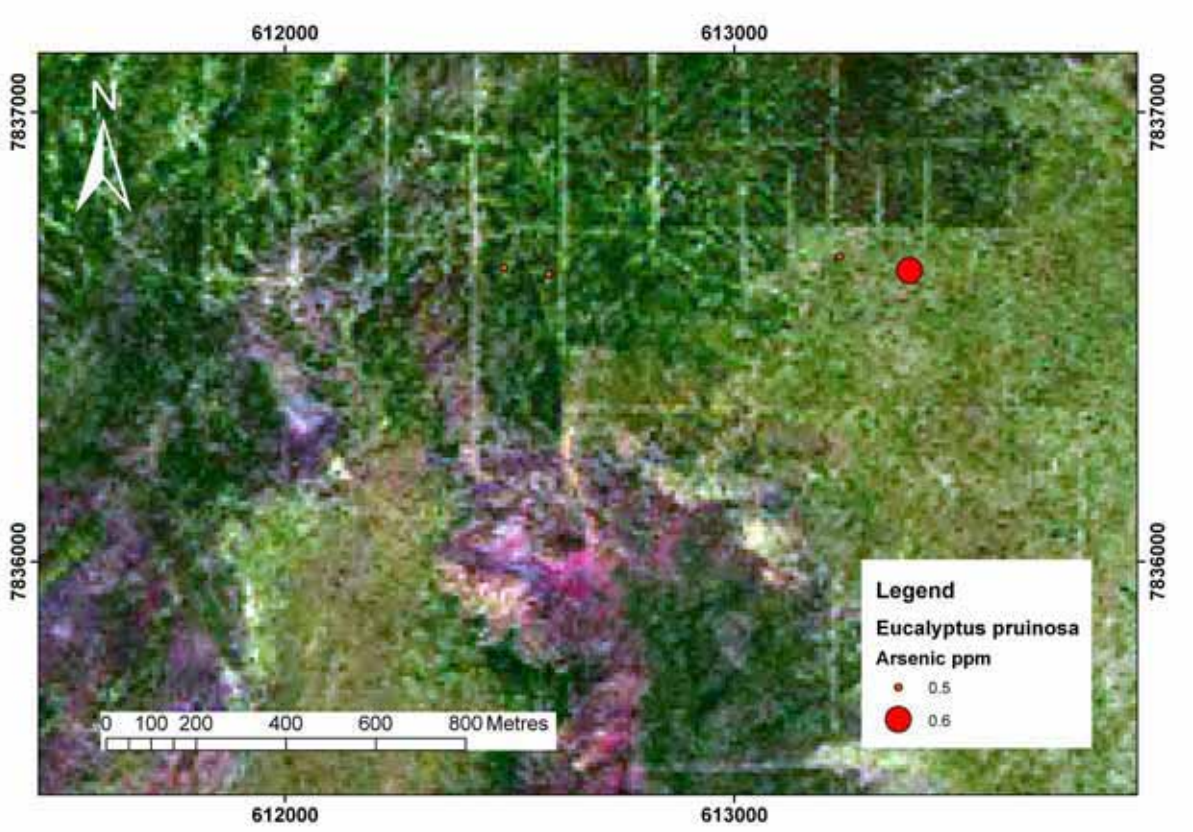

Figure 5.46: Plots of As concentration for *Eucalyptus pruinosa* overlying the SPOT of the Hyperion Prospect

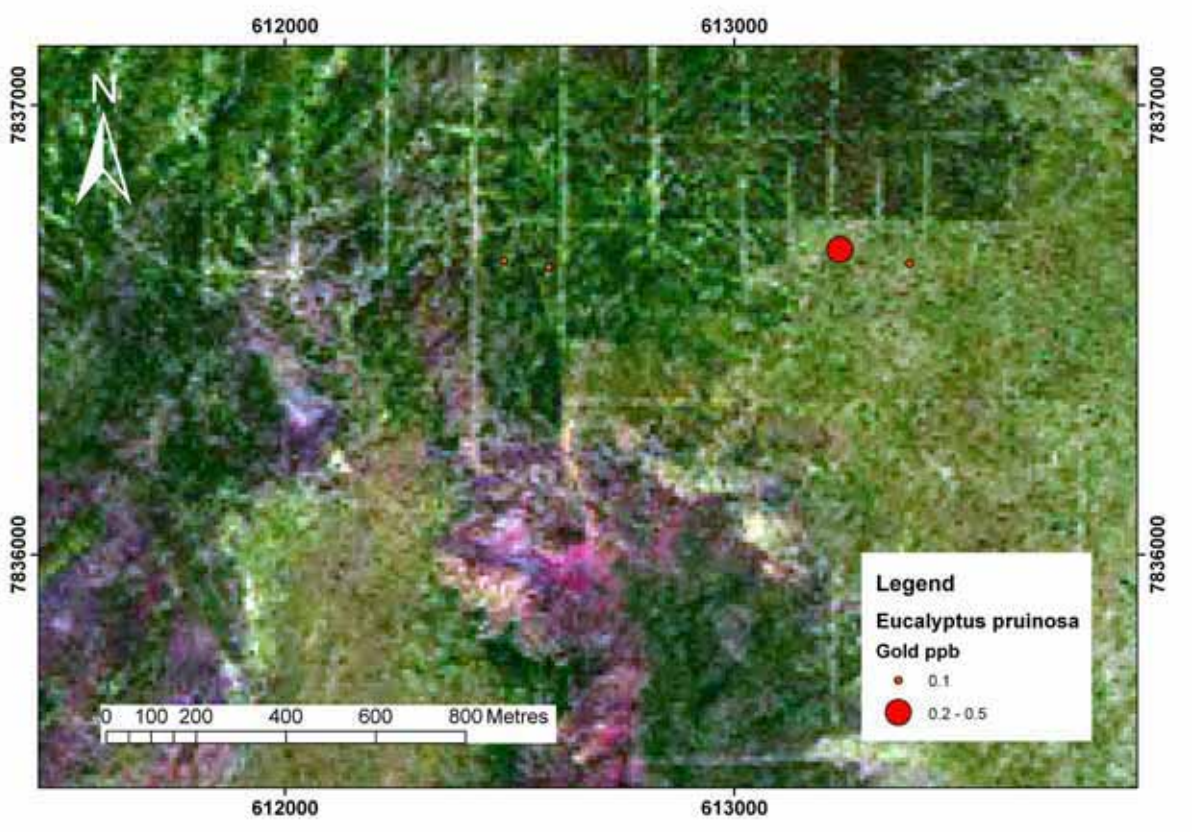

Figure 5.47: Plots of Au concentration for *Eucalyptus pruinosa* overlying the SPOT of the Hyperion Prospect

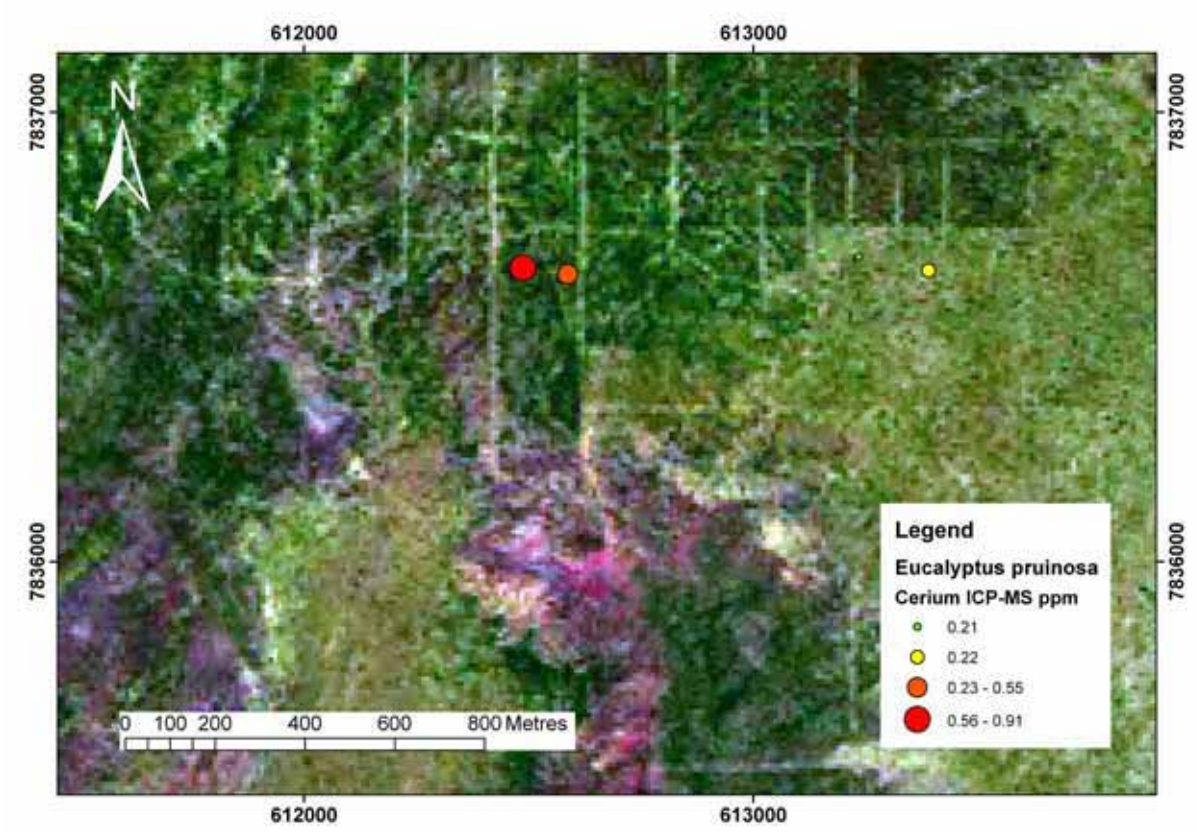

Figure 5.48: Plots of Ce (ICP-MS) concentration for *Eucalyptus pruinosa* overlying the SPOT of the Hyperion Prospect

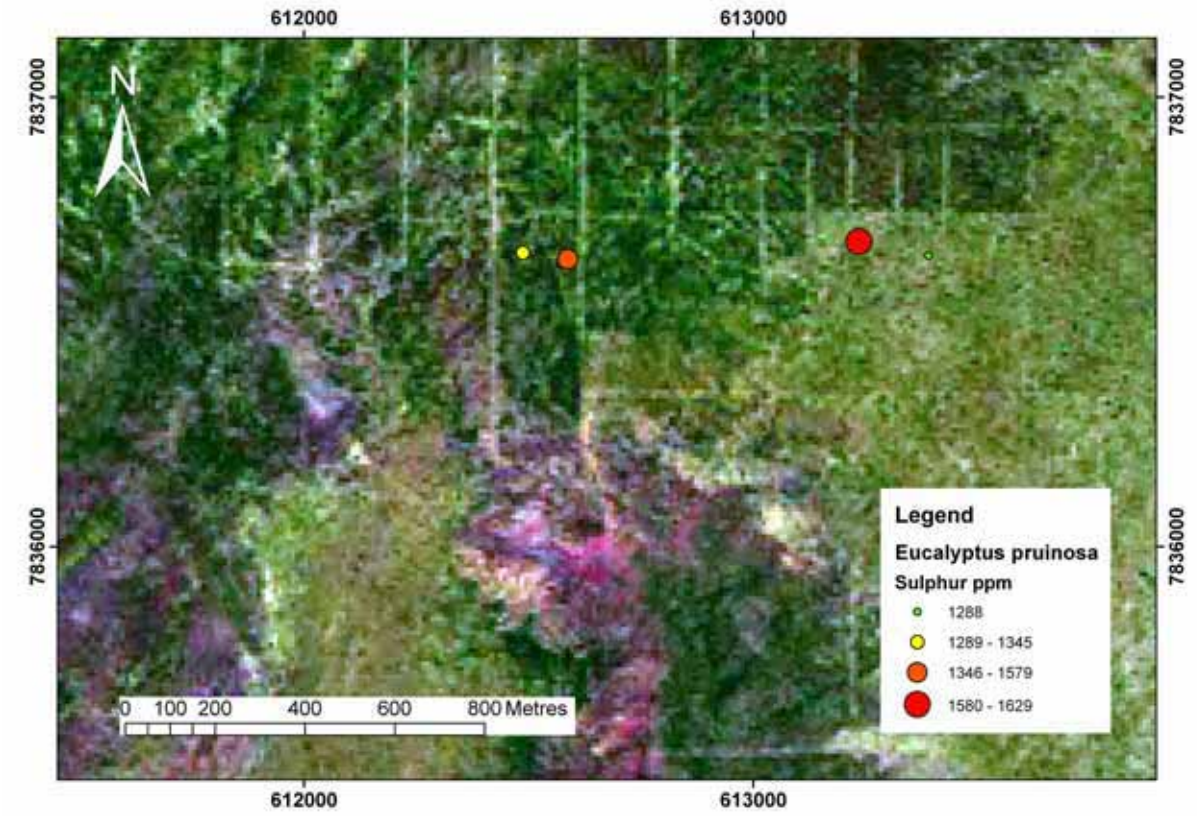

Figure 5.49: Plots of S concentration for *Eucalyptus pruinosa* overlying the SPOT of the Hyperion Prospect

Discussion

The limited data set for this species supports the interpretation of the snappy gum results. There are isolated higher values of Au and As to the east, that may be consistent with eastwards dispersion away from a primary source. The REE patterns are the opposite which is difficult to explain with the limited data set.

5.3.6 *Acacia lysiphloia* (turpentine)

Acacia lysiphloia was relatively abundant, but sparse, in this area, hence it was chosen as a sampling medium. This species however, has sticky phyllodes and stems, so the detrital contamination potential is high. The turpentine results show 3 distinct elemental patterns from the data:

1. Elements anomalous to the east of the transect (P);
2. Elements anomalous to the west of the transect (As, B, Br, Eu, Gd, La, Mg, Mn, Nd, Pr, S, Sm and Y) (Figures 5.51 and 5.52); and,
3. Elements negatively anomalous to the centre of the transect (Al, Ce, Cs, Dy, Er, Li, Sc, Sm and Zn).

There are also elements that are irregularly distributed (Ba, Ca, Cu, Fe, K, Na, Ni, Rb, Sr, Yb, Zn and Zr). Elements that were below analytical detection limit were Ag, Au, Be, Bi, Cd, Co, Cr, Ga, Hf, Ho, In, Ir, Lu, Mo, Nb, Pb, Re, Sb, Sc, Se, Sn, Ta, Tb, Te, Th, Ti, Tl, Tm, U, V and W.

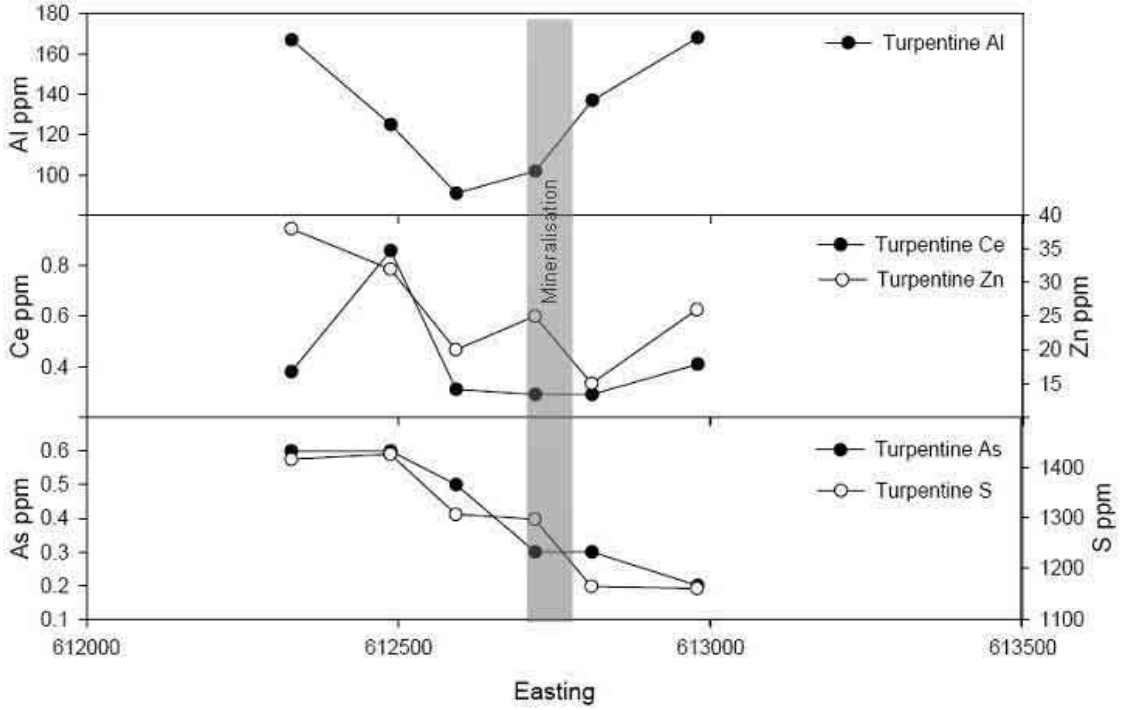

Figure 5.50: *Acacia lysiphloia* elemental cross section across the Hyperion prospect

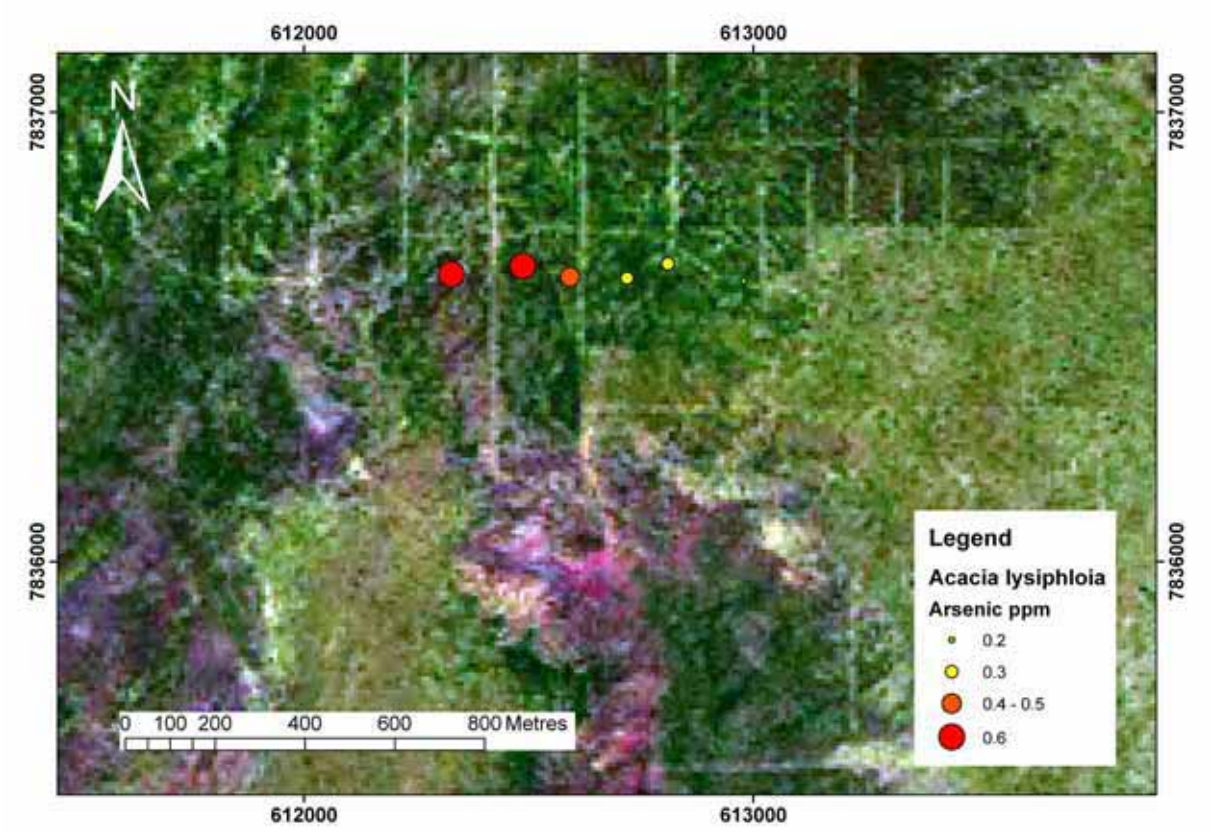

Figure 5.51: Plots of As concentration for *Acacia lysiphloia* overlying the SPOT of the Hyperion Prospect

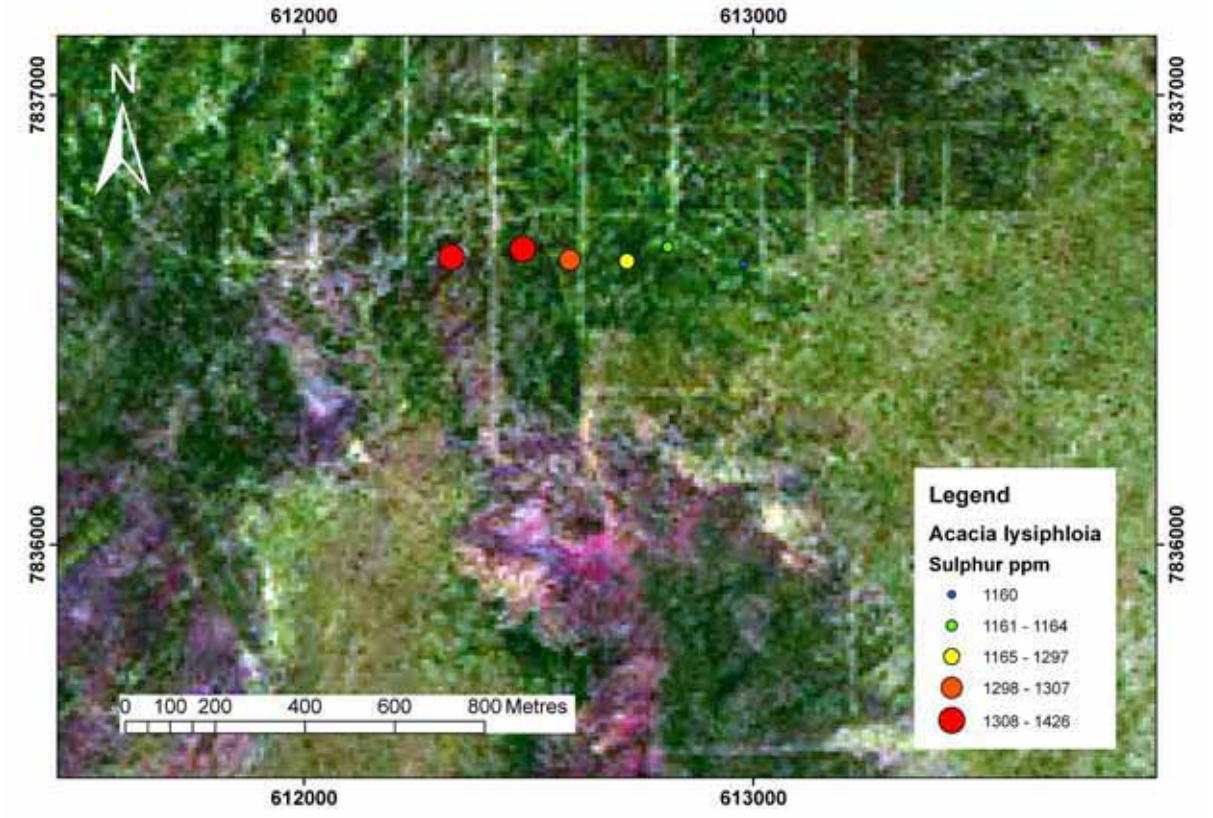

Figure 5.52: Plots of S concentration for *Acacia lysiphloia* overlying the SPOT of the Hyperion Prospect

Discussion

In general the turpentine results show the inverse trends from the snappy gum and silver box (Figure 5.50). Since those results show a trend of higher values to the east, within pathfinder elements, due to surficial and/or groundwater dispersion, then this process must not be as important an influence on the chemical composition of turpentine phyllodes. A factor likely affecting this concentration is wind, with the dominant wind direction in the Tanami region from east to west. The turpentine phyllodes are very sticky and therefore act as an effective dust trap. The anomalies generated by this species are therefore directly related to wind blown particles which become trapped upon the phyllodes. This could be seen in the bottom of the sample bag as some dust had fallen off and collected in the bottom after drying. This indicates that *Acacia lysiphloia* would not be an ideal sampling media for a phyto-exploration project.

5.3.7 Species Differences

Probability plots were created within the program IoGas for each element, using different colours for each different species from the Hyperion survey. Several of the key results are shown in Figures 5.53-5.57. Turpentine phyllodes are shown to have the highest levels of contamination of all the plants, but all species showed similar levels of contamination, which was deemed insignificant.

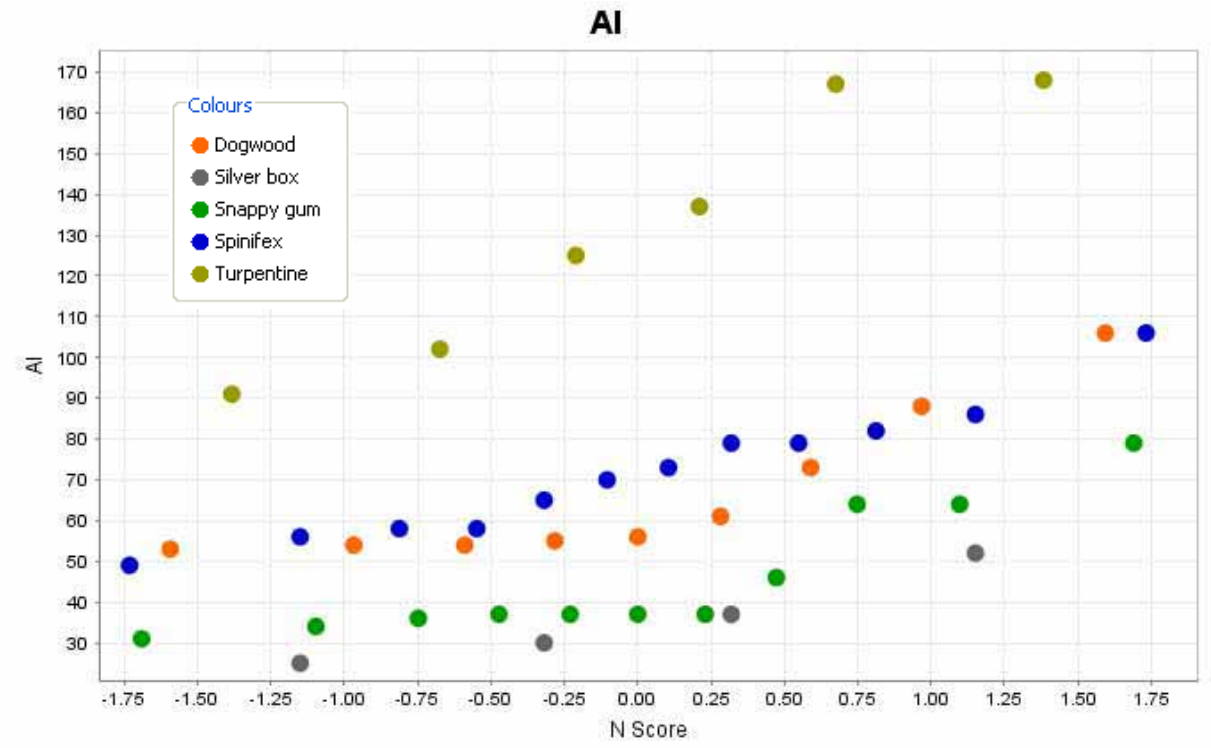

Figure 5.53: Al results split by species at the Hyperion Prospect.

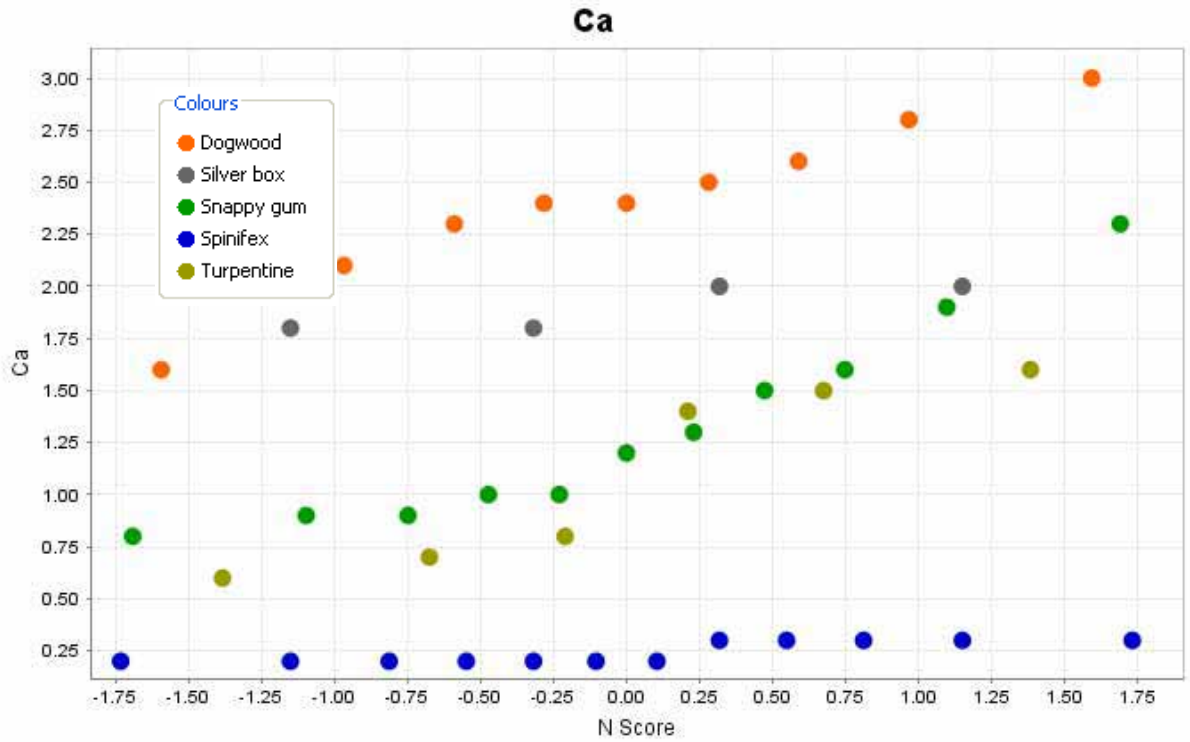

Figure 5.54: Ca results split by species at the Hyperion Prospect.

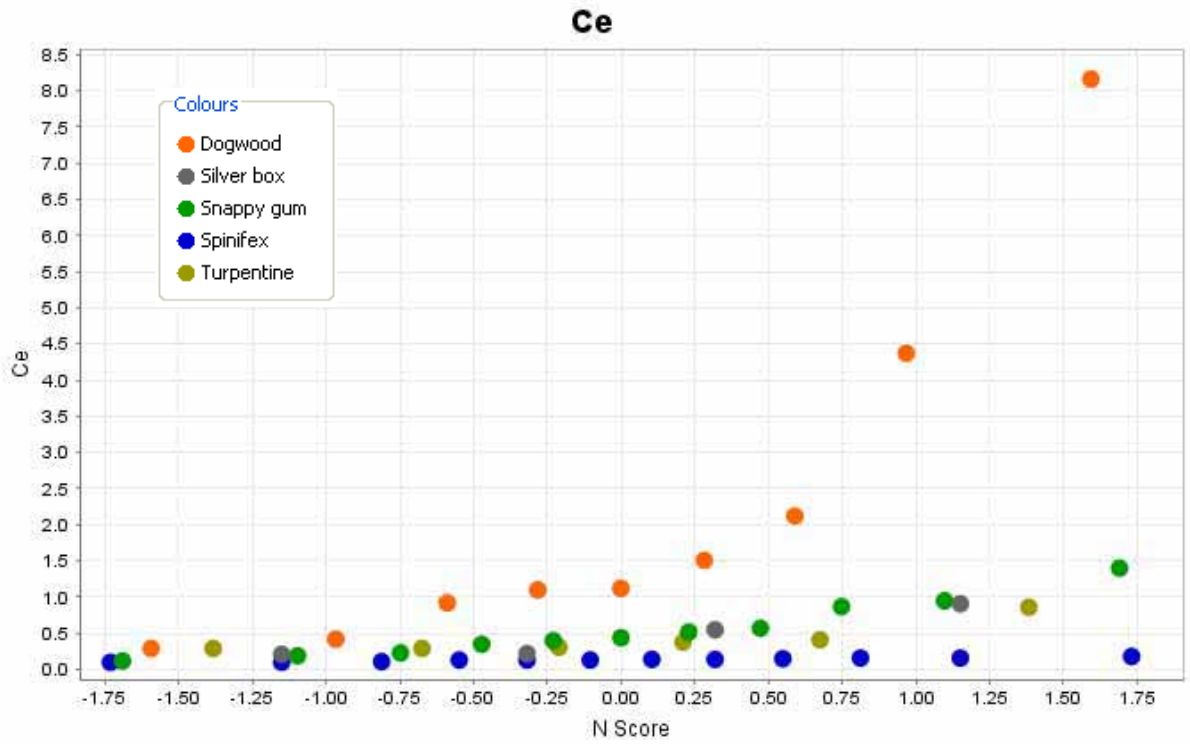

Figure 5.55: Ce results split by species at the Hyperion Prospect.

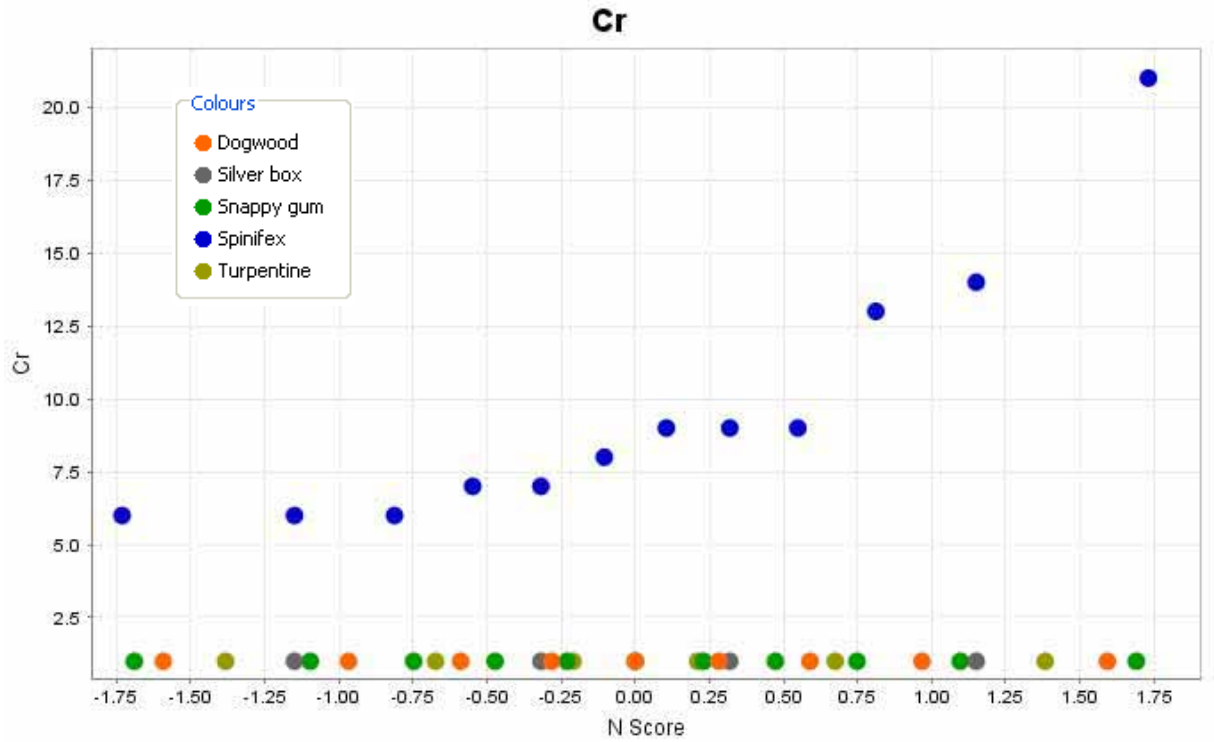

Figure 5.56: Cr results split by species at the Hyperion Prospect.

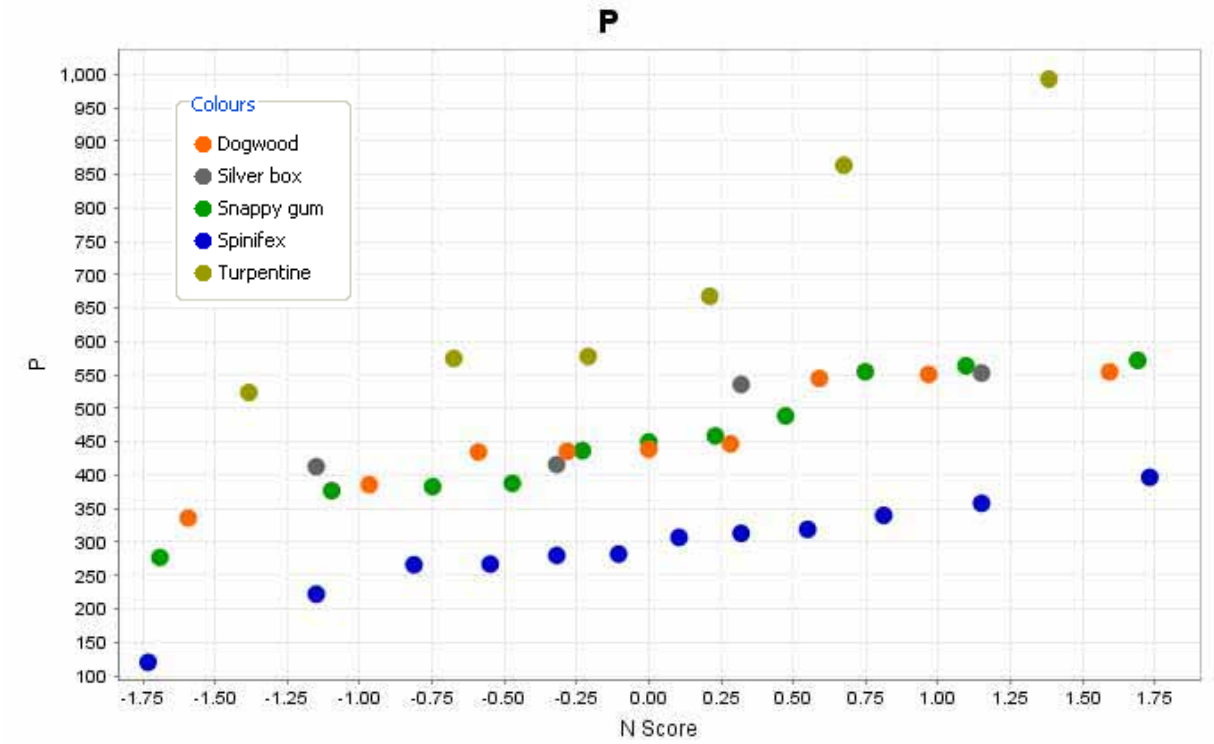

Figure 5.57: P results split by species at the Hyperion Prospect.

There is little consistency between the pathfinder elemental responses (Au, As, REE, S and Zn) between the different plant species. This seems to be due to the different habit of the plants examined in this case, as each species seems to draw elements from a different source.

There was no distinct anomaly to background split highlighted by the probability plots. However, several of the elements were particularly different with respect to species (Figures 5.55 and 5.56). This shows that *Acacia coriacea* is able to uptake significantly higher REE than the other species, the reason for this is unknown (Figure 5.55). *Triodia pungens* can

accumulate Cr up to 21 ppm which is over an order of magnitude greater than any other species (Figure 5.56). This is similar to that seen at the Coyote Prospect but the greatest value is only half that seen at Coyote. In general, different species uptake elements at different rates, which indicates that species sampling is critical in biogeochemical orientation surveys.

Phosphorous is again fairly consistent between the species, however, the soft spinifex has slightly lower levels than the other species and turpentine has slightly higher (Figure 5.57). This may be due to turpentine being fast growing and hence needing more P for fast growth, and spinifex is slow growing and adapted for nutrient poor soils.

5.3.8 Elemental correlations

The elemental correlations generated by the Hyperion assays are rather misleading due to the small number of samples. The fewer samples in the data set, the more correlations are generated because of the lack of significant different samples in the set. There are the usual, expected correlations within all the plant species and each individual species; however, there are only a few points for each plant species and a lot higher correlation values are generated because of the small sample size. Some of the correlations can be seen visually in Figures 5.58-5.64. There is a strong correlation between the detrital contaminant elements (Al, Fe, Th and Zr, Figure 5.58), Ca and Sr are highly correlated (0.93, Figure 5.61), the two techniques (ICP-MS and INAA) are also highly correlated as shown by the Ba results (0.98, Figure 5.60). There is a high, positive correlation between As and Br (0.96, Figure 5.59) which is present in all the plant species. This correlation is unique to the Hyperion Prospect and is not fully understood.

All the REE are highly, positively correlated with each other, highlighted in particular by the elevated concentrations of the dogwood results (Figure 5.62). Dogwood also has high correlations between REE and S and P (Figures 5.63 and 5.64), the correlation with P can be explained by the roots of the dogwood actively dissolving monazites which are a REE-phosphate mineral. These are not detrital monazites as there was no correlation between the REE and dust contaminant elements (Al, Fe, Hf Zr) which would have coated the monazites if they were not primary.

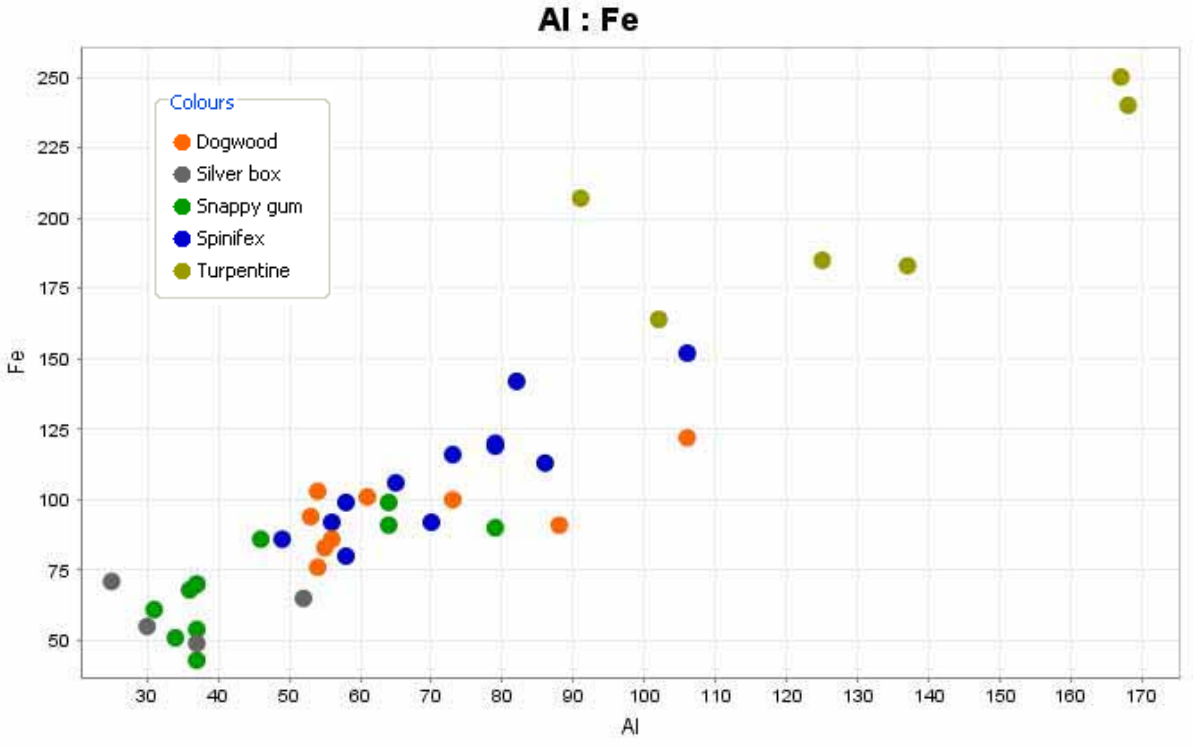

Figure 5.58: Al and Fe visual correlation split by species at the Hyperion Prospect.

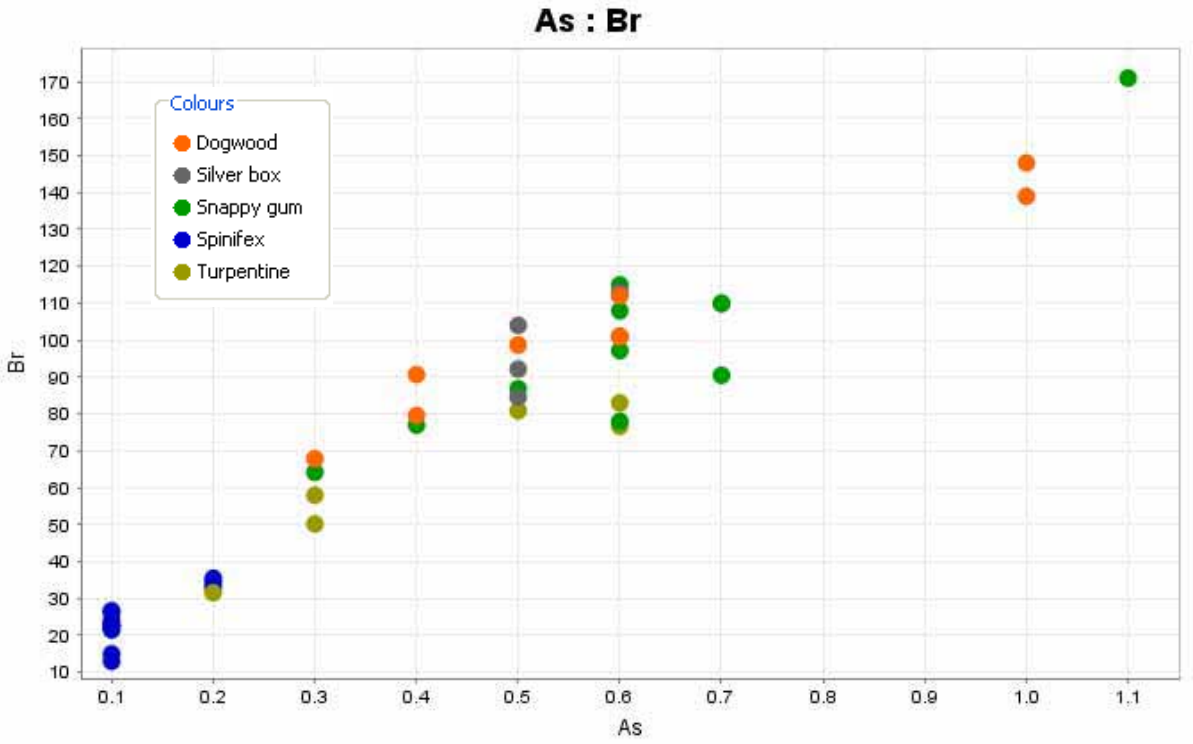

Figure 5.59: As and Br visual correlation split by species at the Hyperion Prospect.

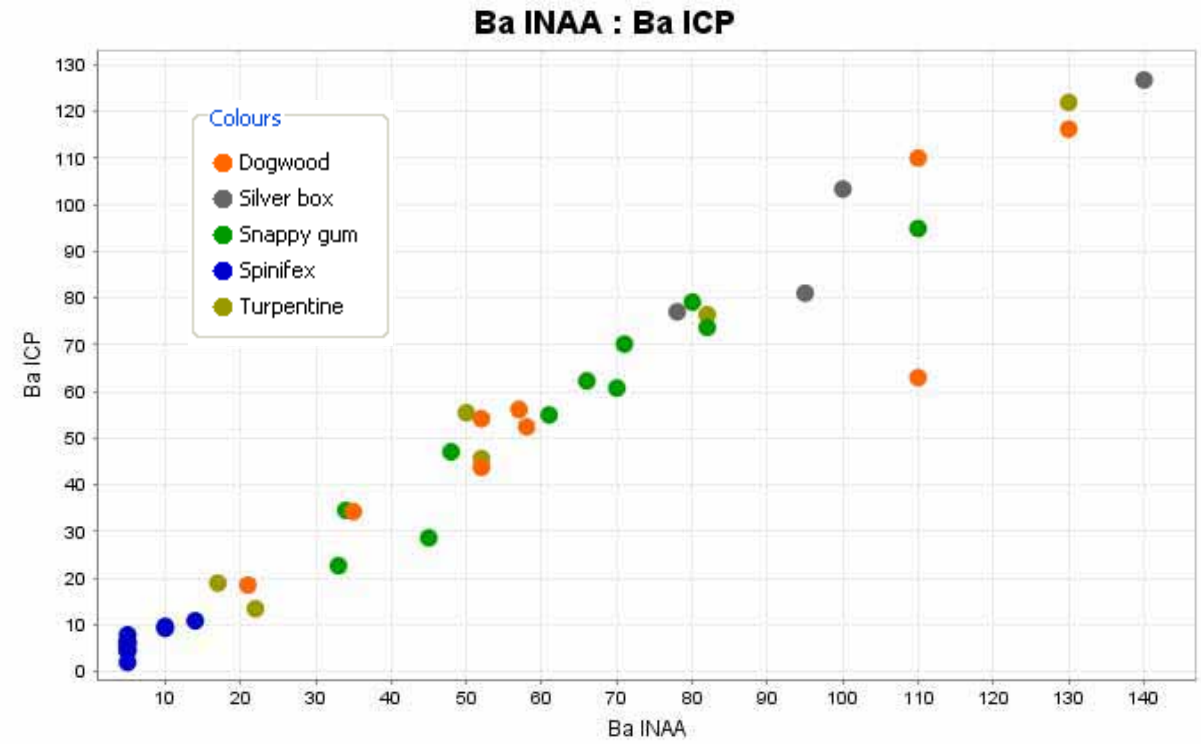

Figure 5.60: Ba INAA and Ba ICP visual correlation split by species at the Hyperion Prospect.

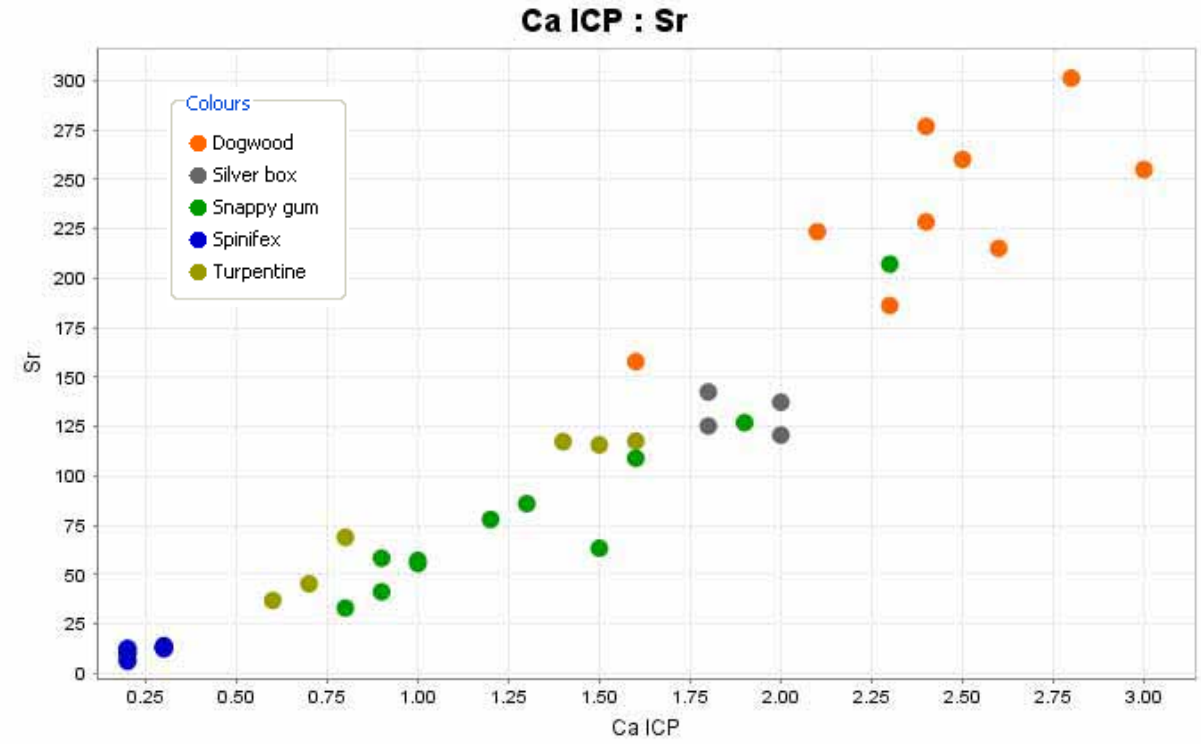

Figure 5.61: Ca and Sr visual correlation split by species at the Hyperion Prospect.

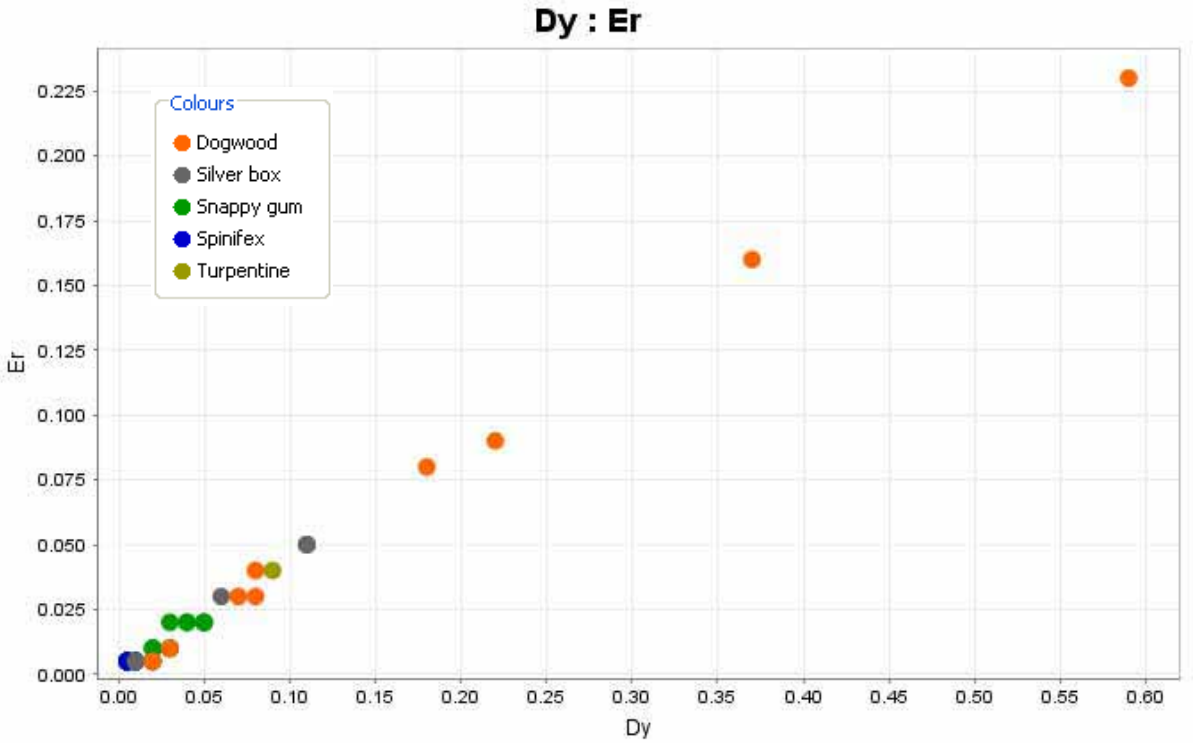

Figure 5.62: Dy and Er visual correlation split by species at the Hyperion Prospect.

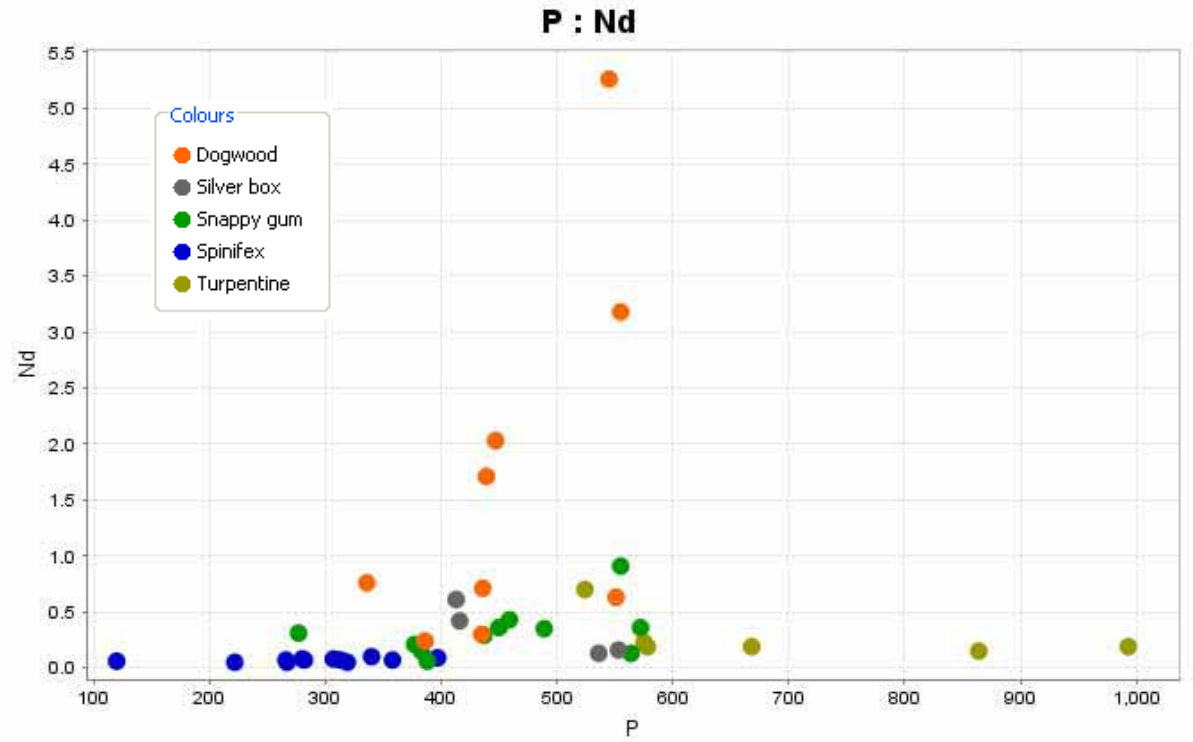

Figure 5.63: P and Nd visual correlation split by species at the Hyperion Prospect.

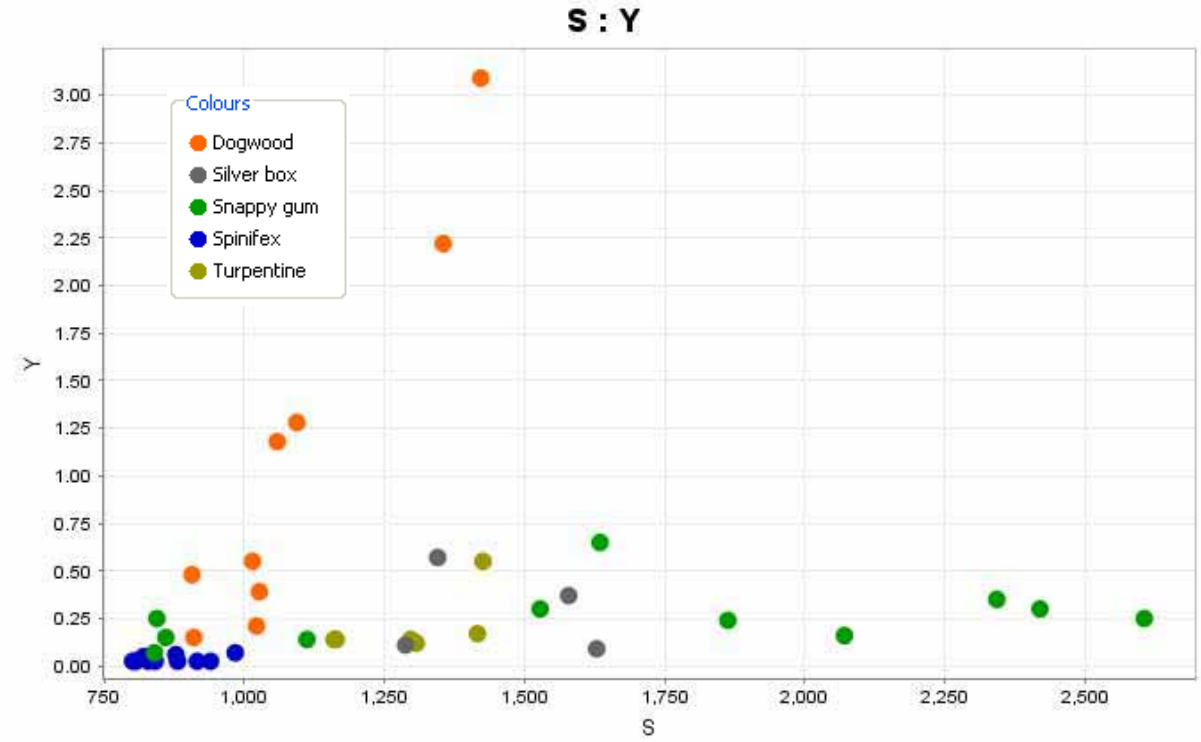

Figure 5.64: S and Y visual correlation split by species at the Hyperion Prospect.

5.4 Geobotany and Biogeochemistry of the Titania Prospect

5.4.1 Site specific methods

The Titania Prospect in the Northern Territory was an area of Au mineralisation (native Au and in arsenopyrite and chalcopyrite), hosted in multiple fine-grained siltstones related to east-west deformational structures, buried by transported cover ranging from 15-30 m thick (Newmont drill logs, (Readford 1999)). It is on the western margins of a large palaeo- and contemporary drainage system. Groundwater is closer to the surface than at the other sites and its exaporation contributes to gypsum deposits on the soil surface from when the groundwater rises to the surface causing ephemeral swamps and bogs. The groundwaters are also more saline contributing to a large salt lake to the east of the mineralised zone. Since the other sites were simple single transects, Titania was chosen as a site to expand the methodology to a gridded array of samples in a 'footprint' study. The site had suffered a fire about 6 months before being sampled and this limited some availability of plants. However, there also had been no rain over the site since that time, meaning that plants with green foliage at that time must be sourcing water from the water table (4 m depth at this time). Vegetation assemblages, tree and large shrub species and tree height were recorded along seven adjacent 2 km long N-S transects over the Titania mineralisation and adjacent area in October 2005. The 322 leaf samples were collected from individual plants at 250 m spacing along the transect grid, the line spacing was 500 m (Figure 5.65). This dot point map could be grouped to provide a rough vegetation map, shown in Figure 5.66.

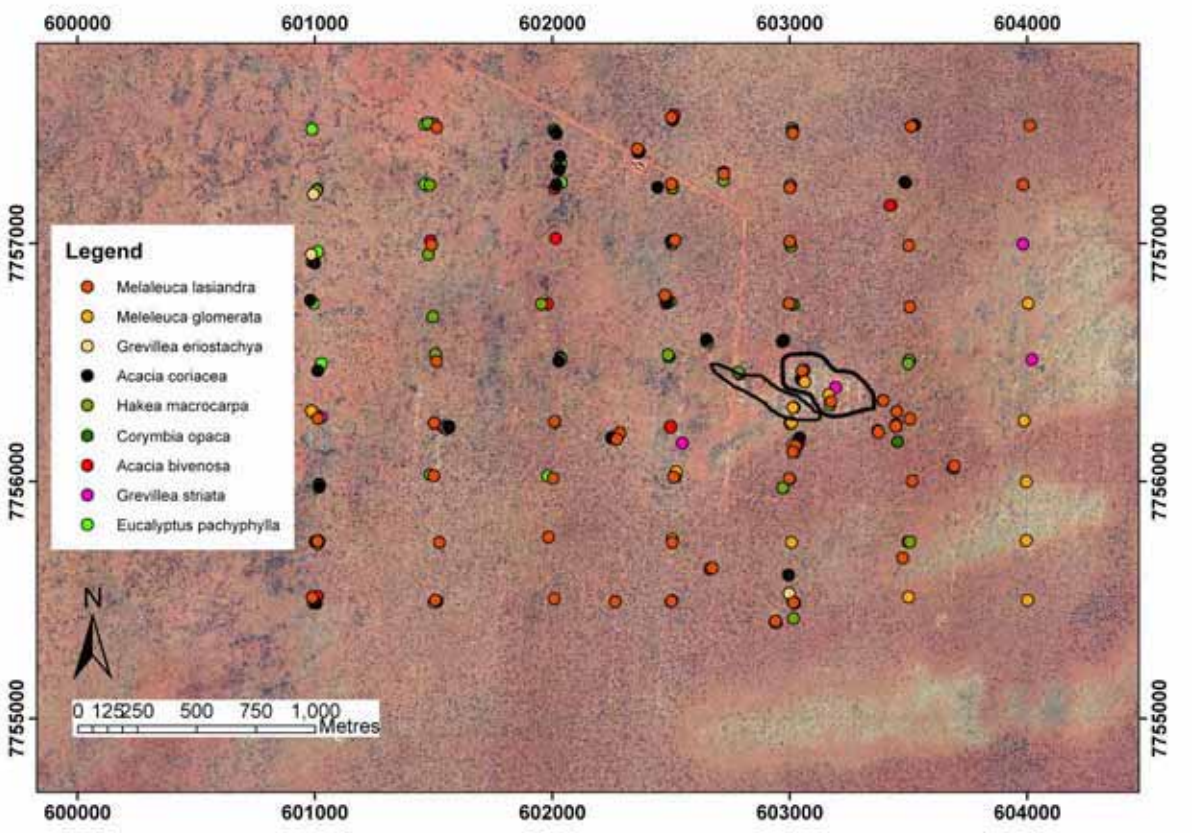

Figure 5.65: Vegetation distribution across the Titania Prospect overlaying the orthophoto

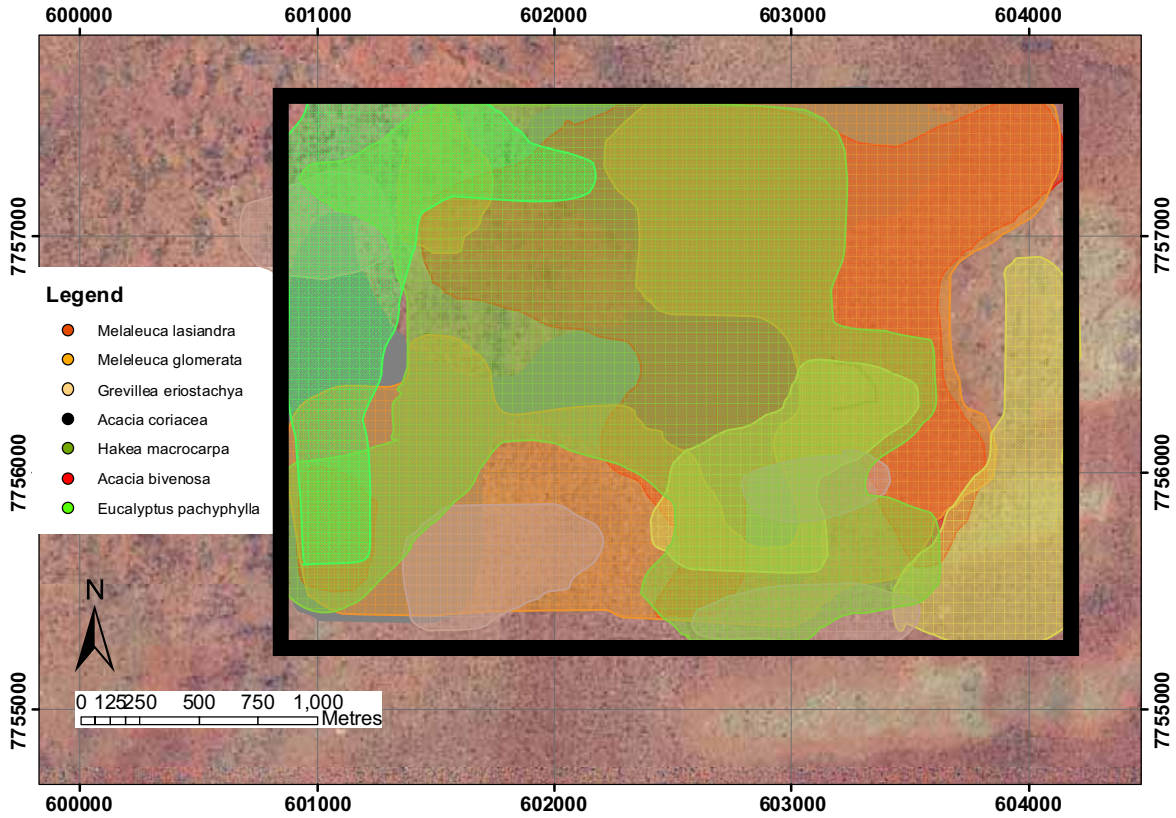

Figure 5.66: Contoured vegetation map over the Titania field site.

This simplified map highlights the different broad vegetation communities over the site and the landforms which they correspond to. In the southern region of the site there are areas of *Grevillea eriostachya* and *Melaleuca lasiandra* with other widespread species, which colonise the sand dunes. The west and north-western areas are colonised by *Eucalyptus pachyphylla* with other widespread species, which correspond to where the transported cover is thinnest and with hard-pan ferruginous materials cropping out.

5.4.2 *Triodia pungens* (soft spinifex)

The most common species over this site was *Triodia pungens*, it showed the remnants of burnt parts within the plants but in general they had all resprouted and had available foliage. The soft spinifex results show 4 distinct elemental patterns:

1. Elements that are elevated over the mineralisation (As, Au, Ce, Hg, La, U, Y and Zn);
2. Elements less abundant over mineralisation (B, Cr, Mn, Nb, Ni, Pb and Ta);
3. Elements elevated to the south-east (Ba, Cd, Cu, K, Mo, Na, P, Re, S, Sc and Th); and,
4. Elements elevated to the north-west (Ag, Bi, Co, Cs, Ge, Hf, Li, Rb, Sb and Sn).

There are also elements that are irregularly distributed (Al, Ca, Fe, Ga, Mg, Se, Sr, Ti, V and Zr). Elements that were below analytical detection limit were Be, In, Pd, Pt, Tb, Te, Tl and W.

The results from the Titania Prospect have indicated that spinifex biogeochemistry show a zone of high As contents (800 m wide) that has minimal dispersion away from the mineralised zone, Figure 5.67. The highest concentrations are directly over mineralisation (1.9 ppm). This is complemented by two elevated Au analyses over mineralisation (Figure 5.68). The highest value is directly over mineralisation (2.0 ppb), however, it is only 2 points

which reduces the statistical viability which means the multi-element suite becomes important. Similar to the Coyote Prospect, Zn and S are closely associated with mineralisation, but with greater dispersion. These elements have much larger dispersion haloes extending towards the south-east. High Zn contents define a zone (1 km) towards the south-east of the area, with the highest value (38.6 ppm) directly to the south-east of mineralisation rather than directly overlying it (Figure 5.69). This is complemented by the more mobile S halo, which has a zone of elevated values (2.5 km wide by 1.5 km long) towards the south-east of the area, with the highest values of 0.17% directly over and to the south-east of the mineralisation (Figure 5.70). The S would be sourced from sulphides (pyrite, chalcopyrite and arsenopyrite) that comprise the ore. These sulphides would be oxidised to sulphates by interaction with groundwaters which would then disperse the sulphate with the groundwater flow. Once the sulphate reaches the root zone of the plants it would be transported across the root membrane by the sulphate ion transporter and then transported to the aerial tissues by osmotic pressure (Frank et al., 2000). The difference in width and magnitude of anomalism is due to the mobility of the individual element, primary dispersion from mineralisation, and secondary dispersion of elements due to mechanical and/or climatic factors (Nicolls *et al.* 1965).

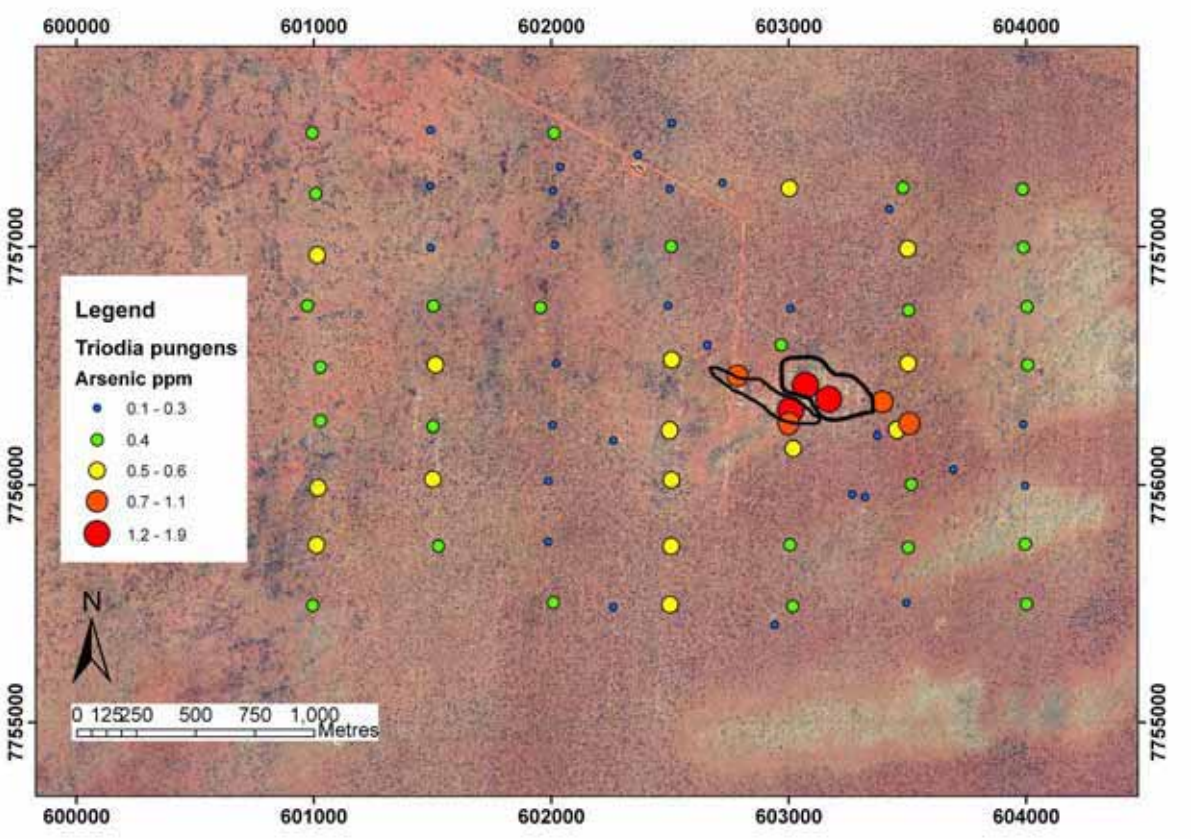

Figure 5.67: Plots of As concentration for *Triodia pungens* overlying the orthophoto of the Titania Prospect.

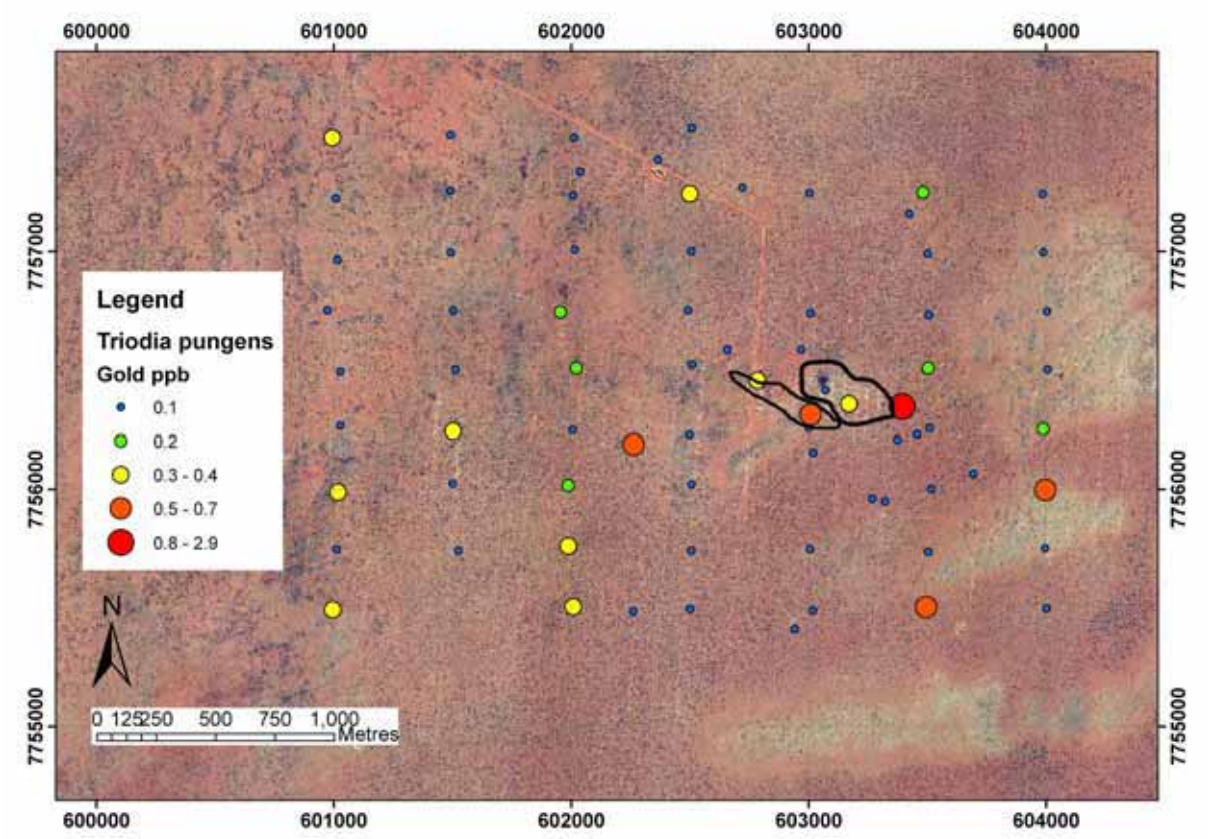

Figure 5.68: Plots of Au concentration for *Triodia pungens* overlying the orthophoto of the Titania Prospect.

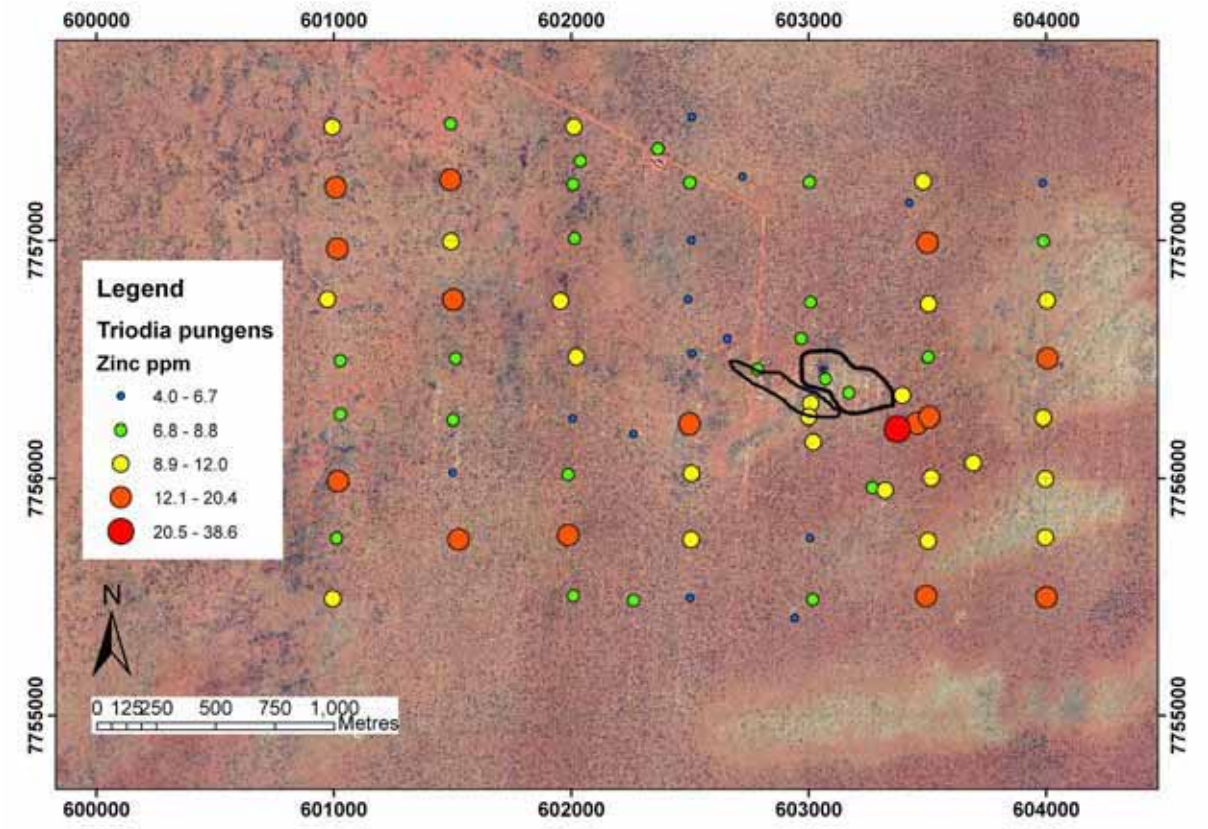

Figure 5.69: Plots of Zn concentration for *Triodia pungens* overlying the orthophoto of the Titania Prospect.

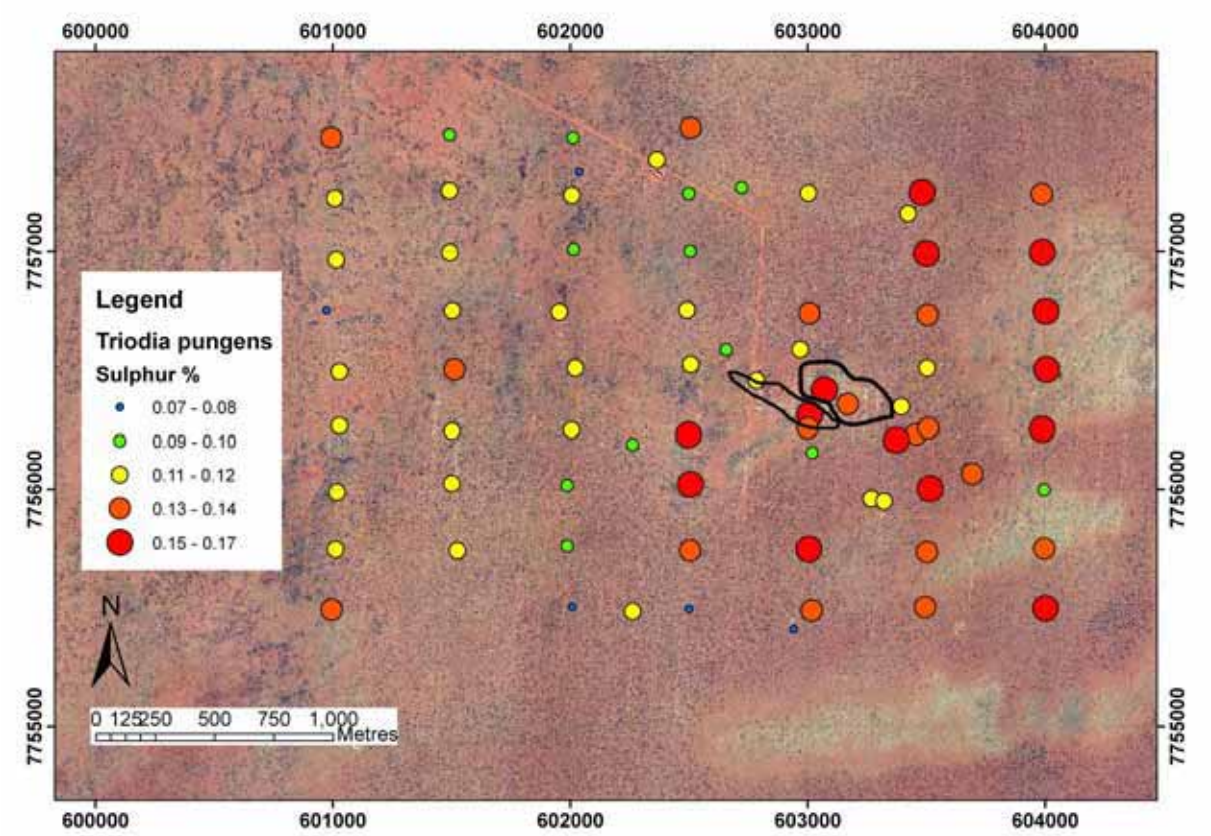

Figure 5.70: Plots of S concentration for *Triodia pungens* overlying the orthophoto of the Titania Prospect.

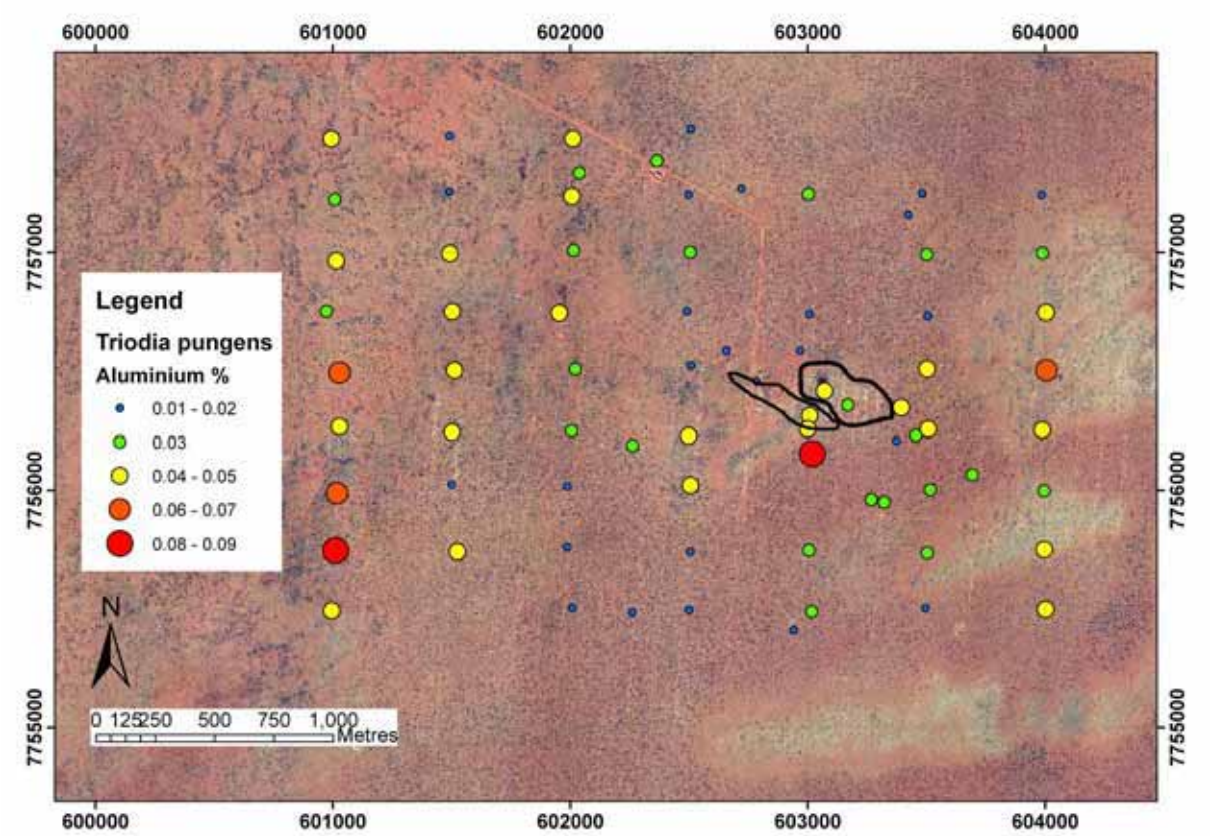

Figure 5.71: Plots of Al for *Triodia pungens* concentration overlying the orthophoto of the Titania Prospect.

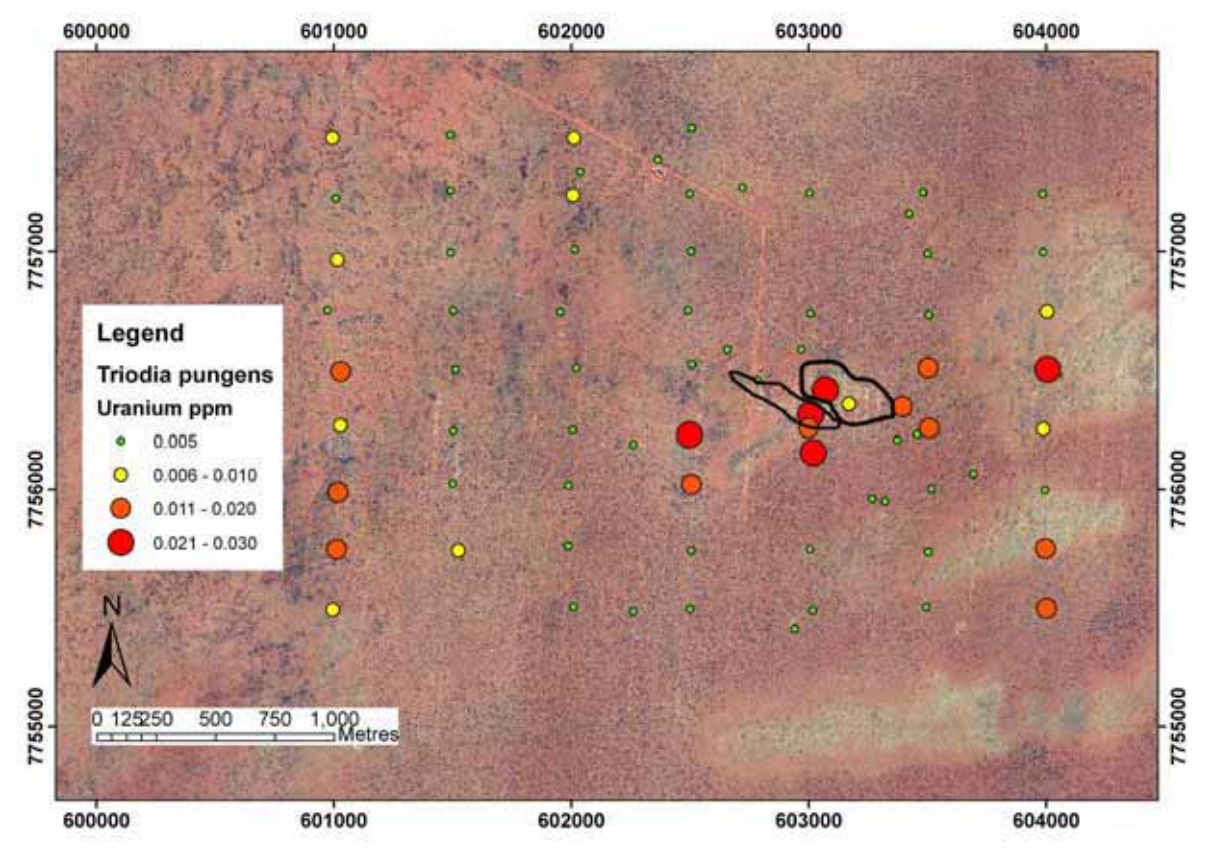

Figure 5.72: Plots of U for *Triodia pungens* concentration overlying the orthophoto of the Titania Prospect.

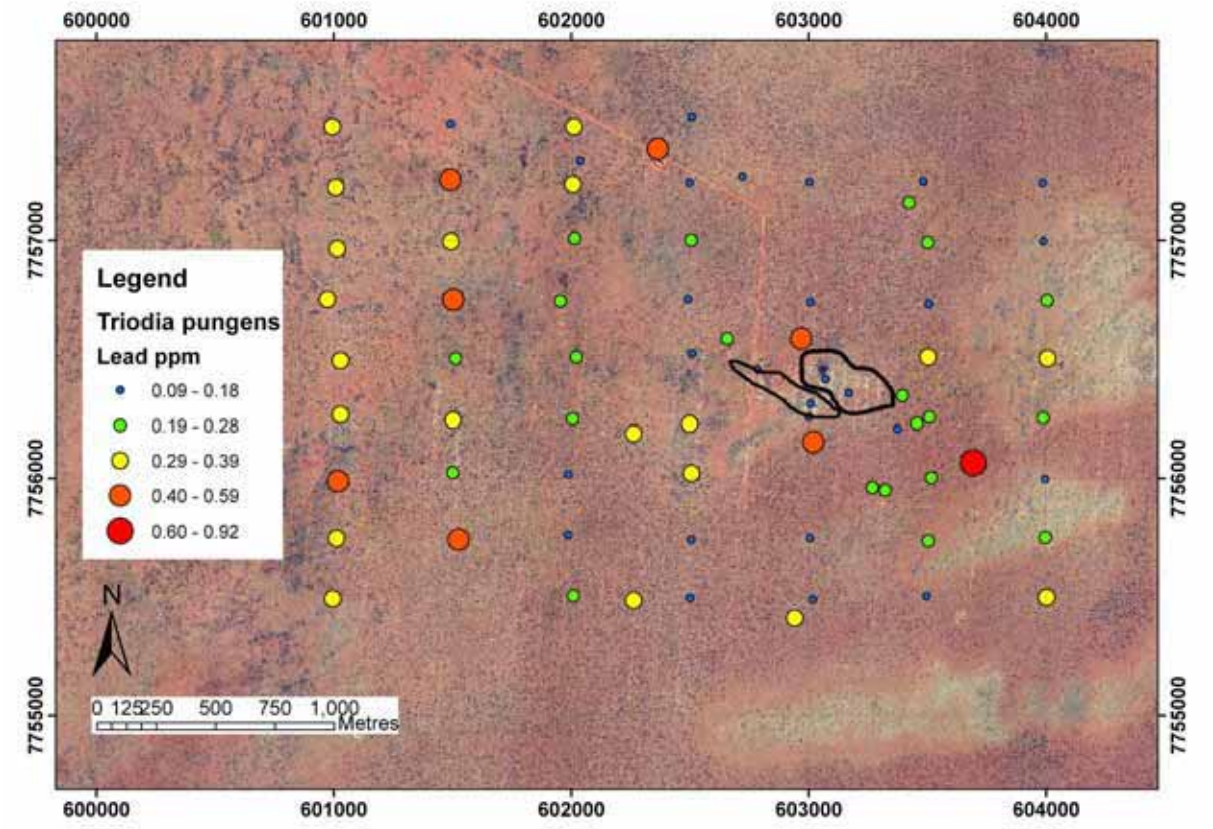

Figure 5.73: Plots of Pb concentration for *Triodia pungens* overlying the orthophoto of the Titania Prospect.

Elements generally associated with detrital contamination (Al, Fe, Hf, Th and Zr) show an irregular distribution. They particularly highlight plants that have greater dust trapping

capacity (Figure 5.71). Although the levels of these elements are higher in the spinifex than in most of the other plants (since they are lower to the ground) the lack of association with any of the important pathfinders shows that the anomaly is unlikely to be generated from detrital contamination.

There is zone of elevated U over mineralisation close to the same size as the As anomaly (Figure 5.72). A zone of lower Pb assays overlies the mineralisation site (Figure 5.73). This is unexpected considering that there is Pb within the ore body associated with the primary sulphides. One explanation for this could be from the phenomenon found by (Nicolls *et al.* 1965a), where *Triodia pungens* would not grow in areas of higher than normal Pb. In this case it is possible that the plants may be actively excluding the element when the levels are higher. Alternatively Pb could be bound in non-biologically accessible compounds directly over the mineralisation but has been transformed into a more useable form as the element is dispersed away.

Discussion

There are four distinct spatial patterns to the elemental distribution over the Titania Prospect. The highest values are either: directly over mineralisation (Au, As), and directly related to the ore body (although Au has more anomalous sites outside of the mineralisation due to 'nugget' effects, the greatest values are over mineralisation); highest towards the south-east and related to groundwater (hydraulic conductivity and salt concentrations); or, highest towards the northwest relating to the ferruginous duricrust which is exposed there (however iron oxides and hydroxides bind and immobilise elements so would not be accessible by plants), the shallower bedrock there, or a negative accumulation due to the groundwater movement. Since spinifex slightly lowers the pH around their root systems. This would impact upon the mobility of certain elements: from the highly mobile (S, Mo, U, Na, Sr, Zn, and Cu) that have the southeast spatial trend; to the moderately mobile (As and Au) that centre over mineralisation; to the immobile (Al, Cr, Cs, Fe, Li, Mn, Pb, Rb, Sn, Ti, Zr and REE). Several elements have different trends compared to that expected from slightly acidic conditions. For instance, Co and Ni have higher values to the northwest that could relate to the shallower bedrock that may include some mafic units. Boron, Ca, and Mg all exhibit irregular trends that relates to them being essential for plant growth and would be taken up to their limits within the plant material. Barium, K and P all exhibit dispersion patterns towards the southeast suggesting that they are mobile within groundwaters, however they are expected to be less mobile. One possibility is that the elements are being bound within the ferruginous duricrust to the northwest and are hence not bioavailable there; hence it actually contributes to forming a lower abundance of these elements.

As was shown at Coyote, *Triodia pungens* is a deep-rooted species (Reid *et al.* 2008; Grigg *et al.* 2008b) that is able to provide localised chemical signatures for the *in-situ* regolith materials that may underlie 15-30 m of surface sediment. In the Tanami region, and possibly many other parts of arid Australia, the spinifex is an excellent biogeochemical exploration sampling media, especially compared to soils, which are typically influenced by sheetflow and aeolian dispersion and dilution, as seen in Chapter 5.4.11. Spinifex would be an ideal sampling media for closely spaced, detailed ore body delineation in the Tanami region and most likely in other hummock-grass dominated parts of the continent and grasslands world-wide.

5.4.3 *Melaleuca lasiandra* (sandhill tea-tree)

Melaleuca lasiandra was a dominant species over this field site. The only restrictions to its range here were to the far west where either the cover was too thin or there was not enough moisture and the far south-east where *Melaleuca glomerata* was dominant (cover thicker and substrate with a greater salt content). The chemical signature of the sandhill tea-tree results shows 4 distinct elemental patterns from the data:

1. Elements that are elevated over the mineralisation (As, Au, Ge, Nb, Sb and V);
2. Elements less abundant over mineralisation (Cr and Se);
3. Elements elevated to the south-east (Ba, Ce, Co, Cu, La, Li, Mn, Na, P, Re, S, Th, U, Y, Zn and Zr); and,
4. Elements elevated to the north-west (Ta and Tl).

There are also elements that are irregularly distributed (Ag, Al, B, Ca, Cs, Fe, Hf, Hg, K, Mg, Mo, Ni, Pb, Rb, Sc, Sn, Sr and Ti). Elements that were below analytical detection limit were Be, Bi, Cd, Ga, In, Pd, Pt, Te and W.

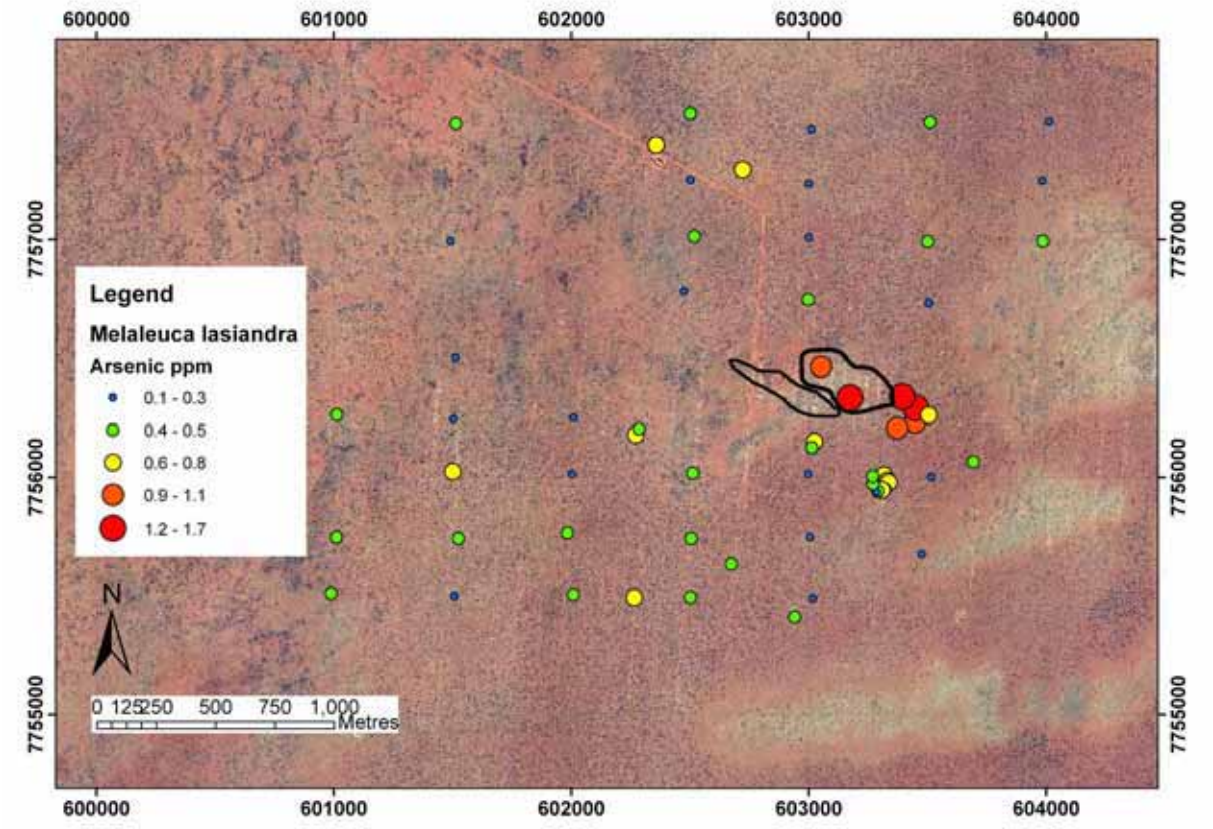

Figure 5.74: Plots of As concentration for *Melaleuca lasiandra* overlying the orthophoto of the Titania Prospect.

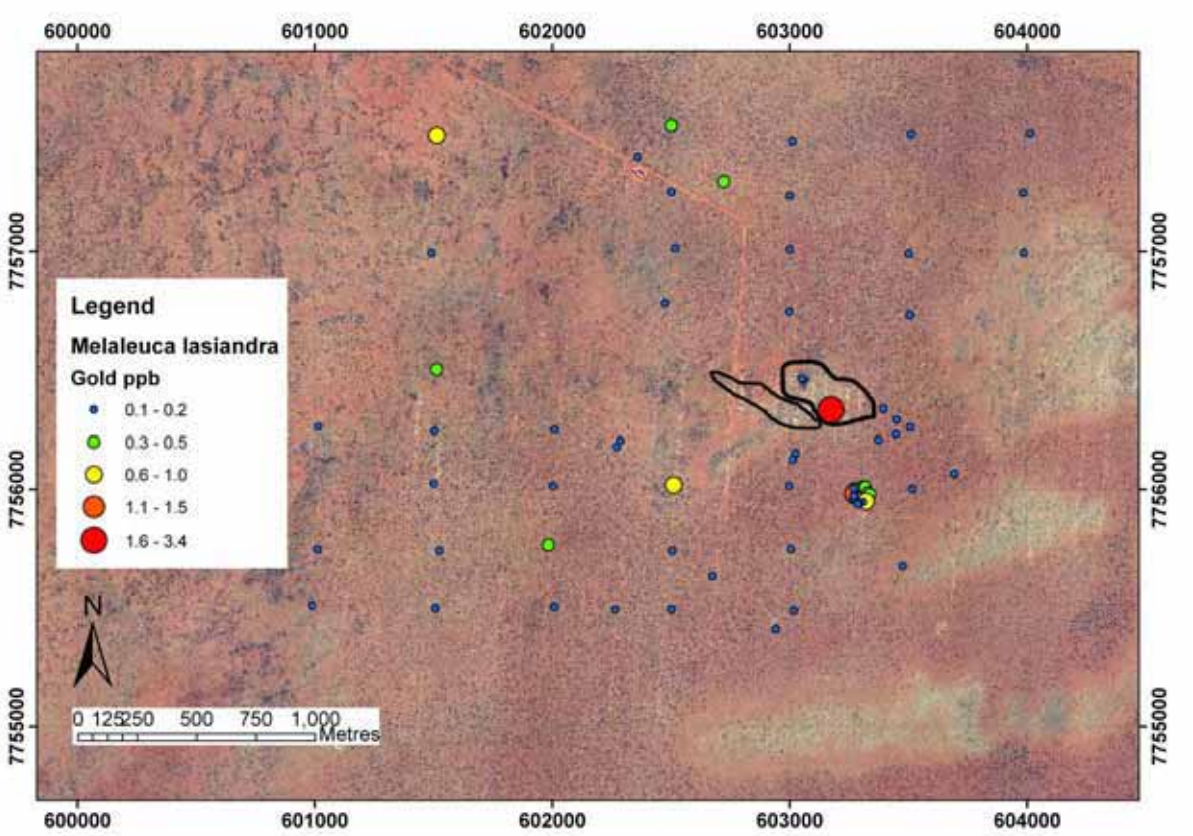

Figure 5.75: Plots of Au concentration for *Melaleuca lasiandra* overlying the orthophoto of the Titania Prospect.

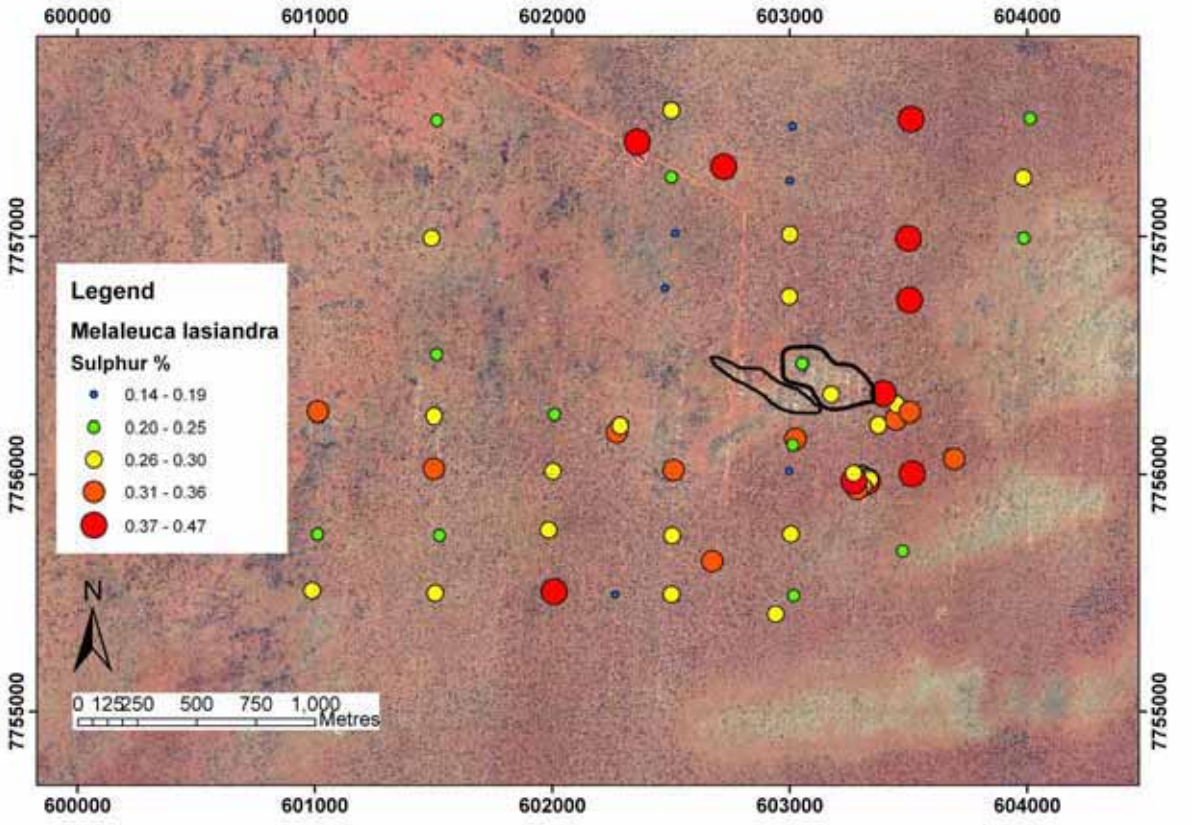

Figure 5.76: Plots of S concentration for *Melaleuca lasiandra* overlying the orthophoto of the Titania Prospect.

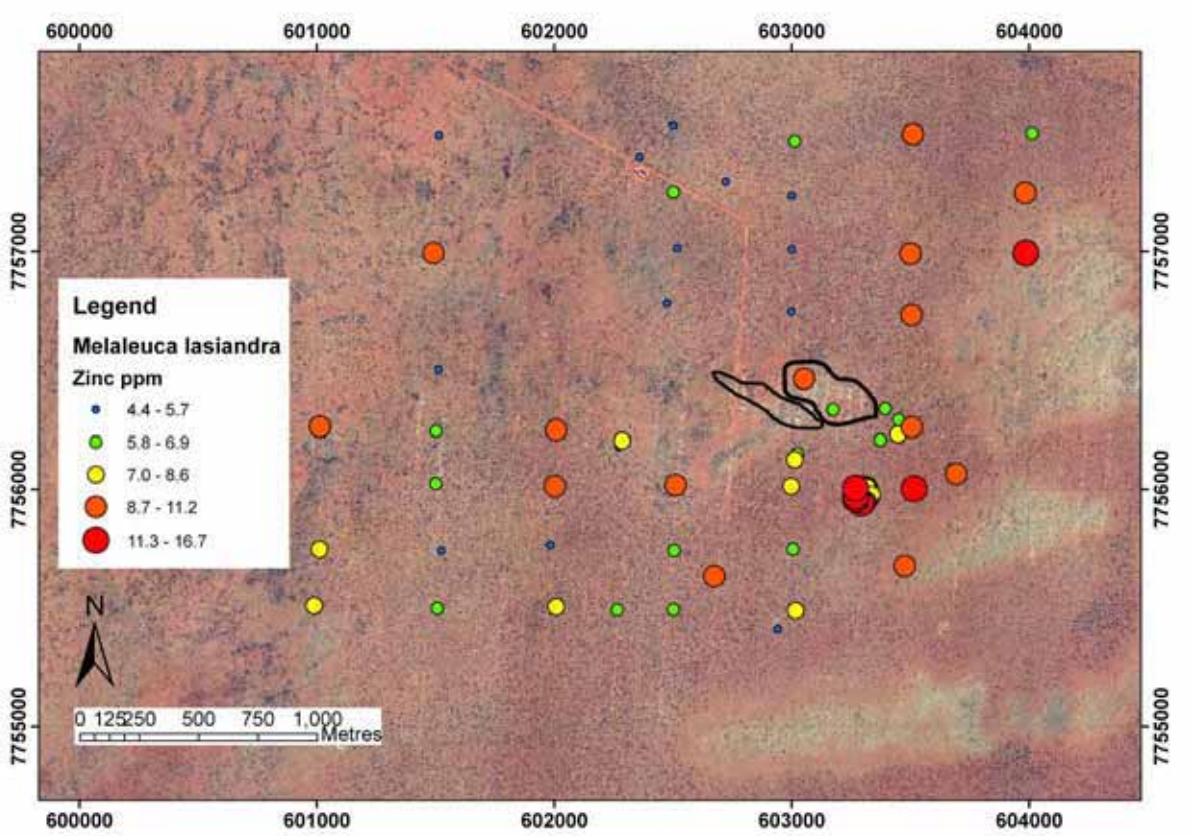

Figure 5.77: Plots of Zn concentration for *Melaleuca lasiandra* overlying the orthophoto of the Titania Prospect.

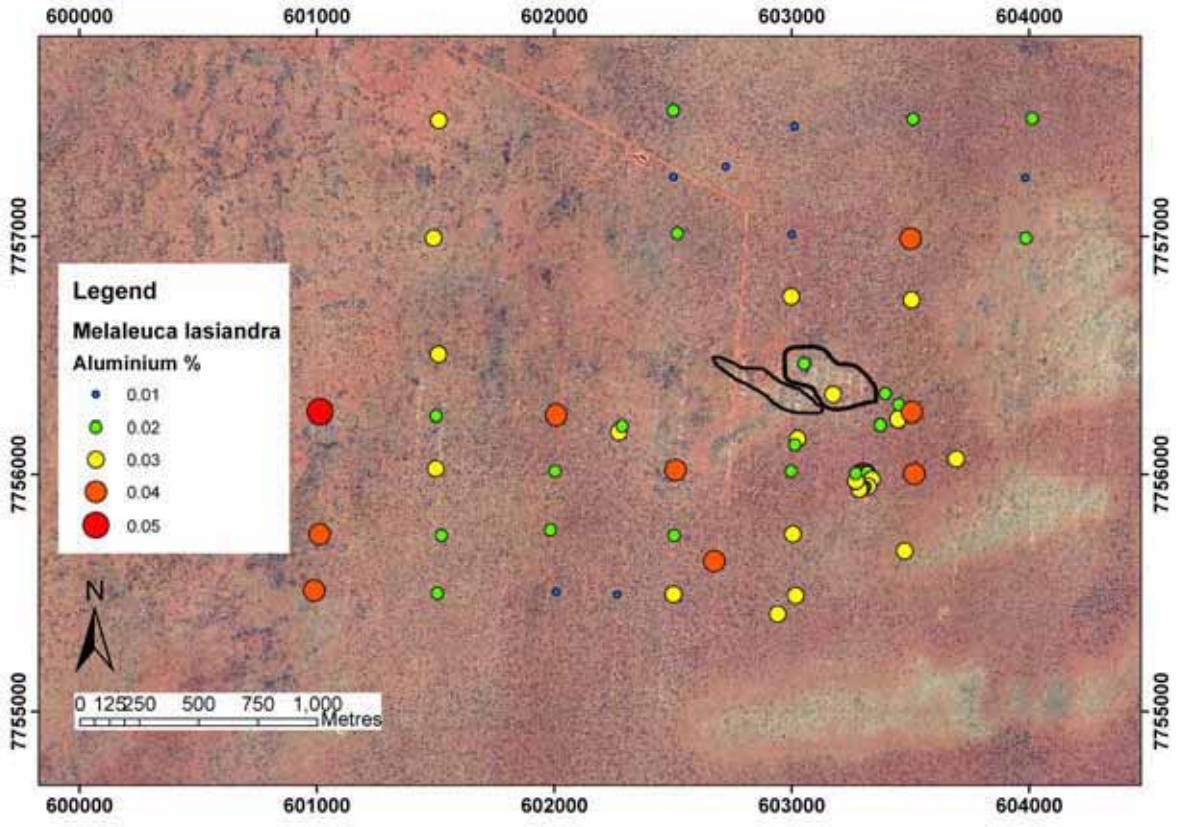

Figure 5.78: Plots of Al for *Melaleuca lasiandra* concentration overlying the orthophoto of the Titania Prospect.

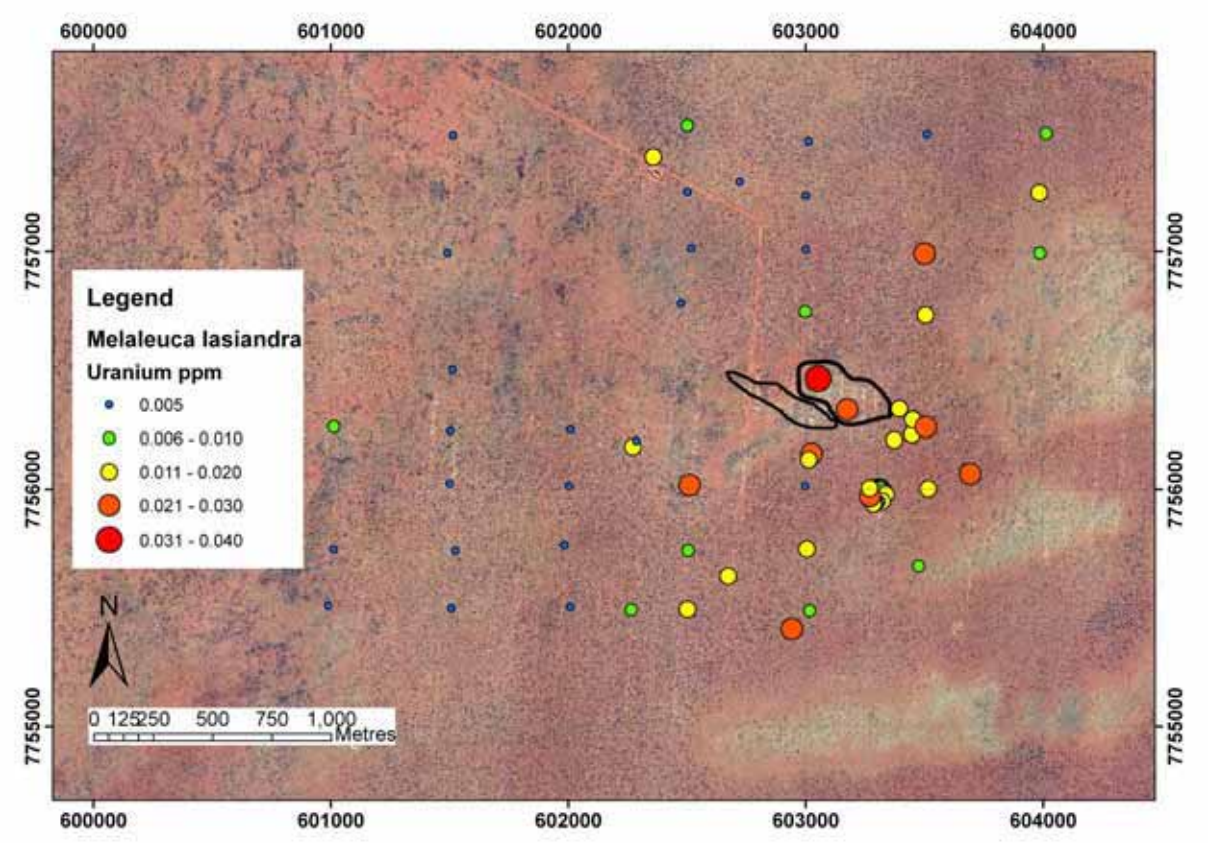

Figure 5.79: Plots of U for *Melaleuca lasiandra* concentration overlying the orthophoto of the Titania Prospect.

The biogeochemical assay results for *Melaleuca lasiandra* leaves show similar trends to the spinifex results. An exceptionally high, elevated Au assay corresponds to directly over mineralisation (Figure 5.75, 3.4 ppb, 1 point). A zone of high As assays occurs over mineralisation and up to 500 m to the south-east (Figure 5.74, 1.7 ppm). The zones of high Zn and S assays, however, are not centred over the mineralisation but instead are offset to the south-east. Zinc has a maximum assay of 16.7 ppm and within a 1 km by 1 km zone of high assays (Figure 5.77), and S (Figure 5.76) has a maximum assay of 0.47% within a 1 km by 1.5 km zone of high assays. The distribution of *Melaleuca lasiandra* plants was more restricted than that of the spinifex, resulting in gaps within its sampling grid. The distribution of these plants was closely associated with low lying parts of the landscape, such as depositional plains, dune swales and the margins of clay pans.

The biogeochemical expression of mineralisation is dispersed towards the south-east and is more pronounced within the multi-element suite. Also, U, which was elevated over mineralisation within the spinifex results, tends to reflect greater dispersion within the tea-tree results (Figure 5.79). Other elements that are not shown here, such as Cu, Pb and REE, show similar trends to the As results, which aid in expressing the mineralisation. Elements typically associated with detrital contamination, such as Al, Fe, Ti and Zr, all had low concentrations and were evenly distributed across the field site (Figure 5.78).

Discussion

Melaleuca lasiandra expresses the mineralisation as a primary zone of Au and As directly over the mineralisation, but the Zn and S halos are dispersed towards the south-east in the direction of groundwater flow towards the major palaeodrainage system, since the S (as sulphate) would be moving within the groundwater (Kirste, 2007). This indicates that this species is being influenced both by the elements relating to the primary mineralisation and dispersion towards the palaeodrainage system, most likely as groundwater dispersion.

Both *Triodia pungens* and *Melaleuca lasiandra* can detect primary mineralisation through up to 15 m of transported cover materials with a sample spacing of 250 m. While they both have proven to be most effective at detecting the known mineralisation extents in this area, *Melaleuca lasiandra* has a more restricted distribution due to its growth preferences. Therefore the implication is to use spinifex as a biogeochemical sampling medium in areas of thick transported cover and this can be used at spacings of 50 to 250 m without diminished expression.

5.4.4 *Melaleuca glomerata* (inland paperbark)

Melaleuca glomerata had a limited distribution over the field site, mostly restricted to areas of thicker cover and higher water content. The inland paperbark results show 4 distinct elemental patterns from the data:

1. Elements that are elevated over the mineralisation (As, Au, B, Cr, Cu, Ge, Nb, Ni, Pb, S, Sb, Se, Sn, Ta and U);
2. Elements less abundant over mineralisation (Ba and Cd);
3. Elements elevated to the south-east (Ag, Al, Ca, K, Li, Mg, Mo, Na, P and Zn); and,
4. Elements elevated to the north-west (La, Rb, Sr, Th, Tl and Y).

There are also elements that are irregularly distributed (Ce, Co, Cs, Fe, Hf, Hg, Mn, Re, Ti, V and Zr). Elements that were below analytical detection limit were Be, Bi, Ga, In, Pd, Pt, Sc, Te and W.

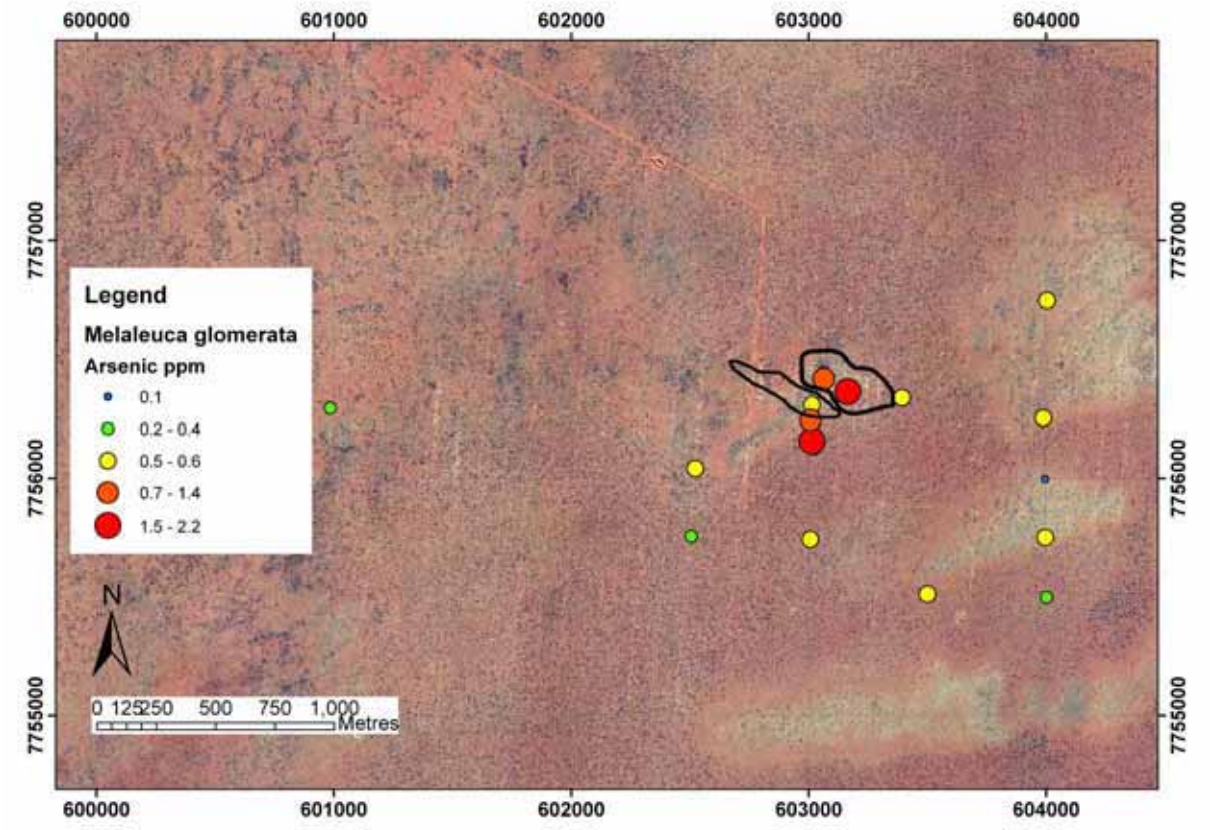

Figure 5.80: Plots of As concentration for *Melaleuca glomerata* overlying the orthophoto of the Titania Prospect.

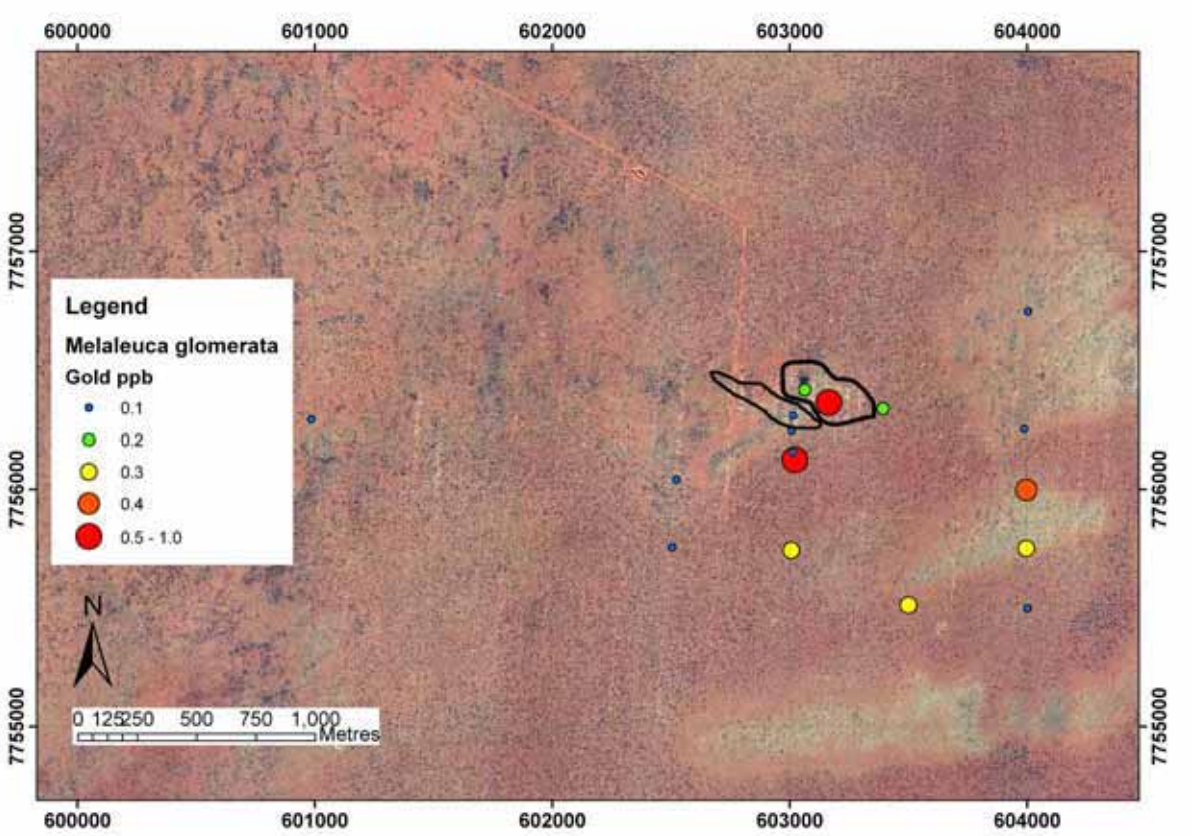

Figure 5.81: Plots of Au concentration for *Melaleuca glomerata* overlying the orthophoto of the Titania Prospect.

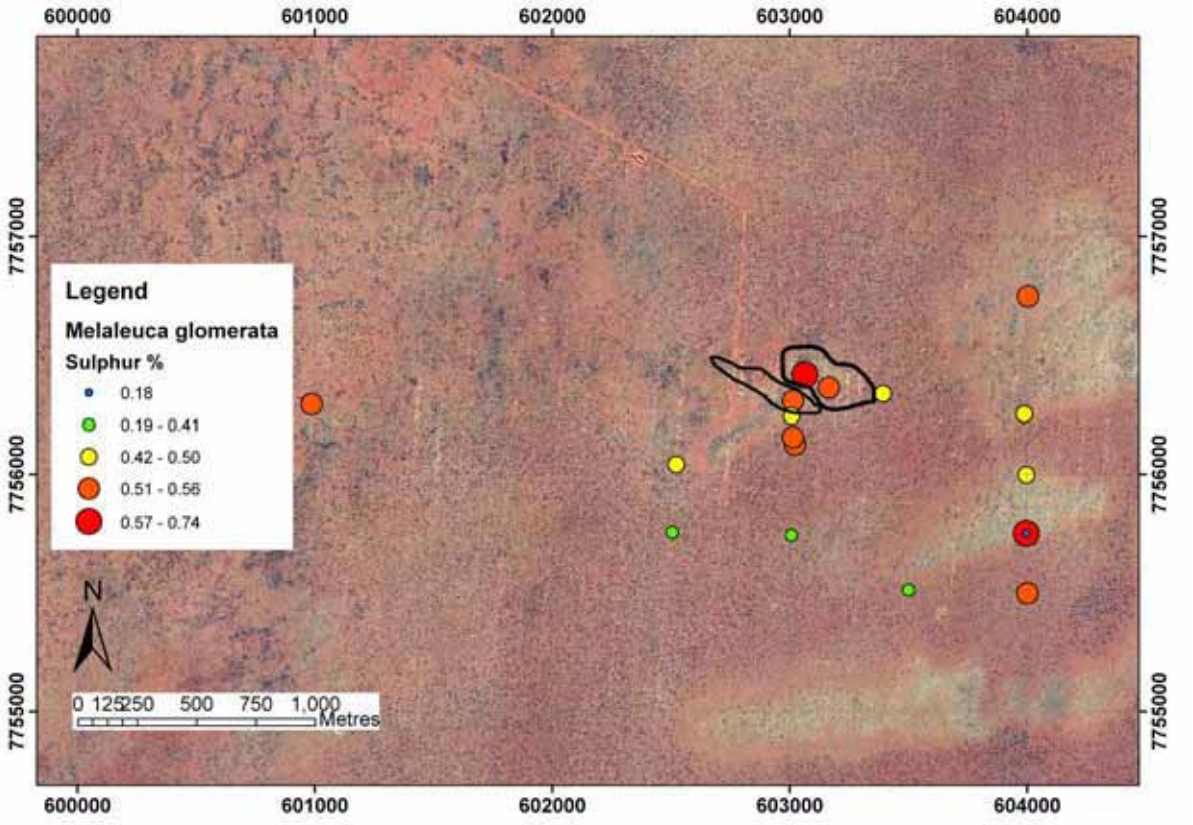

Figure 5.82: Plots of S concentration for *Melaleuca glomerata* overlying the orthophoto of the Titania Prospect.

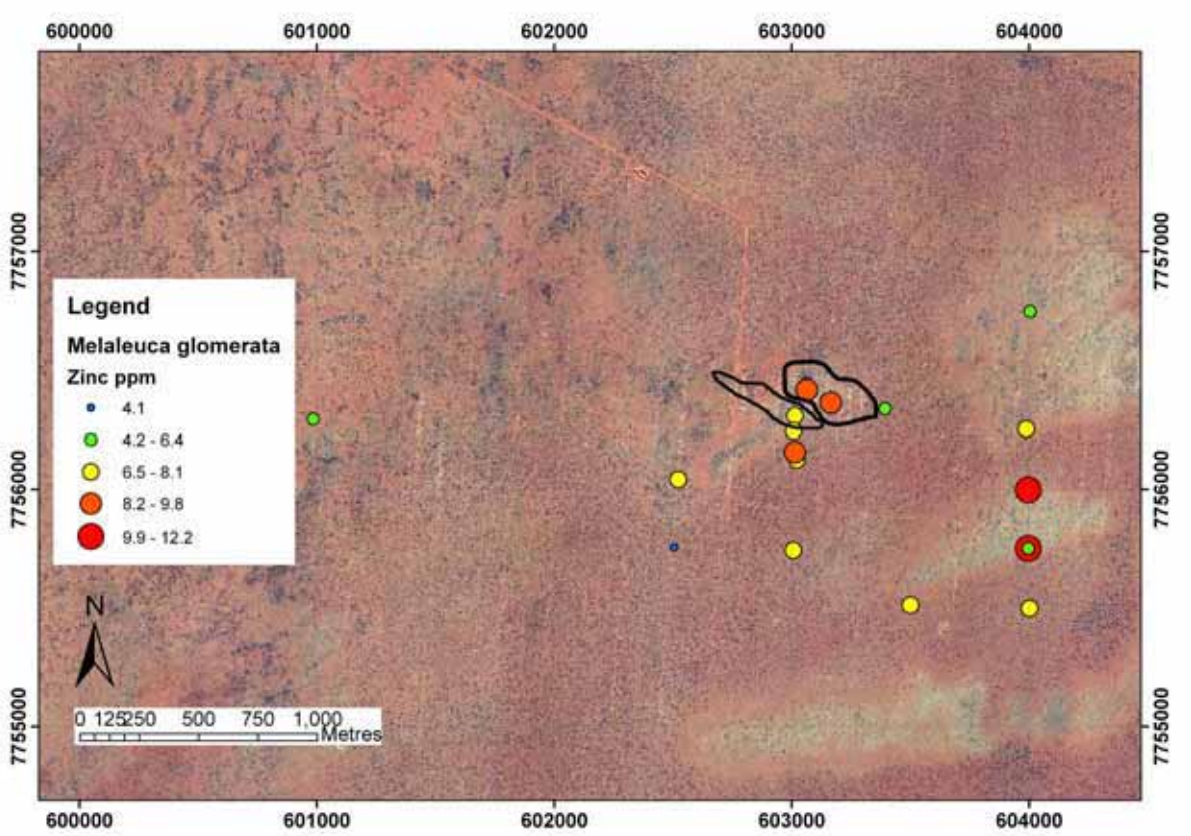

Figure 5.83: Plots of Zn concentration for *Melaleuca glomerata* overlying the orthophoto of the Titania Prospect.

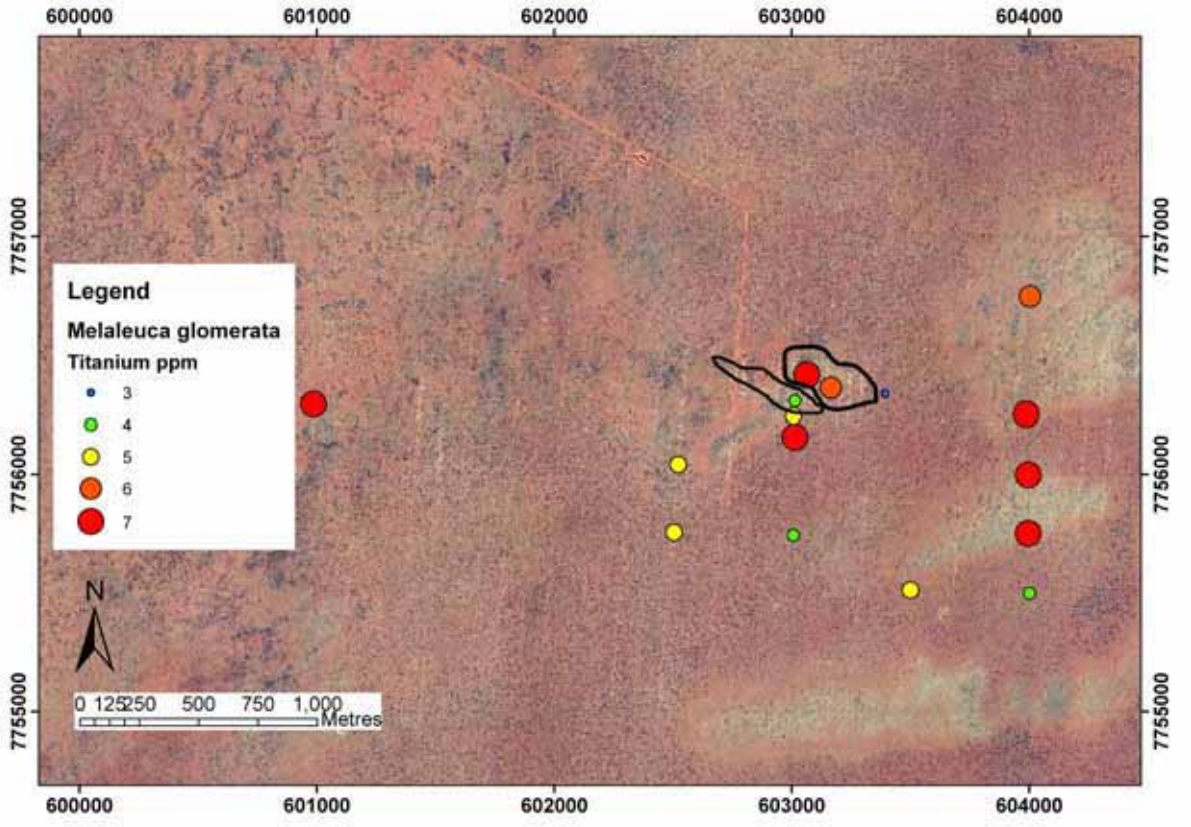

Figure 5.84: Plots of Ti concentration for *Melaleuca glomerata* overlying the orthophoto of the Titania Prospect.

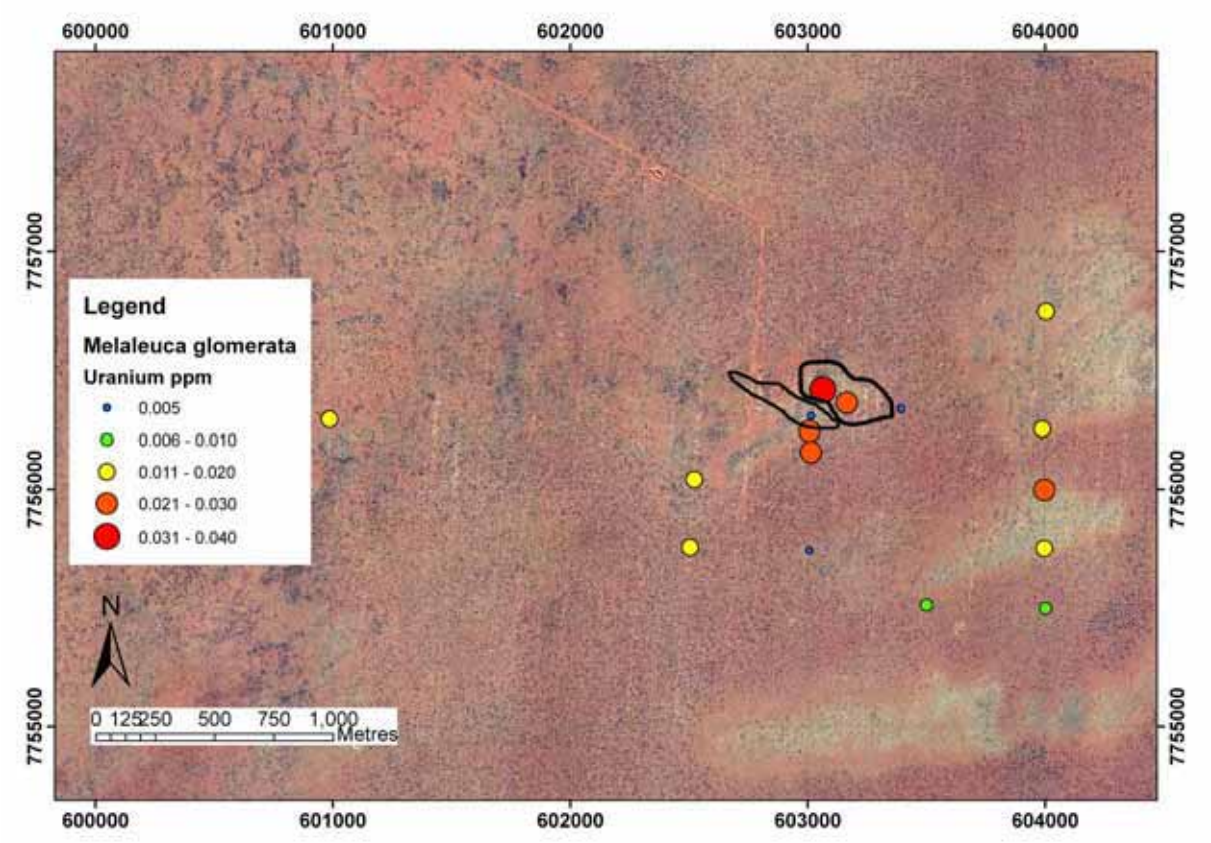

Figure 5.85: Plots of U concentration for *Melaleuca glomerata* overlying the orthophoto of the Titania Prospect.

The highest assay values of Au, and As are from samples directly over the zone of mineralisation (Figures 5.80 and 5.81). Even with the limited distribution of this species those trends are prominent. The Zn and S assays correspond to the same trend as those of the soft spinifex and the sandhill tea-tree, assays with moderately high values over the mineralisation and high values to the south-east of the mineralisation (Figures 5.82 and 5.83). The U results (Figure 5.85), are more closely related to those of the soft spinifex, showing high values over the mineralisation. This species also had a greater potential for detrital contamination than *Melaleuca lasiandra* (Figure 5.84). This is partially due to the species growing on lower lying areas that collect more wind blown dust and were hardest hit by the fire, but also this species typically has a cathedral termite mound growing in the centre of it, providing a local source of detrital particles.

5.4.5 *Acacia bivenosa* (two-nerved wattle)

The two-nerved wattle results show 4 distinct elemental patterns:

1. Elements that are elevated over the mineralisation (As, Ca, Cd, Co, Hf, Mo, Pb, Ta and U);
2. Elements in low abundance over mineralisation (Au, Hg and Na);
3. Elements elevated to the south-east (Ce, Cr, Fe, La, Mn, Nb, Re, Ti and Y); and,
4. Elements anomalous to the north-west (Ag, Cs, Li, Rb, Te and Tl).

There are also elements that are irregularly distributed (Al, B, Ba, Cu, Ge, K, Mg, Ni, P, S, Sb, Se, Sr, Th, Zn and Zr). Elements that were below analytical detection limit were Be, Bi, Ga, In, Pd, Pt, Sc, Sn, V and W.

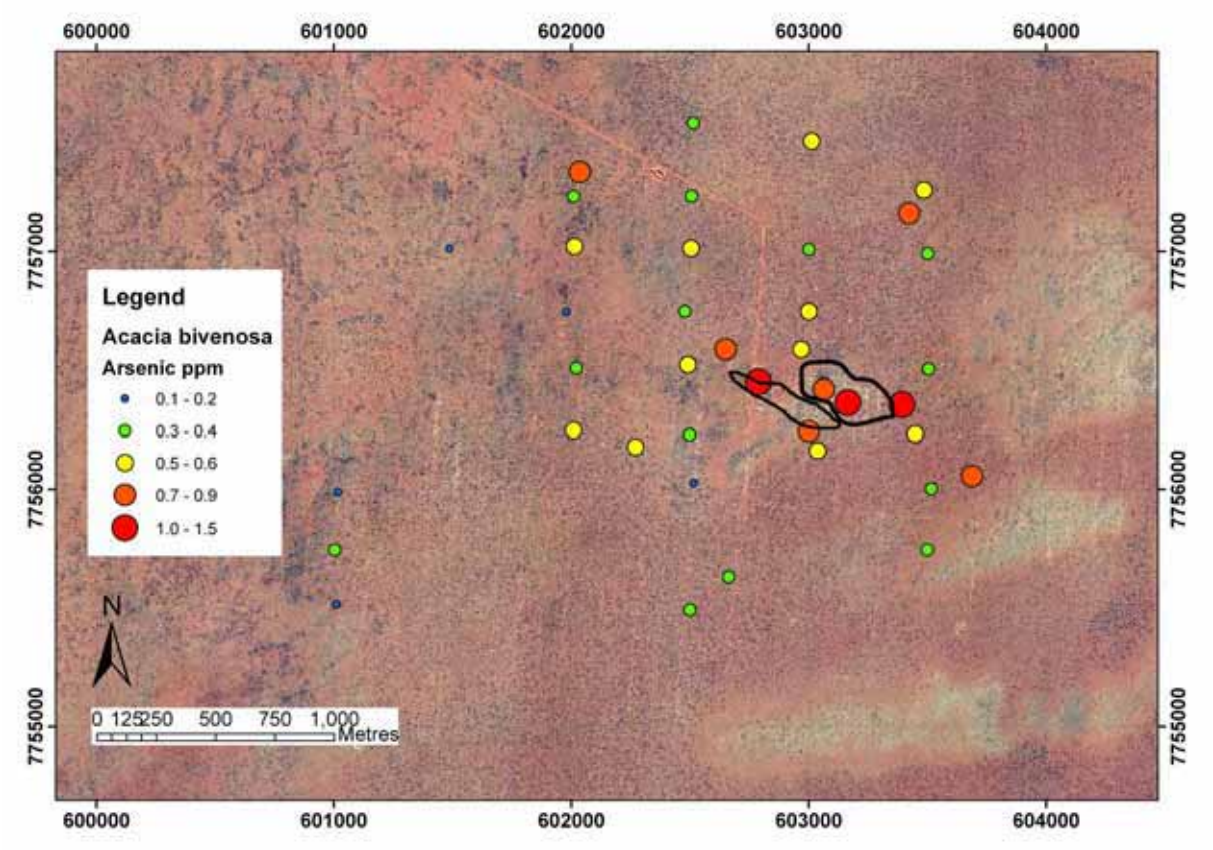

Figure 5.86: Plots of As concentration for *Acacia bivenosa* overlying the orthophoto of the Titania Prospect.

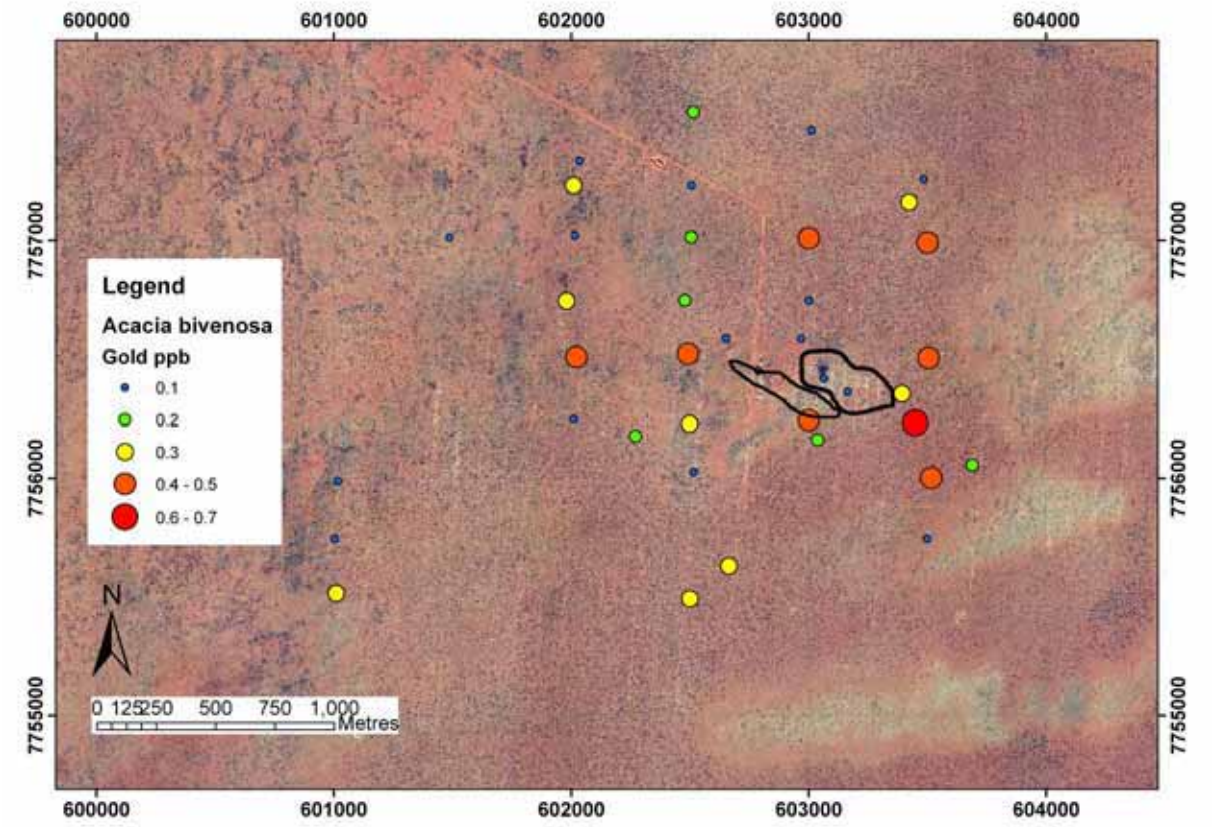

Figure 5.87: Plots of Au concentration for *Acacia bivenosa* overlying the orthophoto of the Titania Prospect.

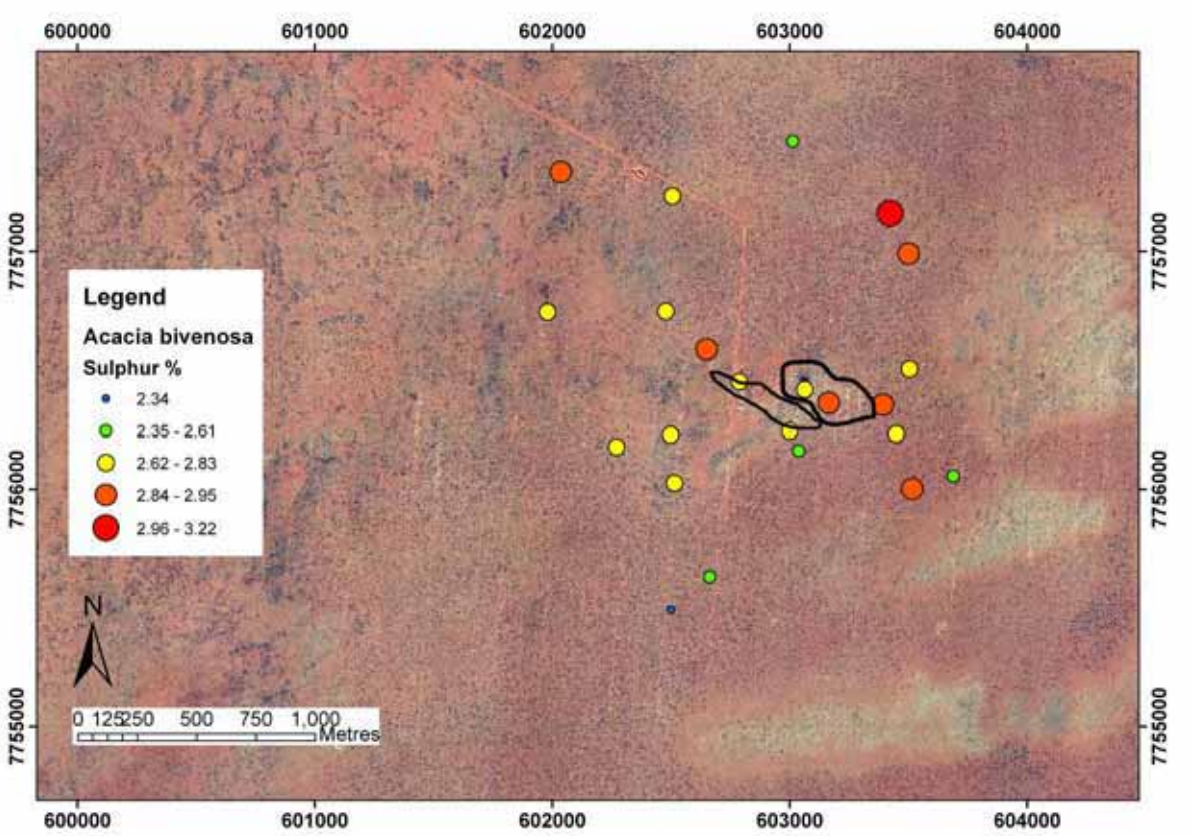

Figure 5.88: Plots of S concentration for *Acacia bivenosa* overlying the orthophoto of the Titania Prospect.

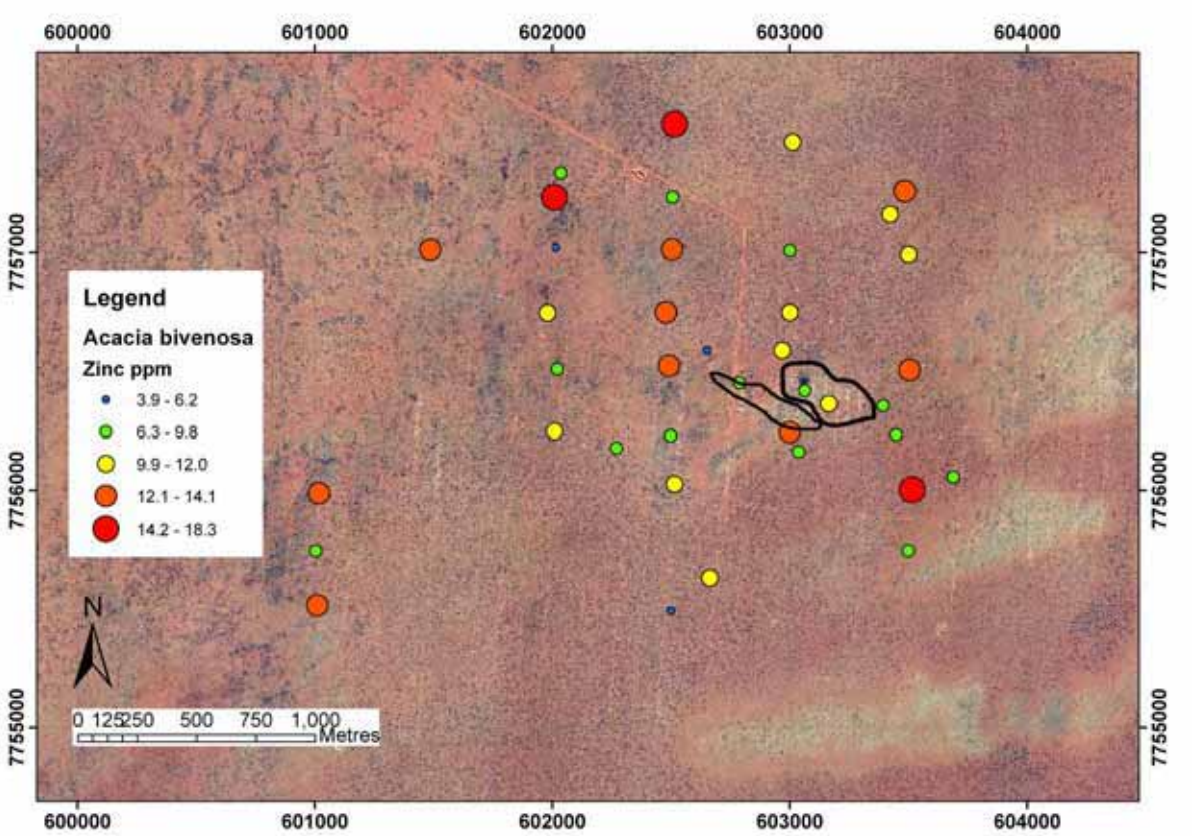

Figure 5.89: Plots of Zn concentration for *Acacia bivenosa* overlying the orthophoto of the Titania Prospect.

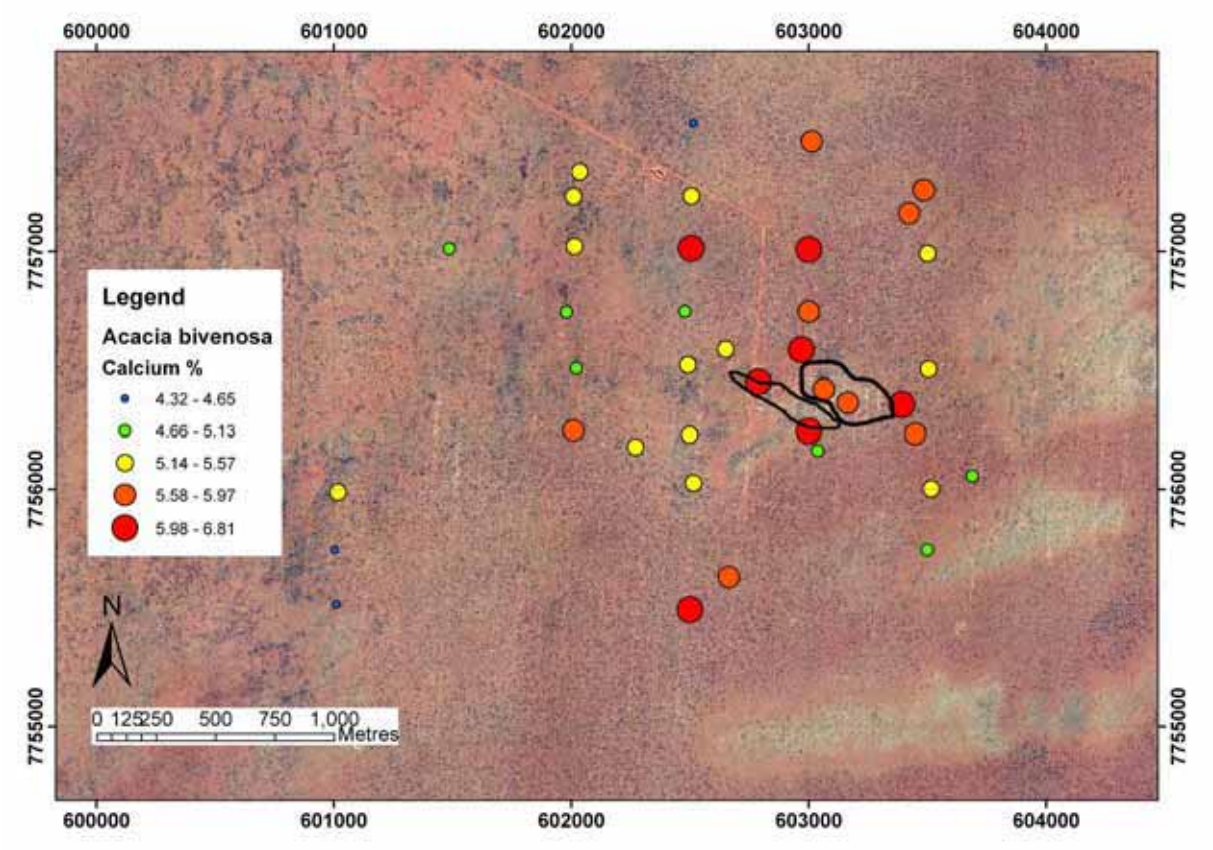

Figure 5.90: Plots of Ca concentration for *Acacia bivenosa* overlying the orthophoto of the Titania Prospect.

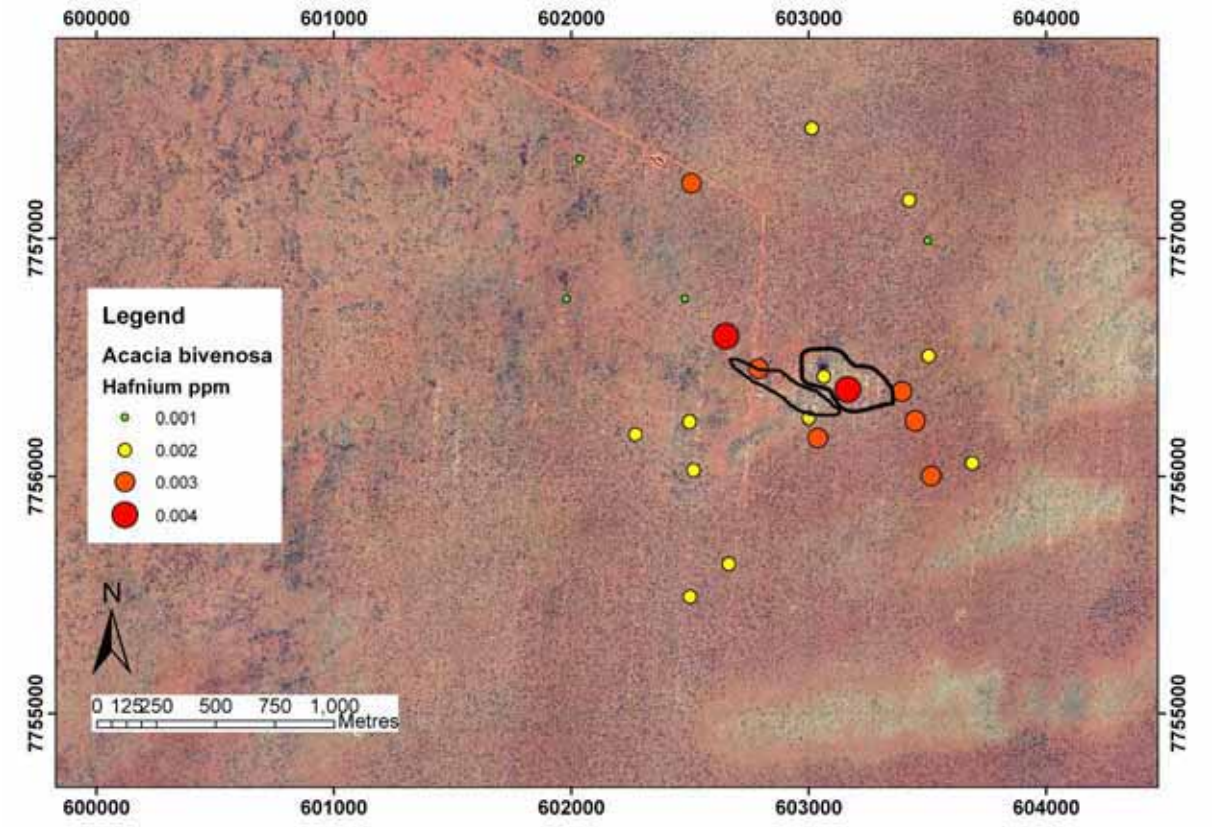

Figure 5.91: Plots of Hf concentration for *Acacia bivenosa* overlying the orthophoto of the Titania Prospect.

The chemical composition of the *Acacia bivenosa* phyllodes constrained a zone of moderately elevated Au assays (maximum 0.7 ppb) up to 1 km away from the mineralisation in all directions (Figure 5.87). The zone of high As assays (maximum 1.5 ppm) spatially corresponds with the 800 m wide zones defined for both the *Triodia* and *Melaleuca* assays (Figure 5.86). The spatial patterns for Zn and S assays for *Acacia bivenosa* however, are very different than for the other two plant species. High assays for both elements plot as a zone radiating from the mineralisation zone: Zn (Figure 5.89) with 18.3 ppm, 1.5 km by 1.5 km, and S (Figure 5.88) with 3.22%, 1.5 km by 1.5 km.

Other results of significance for this species focus on the higher amounts of Ca, Sr and S that is taken up (Figure 5.90). This will be addressed in greater detail in the species differences section; however, the spatial patterns for these elements do not show any relationship to the other plant species. *Acacia bivenosa* emphasises high values radiating from the centre of the grid, the other species tend to show south-easterly dispersion patterns indicating another process must influence the uptake of these elements.

The potential for detrital contamination of this species is generally low, as shown by the Hf results (Figure 5.91). This is most likely because it is a fast growing and shallow rooted plant with thick waxy phyllodes which would collect minimal dust.

Discussion

Acacia bivenosa represents the mineralisation within the Au and As results in a similar manner to the other two species. It shows a different dispersion pattern within the Zn and S results with these elements dispersed evenly in all directions away from the mineralisation zone. This indicates that these results are not being influenced by the dispersion towards the palaeodrainage system. This dispersion pattern is more closely linked to the surface flow patterns and the generation of gypsum at the surface of the soil which was observed at the site (Figure 5.92), however there was no soil chemistry or mineralogy to support this as S is difficult to analyse through ICP-MS in soils and XRF samples were not run. If the Au and As anomaly of this species is linked to a surface dispersion pattern then this anomaly must be from either drill spoil or a naturally occurring surficial expression possibly related to biogeochemical element cycling from depth and to the surface. This surficial signature is supported by this species having many shallow lateral roots.

Figure 5.92: Gypsum crystals precipitated onto the soil surface near the turkeys nest at the Titania prospect.

All plant species examined were able to provide a variably focussed expression to the mineralisation using the multi-element haloes discussed above. However, *Acacia bivenosa* is shallow rooted and displayed an obvious surface dispersion pattern that may be correlated with drill spoil seen in the area. Hence this species would not be an ideal sampling medium for penetrative mineral exploration.

5.4.6 *Acacia coriacea ssp. sericophylla* (dogwood)

Acacia coriacea is a very common species across the Tanami region and over the Titania prospect. The limitations to its distribution are where the cover is too thin (north-west corner of the grid) and where the subsurface is highly saline (south-east). The dogwood results show 4 distinct elemental patterns:

1. Elements that are elevated to the north (As, Ba, Ca, Cd, Cu, Hg, Li, Sn, Sr, Ta, Te, Tl and U);
2. Elements in low abundance to the south (Mo and P);
3. Elements elevated to the east (Mn, Na, Nb and Se); and,
4. Elements anomalous to the west (Al, Ce, Cs, K, Pb, Rb, T and Zr).

There are also elements that are irregularly distributed (Au, B, Co, Cr, Fe, Ge, Hf, La, Mg, Ni, Re, S, Sb, Sc, Th, V and Zn). Elements that were below analytical detection limit were Ag, Be, Bi, Ga, In, Pd, Pt, W and Y.

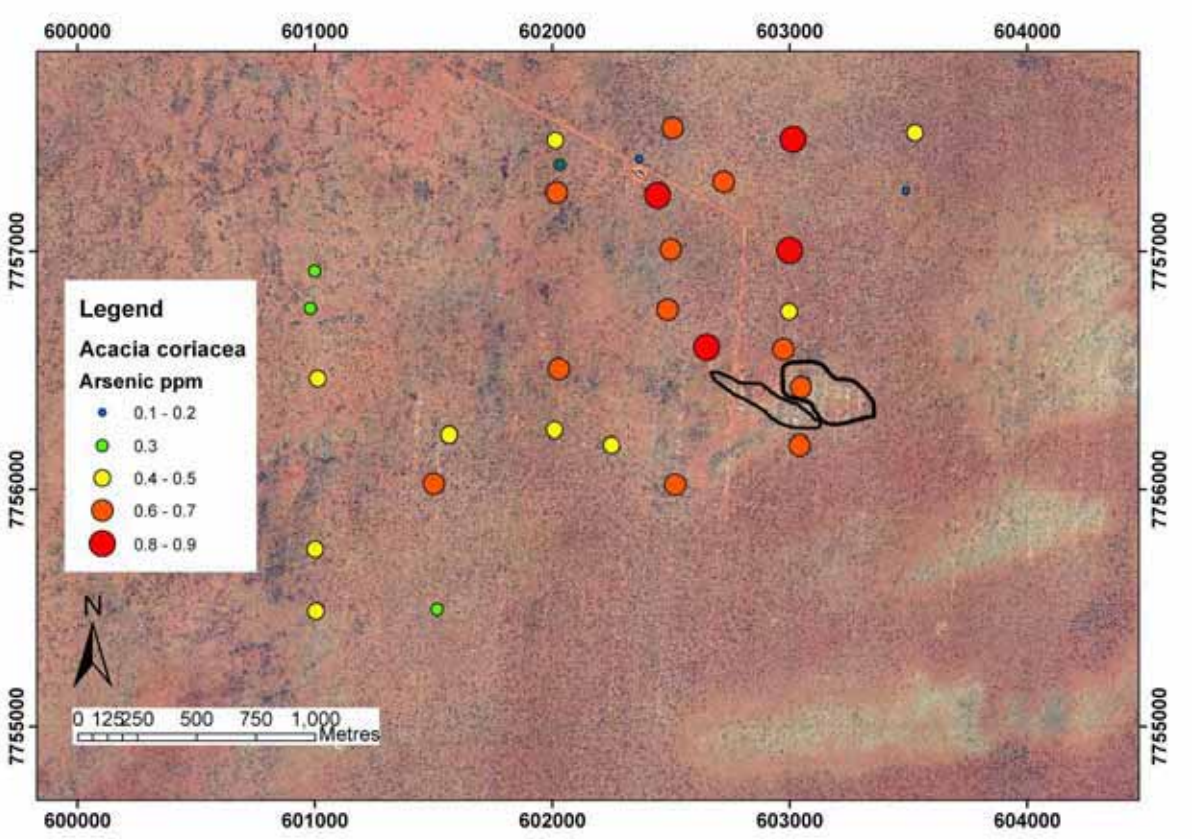

Figure 5.93: Plots of As concentration for *Acacia coriacea* overlying the orthophoto of the Titania Prospect.

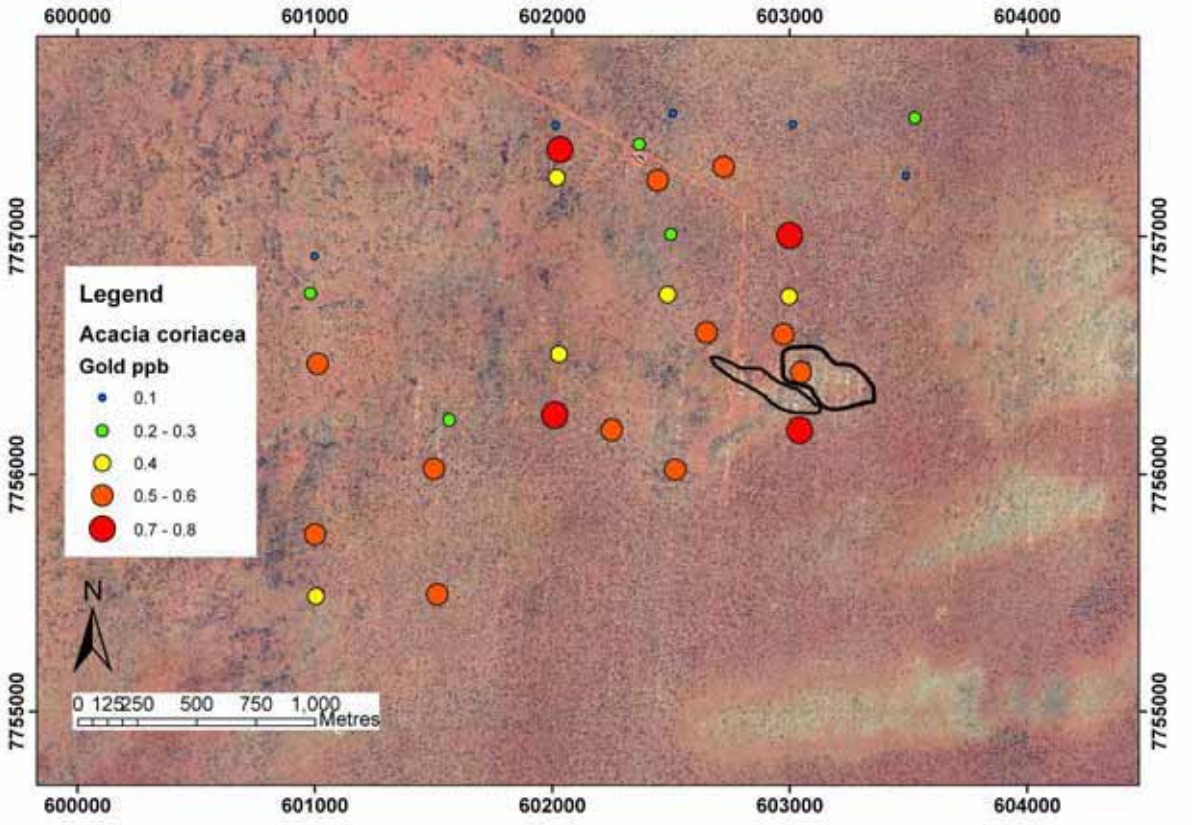

Figure 5.94: Plots of Au concentration for *Acacia coriacea* overlying the orthophoto of the Titania Prospect.

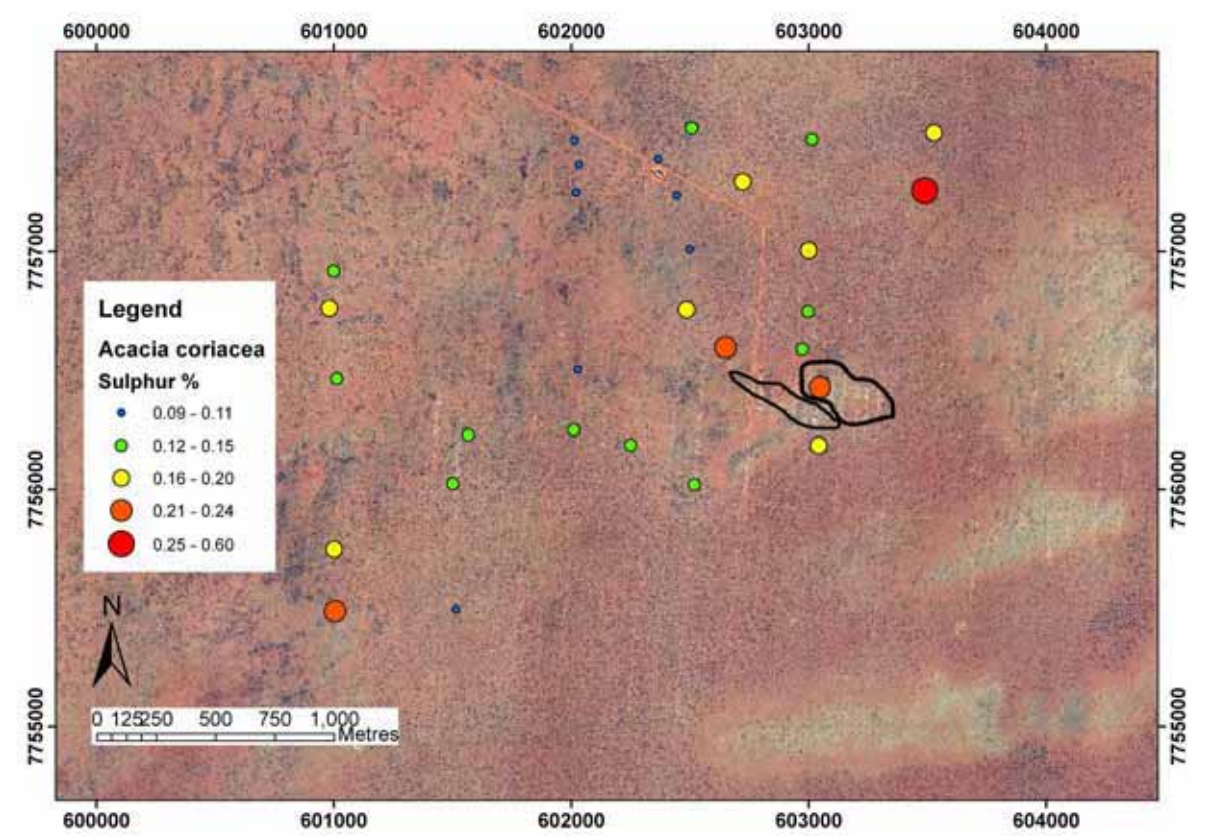

Figure 5.95: Plots of S concentration for *Acacia coriacea* overlying the orthophoto of the Titania Prospect.

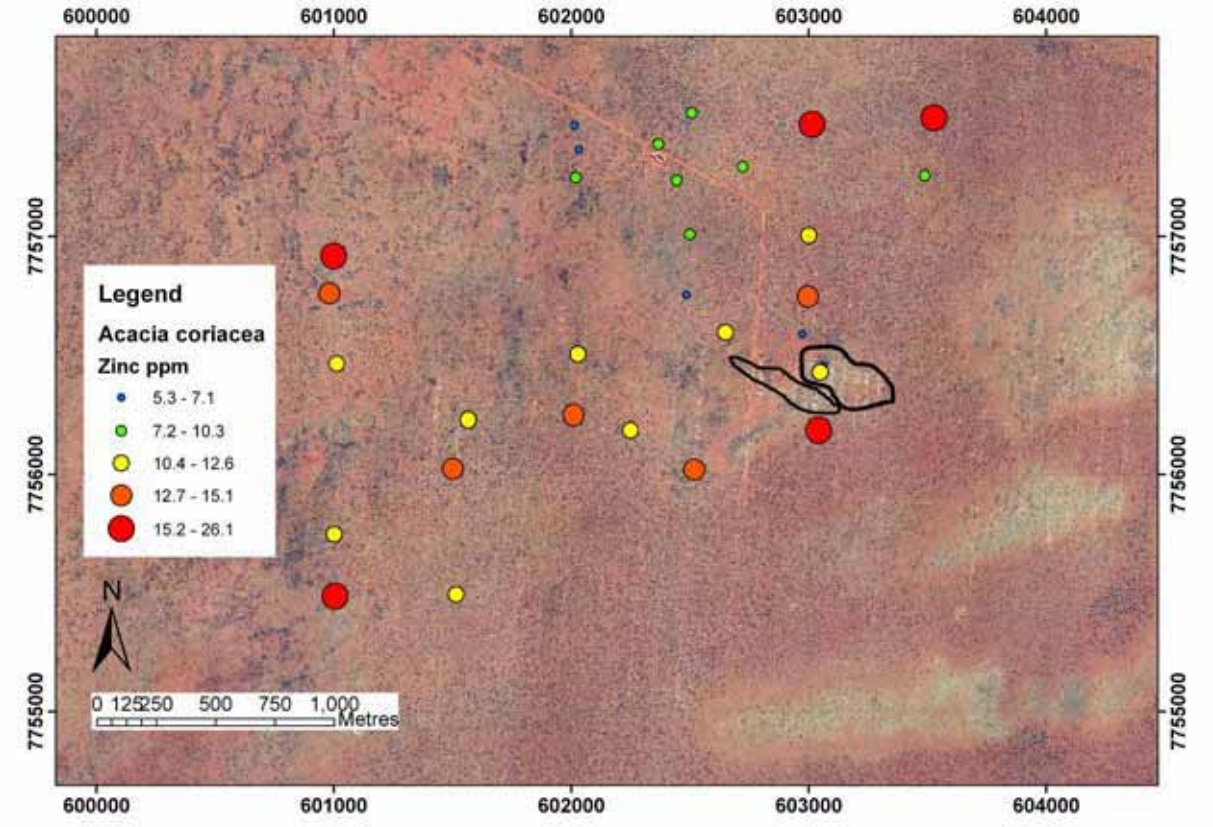

Figure 5.96: Plots of Zn concentration for *Acacia coriacea* overlying the orthophoto of the Titania Prospect.

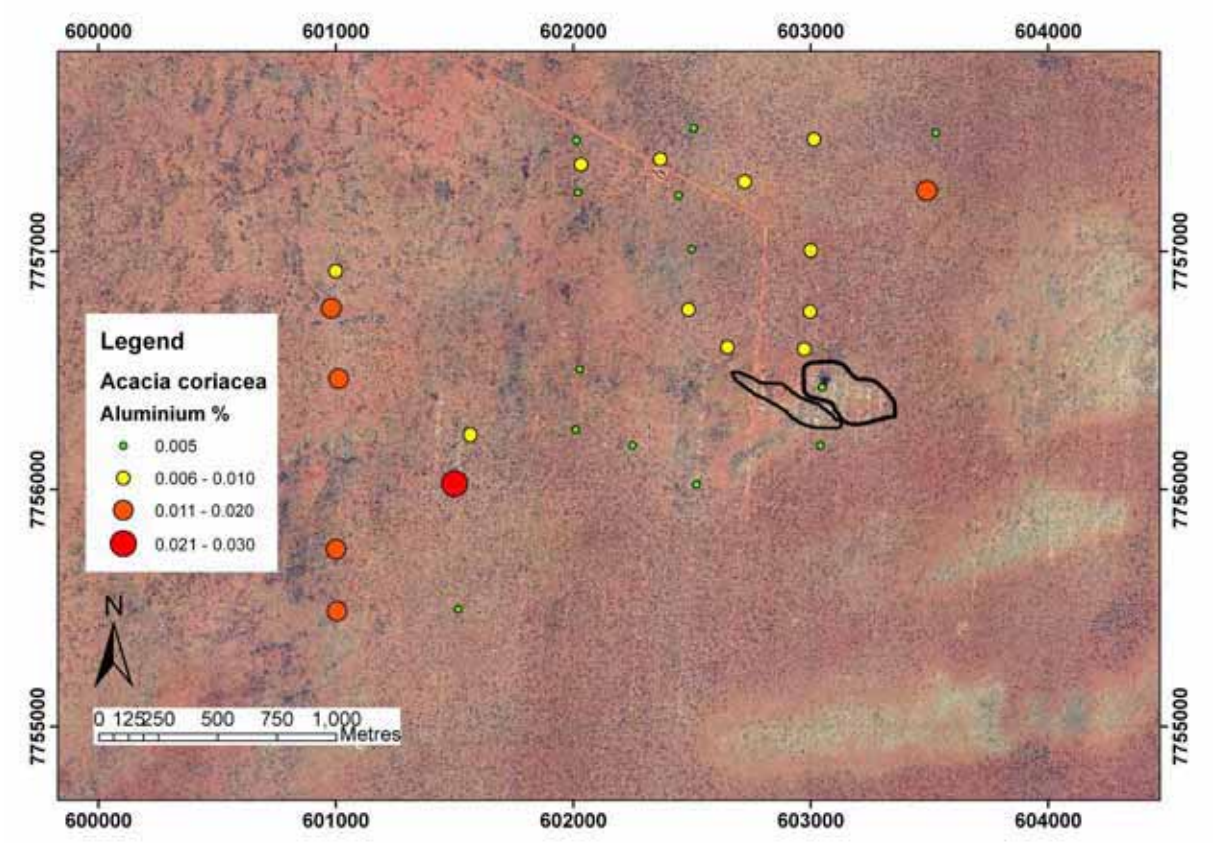

Figure 5.97: Plots of Al concentration for *Acacia coriacea* overlying the orthophoto of the Titania Prospect.

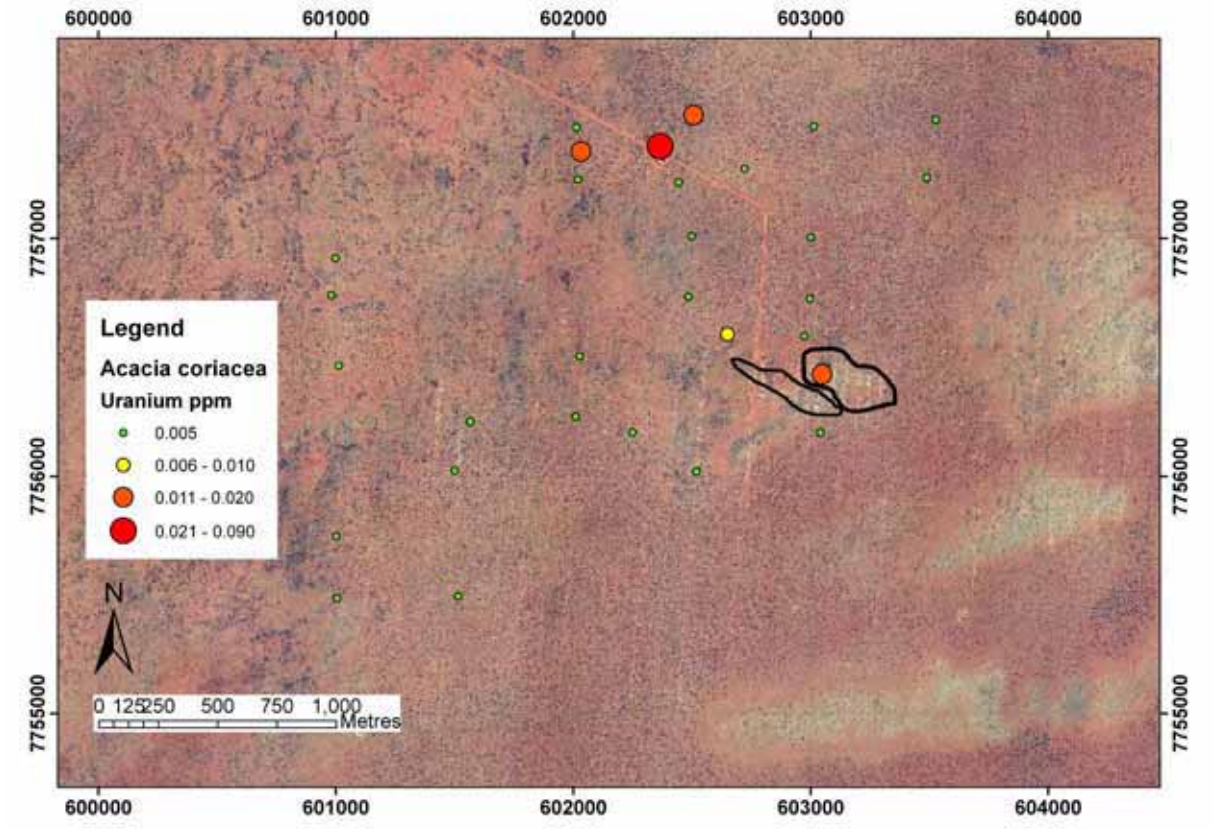

Figure 5.98: Plots of U concentration for *Acacia coriacea* overlying the orthophoto of the Titania Prospect.

The dogwood chemical results are the most difficult to interpret of all the plant species. There appears to be very little correlation between the chemical patterns of this species and any of the others. Most *Acacia* species of this form (tall, gnarled and long-lived) seem to

have a few surface lateral roots and a deep 'carrot-like' sinker root (Anand *et al.* 2007). The chemical characteristics are intermediate between the surface sampling of *Acacia bivenosa* and the deeper sampling of the soft spinifex and *Melaleuca* species. Elements do not appear to be directly associated with the mineralisation, however, there is a large zone of elevated Au and As around the centre of the grid (Figures 5.93 and 5.94). This zone is about 1 km wide and 1.5 km long (within the spacings of the grid) and S and Zn concentrations are in low abundance in this area (Figures 5.95 and 5.96).

Detrital contamination is minimal within all samples, as shown by the Al results (Figure 5.97). This would be due to the fire generating fresh, clean phyllodes and that they are generally waxy helping prevent dust build-up. The U results show a single detectable point over the mineralisation, but the largest value is next to the old exploration site office, which may be from contamination (Figure 5.98).

Discussion

Acacia coriacea does not seem to represent mineralisation within any of the multi-element suite. Similar to the results at the Hyperion Prospect, the dogwood samples contained the highest levels of REE, but the full suite was not sampled at this site. The distribution of this plant is also restricted in this terrain, which would indicate that this species would not be useful as a phyto-exploration sampling medium at any sampling scale.

5.4.7 *Corymbia opaca* (desert bloodwood)

Corymbia opaca had a very limited distribution over this site. There were only 8 plants in the area, but since the species was sampled at the Coyote Prospect, it was decided to sample it to see if there was correlation. *Eucalyptus/Corymbia* species do not appear to be able to tolerate either the increased water close to the palaeo-drainage system, or the increased salt content within the groundwater. The desert bloodwood results show 5 distinct elemental patterns:

1. Elements that are elevated over the centre (Al, As, B, Ca, Cd, Fe, Ge, Hf, Hg, Sb, Sr and U);
2. Elements elevated to the north (Ba, Cr, Cu, Li, Mo, P, Se, Ta, Ti, Tl and Zr);
3. Elements elevated to the south (Re and S);
4. Elements elevated to the east (Au, Pb and Zn); and,
5. Elements elevated to the west (Ce, Co, Cs, La and Rb).

There are also elements that are irregularly distributed (K, Mg, Mn, Na, Ni and Y). Elements that were below analytical detection limit were Ag, Be, Bi, Ga, In, Nb, Pd, Pt, Sc, Te, Th, V and W.

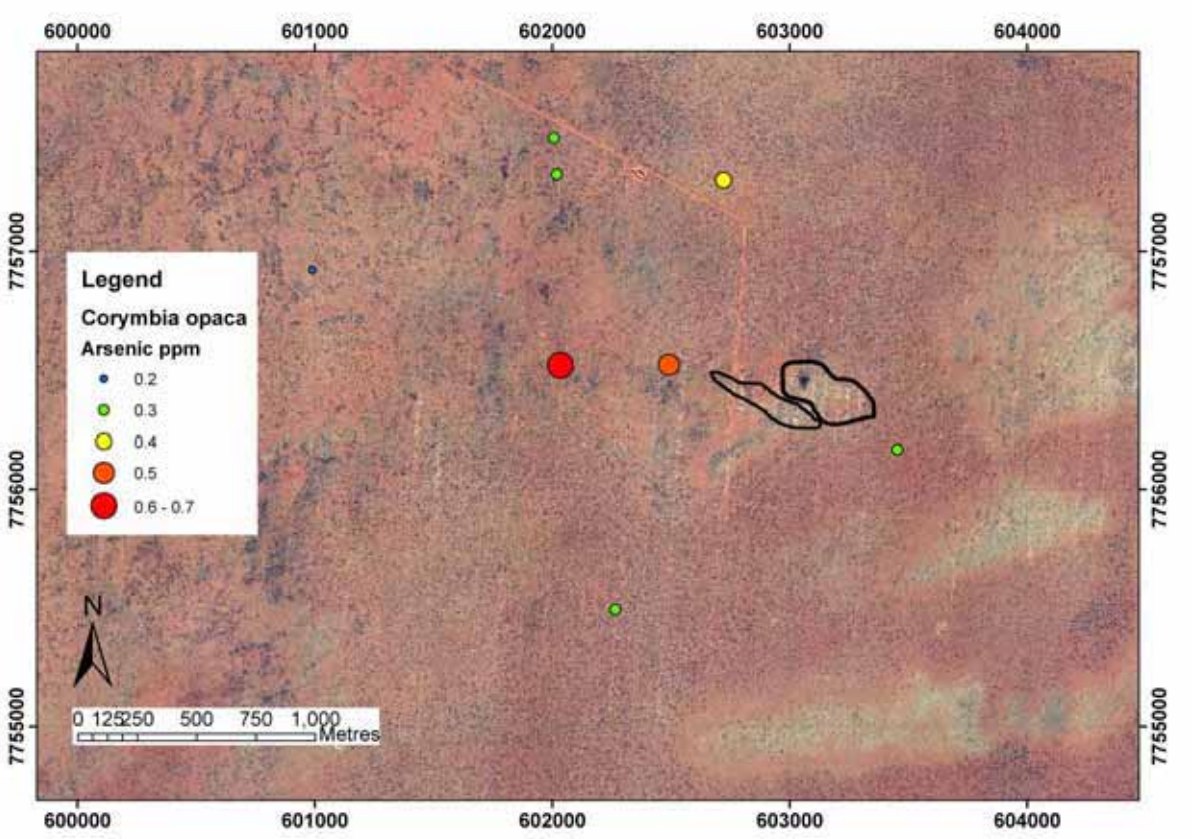

Figure 5.99: Plots of As concentration for *Corymbia opaca* overlying the orthophoto of the Titania Prospect.

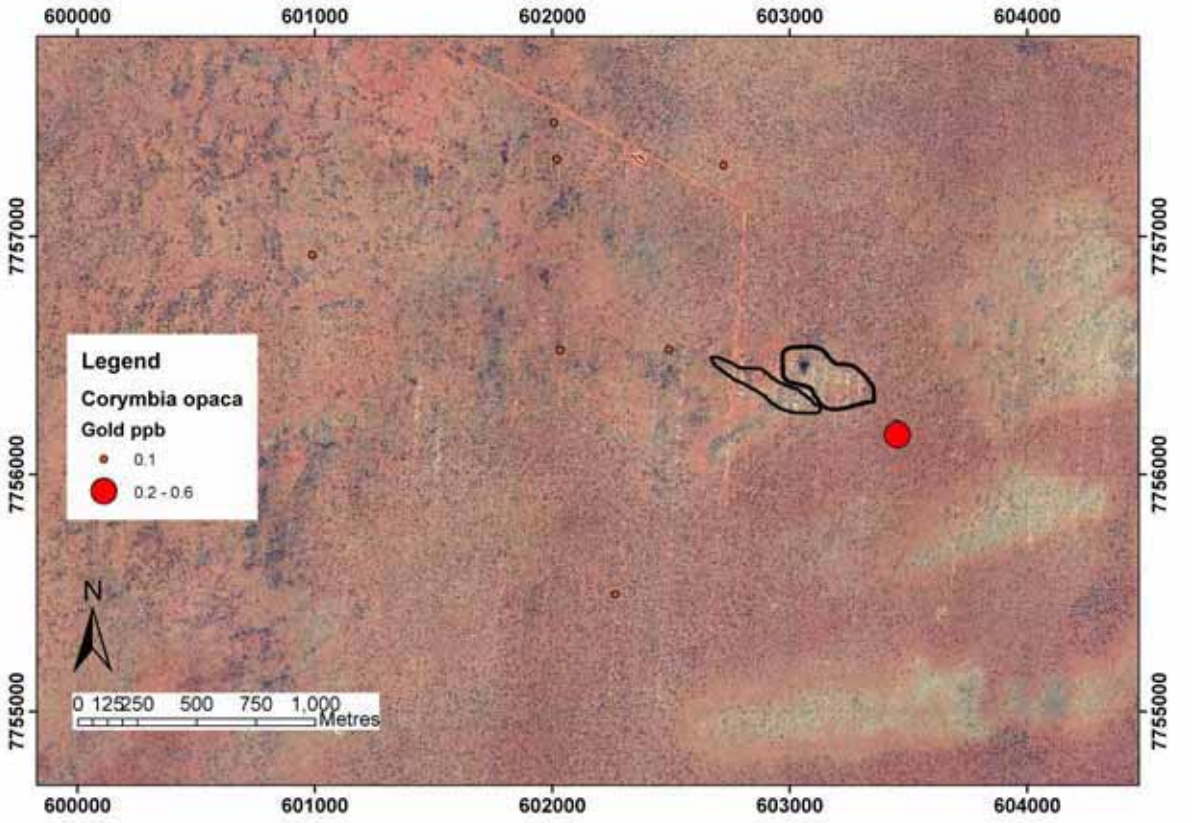

Figure 5.100: Plots of Au concentration for *Corymbia opaca* overlying the orthophoto of the Titania Prospect.

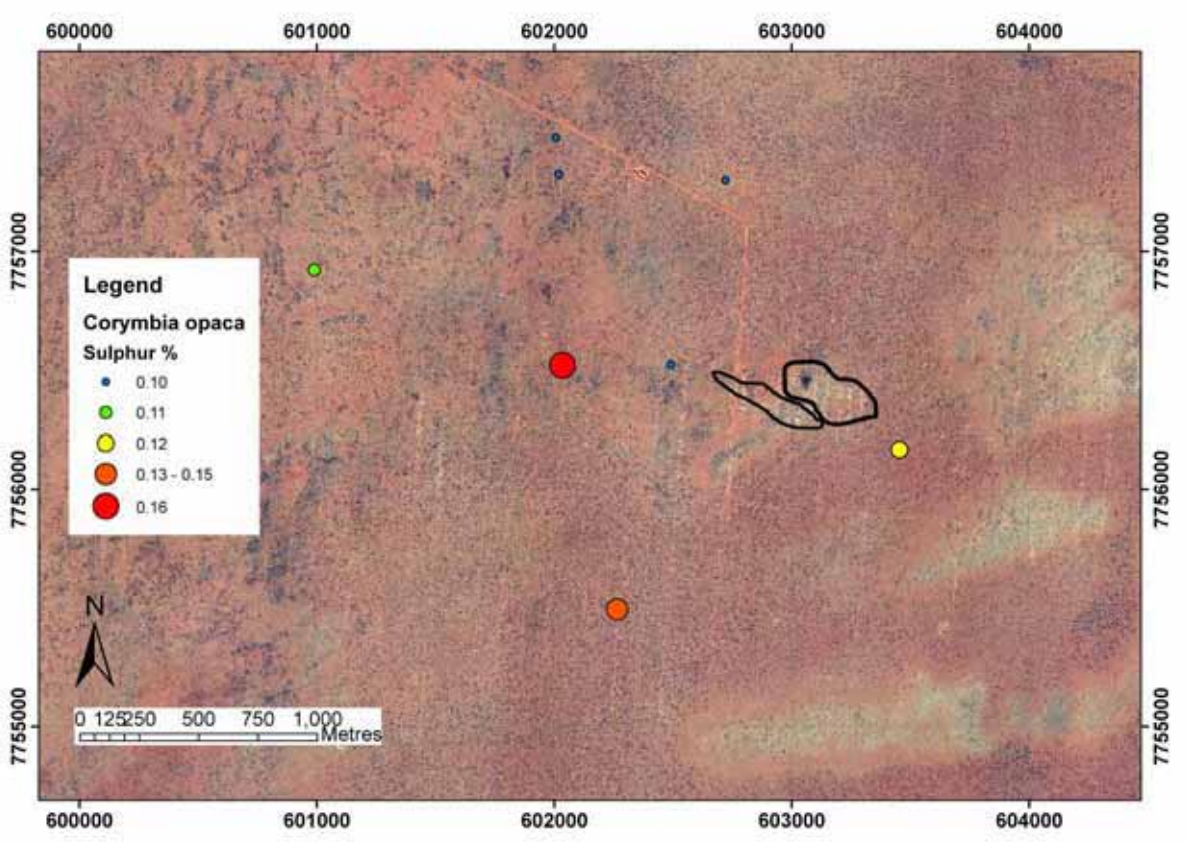

Figure 5.101: Plots of S concentration for *Corymbia opaca* overlying the orthophoto of the Titania Prospect.

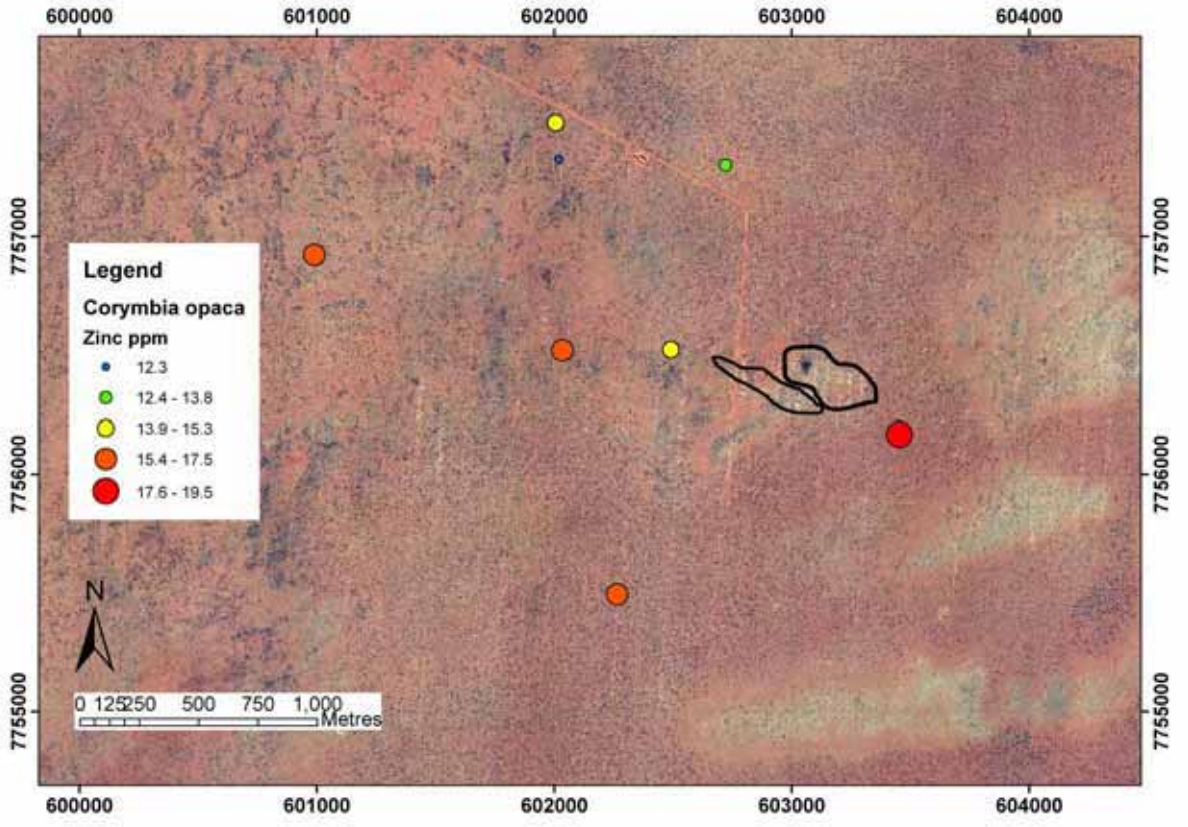

Figure 5.102: Plots of Zn concentration for *Corymbia opaca* overlying the orthophoto of the Titania Prospect.

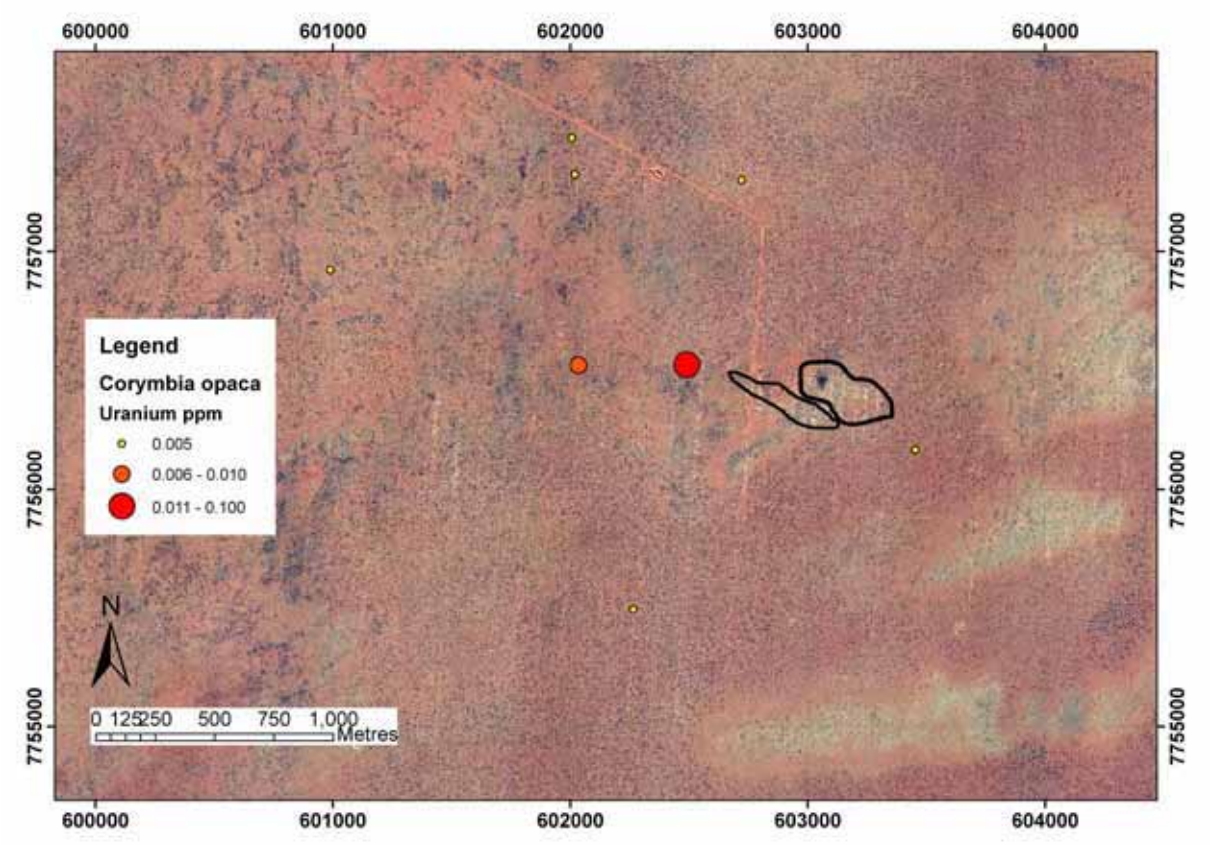

Figure 5.103: Plots of U concentration for *Corymbia opaca* overlying the orthophoto of the Titania Prospect.

Discussion

The significance of interpretations from this data set are limited, however, the highest Au and Zn values are from the south-east of the mineralisation showing the similar trend as the *Triodia* and *Melaleuca* species results (Figures 5.100 and 5.102). The As and U results are highest at the western margin of mineralisation (Figures 5.99 and 5.103), but S seems to be irregularly distributed (Figure 5.101).

The implications are that this species would not be an effective sampling medium where the cover thickness is great and/or the salinity of the subsurface/groundwater is high.

5.4.8 *Eucalyptus pachyphylla* (red-budded mallee)

Eucalyptus pachyphylla also had a very limited distribution over this field site. It was restricted to the far west of the grid where the cover was thinnest and there was sub-cropping ferricrete (Fe-oxide cemented gravels). Therefore the patterns generated in the data could not be directly related to the mineralisation. The red-budded mallee results show 3 distinct elemental patterns:

1. Elements that are elevated to the north (Ag, Ca, Ce, Co, La, Li, Rb, Y and Zn);
2. Elements elevated to the south (Au, Cd, Sb and U); and,
3. Elements elevated over the centre (Al, Cr. Cs, Fe, Mo, Pb, Sc, Th and Zr).

There are also elements that are irregularly distributed (As, B, Ba, Cu, Hf, Hg, K, Mg, Mn, Ni, P, Re, S, Sr, Ta, Ti and Tl). Elements that were below analytical detection limit were Be, Bi, Ge, Ga, In, Mo, Na, Nb, Pd, Pt, Se, Sn, Te, V and W.

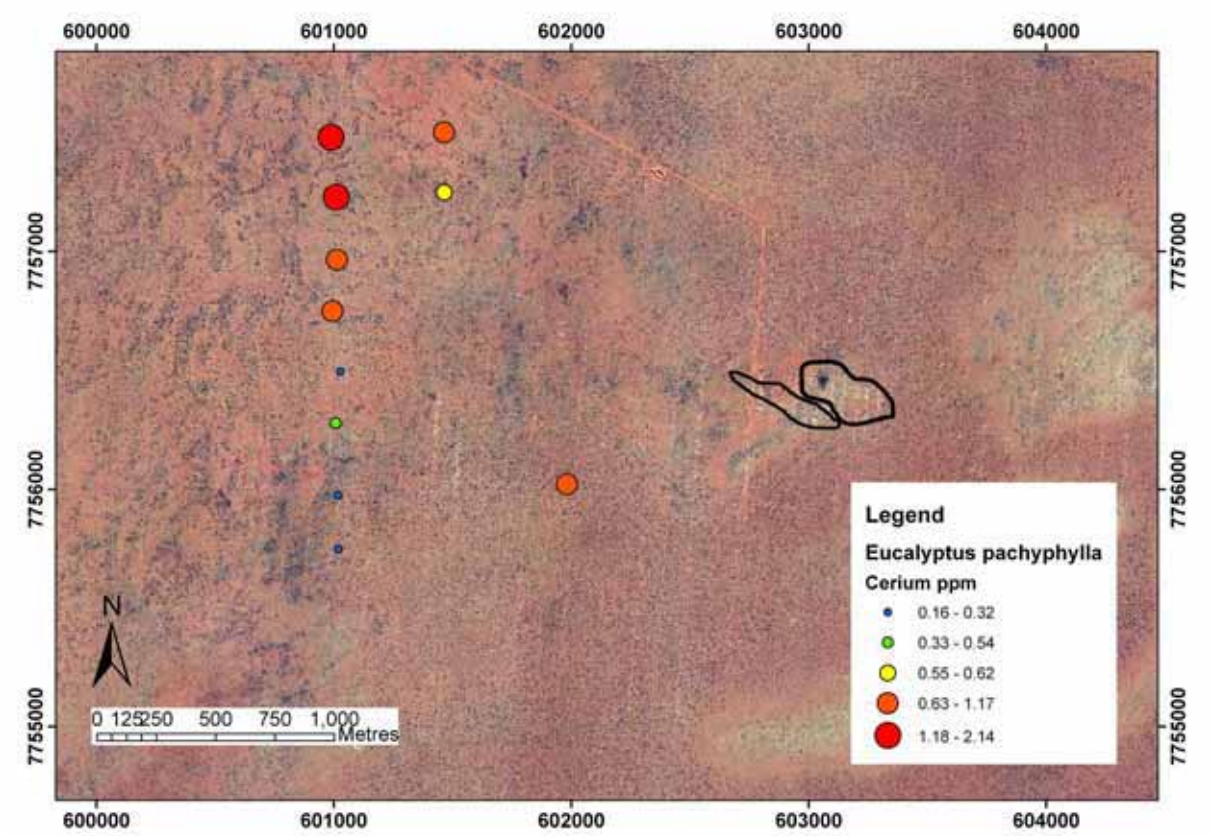

Figure 5.104: Plots of Ce concentration for *Eucalyptus pachyphylla* overlying the orthophoto of the Titania Prospect.

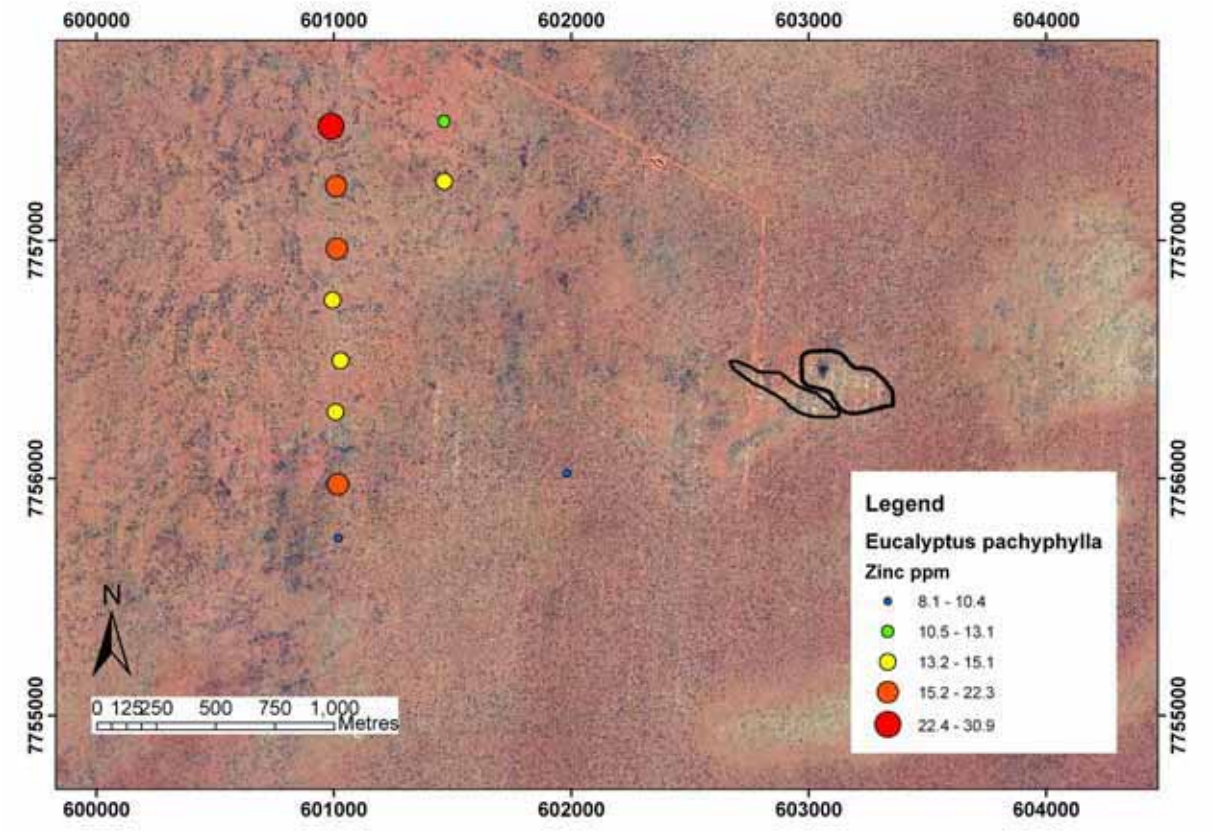

Figure 5.105: Plots of Zn concentration for *Eucalyptus pachyphylla* overlying the orthophoto of the Titania Prospect.

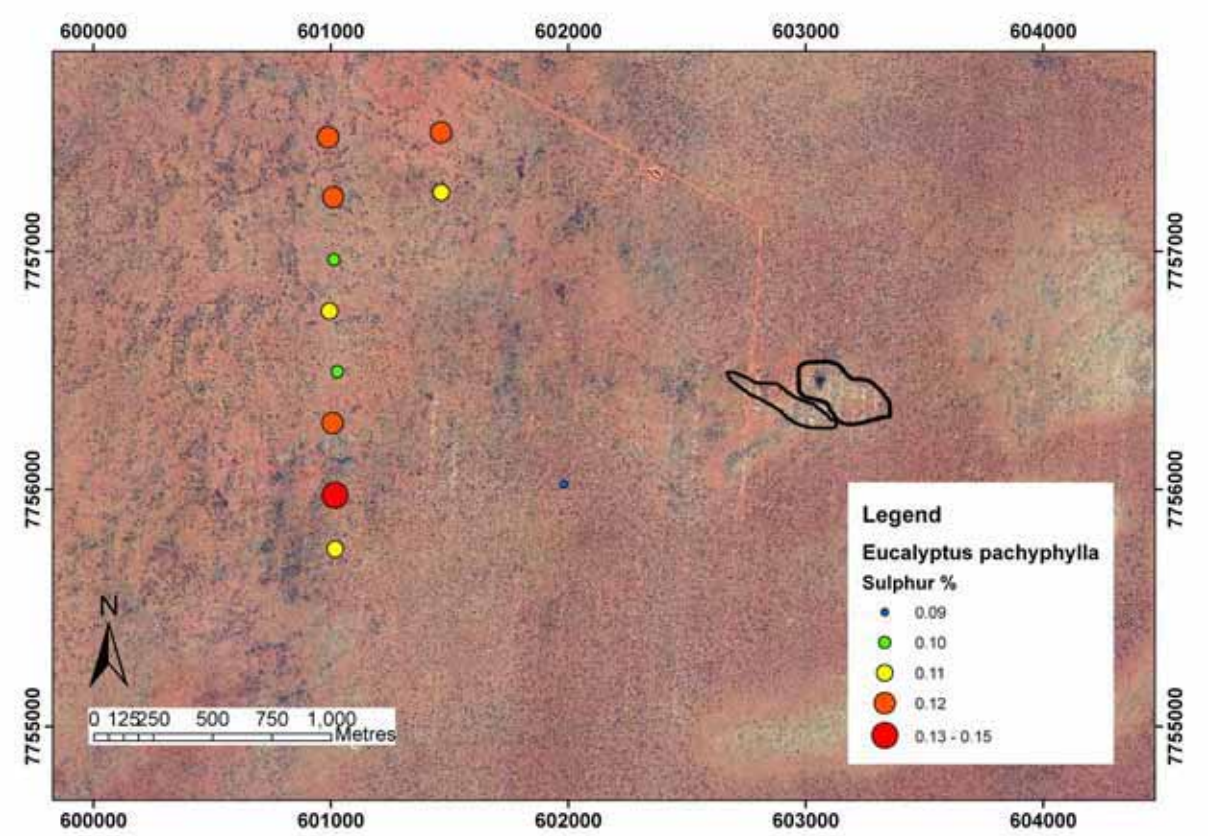

Figure 5.106: Plots of S concentration for *Eucalyptus pachyphylla* overlying the orthophoto of the Titania Prospect.

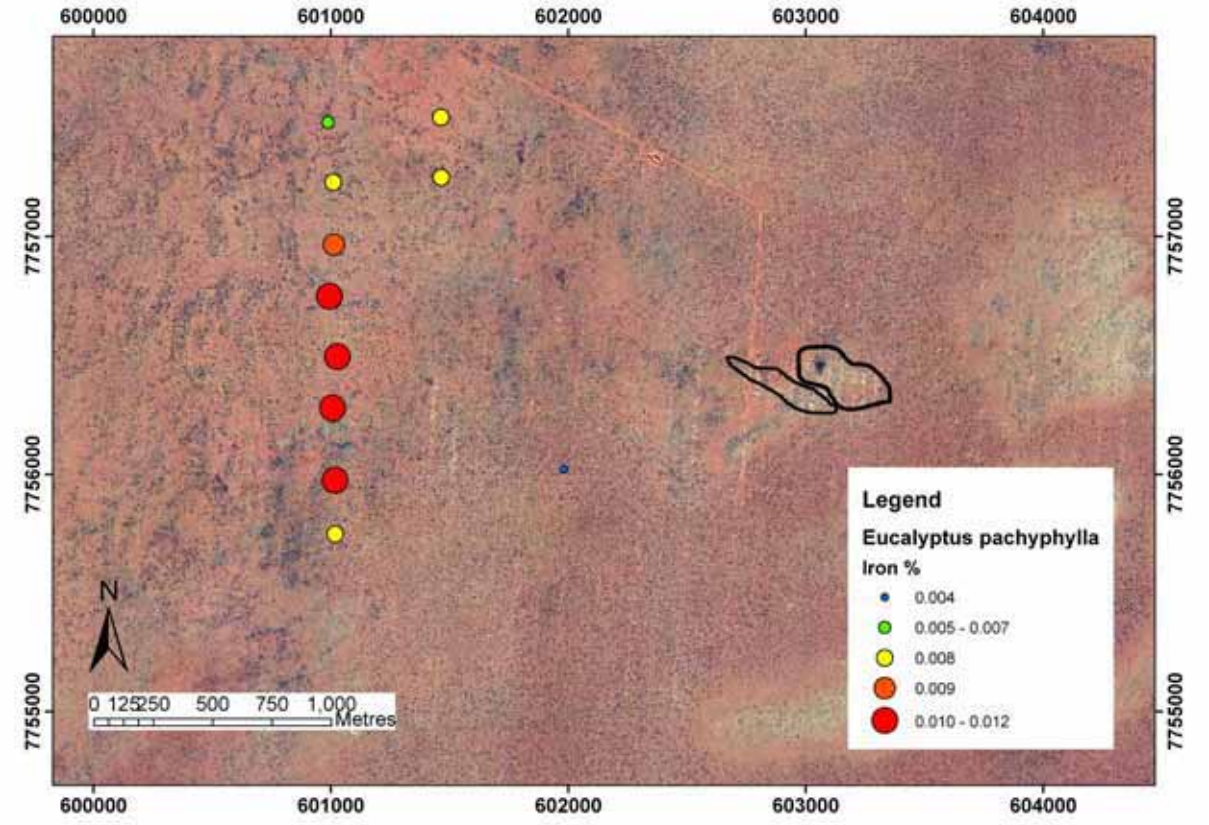

Figure 5.107: Plots of Fe concentration for *Eucalyptus pachyphylla* overlying the orthophoto of the Titania Prospect.

Discussion

The red-budded mallee results were difficult to put into context as they did not extend across the mineralisation. Both As and Au were close to or below analytical detection limit (0.3 ppm and 0.2 ppb respectively). The Zn and S results are opposite trending which is contradictory to the other plant species but could be explained by Zn being hosted in Fe-oxides whereas S is flushed out of the system (Figures 5.105 and 5.106). The REE (Figure 5.104) show increasing values to the north of the transect, which is different from the Fe content of the leaves (Figure 5.107). If they had the same pattern then it would be possible to say that the source of REE was detrital monazites (most common source of REE), however this correlation is poor so it is more likely that the monazites are bedrock hosted which matches well with cover thickness decreasing to the north and west of the area.

5.4.9 *Grevillea striata* (beefwood)

Grevillea striata was widespread across the field site but it did not respond as well to the fire as the other species. Hence there were few samples able to be collected. The beefwood results show 4 distinct elemental patterns:

1. Elements that are elevated over the mineralisation (Ag, Al, As, Au, Ca, Cd, Ce, Fe, Hf, Hg, K, La, Mg, Mo, Na, S, Sn, Ti and Zr);
2. Elements elevated to the east (Ni);
3. Elements elevated to the south (Ba, Cu and Se); and,
4. Elements elevated to the west (Mn).

There are also elements that are irregularly distributed (B, Co, Cr, Cs, Li, P, Pb, Rb, Sb, Sr, Ta, Y and Zn). Elements that were below analytical detection limit were Be, Bi, Ge, Ga, In, Nb, Pd, Pt, Re, Sc, Te, Th, Tl, U, V and W.

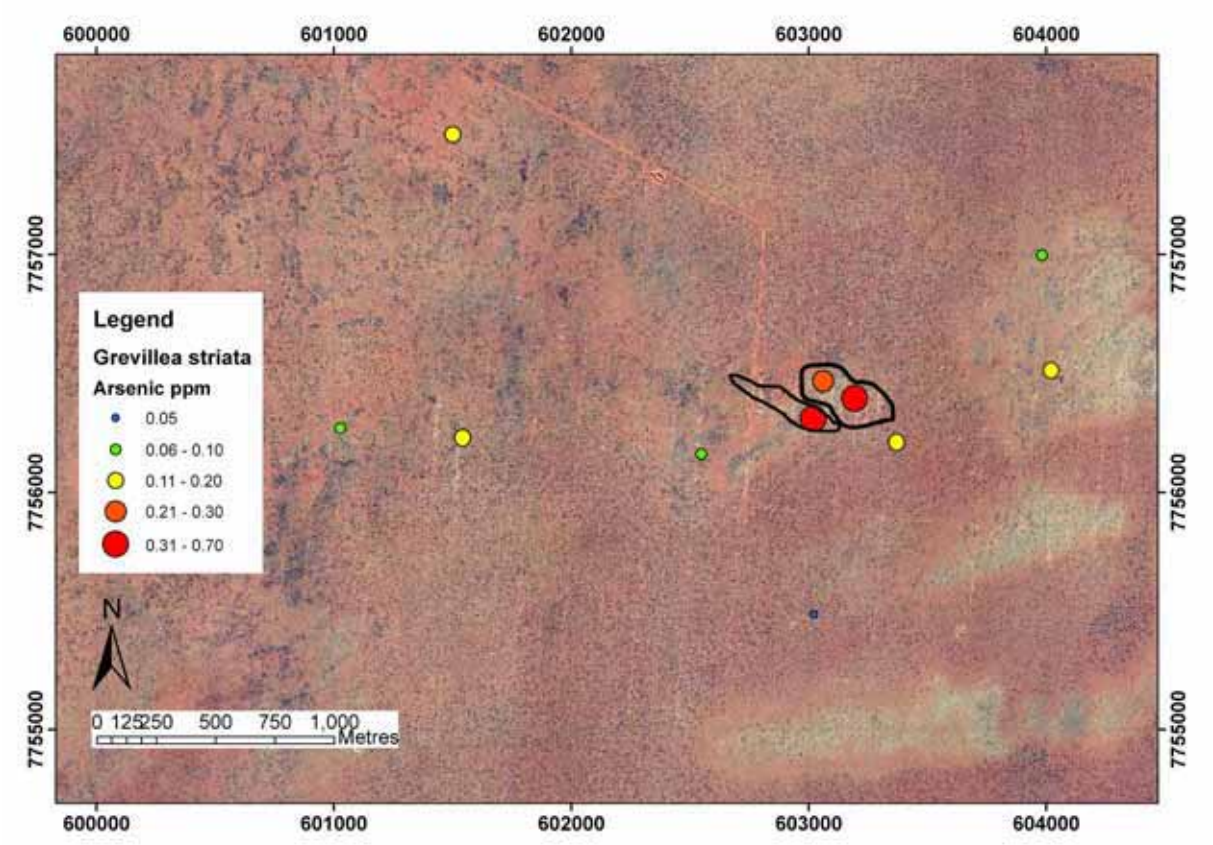

Figure 5.108: Plots of As concentration for *Grevillea striata* overlying the orthophoto of the Titania Prospect.

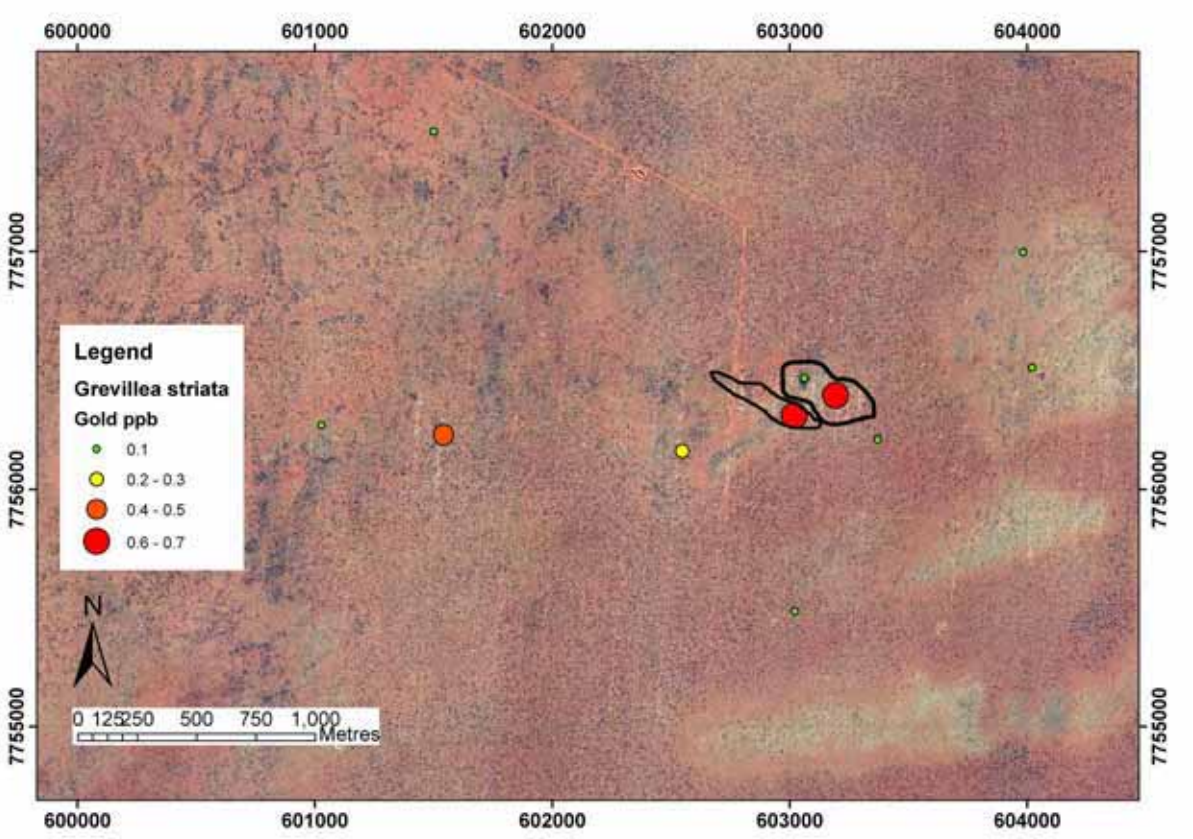

Figure 5.109: Plots of Au concentration for *Grevillea striata* overlying the orthophoto of the Titania Prospect.

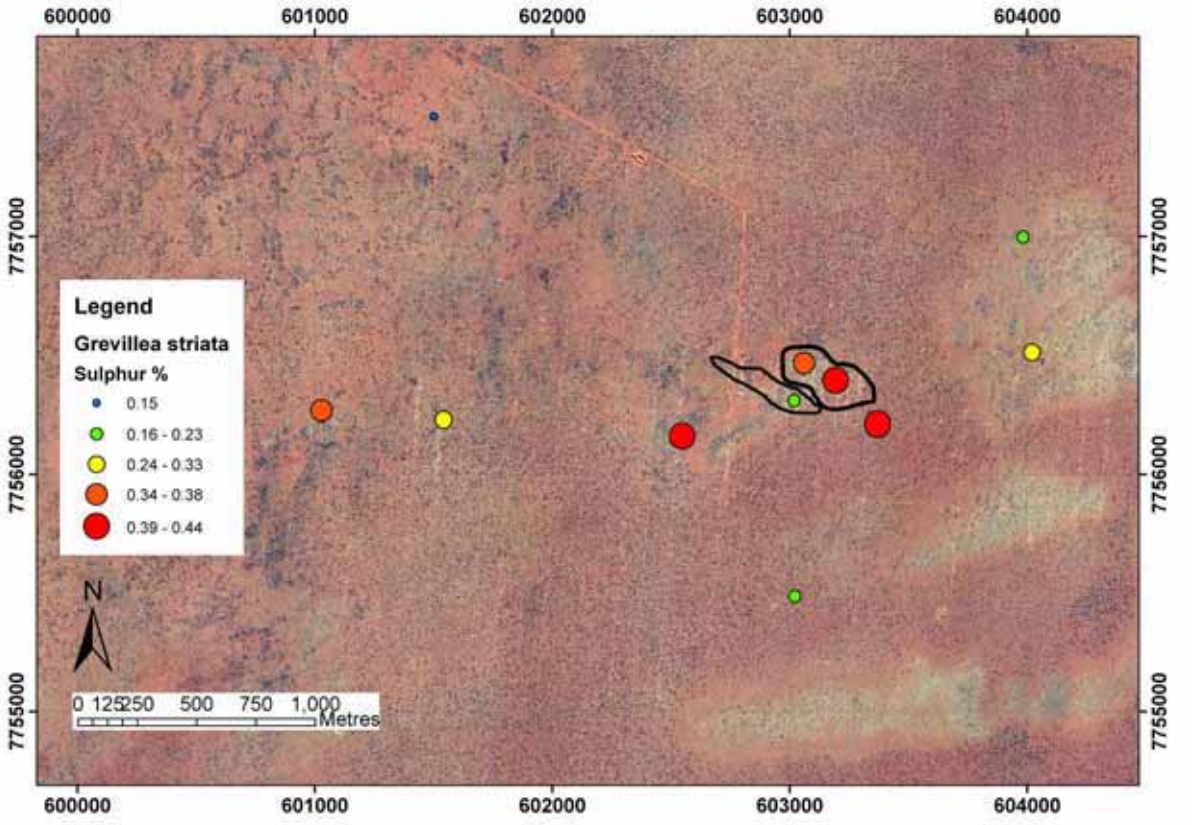

Figure 5.110: Plots of S concentration for *Grevillea striata* overlying the orthophoto of the Titania Prospect.

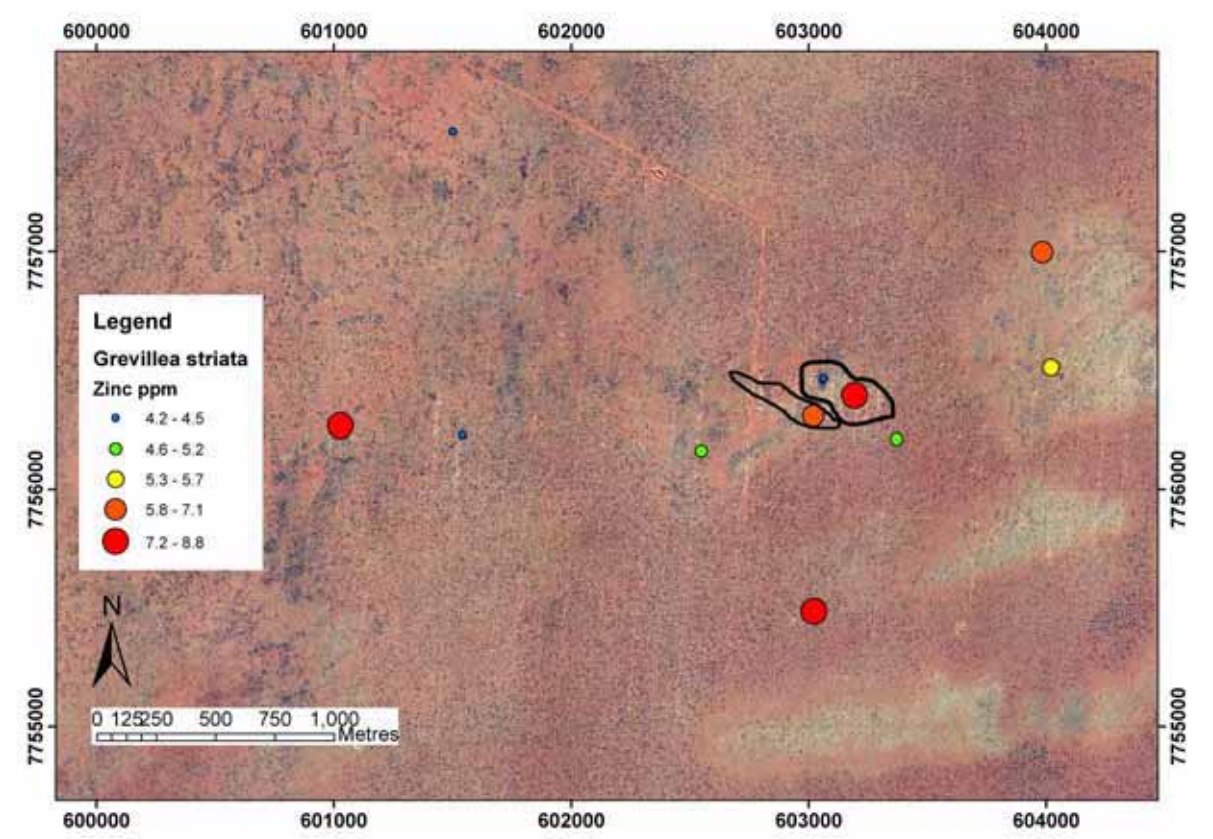

Figure 5.111: Plots of Zn concentration for *Grevillea striata* overlying the orthophoto of the Titania Prospect.

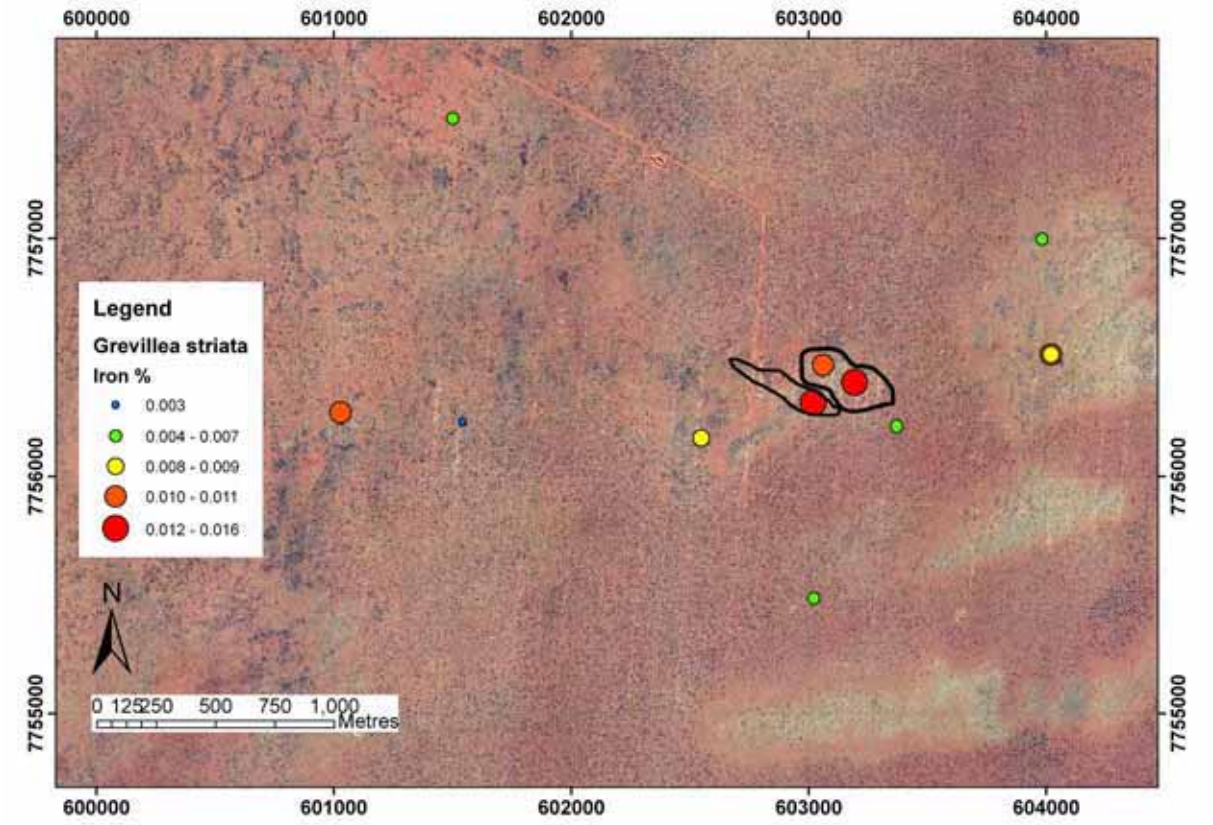

Figure 5.112: Plots of Fe concentration for *Grevillea striata* overlying the orthophoto of the Titania Prospect.

Discussion
The beefwood results are rather misleading because there were few samples collected and most of them were very close to the zone of mineralisation. Hence, most of the elements show high values over the mineralisation. This is compounded by the detrital contamination with this species, as shown by the high Fe assays (Figure 5.112). This species collected visible dust within the leaf veins which may indicate that the mineralisation anomalies could be generated by drill spoil dust.

There is a 0.7 ppm As peak concentration corresponding with a 0.7 ppb Au concentration and a 0.44% S concentration (Figures 5.108 - 5.110). There is an elevated Zn assay (8.8 ppm) that corresponds with these, but there are also high values away from the mineralisation (Figure 5.111). The Zn values within this species are particularly low considering the other values at this site.

The implications for this species is that more information is required and further studies needed to determine if this species is truly detecting the primary mineralisation or if it is hosting detrital contamination from dust collected on the leaves.

5.4.10 *Hakea macrocarpa* (corkwood)

Hakea macrocarpa was one of 2 corkwood species growing over the Titania Prospect. In general it was easy to tell the difference between the 2 because *H. macrocarpa* has wide flat leaves with a large central vein and *H. lorea* had long, 'shoe-string' leaves. Both species grew together, but not where the cover became thick in the south-east, or where it was thin in the north-west. The corkwood results show 6 distinct elemental patterns:

1. Elements that are elevated over the mineralisation (As);
2. Elements in low abundance over mineralisation (Ni, Pb and Sb);
3. Elements elevated to the north (Ag, B and Mg);
4. Elements elevated to the south (Mo);
5. Elements elevated to the east (Na and Nb); and,
6. Elements elevated to the west (Al, Au, Ce, Co, Cs, Cu, La, Li, Th, Ti, Y, Zn and Zr).

There are also elements that irregularly distributed (Ba, Ca, Cd, Cr, Fe, Hf, Hg, K, Mn, P, Rb, S, Sc, Se, Sr and Ta). Elements that were below analytical detection limit were Be, Bi, Ge, Ga, In, Pd, Pt, Re, Sn, Te, Tl, U, V and W.

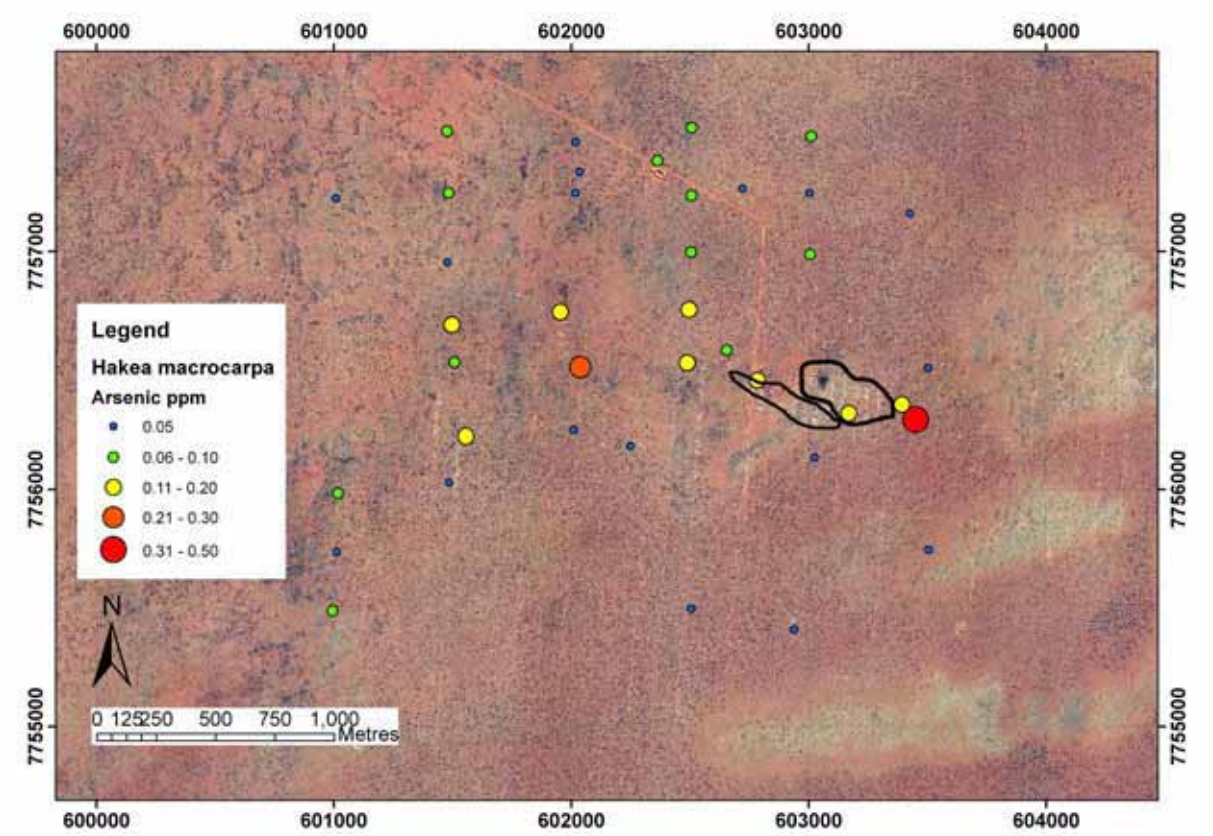

Figure 5.113: Plots of As concentration for *Hakea macrocarpa* overlying the orthophoto of the Titania Prospect.

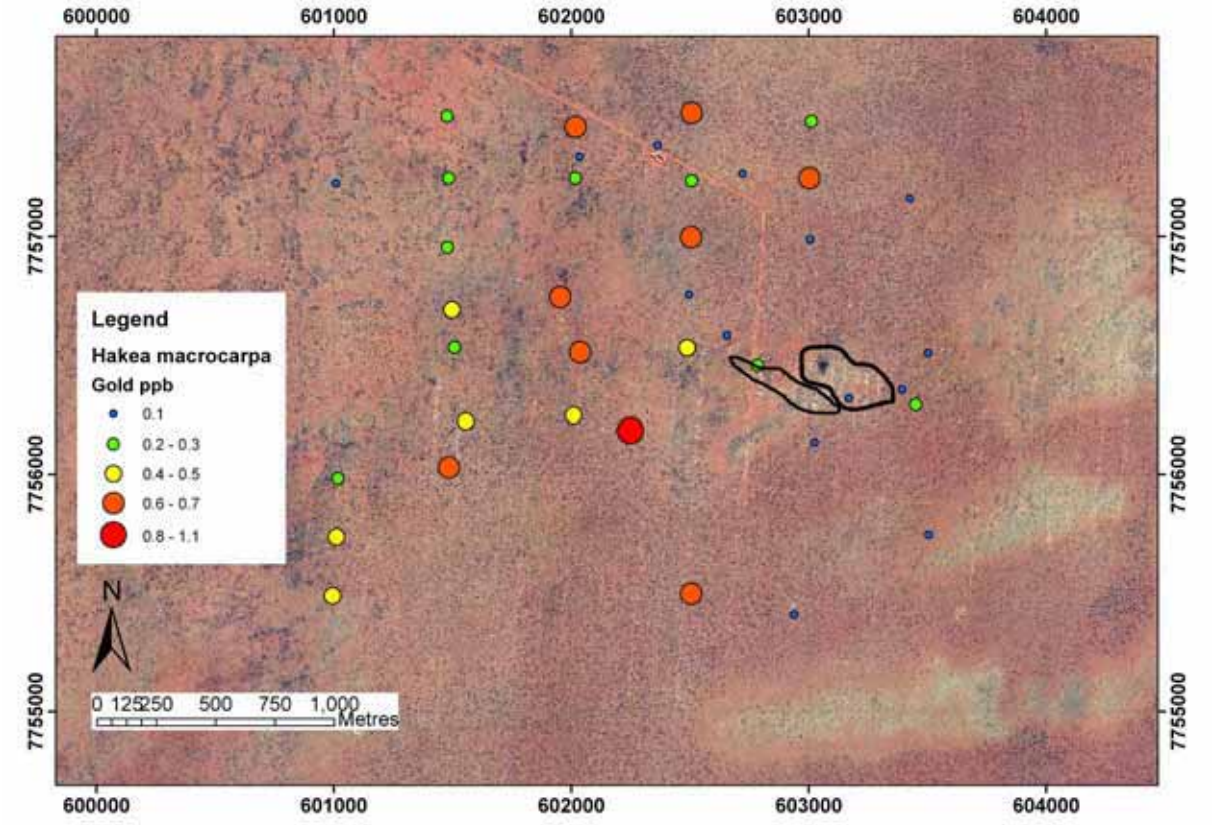

Figure 5.114: Plots of Au concentration for *Hakea macrocarpa* overlying the orthophoto of the Titania Prospect.

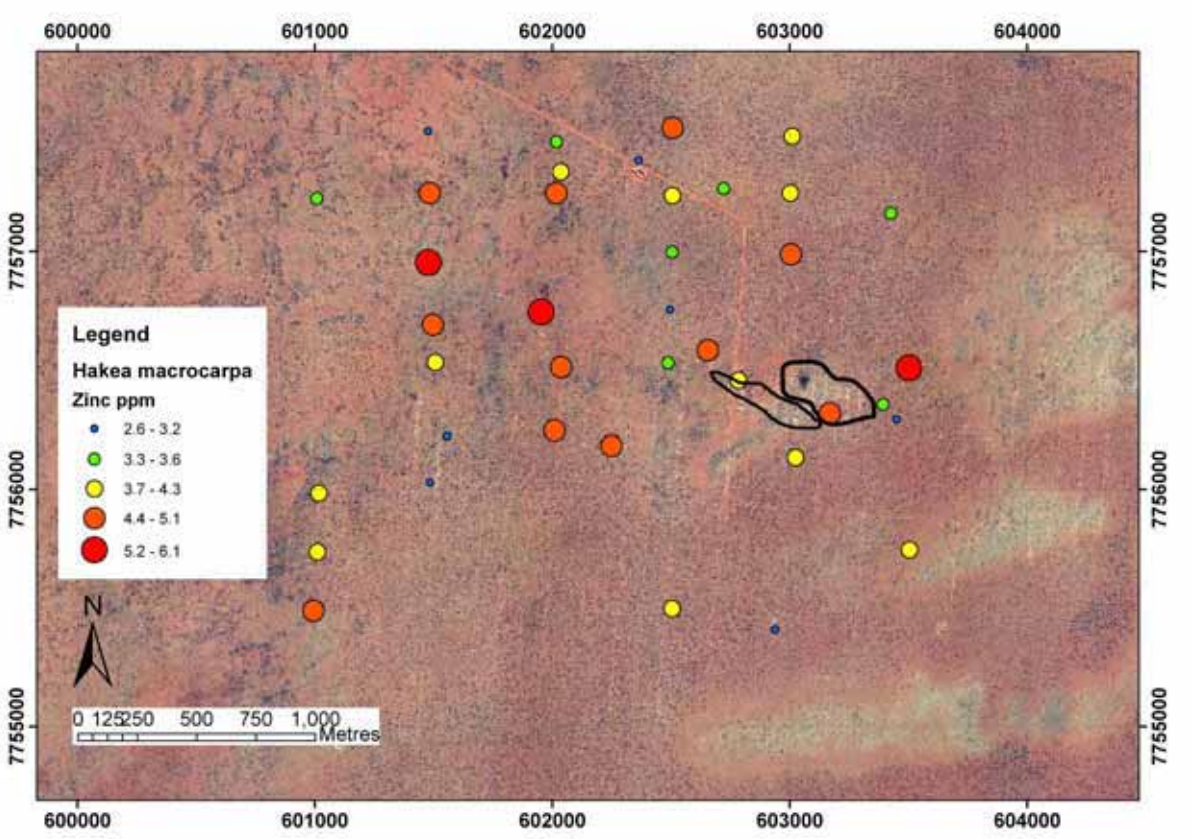

Figure 5.115: Plots of Zn concentration for *Hakea macrocarpa* overlying the orthophoto of the Titania Prospect.

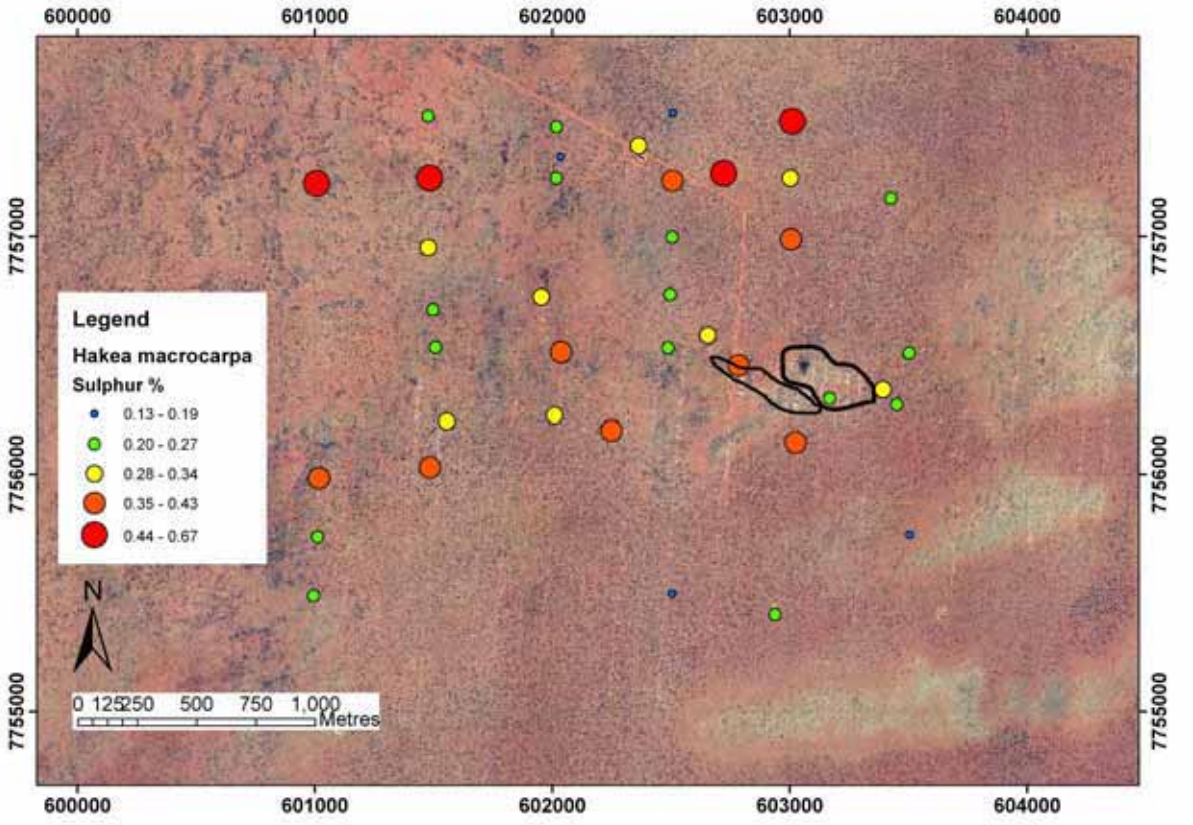

Figure 5.116: Plots of S concentration for *Hakea macrocarpa* overlying the orthophoto of the Titania Prospect.

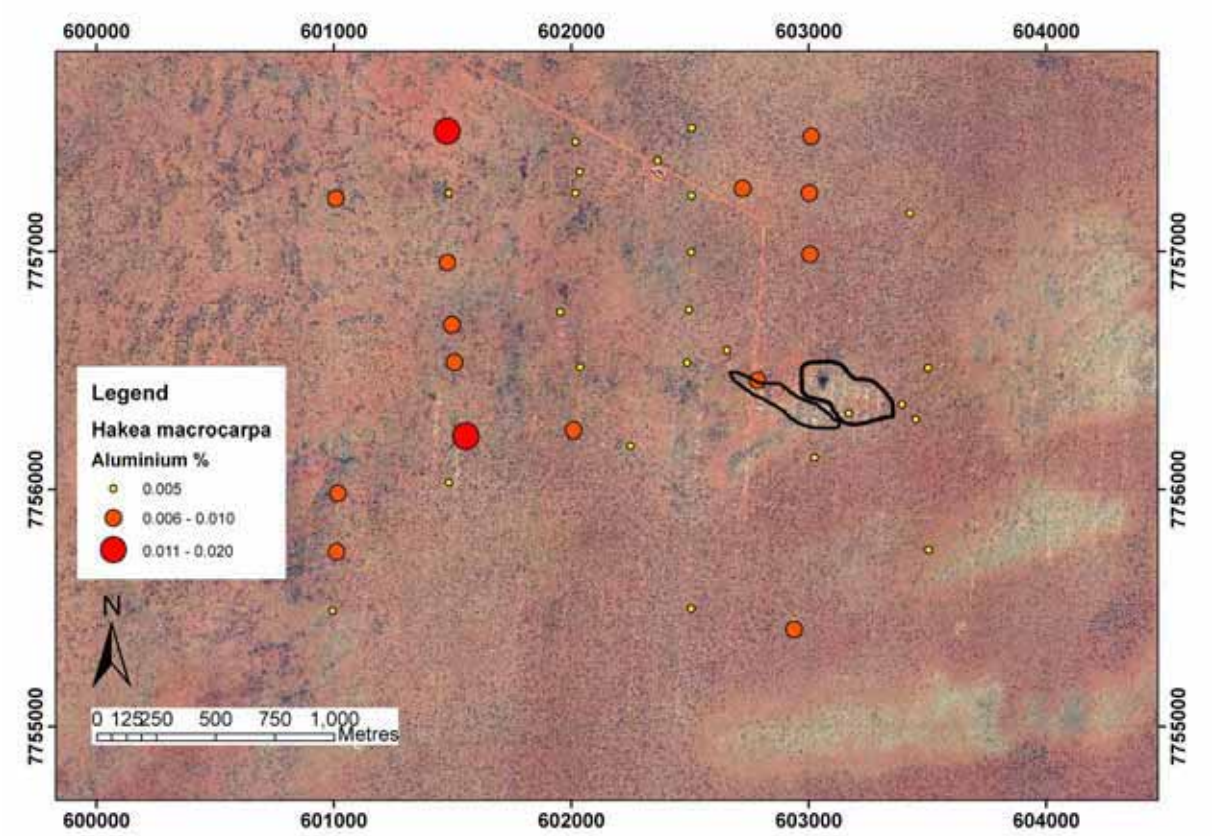

Figure 5.117: Plots of Al concentration for *Hakea macrocarpa* overlying the orthophoto of the Titania Prospect.

Discussion

The corkwood results are difficult to put into context and tend to produce similar spatial patterns to the dogwood results. There is a single peak As assay (0.5 ppm, Figure 5.113) which is very close to the mineralisation, but there are several points over mineralisation that have low concentration. The Au results are high (1.1 ppb, Figure 5.114) to the west of the mineralisation across a wide zone. This possible reflects the Lamaque mineralisation that is a shallower super-gene Au deposit that was not detected by the other plant species. Similar to the *Acacia bivenosa* and *Acacia coriacea* results, the Zn and S plots (Figures 5.115 and 5.116) show higher values around the centre-west and north of the gridded area. This may show a greater surficial influence on the chemistry but it is not as strong as with the two-nerved wattle results.

Detrital contamination within the results of this species is very low, as supported by the low Al results, which are barely above analytical detection limit (Figure 5.117). The implications of this are that the surficial nature of the signal is more likely generated by actual root uptake rather than contamination. This species may be a useful addition in a biogeochemical sampling program as it may detect secondary deposits higher within the profile than the deeper rooted species. Further information is required to know if these values do match with the predicted Lamaque deposit.

5.4.11 Topsoil / Cryptogam samples

Topsoil samples were collected over the Titania Prospect as outlined in the methods chapter. These samples corresponded to 2 time periods: October 2005 which was after a prolonged 'dry' season; and, August 2006, which was 6 months after the 1 in 1000 year flooding event. The second set of soil samples did not correspond to the full grid but followed the hydrogeochemical sampling carried out by Dirk Kirste (CRC LEME/Simon Fraser University). Some of the sites do correspond and the differences between those results are significant.

Before flooding (October 2005)

The topsoil sampling in October showed 3 different spatial patterns:

1. Elements high over the centre Al, As, Au, Cd, Li, Mg, Ni, Pt, Te, U, Zn; (Figures 5.118 – 5.120, 5.124)
2. Elements high to the west Bi, Ce, Co, Cr, Cs, Cu, Fe, Ga, La, Mn, Pb, Rb, Sb, Sc, Sn, Th, Ti, Tl, Y; (Figures 5.121 and 5.123) and,
3. Elements high to the east Ca, K, Na, Nb, P, Pd, S, Se, Sr. (Figure 5.122)

There were also elements with an irregular distribution Ag, Ba, Be, Hf, Hg, Mo, Zr.

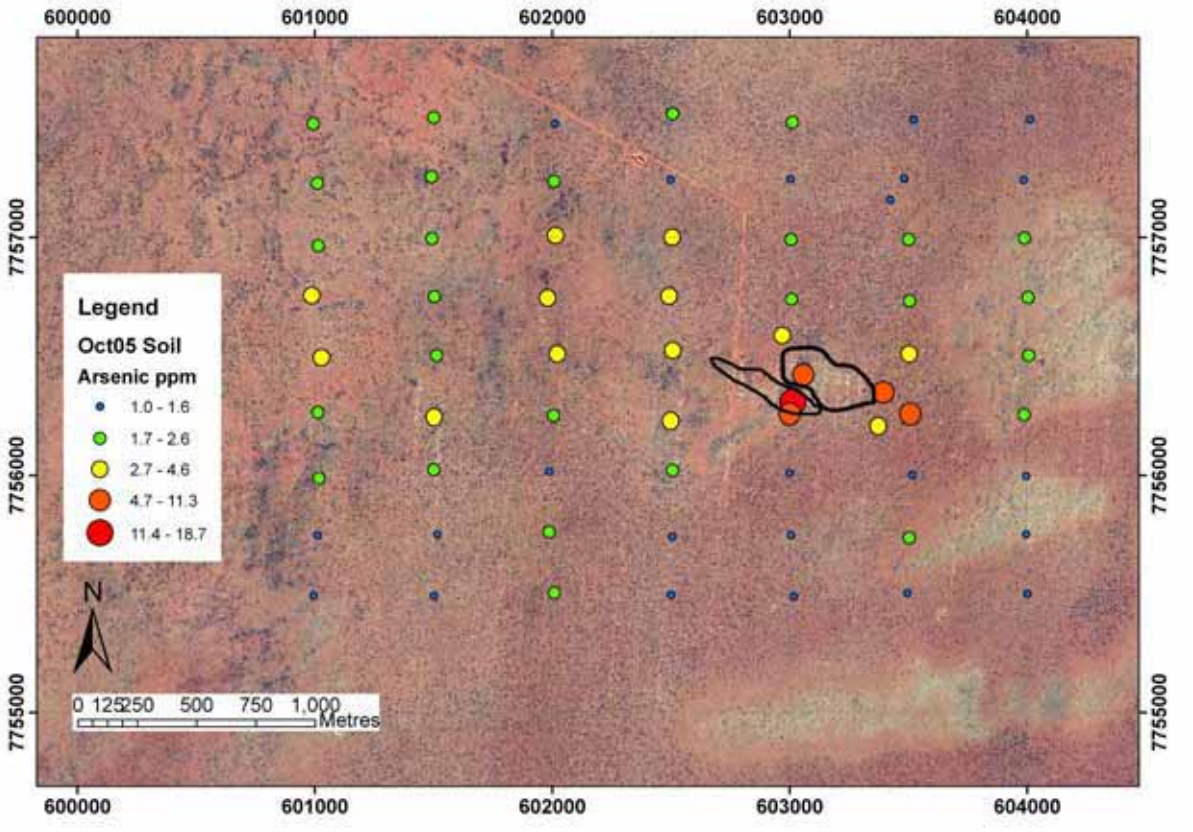

Figure 5.118: Plots of As concentration for cryptogam samples overlying the orthophoto of the Titania Prospect.

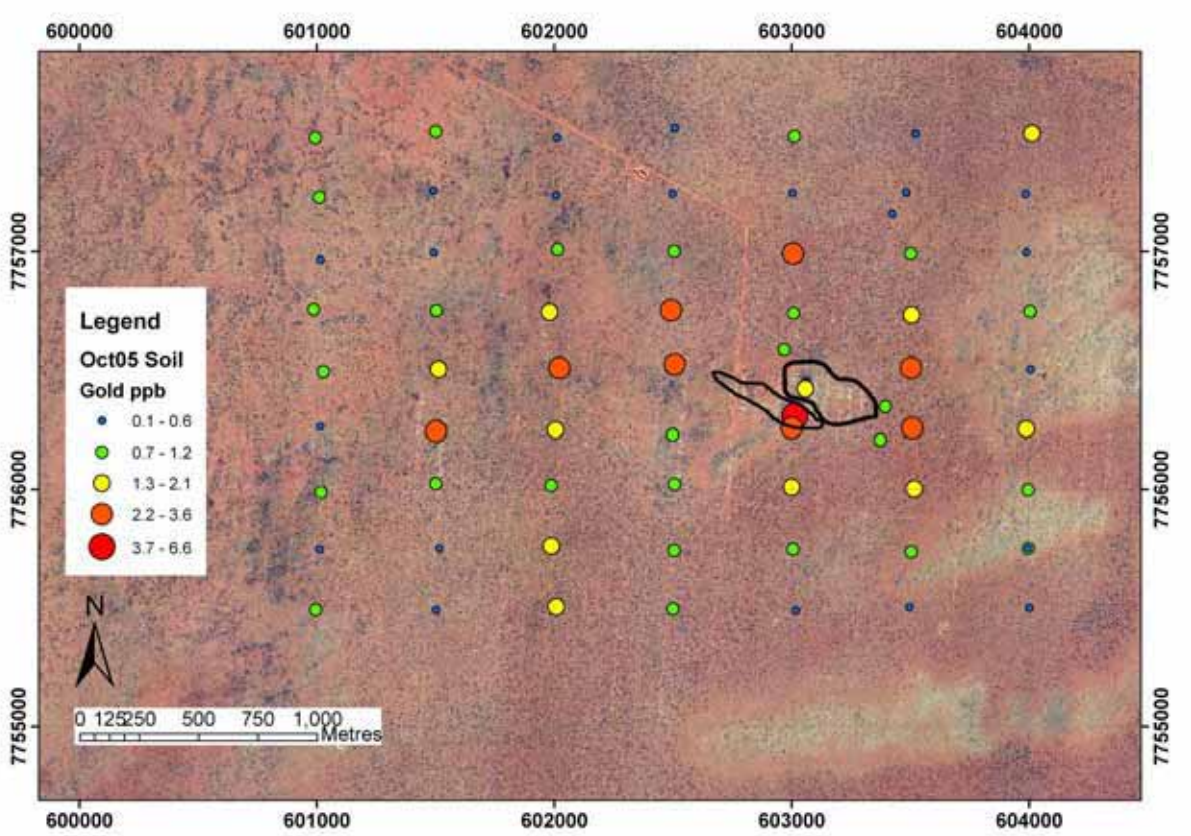

Figure 5.119: Plots of Au concentration for cryptogam samples overlying the orthophoto of the Titania Prospect.

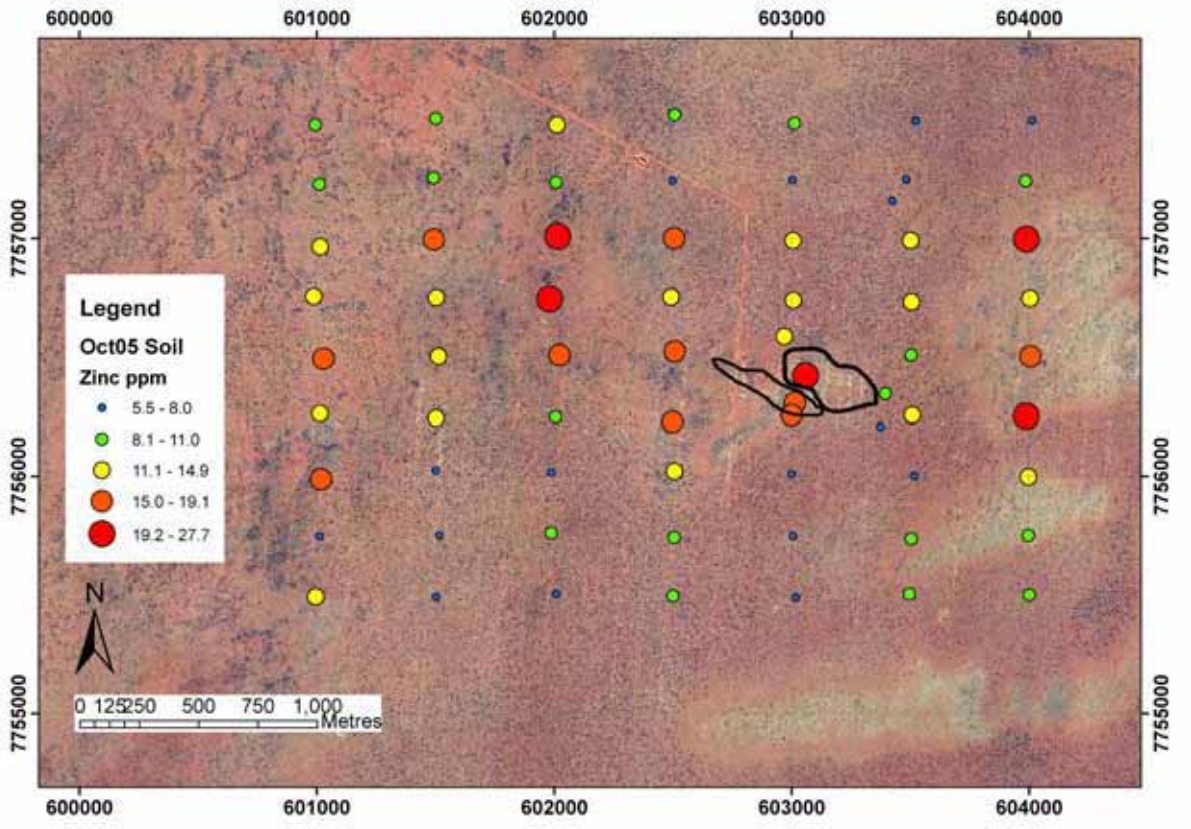

Figure 5.120: Plots of Zn concentration for cryptogam samples overlying the orthophoto of the Titania Prospect.

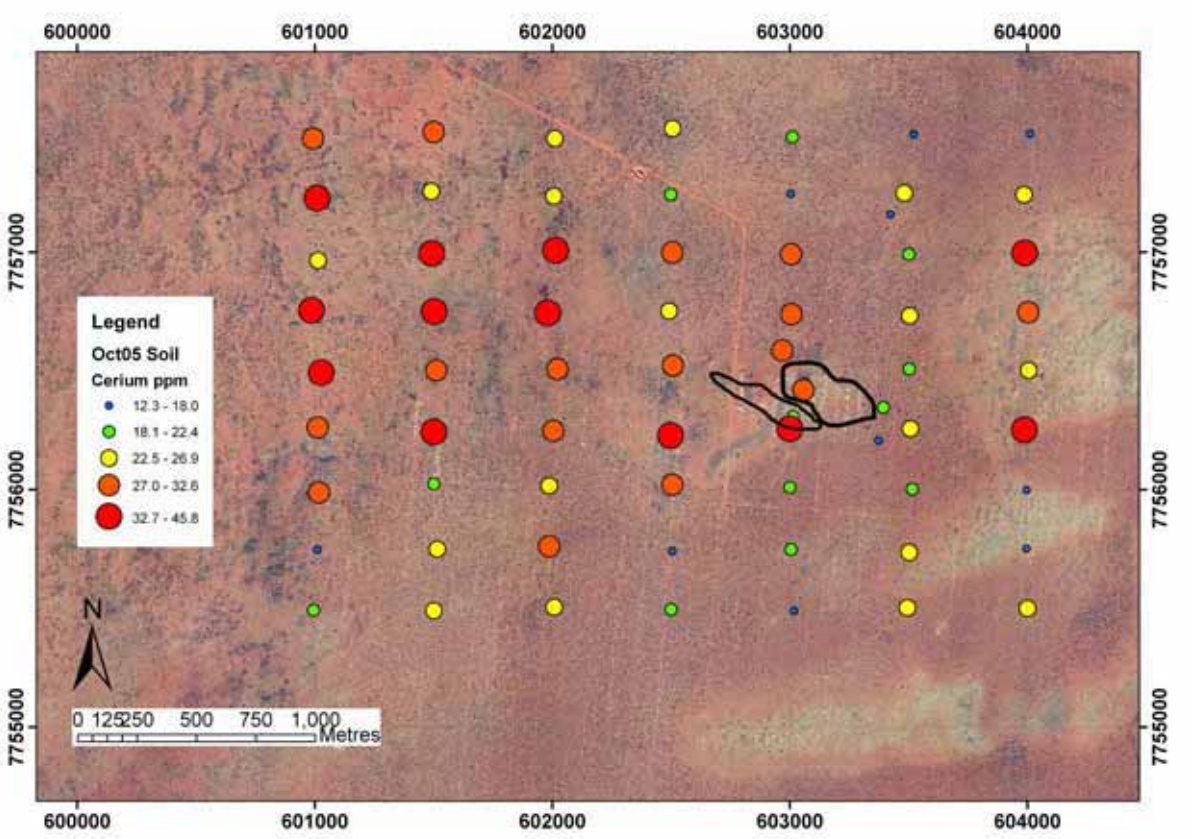

Figure 5.121: Plots of Ce concentration for cryptogam samples overlying the orthophoto of the Titania Prospect.

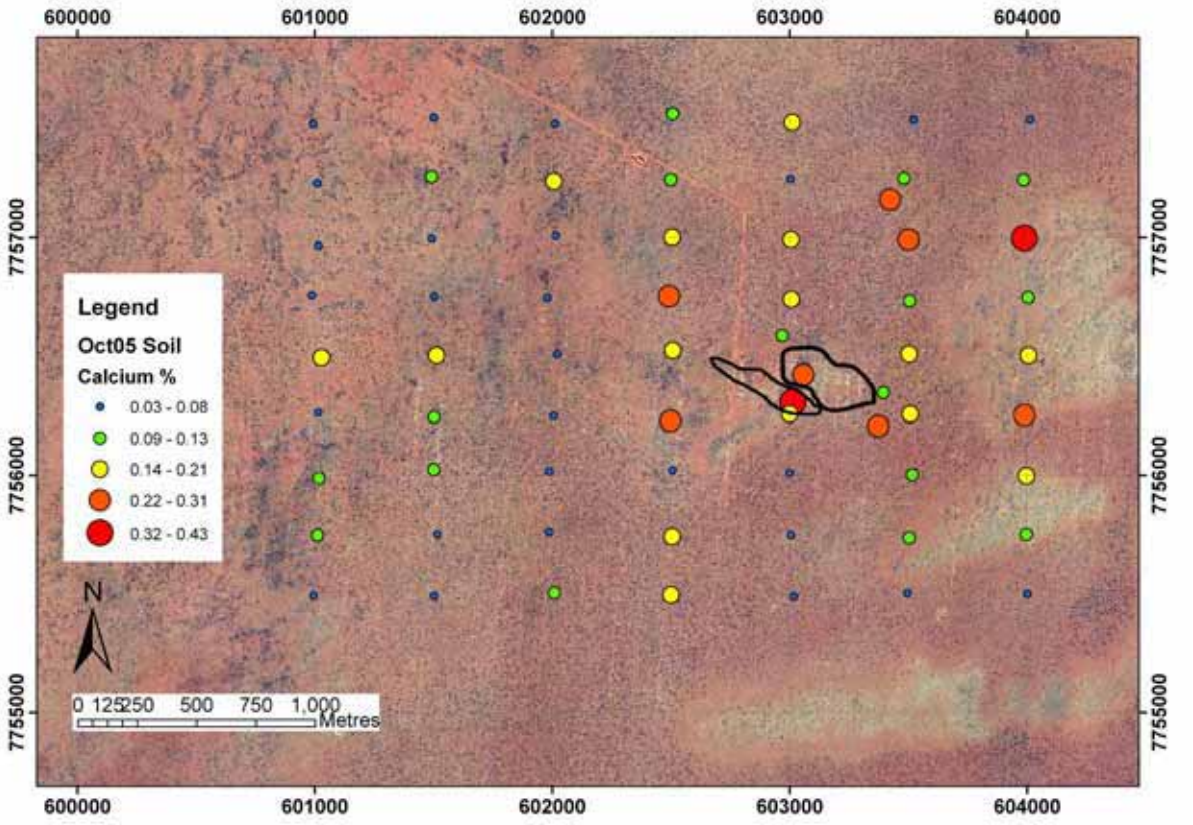

Figure 5.122: Plots of Ca concentration for cryptogam samples overlying the orthophoto of the Titania Prospect.

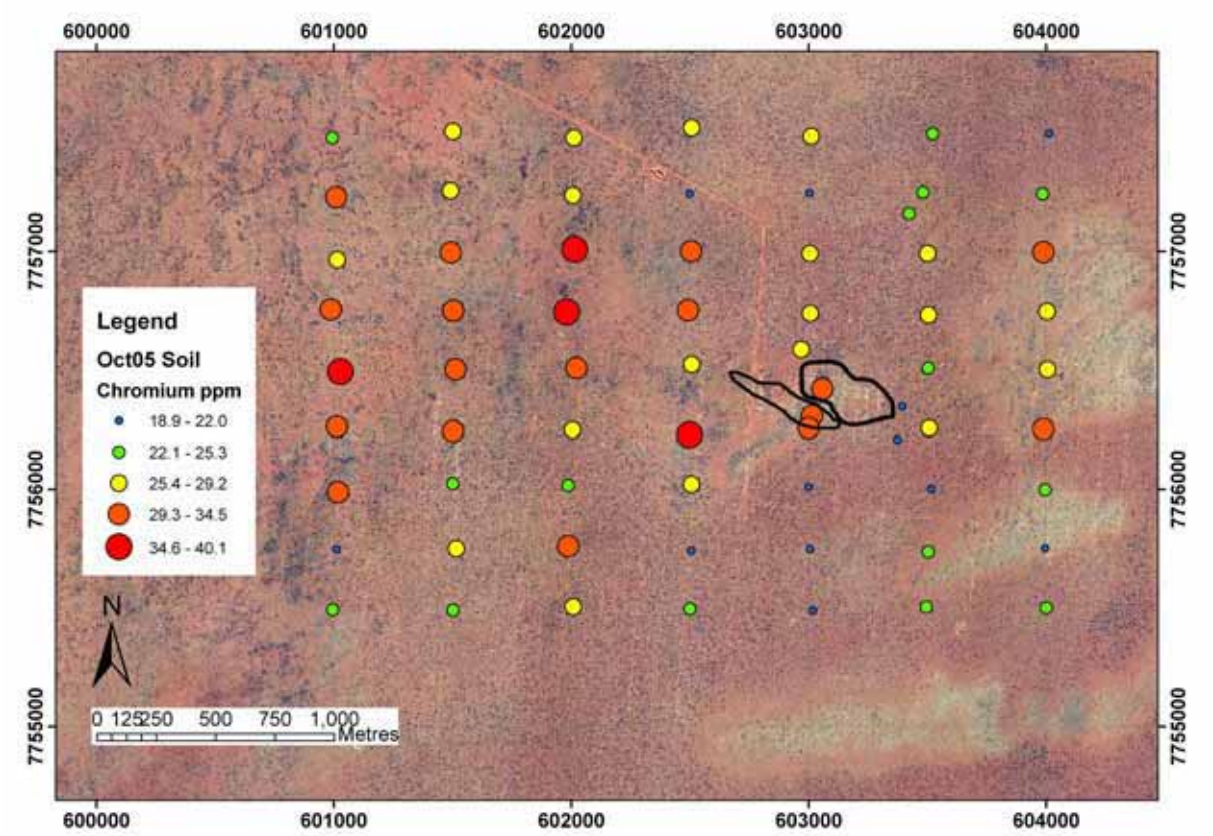

Figure 5.123: Plots of Cr concentration for cryptogam samples overlying the orthophoto of the Titania Prospect.

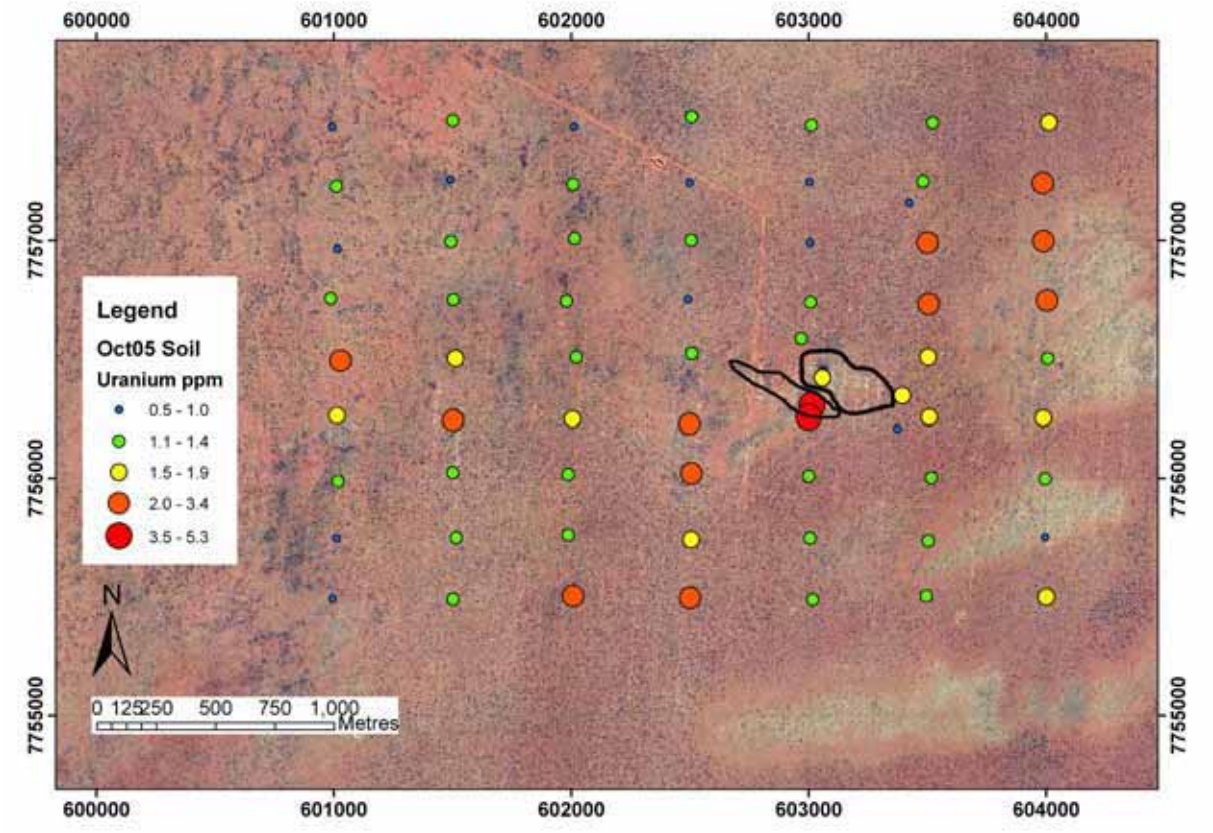

Figure 5.124: Plots of U concentration for cryptogam samples overlying the orthophoto of the Titania Prospect.

In general, the topsoil samples produced broader geochemical anomalies of generally higher magnitude than the vegetation samples. There were some general trends in the data, most of

which are easily linked to surface dispersion processes. The more mobile elements tend to accumulate towards the eastern edge of the grid area, due to that area being down-slope of the rest of the grid and hence being a local depositional point. The less mobile elements tended to be more concentrated to the west of the transect where they are either bound up within iron oxides and hydroxides or directly associated with the shallower transported cover. Other elements are high within a wide swath across the centre of the grid, covering the mineralised zone. Several of these elements correspond very closely with those within the plants (e.g. As, Au, Zn and U) (Figures 5.118-5.120 and 5.124). Sulphur is very difficult to analyse from soil samples and the results were mostly below detection. The Ca results represent the distribution of Ca-carbonates and surficial gypsum growth (Figure 5.122).

Discussion

This field site is subjected to flooding in most years, which has a great impact upon the soil chemistry. There is very little residence time for minerals at the landsurface before there is a flood event and the minerals break down and are dispersed across the environment. Since there had been an extended dry period prior to flooding it is possible that these results are more influenced by wind movements.

Since the spatial extend of the mineralisation signature produced by these results is so large it would be necessary to follow up with close spaced drilling to delineate the mineralisation which would not have been as essential with the vegetation results.

The Cr results of the soils have the same magnitude and range of the spinifex results, which is much greater than the other plants (Figure 5.123). There are several possible explanations for this: the spinifex could uptake the Cr from the soil incorporating it into the plant (but since there are few surface feeder roots this seems unlikely); the spinifex could take up Cr from depth, then via leaf drop could add Cr to the topsoil and over time the levels could equilibrate; or, the spinifex could uptake the Cr from depth and termites could eat the spinifex transferring the Cr to the termite mound and when the mound breaks up the Cr is then incorporated into the soil. Further investigations of Cr at depth would need to be examined before this question could be fully answered.

After flooding (August 2006)

The topsoil samples from August 06 showed 4 distinct spatial patterns:

1. Elements high over the centre As, Au, Cr, Cu, U, V; (Figures 5.125 and 5.126)
2. Elements high to the west Ag, Al, Be, Ca, Cd, Mg, Rb, Zn; (Figure 5.127)
3. Elements high to the east S; (Figure 5.129) and,
4. Elements high to the south Bi, Ce, Co, Cs, Ga, La, Mo, Ni, P, Sb, Sc, Te, Th, Tl, W, Y. (Figure 5.128)

Elements with irregular distributions Ba, Fe, Hf, Hg, K, Li, Mn, Na, Nb, Pb, Pd, Se, Sn, Sr, Ti, Zr.

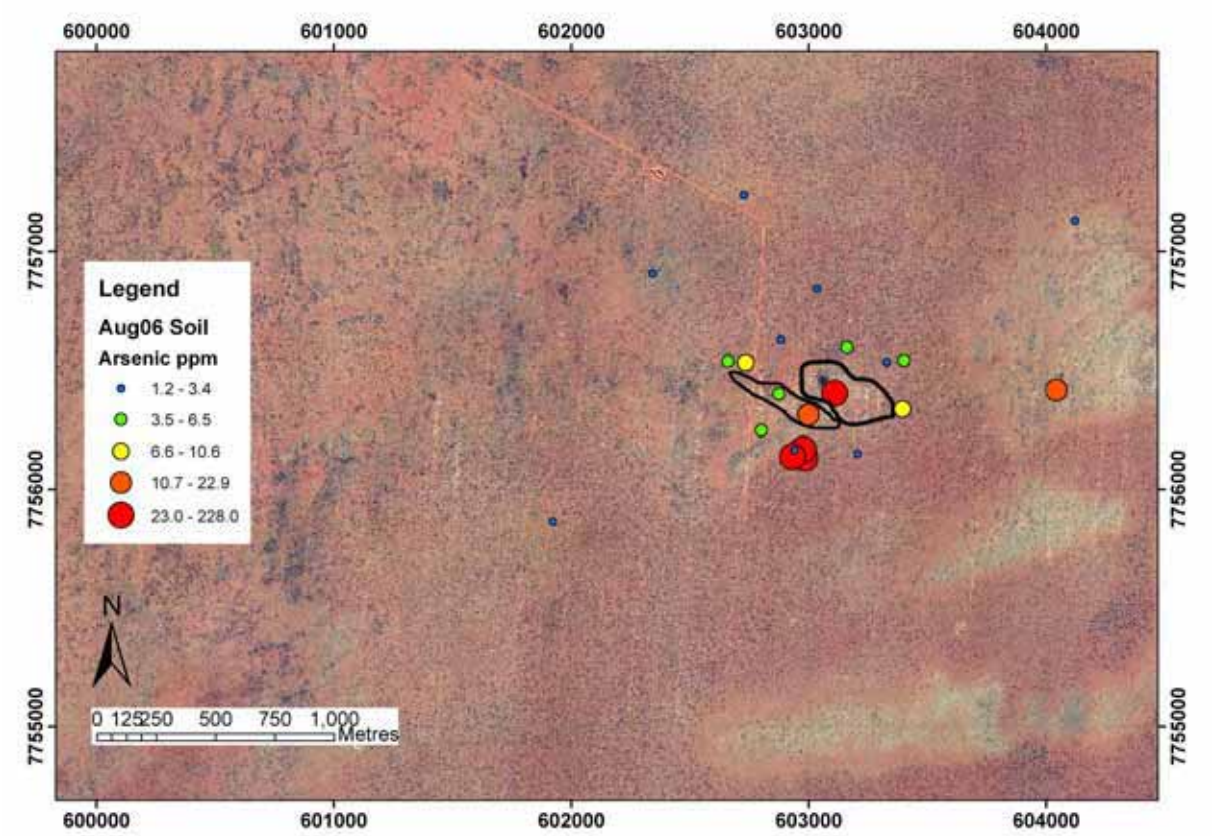

Figure 5.125: Plots of As concentration for cryptogam samples overlying the orthophoto of the Titania Prospect.

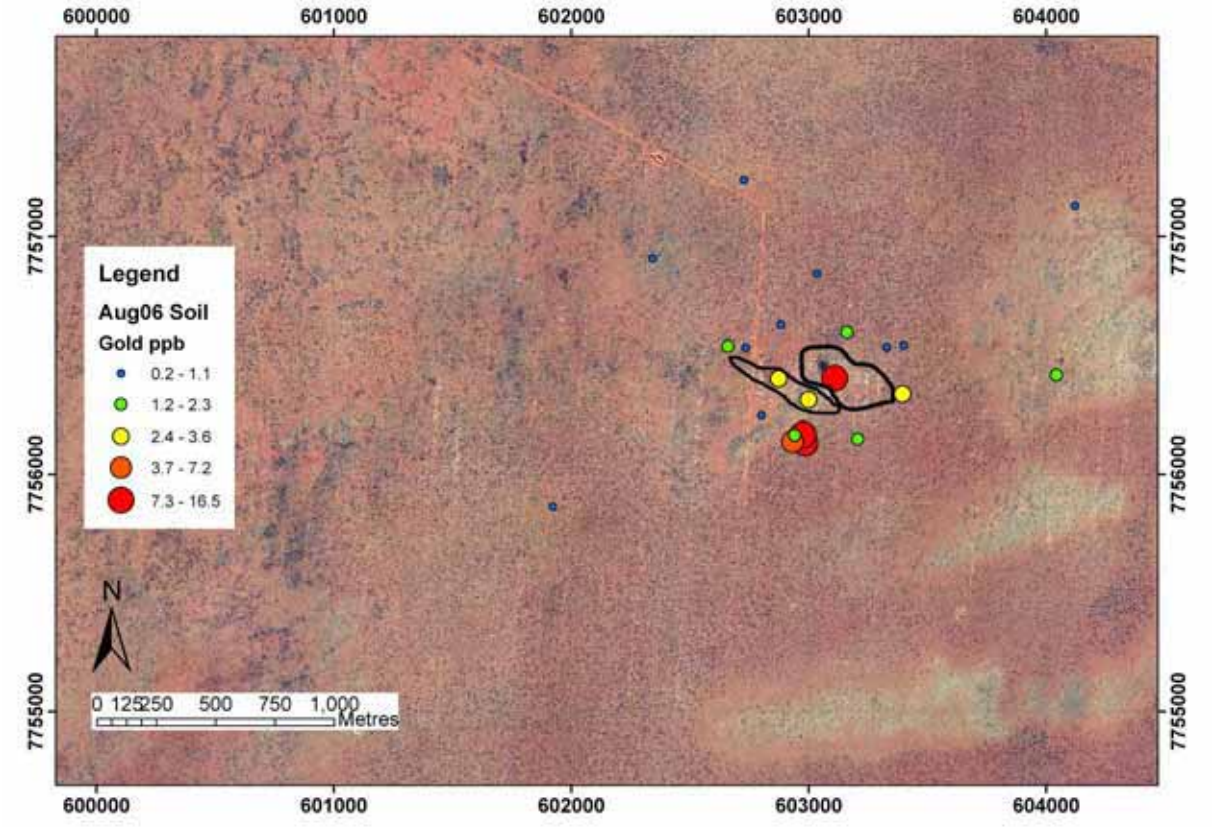

Figure 5.126: Plots of Au concentration for cryptogam samples overlying the orthophoto of the Titania Prospect.

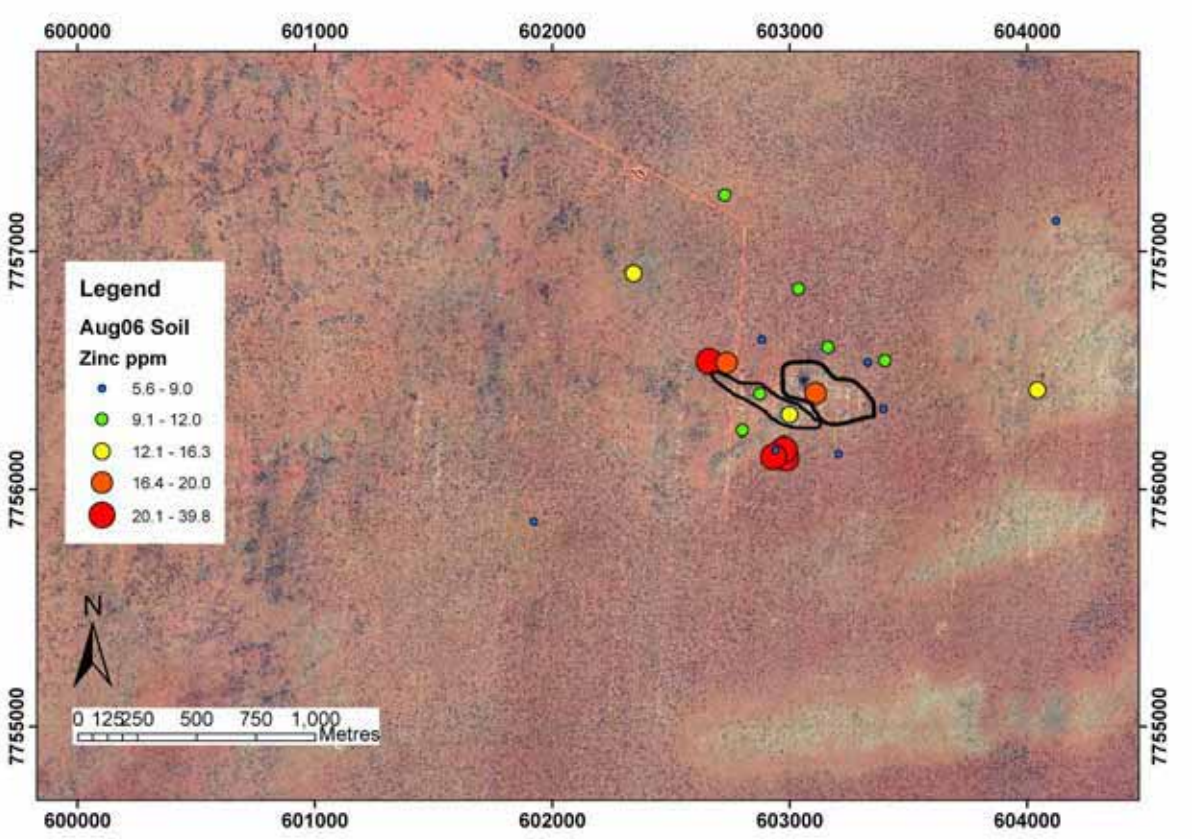

Figure 5.127: Plots of Zn concentration for cryptogam samples overlying the orthophoto of the Titania Prospect.

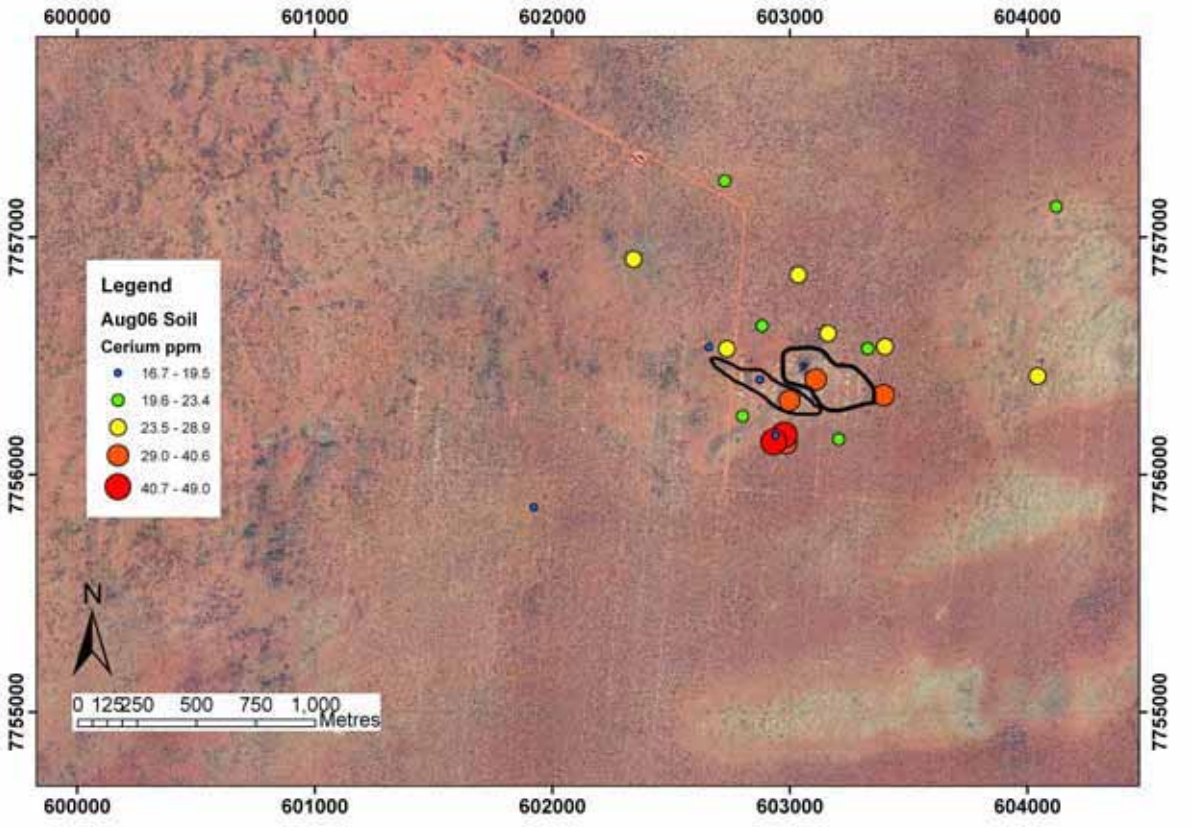

Figure 5.128: Plots of Ce concentration for cryptogam samples overlying the orthophoto of the Titania Prospect.

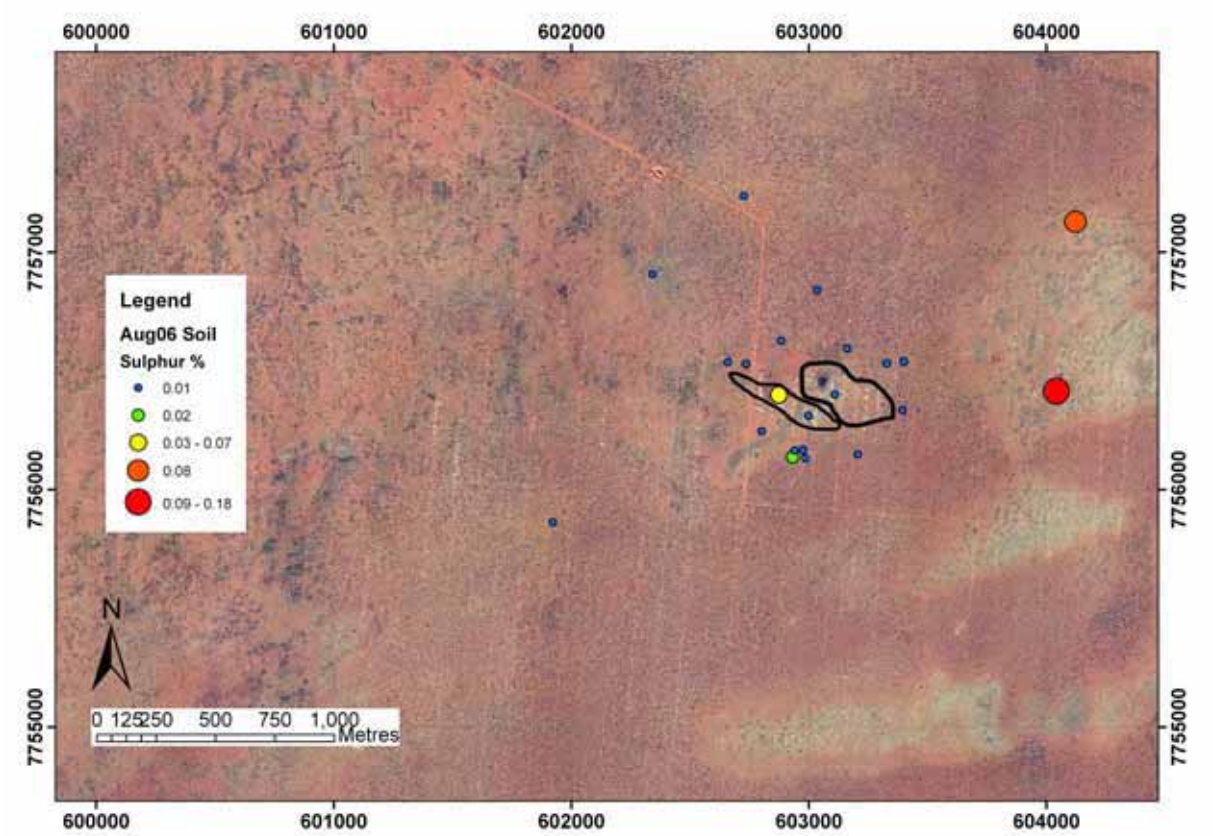

Figure 5.129: Plots of S concentration for cryptogam samples overlying the orthophoto of the Titania Prospect.

Discussion

The soil samples collected in the August 2006 field trip did not cover the full grid, limiting direct comparisons. There are however, some distinct differences in the magnitude and patterns of soil geochemistry generated after the rain event. While the As and Au results express the underlying mineralisation area, the magnitude of those values are much greater after rain (18 ppm to 228 ppm for As, and 6.6 ppb to 16.5 ppb for Au) (Figures 5.125 and 5.126). The rain event was very large and the area directly over the mineralisation is a local depression and ephemeral swamp which would collect material washed into it. The area has a large amount of drill spoil at the surface that could have been washed into this depression. Sulphur was above detection in this sample set (Figure 5.129) which was different from the previous results indicating that S which is able to be detected in the soil has been increased implying that the soil is more S rich that before flooding. The S could be sourced from the flood waters or simply washed into the swampy area from further out.

Some of the ranges of the geochemical assay results have been enhanced, such as for As and Au, but most have moved laterally, whereas, some had stayed relatively constant, as with Zn (Figure 5.127). The implications of this are that in this environment, temporal constraints on the sampling of the soils is at least as significant as it is with the sampling of vegetation (both are affected by seasonality and rainfall events).

5.4.12 Species Differences

Probability plots were created within the program IoGas for each element, using different colours for each different species from the Titania survey. Several of the key results are shown in Figures 5.130 - 5.141. Spinifex leaves are shown to have the highest levels of

contamination (Fe concentration) of all the plants, followed by the *Melaleuca spp.*, but all species showed similar levels of contamination, which was deemed insignificant.

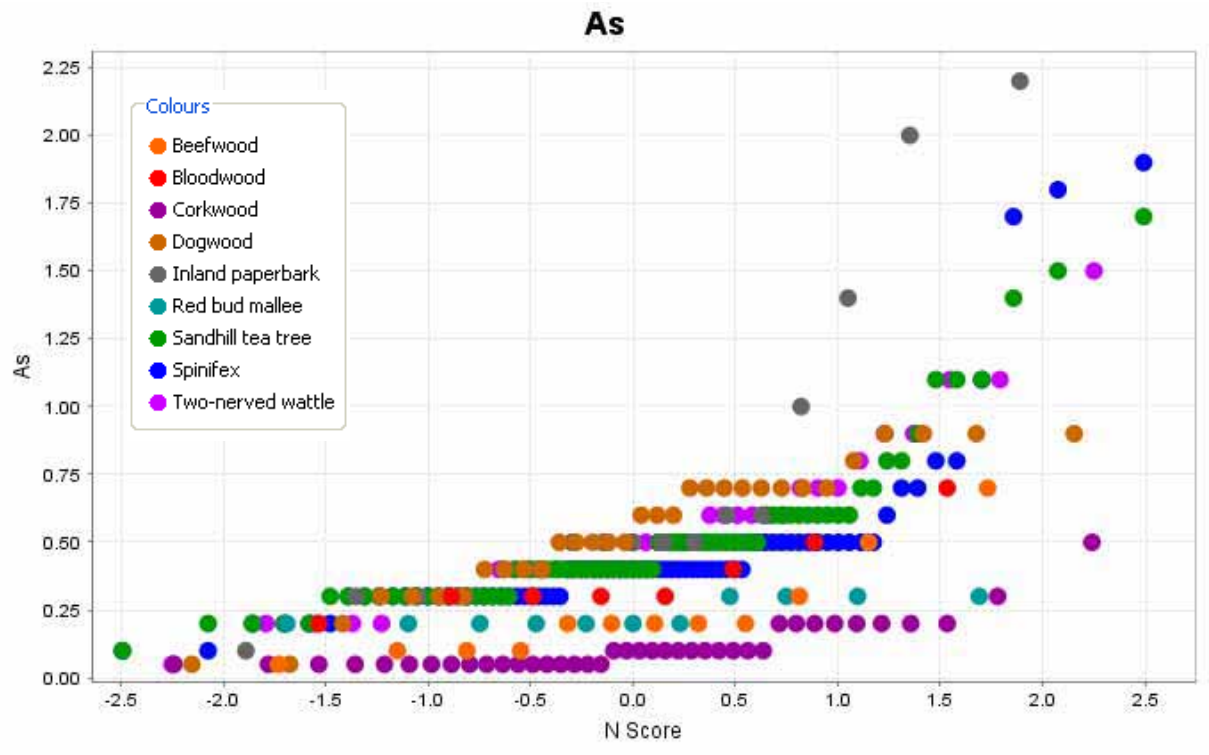

Figure 5.130: As results split by species at the Titania Prospect.

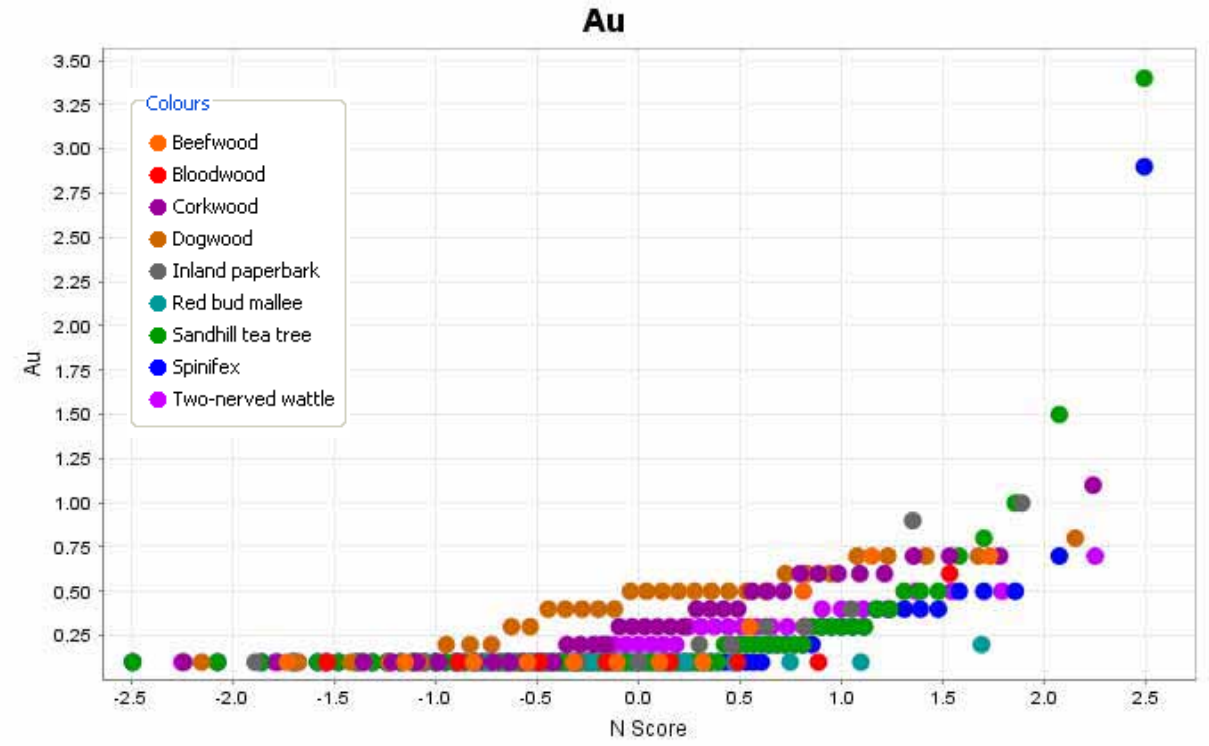

Figure 5.131: Au results split by species at the Titania Prospect.

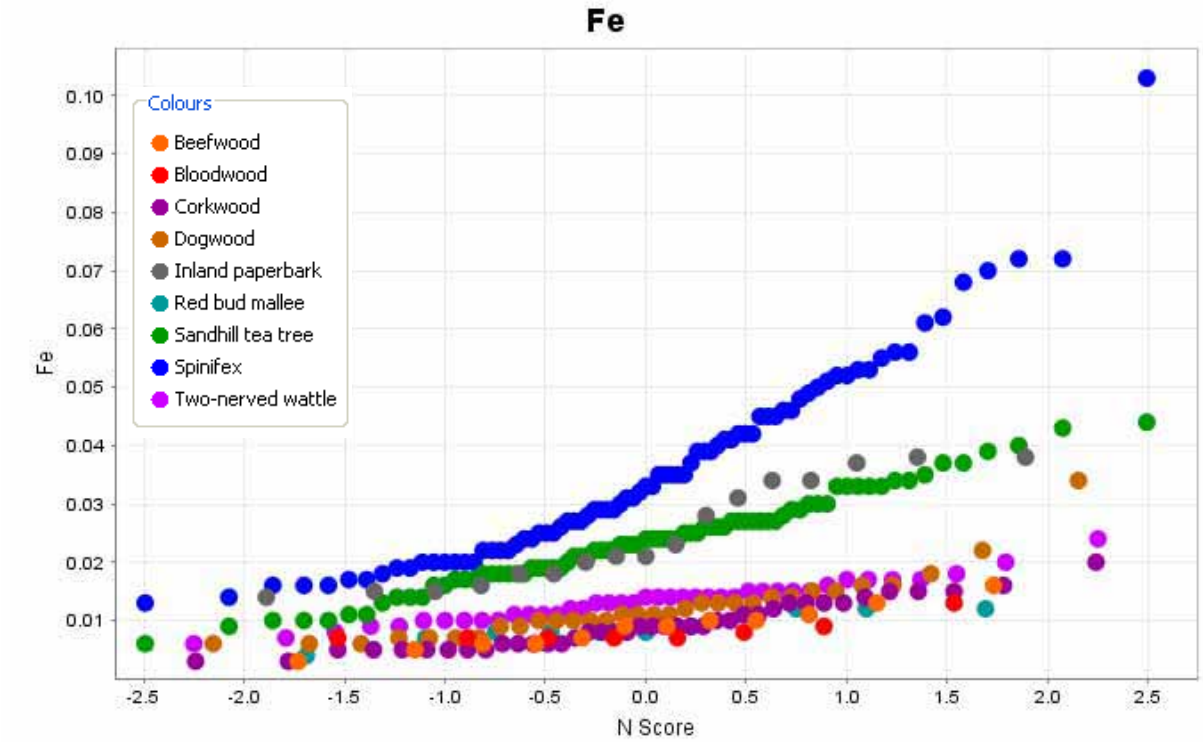

Figure 5.132: Fe results split by species at the Titania Prospect.

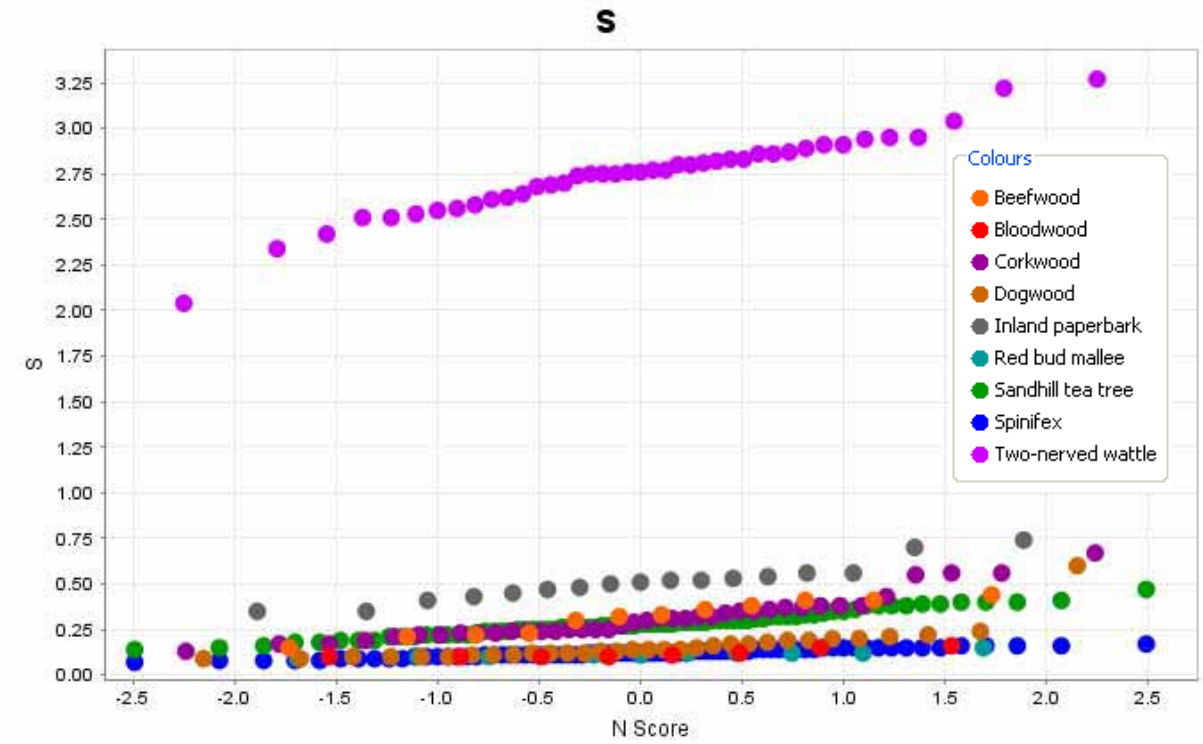

Figure 5.133: S results split by species at the Titania Prospect.

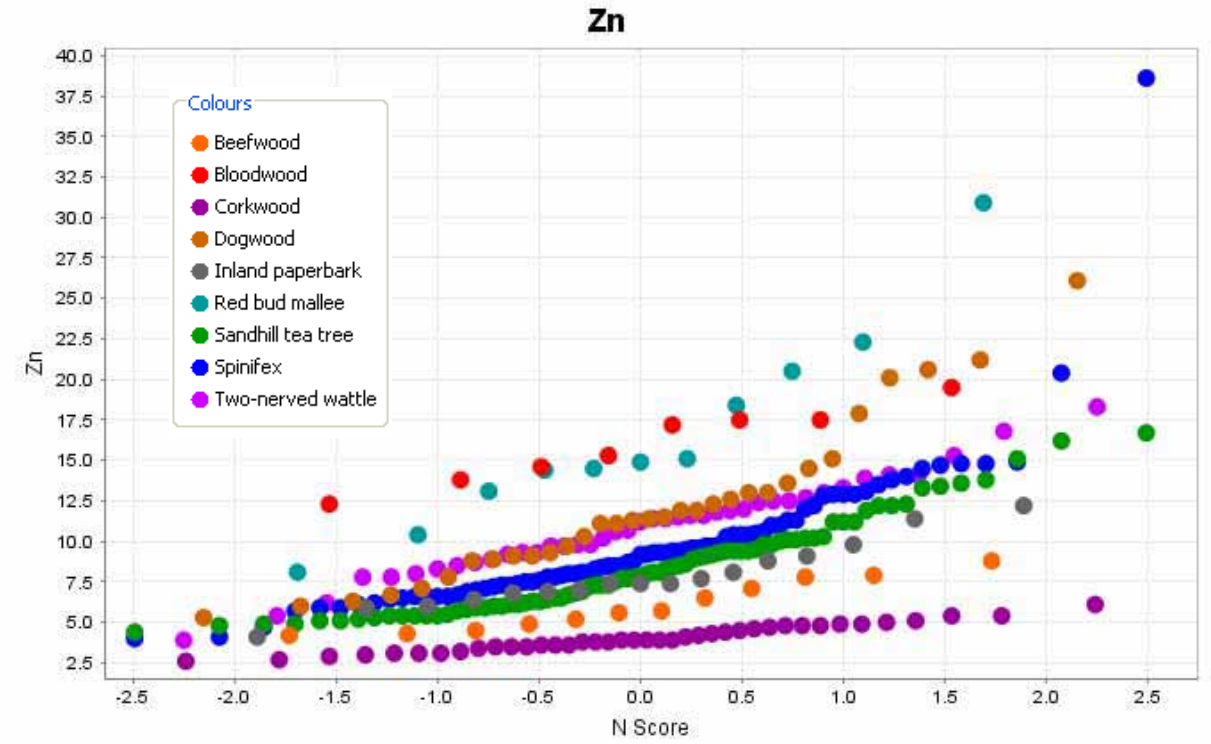

Figure 5.134: Zn results split by species at the Titania Prospect.

There is good consistency between the pathfinder elemental responses for the different plant species, except for S in the *Acacia bivenosa* results. *Acacia bivenosa* has much higher concentrations of Ca, Sr, Mg, Mo and S than the other plant species. This could have several explanations: the plant could be sourcing elements from carbonates at or near the surface, which could explain the Ca, Sr and Mg; the elements could be sourced from gypsum at the surface, which could explain the Ca, Sr and S; or there could be some combination of both. All these solutions highlight that the root system of this species is shallow and is sourcing elements from surficial materials.

Several of the elements were particularly different with respect to species (Figures 5.135 – 5.141). *Corymbia opaca* has much greater values of Co than any of the other plant species, which is not matched up with higher Ni or Fe which are the elements that can usually substitute for Co. *Triodia pungens* can accumulate Cr up to 23 ppm which is over an order of magnitude greater than any other species. This is similar to that seen at the Coyote and Hyperion Prospects but the greatest value is only half that seen at Coyote. *Hakea macrocarpa* is able to uptake much higher levels of Mn than the other species, the concentration values are even higher than that of the soils. Phosphorous is again fairly consistent between the species, which corresponds to P being a limited element in this environment.

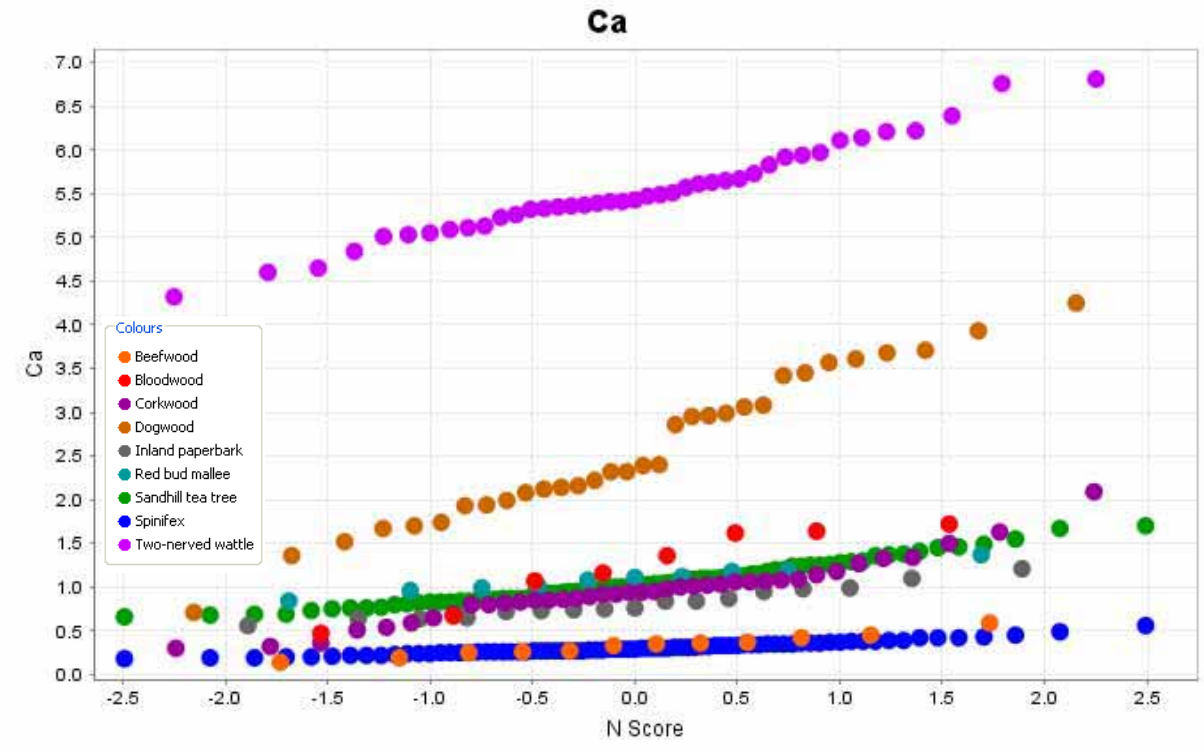

Figure 5.135: Ca results split by species at the Titania Prospect.

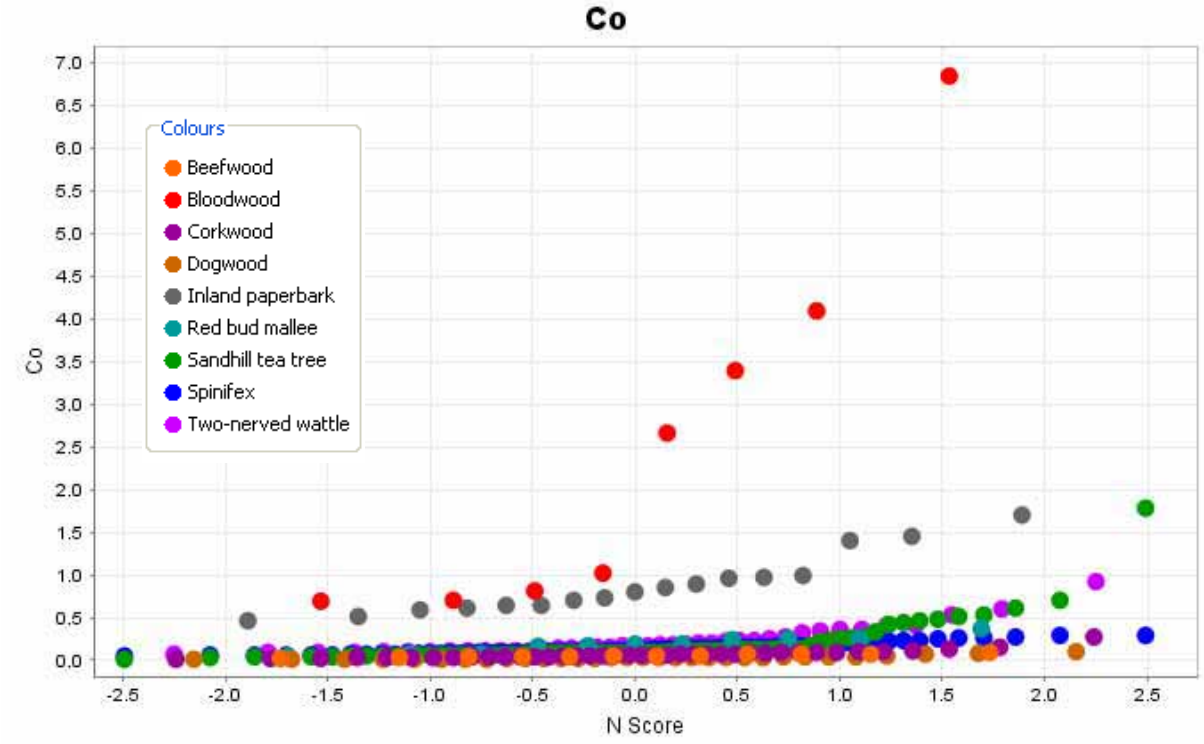

Figure 5.136: Co results split by species at the Titania Prospect.

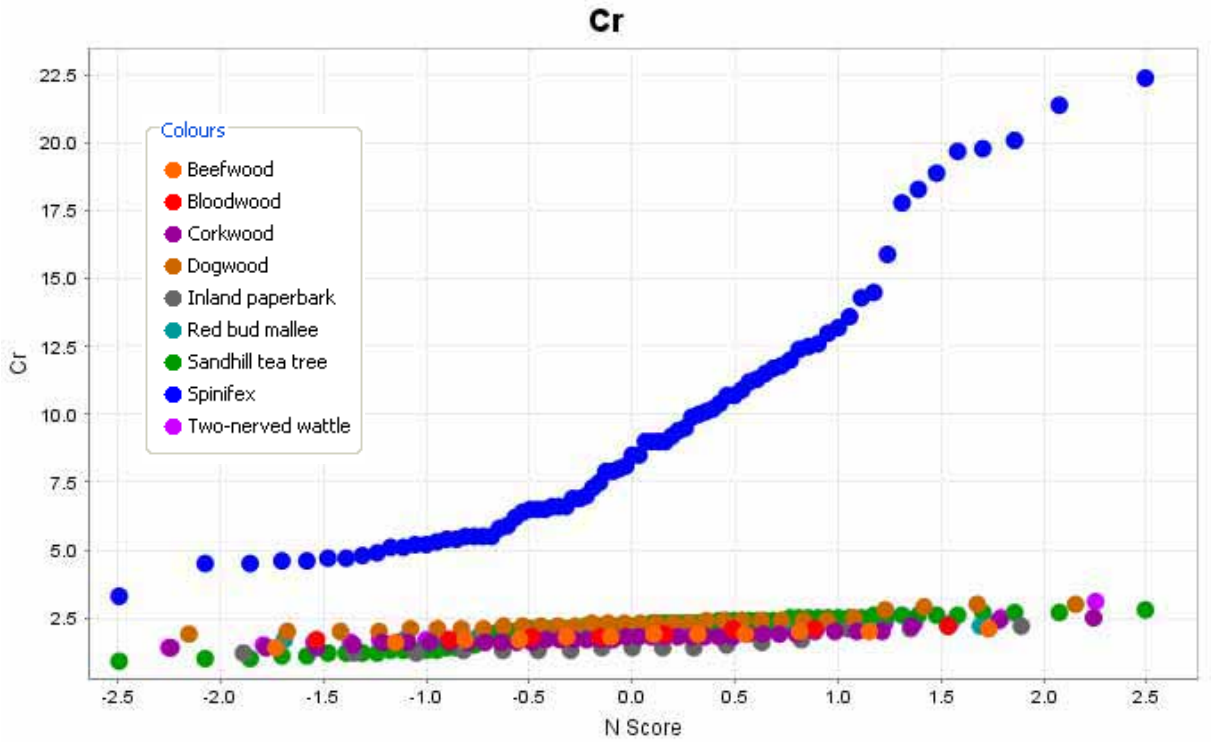

Figure 5.137: Cr results split by species at the Titania Prospect.

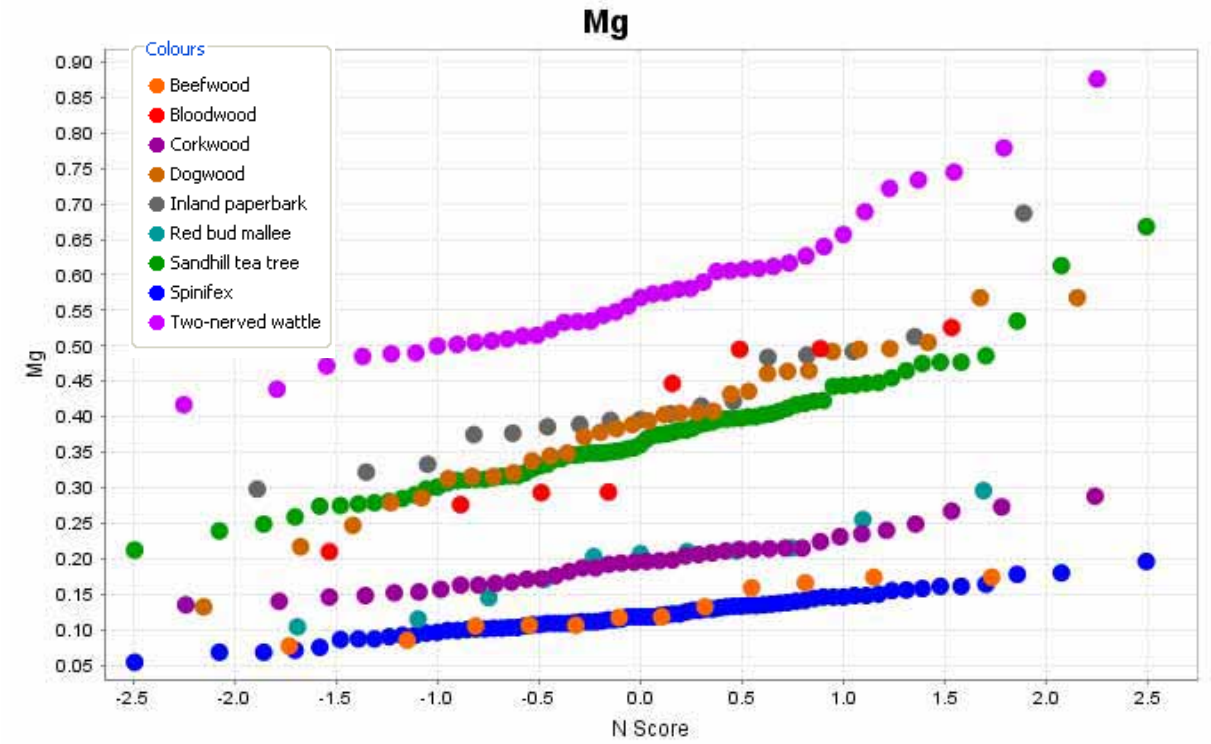

Figure 5.138: Mg results split by species at the Titania Prospect.

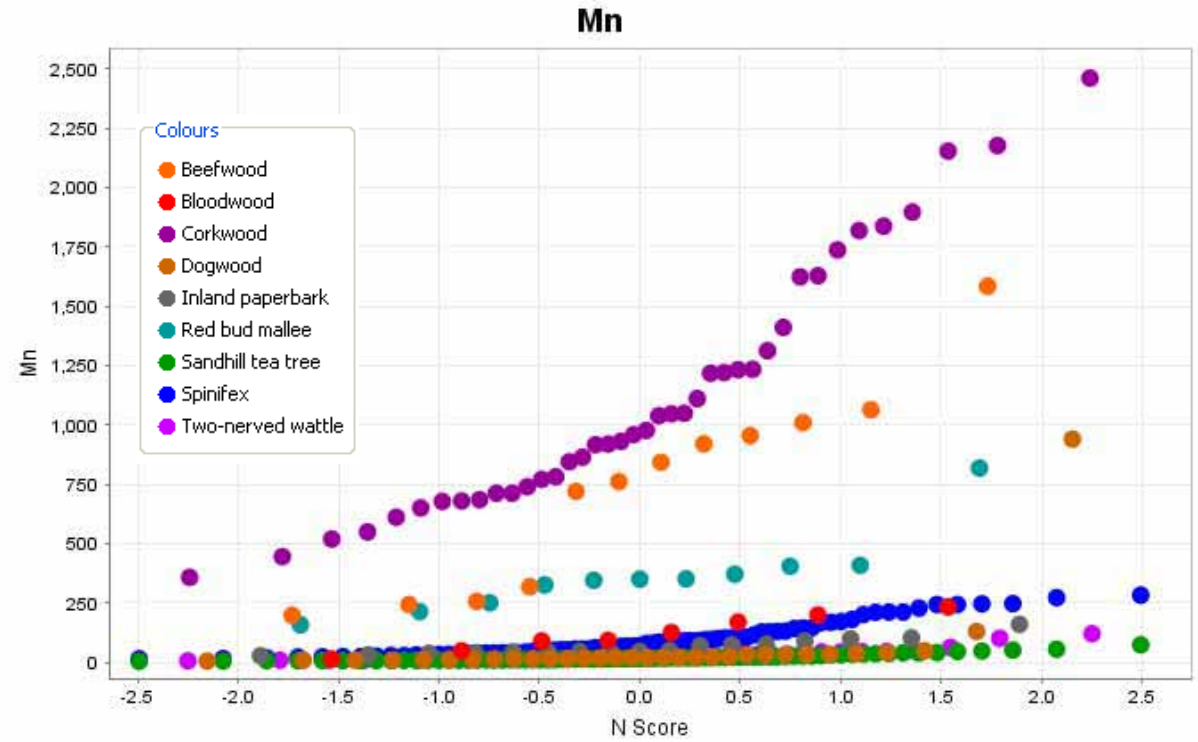

Figure 5.139: Mn results split by species at the Titania Prospect.

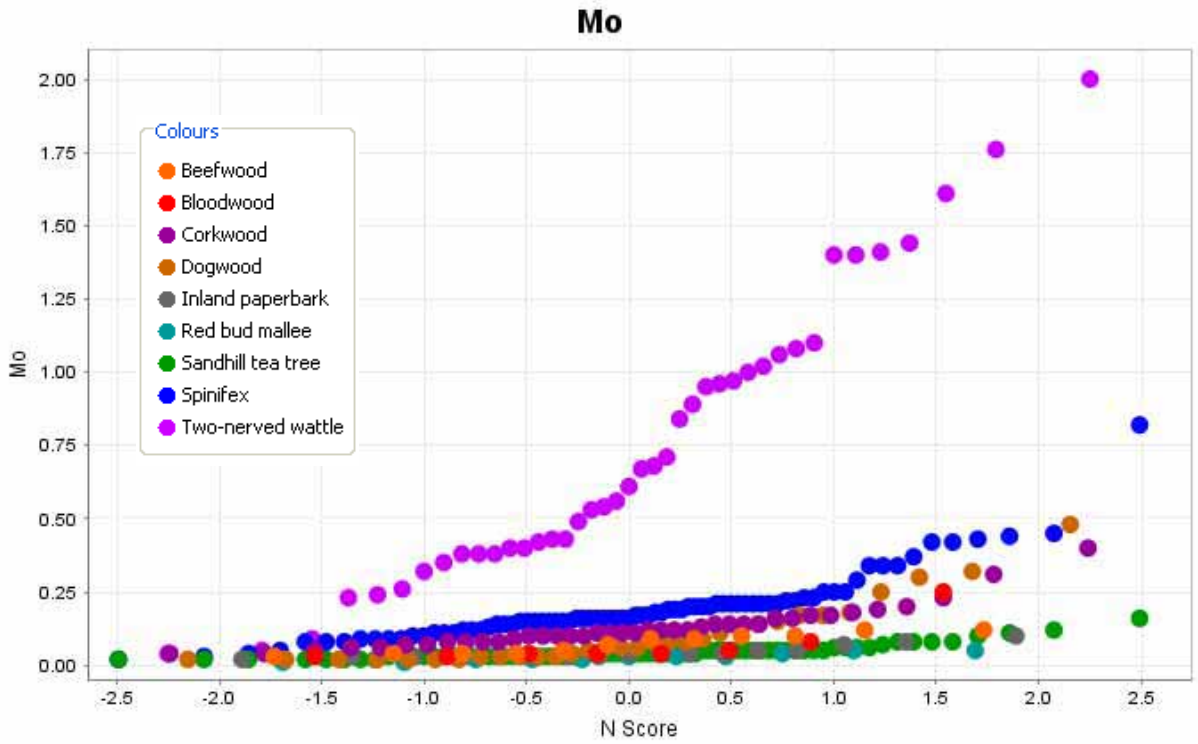

Figure 5.140: Mo results split by species at the Titania Prospect.

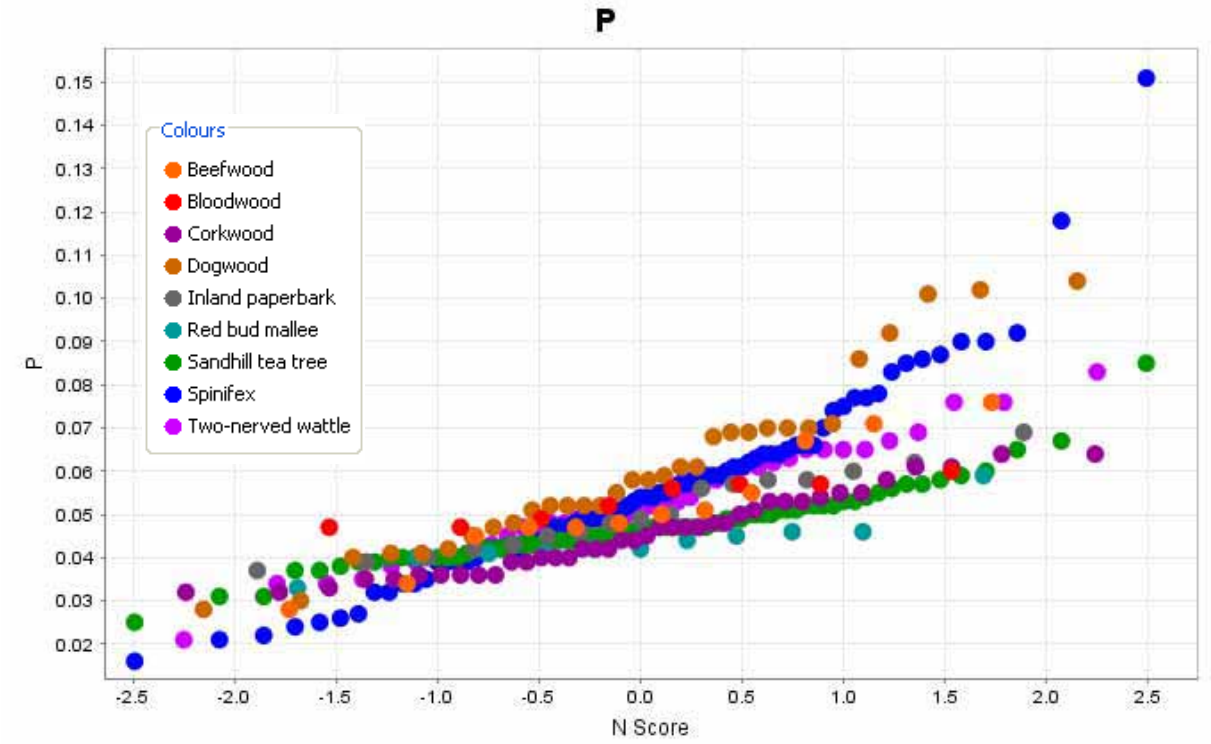

Figure 5.141: P results split by species at the Titania Prospect.

5.4.13 Elemental correlations

There are several different correlations that can be compared from the Titania data: there are the elemental correlations shown in Figures 5.142 – 5.148; correlations between the two soil sample sets (Figure 5.149); and, correlations between plant species and the soil samples (Figures 5.150-5.153). The correlations with the soil data was generated by comparing the average values for each element within each plant or soil set.

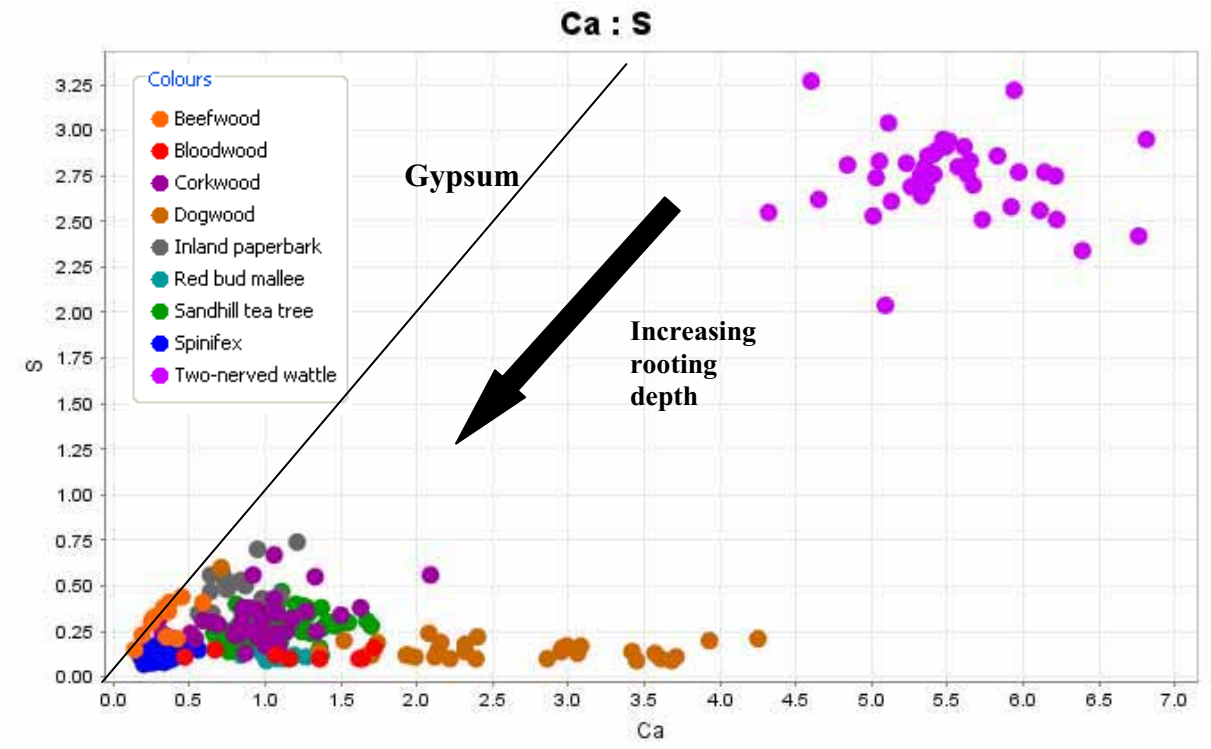

Figure 5.142: Ca and S visual correlation split by species at the Titania Prospect.

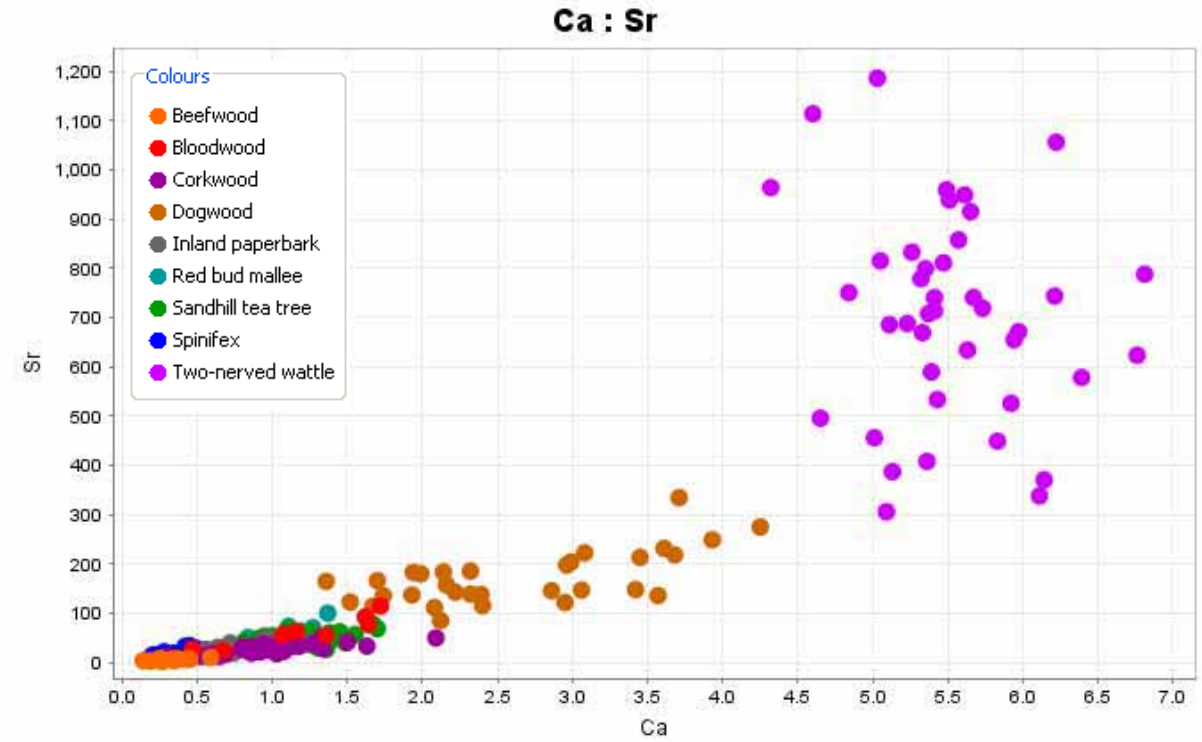

Figure 5.143: Ca and Sr visual correlation split by species at the Titania Prospect.

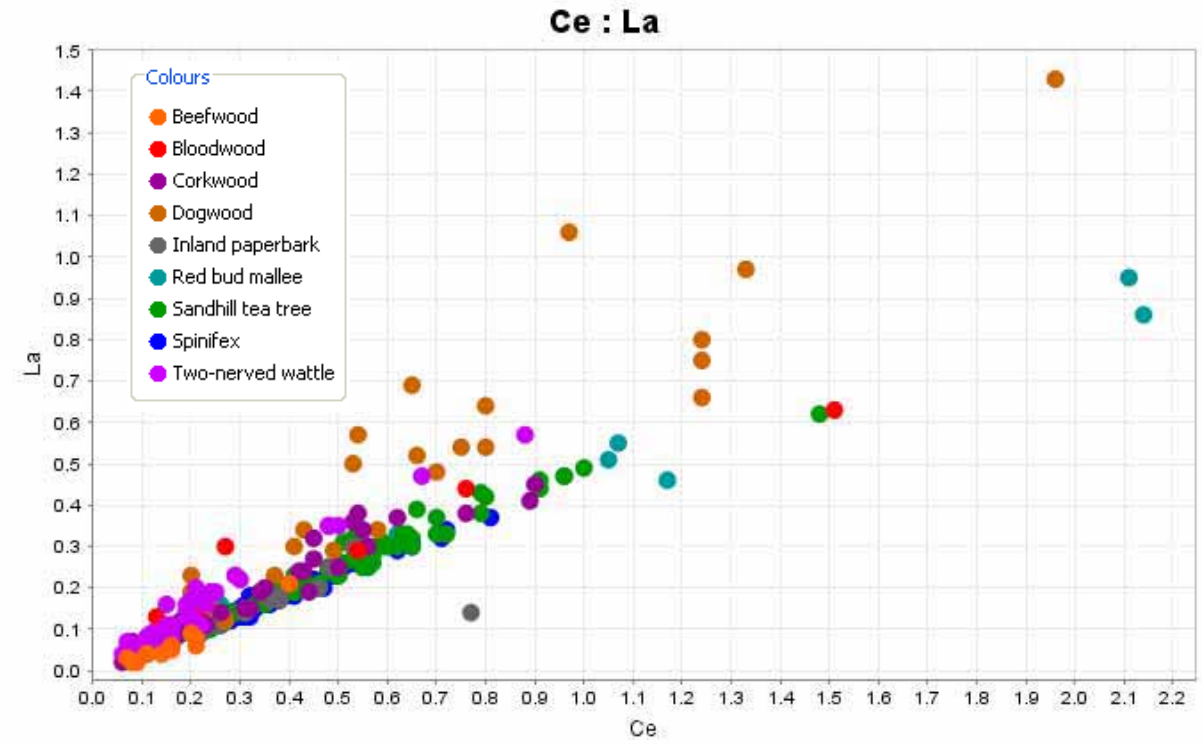

Figure 5.144: Ce and La visual correlation split by species at the Titania Prospect.

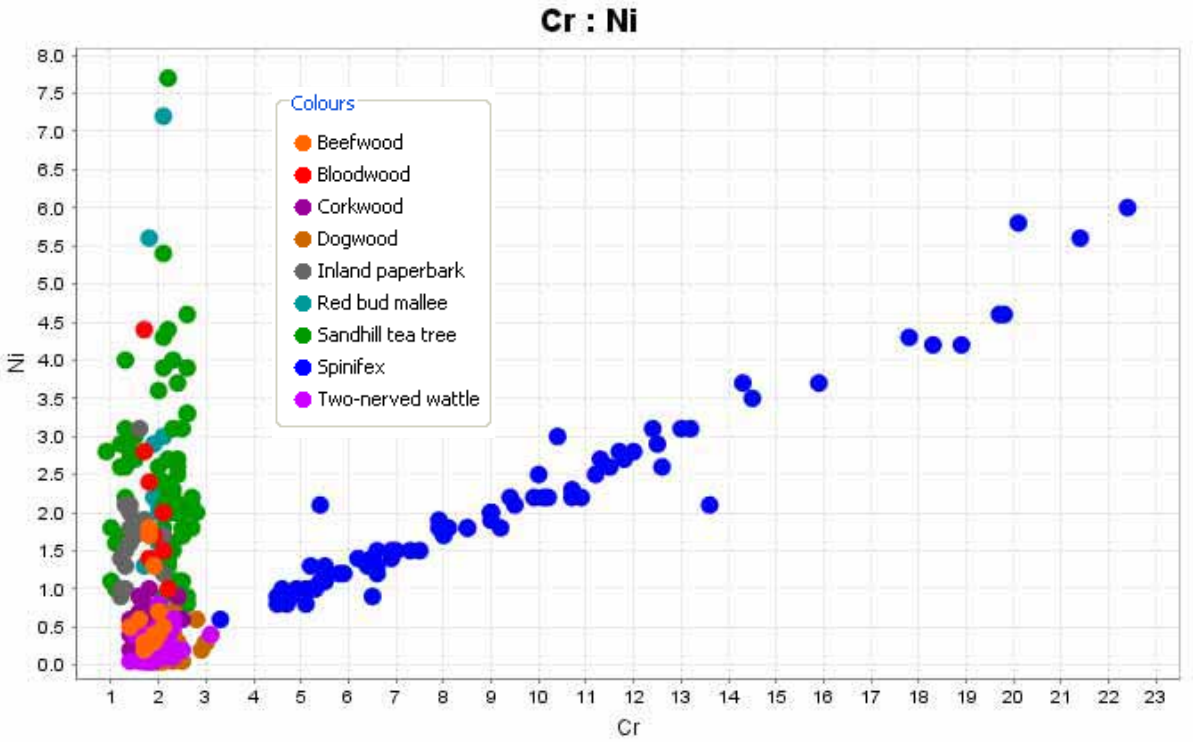

Figure 5.145: Cr and Ni visual correlation split by species at the Titania Prospect.

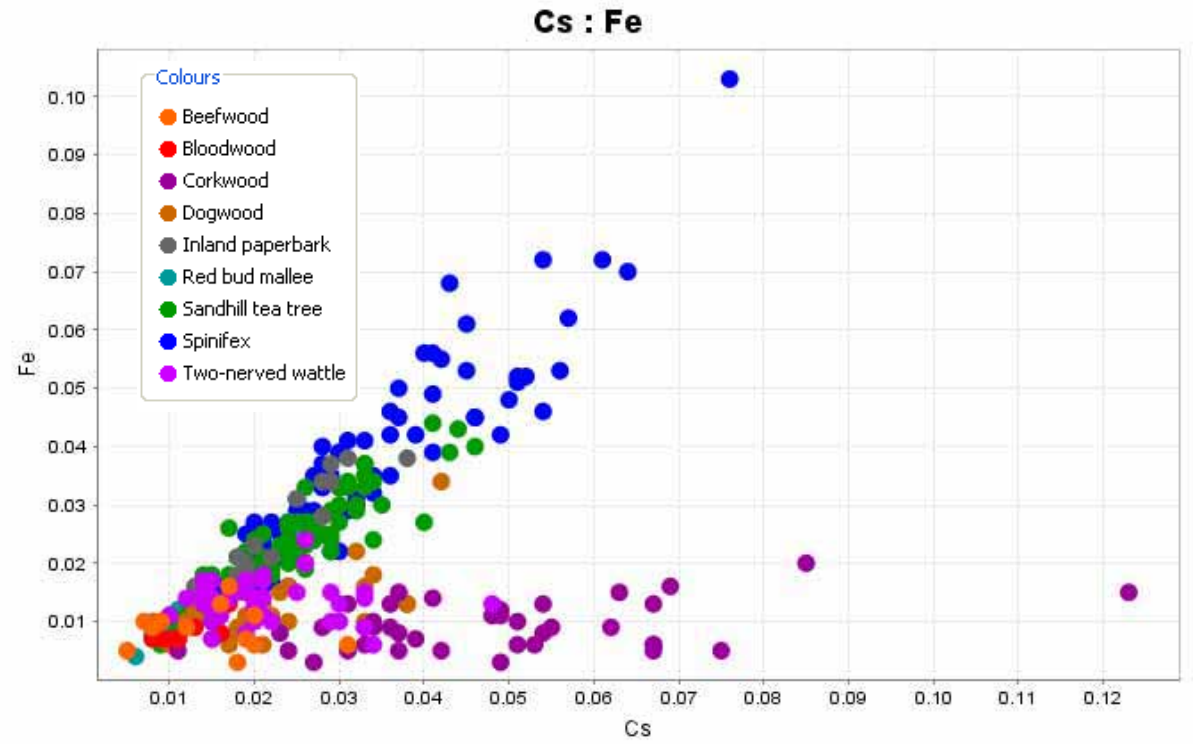

Figure 5.146: Cs and Fe visual correlation split by species at the Titania Prospect.

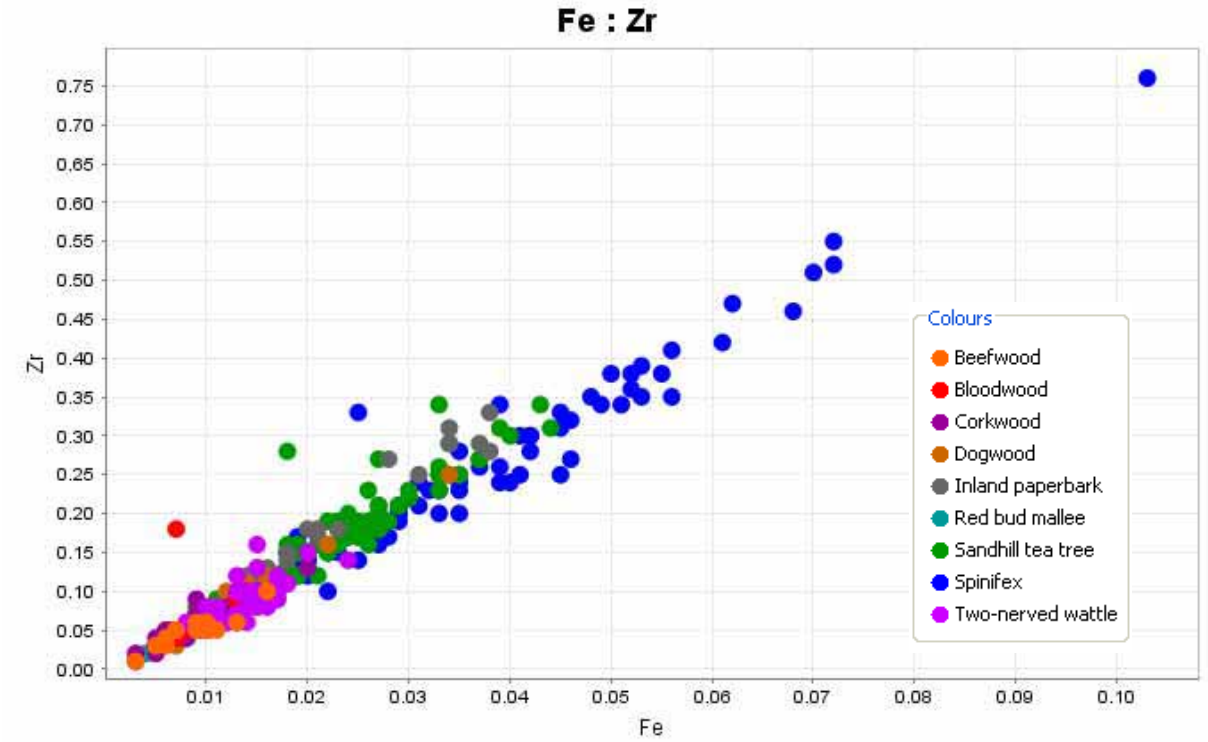

Figure 5.147: Fe and Zr visual correlation split by species at the Titania Prospect.

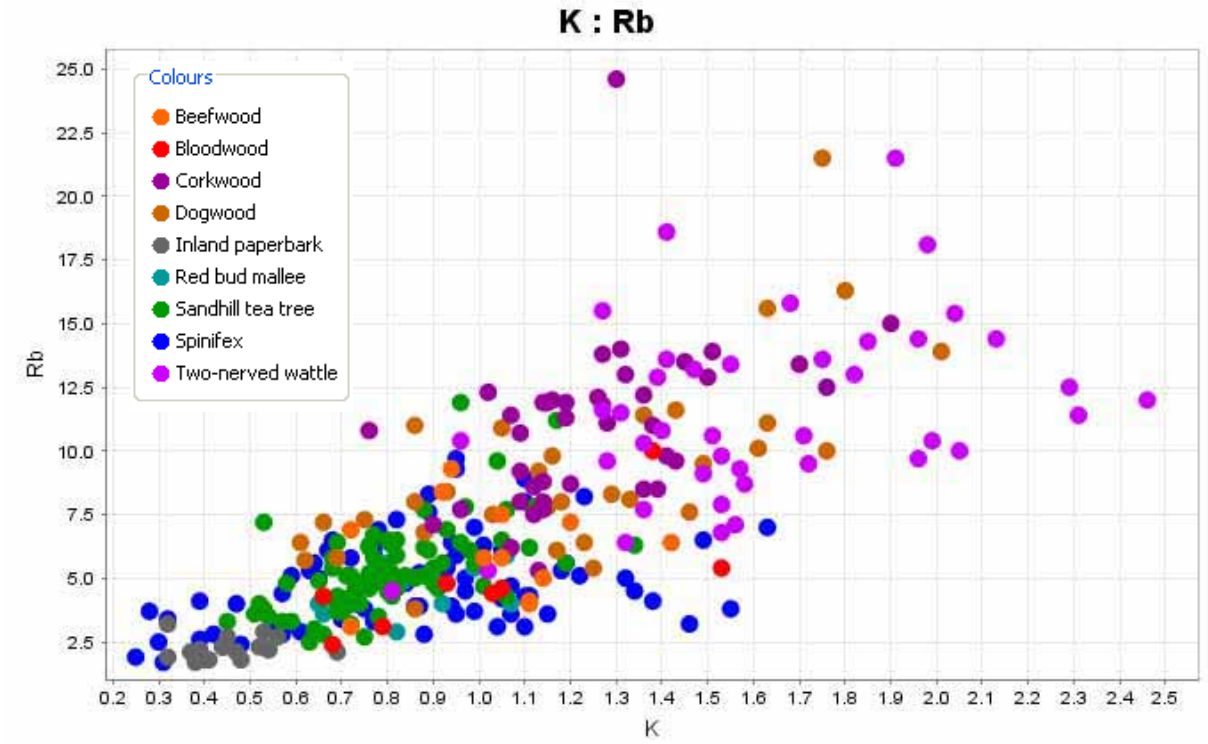

Figure 5.148: K and Rb visual correlation split by species at the Titania Prospect.

The elemental correlations show similar trends to those seen at the other field sites. There are correlations between detrital contamination elements (Al, Fe, Hf, Th, Ti and Zr) in this situation Cs also correlates well with detrital contamination with all plants except corkwood (Fe:Cs is 0.92 in spinifex). All the REE analysed were highly positively correlated within all plant species, as shown by Ce and La (0.92). Calcium was strongly correlated with Sr in all species except *Acacia bivenosa*. The high values of S within the *Acacia bivenosa* assays with high values of Ca and Sr led to the hypothesis that gypsum was being sampled, however, there is no correlation between these elements indicating that if gypsum is being sampled, the

S is being taken up at a different rate than the Ca, and this mechanism within the plant is not related. This could indicate that *Acacia bivenosa* is able to accumulate more S than other species.

Triodia pungens has very high correlation between Cr and Ni (0.98) indicating that in this site these 2 elements must be taken up through the same mechanism and may be interchangeable within the plant structure. Potassium and Rb have a visual correlation but the calculated correlation value (0.52) is not deemed significant.

Correlations between the soil (before flooding) and the soil (after flooding), *Triodia pungens*, *Melaleuca lasiandra*, *Hakea macrocarpa* and *Acacia bivenosa* can be seen in Figures 5.149-5.153.

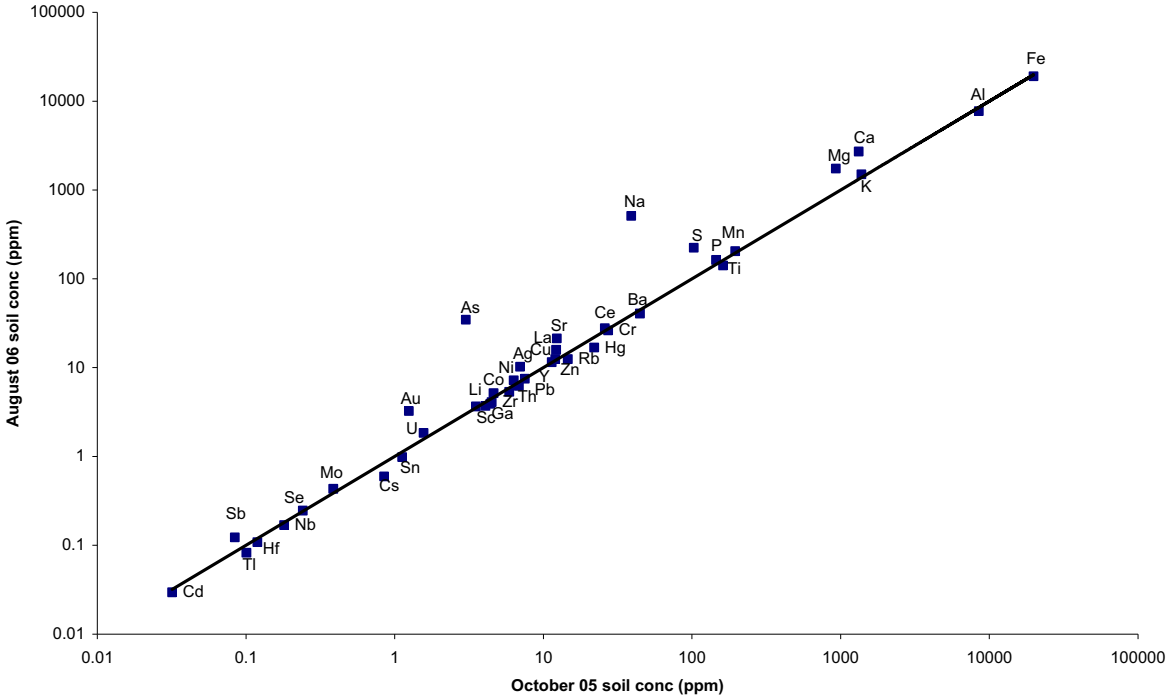

Figure 5.149: Direct comparison between October 05 soil concentrations and August 06 soils. All concentrations are in ppm except for Ag, Au and Hg which are in ppb.

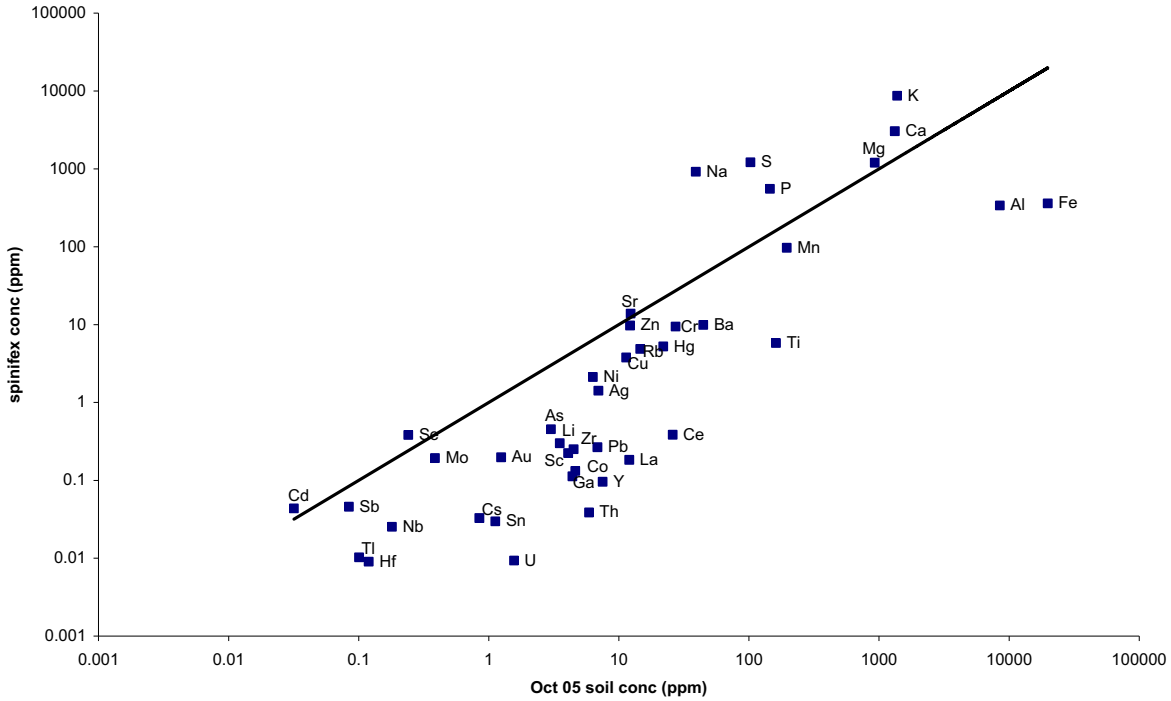

Figure 5.150: Direct comparison between soil concentrations (Oct 05) and *Triodia pungens* concentrations. All concentrations are in ppm except for Ag, Au and Hg which are in ppb.

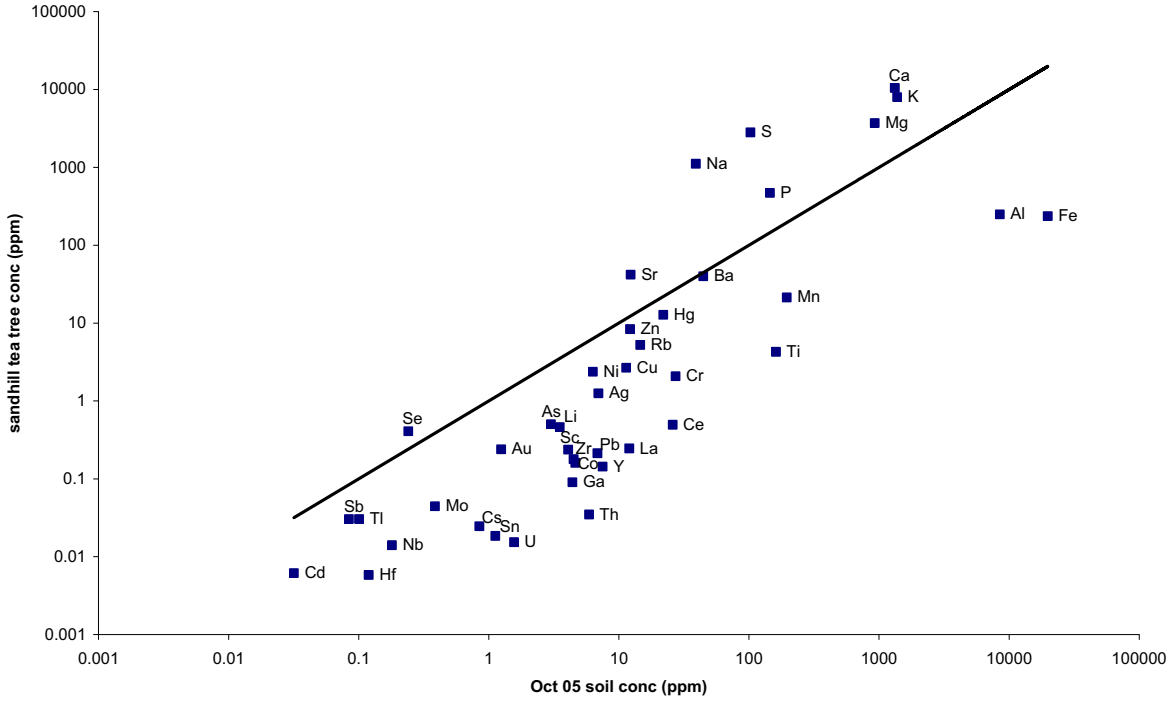

Figure 5.151: Direct comparison between soil concentrations (Oct 05) and *Melaleuca lasiandra* concentrations. All concentrations are in ppm except for Ag, Au and Hg which are in ppb.

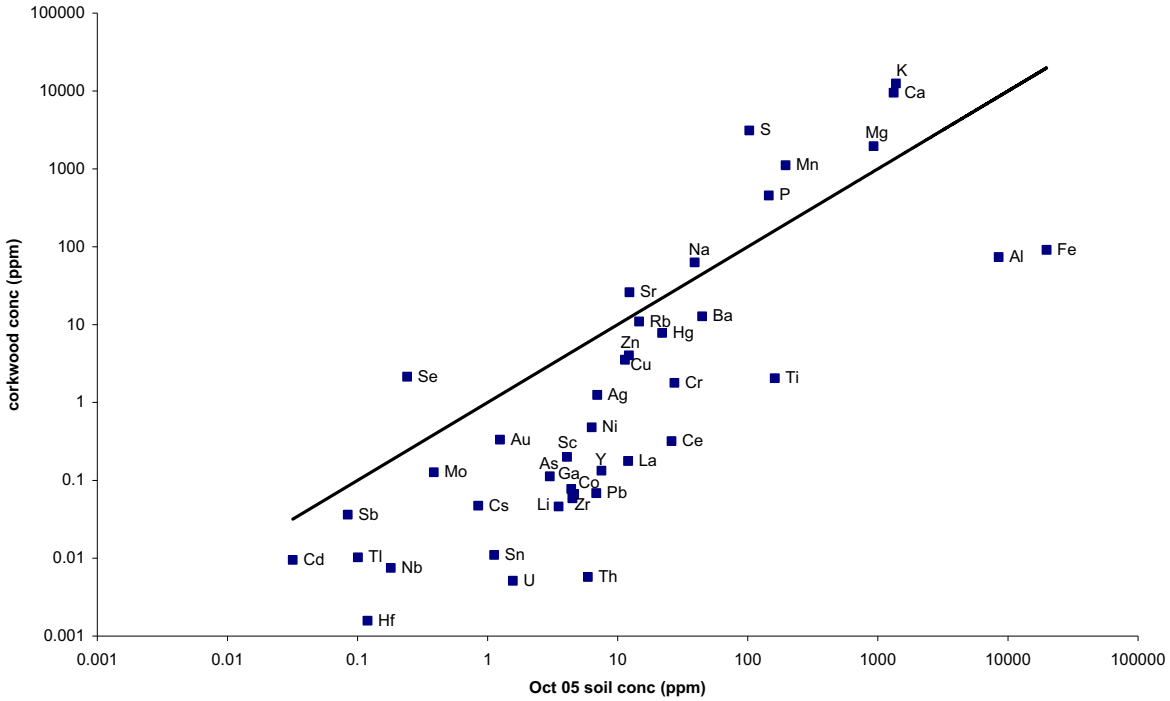

Figure 5.152: Direct comparison between soil concentrations (Oct 05) and *Hakea macrocarpa* concentrations. All concentrations are in ppm except for Ag, Au and Hg which are in ppb.

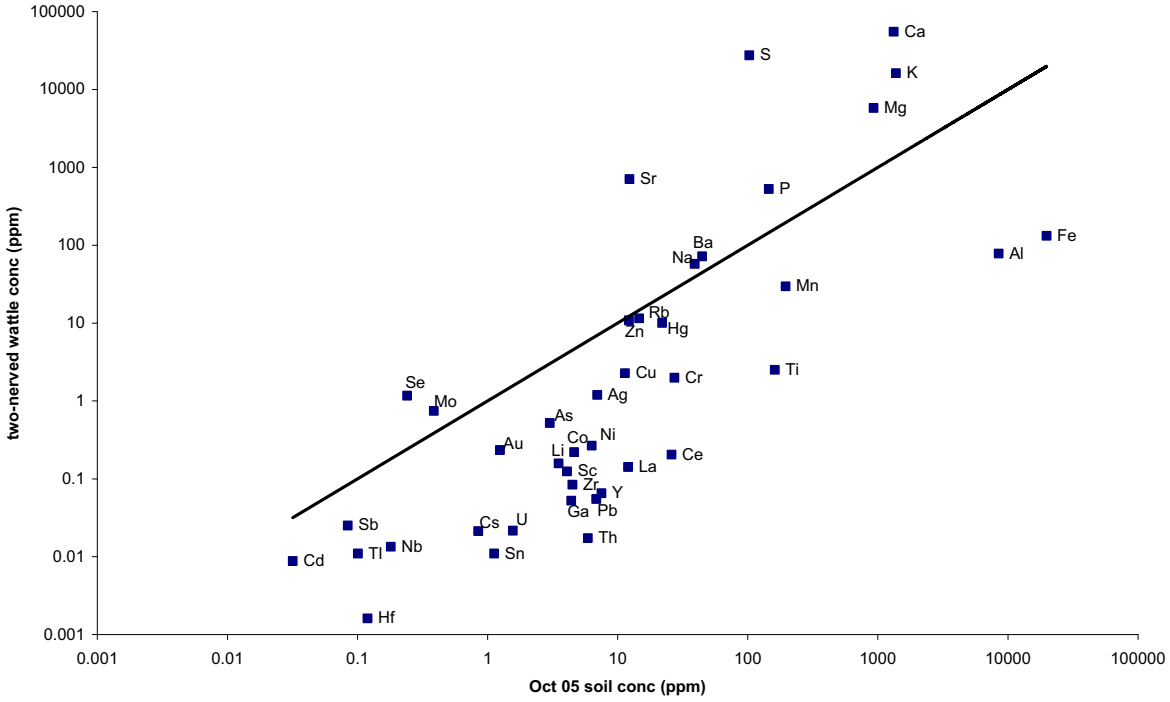

Figure 5.153: Direct comparison between soil concentrations (Oct 05) and *Acacia bivenosa* concentrations. All concentrations are in ppm except for Ag, Au and Hg which are in ppb.

The correlations to the soils data show that in general the two time periods of sampling have consistent levels of all elements except for As, Au and Na which are higher in the August 06 soil samples (after flooding). This indicates that these elements have been accumulated and sediment bearing these elements must have moved into the system.

All the plants show similar trends with respect to the soils. Elements that are considered essential to plant growth (Ca, K, Na, Mg, P, Sr and S) are higher in the plants as the plants accumulate these elements. The other elements are higher in or equal to the amounts within

the soils. There are several exceptions: *Triodia pungens* has Cr levels much higher than those of other plants but this is still on the same level as the soils; *Hakea macrocarpa* has much greater Mn concentrations than those of the other plants and this level actually exceeds that of the soils indicating that corkwood hyperaccumulates Mn; and, *Acacia bivenosa* has much higher concentrations of Ca, Sr, Mg, Mo and S than the other plants, all those except Mo are simply moved further from the 1:1 line but Mo is actually accumulated within this species moving this element from higher values in the soil (as with the other species) to higher values in the plant.

6 Tanami Region – Regional Summary and Discussion

6.1 Interpretation of spatial patterns

In each of the field sites a major challenge is the distinction between surface expression of buried mineralisation and lateral transport and deposition. A combination of recognising the surficial regolith-landform assemblage and utilising the multi-element chemical assays seem to be the best ways to discern this. For instance, depositional landforms such as drainage channels will have a greater tendency towards hosting transported responses, whereas erosional rises will have more locally derived responses. 'Gold-only' responses appear to be variable and are subjected to strong 'nugget' effects. Supportive high responses in other mineralisation-related elements, in particular As, REE, Zn and S, appear to be valuable for interpreting less transported material and anomalies.

6.1.1 Coyote

At the Coyote Prospect, spinifex, snappy gum, desert bloodwood and silver box were all able to express the buried mineralisation or associated dispersion haloes with either all or some of Au, As, S, Zn and REE. Soft spinifex was the most widely distributed species and gave the best 'direct' footprint of the mineralisation zone. This zone varied in length based upon the mobility of each element examined. The original geochemical data at the site showed that there was only a surface As anomaly and the geochemistry of the regolith profile showed barren saprolite to 80 m depth.

Since *Triodia pungens* is a deep-rooted species it is able to give localised chemical signatures for the *in-situ* regolith materials that may underlies 5-15 m of surface sediment (Burbidge 1953; Reid *et al.* 2008; Grigg *et al.* 2008b). In the Tanami region, and possibly many other parts of arid Australia, the spinifex is an excellent biogeochemical exploration sampling medium, especially compared to soils, which are typically influenced by complexities of sheetflow and aeolian dispersion and dilution. The vegetation results have very sharp cut-offs to the generated anomalies in this system. There are high values next to values that are below the detection limit of the analysis technique. This makes it less useful in a regional sampling program, but spinifex would be an ideal sampling medium for closely spaced, detailed ore body delineation in the Tanami region and most likely in other hummock grass-dominated parts of the continent and grasslands world-wide.

Eucalyptus brevifolia had a distinct geobotanical anomaly related to the Coyote Fault. This means that botanical mapping of the distribution of this species could be used as a surrogate for interpretive structural geology maps. However, the elemental distributions showed a widely dispersed halo within Zn and S that decreased gradually to the south of the transect.